Charles University
Faculty of Science

Molecular and Cellular Biology, Genetics and Virology

Ing. Radka Štorchová

Molecular mechanisms of Wip1 phosphatase function in DNA damage response

Molekulární mechanismy funkce Wip1 fosfatázy v buněčné odpovědi na poškození DNA

Doctoral thesis

Supervisor: MUDr. Libor Macůrek, Ph.D.

Prague, 2023

Prohlášení:

Prohlašuji, že jsem závěrečnou práci zpracovala samostatně a že jsem uvedla všechny použité informační zdroje a literaturu. Tato práce ani její podstatná část nebyla předložena k získání jiného nebo stejného akademického titulu.

V Praze dne

.....

Radka Štorchová

ACKNOWLEDGEMENTS

First of all, I would like to express my gratitude to my supervisor Libor Macůrek for letting me pursuit my Ph.D. studies in his laboratory and for his supervision and support over the years. I would also like to thank my colleagues, both past and present, from the team for a pleasant working environment and inspiring discussions, especially to Matouš Palek and Kamila Burdová, with them I was working closely on the projects. I would also like to thank to my family and especially my husband for their continuous support over the years of my PhD and now also to my daughter for letting me finish writing of the thesis.

ABSTRACT

Human cells are constantly exposed to diverse factors causing DNA lesions, which activate the DNA damage response (DDR). Depending on the severity of DNA damage, DDR can promote temporary cell cycle arrest (checkpoint), permanent growth arrest (senescence) or programmed cell death (apoptosis). DDR signalling is regulated by a cascade of post-translational modifications, where key mediators are represented by protein kinases ATM, ATR and DNA-PK. Wip1 phosphatase (encoded by PPM1D gene) plays an important role in DDR termination by dephosphorylation of many targets of these kinases.

In this thesis, we investigated checkpoint-independent functions of PPM1D in cells and described several new substrates. We discovered, that PPM1D interacts with the shelterin complex and localizes at telomeres. PPM1D dephosphorylates the shelterin component TRF2 at S410. TRF2 S410 phosphorylation enhanced TRF2 interaction with TIN2, indirectly also increasing recruitment of TPP1 to telomeres. Importantly, cells over expressing PPM1D showed increased number of telomeric fusions. These findings might be very relevant for some cancer types, in particular those expressing high levels of PPM1D or carrying C-terminally truncated mutations in PPM1D.

To validate the published substrates and to detect possible new targets of PPM1D, we developed a novel screen based on direct dephosphorylation of proteins in nuclear extracts by purified PPM1D phosphatase. In this way, we detected novel PPM1D targets including BRCA1 S1524 and DBC1 T454. We also proposed a mechanism how PPM1D inhibition stimulates p53 function by increasing its acetylation.

We also studied how PPM1D affects DNA damage repair and found that PPM1D promotes homologous recombination. Importantly, we found that PPM1D inhibition could have synergistic effect with PARP1i on eradicating p53 proficient cancer cells.
Overall, this thesis contributed to better understanding of the checkpoint-independent functions of PPM1D in human cells including its role in telomere maintenance and DNA repair.

Keywords:
DNA damage response, PPM1D phosphatase, telomeres

ABSTRAKT

Lidské buňky jsou neustále vystaveny různým faktorům, které způsobují poškození DNA a aktivují odpověď na poškození DNA (DDR). V závislosti na závažnosti poškození DNA může DDR napomáhat dočasnému zastavení cyklu buněk (kontrolní bod buněčného cyklu, "checkpoint"), trvalému zastavení růstu (senescence) nebo programované buněčné smrti (apoptóze). Signál DDR je regulován kaskádou post-translačních modifikací, kde klíčovými mediátory jsou fosfoproteinové kinázy ATM, ATR a DNA-PK. Fosfatáza Wip1 (kódovaná genem PPM1D) hraje důležitou roli v ukončení DDR fosforylací mnoha cílů těchto kináz.

V této práci jsme zkoumali funkce PPM1D nezávislé na kontrolních bodech buněčného cyklu v buňkách a popsali jsme několik nových substrátů. Zjistili jsme, že PPM1D interaguje se shelterinovým komplexem a nachází se na telomerách. PPM1D desfosforyluje shelterinový protein TRF2 na S410. Fosforylace TRF2 na S410 zvyšovala jeho interakci s TIN2, což nepřímo zvyšovalo množství TPP1 na telomerách. Buňky s overexpresí PPM1D měly zvýšený počet telomerických fúzí. Tato zjištění mohou být velmi důležitá pro některé typy rakoviny, zvláště ty, které vykazují vysoké hladiny PPM1D nebo obsahují mutace v C-konci PPM1D. Pro ověření publikovaných, a detekci možných nových, substrátů PPM1D jsme vyvinuli novou metodu, využívající jaderných extraktů a rekombinantní PPM1D fosfatázy. Touto metodou jsme ověřili několik známých substrátů a detekovali nové substráty PPM1D, včetně BRCA1 S1524 a DBC1 T454. Navíc jsme navrhli mechanismus, kterým PPM1D inhibice zvyšuje acetylaci p53. Studovali jsme také, jak PPM1D ovlivňuje opravu poškození DNA a zjistili jsme, že PPM1D podporuje homologní rekombinaci (HR). Navrhli jsme, že inhibice PPM1D by mohla mít synergické účinky v kombinaci s inhibicí PARP při léčbě rakovinných buněk s nezmutovanou p53. Celkově tato práce přispěla k lepšímu pochopení funkcí PPM1D, nezávislých na kontrolních bodech, v lidských buňkách, včetně role PPM1D při udržování telomer a opravě DNA.

Klíčová slova:

Odpověď na poškození DNA, fosfatáza PPM1D, telomery

LIST OF ABBREVIATIONS

14-3-3	14-3-3 protein family; a large family of signal-transducing adaptor proteins
53BP1	tumour suppressor p53-binding protein 1
ALT	Alternative lengthening of telomeres
ATM	ataxia telangiectasia mutated
ATR	ataxia telangiectasia and Rad3-related protein
ATRIP	ATR interacting protein; required for checkpoint signalling after DNA damage
BER	base excision repair
BRCA1	breast cancer type 1 susceptibility protein
CDC25	M-phase inducer phosphatase
CDK	cyclin-dependent kinases
Chk1	checkpoint kinase 1
Chk2	checkpoint kinase 2
DAXX	death domain-associated protein 6
DCLRE1B	DNA cross-link repair 1B protein (also called SNM1B or Apollo)
DDR	DNA damage response pathways
DNA-PK	DNA-dependent protein kinase
DSBs	DNA double-strand breaks
FACS	fluorescence-activated cell sorting
G1	cell cycle growth phase 1
G2	cell cycle growth phase 2
GAPDH	glyceraldehyde-3-phosphate dehydrogenase
GFP	green fluorescent protein
H2A	a type of histone; a part of nucleosome core particle
H2AX	histone that replaces conventional H2A in a subset of nucleosomes
HCT116	human colon cancer cell line
kb	kilobases
KO	knock-out
MAP	mitogen activated protein kinases

MDC1	mediator of DNA damage checkpoint protein 1
Mdm2	E3 ubiquitin-protein ligase
MdmX	murine double minute
MEFs	murine embryonic fibroblasts
MRE11	meiotic recombination 11
MRN	heterotrimeric protein complex consisting of Mre11, Rad50 and Nbs1
NBS1	Nijmegen breakage syndrome protein 1; nibrin; p95
NF-κB	nuclear factor of κ light polypeptide gene enhancer in B-cells 1
NIH-3T3	mouse embryonic fibroblasts cell line
NLS	nuclear localization sequence
NoLS	nucleolar localization sequence
NUMA1	Nuclear mitotic apparatus protein 1
nt	nucleotide
p21	cyclin-dependent kinase inhibitor 1; CDK-interacting protein 1
p38MAPK	mitogen-activated protein kinase 14; mitogen-activated protein kinase p38 alpha
p53	cellular tumour antigen; acts as a tumour suppressor in many tumour types
PARP	poly(ADP-ribose) polymerase
PCNA	proliferating cell nuclear antigen
PIKK	phosphoinositide three-kinase-related kinase
POT1	Protection of telomeres protein 1
PP2C	serine/threonine-protein phosphatase 2C
PPM1D	gene encoding Wip1 phosphatase, also used as abbreviation for Wip1 phosphatase
pSQ/TQ	ATM/ATR phosphorylable serine or threonine with glutamine at the +1 position
PTEN	phosphatidylinositol-3,4,5-trisphosphate 3-phosphatase
RAD50	DNA repair protein; component of the MRN complex
RAP1	TRF2 interacting protein (also known at TERF2IP)

RING	„Really Interesting New Gene“, zinc finger type domain
RNF168	E3 ubiquitin-protein ligase; RING finger protein 168
RNF8	E3 ubiquitin-protein ligase; RING finger protein 8
ROS	reactive oxygen species; chemically-reactive molecules containing oxygen
RPA	replication protein A
SSB	single-strand break
ssDNA	single stranded DNA
TERF2IP	TRF2 interacting protein (also known at RAP1)
TopBP1	DNA topoisomerase 2-binding protein 1
TPP1	Telomere protection protein 1
TRF1	Telomeric repeat-binding factor 1 (also TERF1)
TRF2	Telomeric repeat-binding factor 2 (also TERF2)
U2OS	human osteosarcoma cell line
Wip1	wild-type p53-induced phosphatase 1
WT	wild-type

TABLE OF CONTENTS

1 INTRODUCTION

1.1 DNA damage and mechanisms of DNA repair

Cells are constantly exposed to diverse factors, either exogenous (UV, IR, chemicals) or endogenous (replication stress and cellular metabolism), causing DNA lesions. The most deleterious type of DNA damage are double strand breaks (DSBs) which can lead to chromosome rearrangements such as chromosome deletions and translocations. The initiation of DNA repair depends on the activation of DNA damage response (DDR) [1].

To resolve the DSBs, cells activate a sophisticated signaling cascade called DNA damage response (DDR) pathway, which can coordinate cell cycle progression and DNA repair. To prevent duplication or segregation of damaged DNA, DDR pathways can activate temporary cell cycle arrest (checkpoint), permanent growth arrest (senescence) or programmed cell death (apoptosis). DDR is regulated by posttranslational modifications, especially by phosphorylations. The main composition of DDR pathway can be categorized into DNA damage sensors, transducers (phosphatidyl-inositol 3-kinase-related kinase protein kinases: ATM/ATR), mediators, and effectors (Figure 1). DSBs are detected by MRN (Mre11-Rad50-Nbs1) complex, which contributes to recruitment and activation of Ataxia telangiecstasia mutated kinase (ATM). Single stranded DNA is sensed by RPA which recruits (ATM and Rad3-related kinase (ATR) kinase via ATR-interacting protein (ATRIP). ATM/ATR then propagate the signal through many phosphorylations. ATM/ATR phosphorylate histone H2AX at S139, which mediates recruitment of DNA damage mediators (BRCA1, 53BP1). Then with the help of mediator proteins, phosphorylate and thus activate the effector kinases Chk1 and Chk2. Those can induce a checkpoint arrest by targeting Cdc25 family of phosphatases [2]. ATR/ATM and Chk1/2 kinases also phosphorylate and thereby stabilize tumor suppressor p53, which triggers expression of multiple target genes leading to either cell cycle arrest to permit DNA repair or senescence or apoptosis, depending on the severity of the DNA damage [1, 3, 4].

To orchestrate the DDR, there are three important phosphatidylinositol 3-kinase related kinases (PIKK): ATM, ATR and DNA-dependent protein kinase (DNA-PK). ATR is activated by ssDNA coated with RPA, which can occur at SSBs or at DSBs after resection. ATM and DNA-PK can be activated by DSBs. Once activated, ATM

phosphorylates hundreds of substrates and DNA-PK regulates smaller subgroup of targets, which are involved in DSB ends ligation [1, 3, 4].

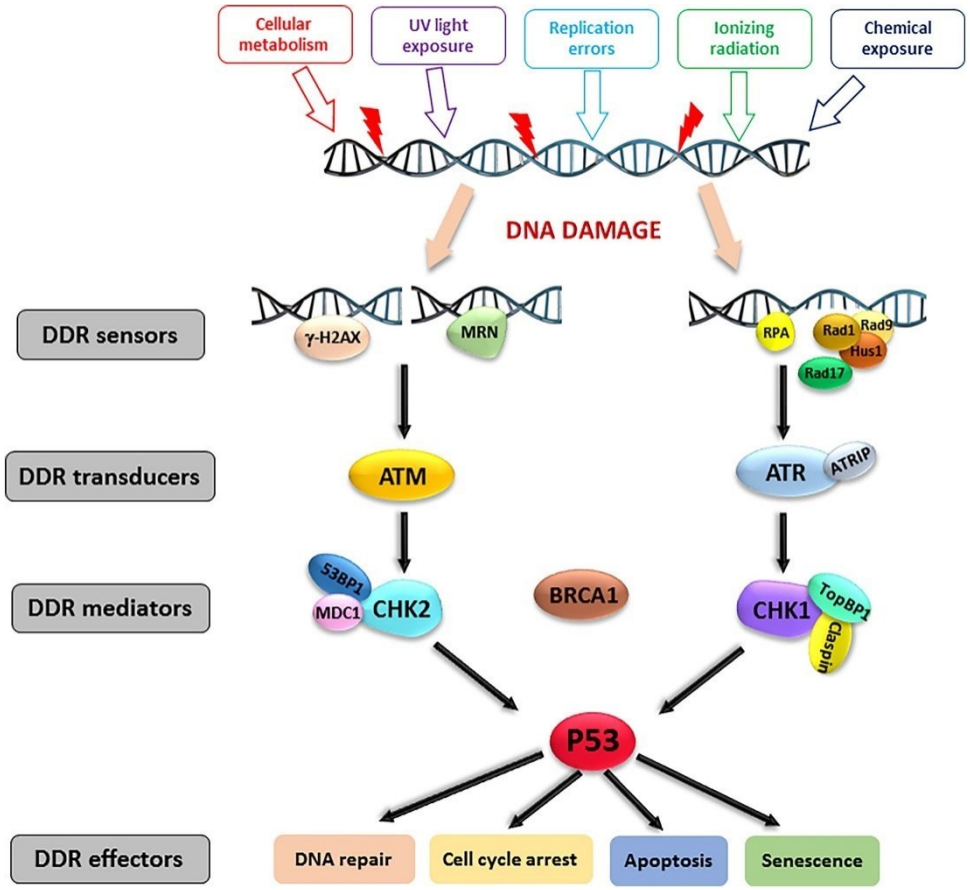

Figure 1: Scheme depicting DNA damage response (DDR) pathway. On the left is signalling after double-stranded breaks (DSBs), on the right after single stranded breaks (SSBs), more details are described in the text above. Adapted from [5].

There are 4 distinct pathways that can repair DSBs: classical non-homologous end joining (c-NHEJ), homologous recombination (HR), alternative end joining (alt-EJ) or single strand annealing (SSA) (Figure 2) [6].

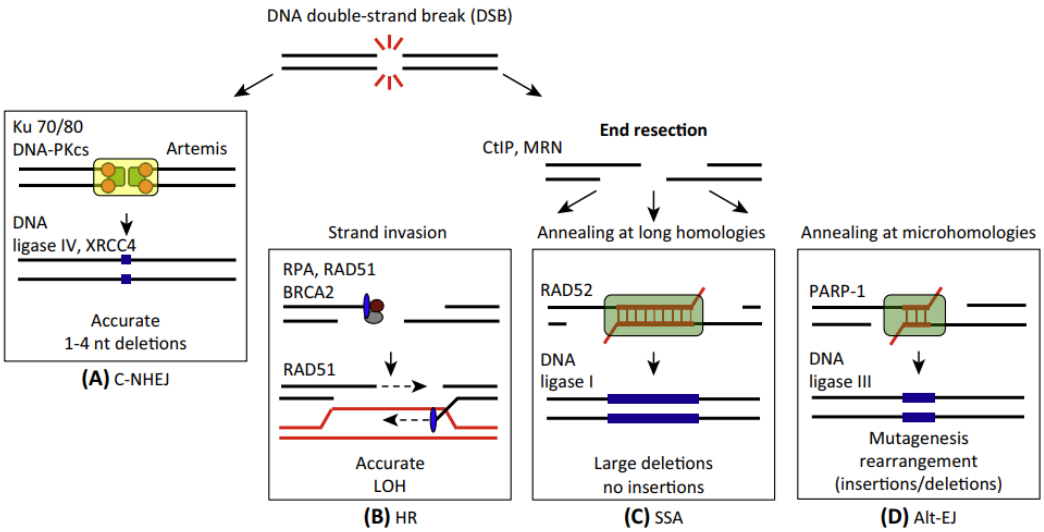

Figure 2: Scheme of four ways to repair DNA double stranded breaks (DSBs).
In cells, where DNA end resection is blocked canonical non-homologous end-joining (c-NHEJ) takes place. If resection occurs, three pathways can compete to repair the break (homologous recombination-HR, single-strand annealing-SSA, alternative end joining Alt-EJ) leading to different outcomes (loss of heterozygosity-LOH, insertions, deletions). Adapted from [6]

Of the four pathways available, two stand out as major pathways to repair DSBs: classical non-homologous end joining (NHEJ) and homologous recombination (HR)[1]. HR and NHEJ compete which will repair the break, the choice is dependent on the local nuclear environment, epigenetic landscape and phase of cell cycle [7, 8].

In mammalian cells, NHEJ is the predominant pathway to repair the two ended DSBs. NHEJ can operate throughout the cell cycle and in principle it directly ligates the DNA ends together, occasionally inducing minor modifications of DNA ends by excision or synthesis prior to ligation if they cannot be ligated directly [9] (see Figure 3). NHEJ starts by recognition of the free DSBs by the Ku70-Ku80 heterodimer (also known as XRCC6-XRCC5). Ku70-Ku80 has strong affinity for DNA with blunt ends or short single-stranded DNA overhangs [10, 11]. DNA bound Ku70-Ku80 recruits DNA-dependent protein catalytic subunit (DNA-PKcs) generating DNA-PK complex or holoenzyme [12]. DNA-PK complex promotes DNA end tethering and enables further recruitment and regulation of NHEJ core factors such as DNA ligase IV (LIG4), X-ray cross-complementing protein 4 (XRCC4), XRCC4-like factor (XLF) and paralogue of XRCC4 and XLF (PAXX).[13, 14]

If needed, DNA-PK can also recruit the additional accessory proteins, including endonuclease Artemis, which promotes DNA-end processing prior to ligation [15]. The complex of XRCC4-LIG4 ligates the DNA ends [16]. XLF stimulates the activity of the

XRCC4-LIG4 complex [17]. PAXX stabilizes the NHEJ machinery including DNA-PKcs on damaged chromatin [18].

The second major pathway of DSBs repair is HR, which is restricted to S phase and G2 phase of the cell cycle, since the DNA template for recombination usually comes from the sister chromatids [19]. HR may happen either at DNA ends which have undergone resection or at post-replicative ssDNA gaps [13]. The resection is initialized by the MRE11-RAD50-NBS1 (MRN) complex which also serves as a scaffold for ATM activation [20]. For efficient "short range" resection (approximately 300 nucleotides from the nick), MRN needs to interact with CtBP-interacting protein (CtIP) [21]. This "short range resection" probably displaces Ku70-Ku80 from DNA ends and enables recruitment and activity of proteins needed for "long range resection": exonuclease 1 (EXO1), endonuclease DNA2 and Bloom syndrome helicase (BLM) generating long 3' ssDNA tail [22]. The emerging ssDNA is rapidly coated with RPA complex, which disables possible pairing with other ssDNA and promotes formation of RAD51 nucleoprotein filament. To proceed with HR, RPA must be exchanged for Rad51 recombinase. This exchange is dependent on many recombination mediators such as BRCA2, BRCA1, BARD1 amd PALB2. BRCA2 probably competes with RPA for ssDNA binding and thus displaces RPA [13].

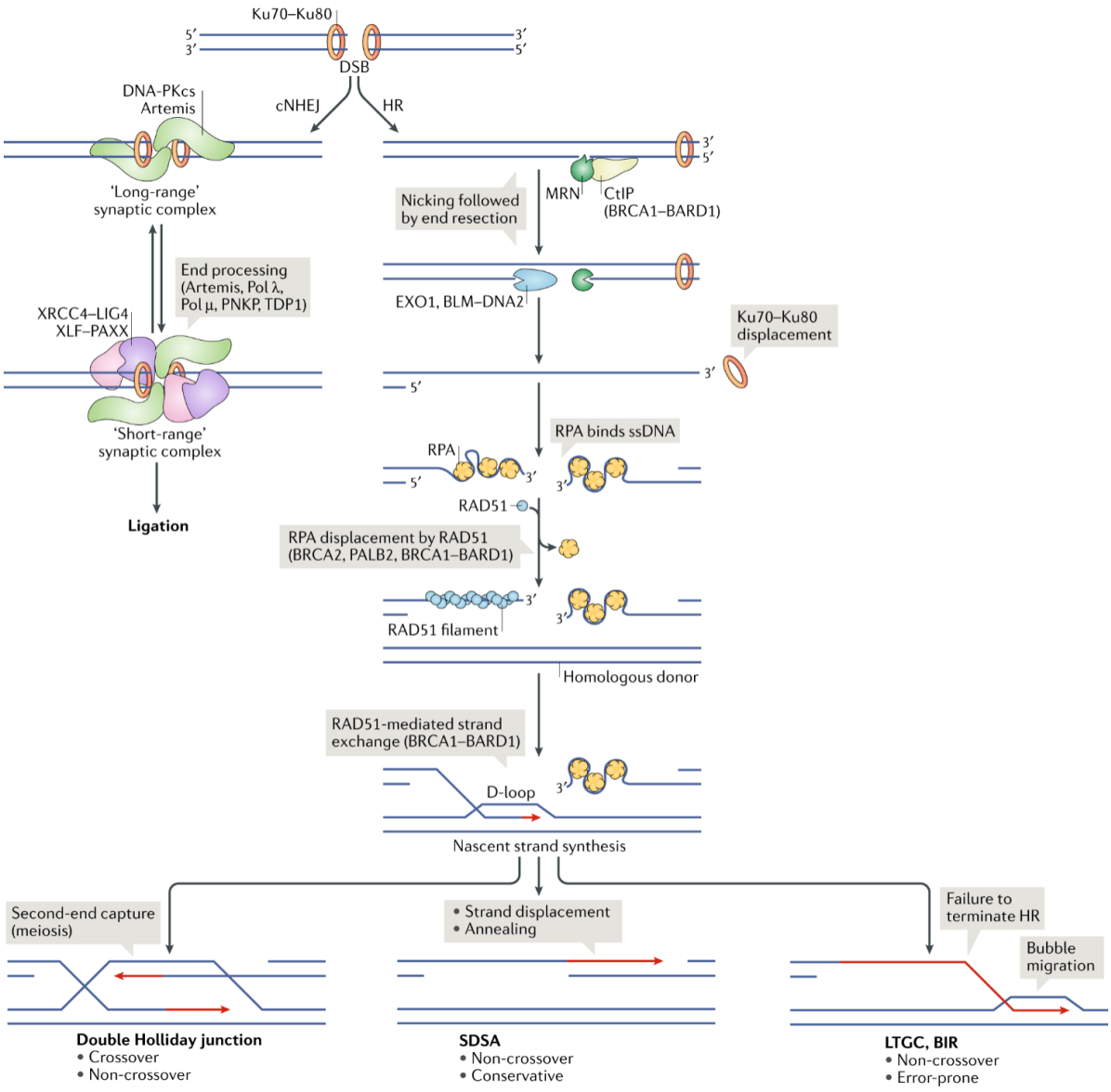

Figure 3: Depiction of the two major pathways (c-NHEJ and HR) for repair of double stranded breaks (DSBs). For further details see the text above. Adapted from [13]

1.2 DNA damage response in the context of chromatin

In eukaryotes, the genomic DNA is packaged into very complex structure called chromatin, which is organized into arrays of nucleosomes [23]. Nucleosomes, consist of 146-147 bp of DNA wrapped around histone octamer formed by two H2A, H2B dimers and one $(H3\text{-}H4)_2$ tetramer [24]. Histone H1 functions as a linker histone, binding between nucleosomes and adjusting the chromatin compaction and folding [25]. DNA is wrapped around histone proteins and associates with nonhistone components that promote higher-order fiber folding [26, 27].

The first model about impact of chromatin on DNA repair was „access-repair-restore“ model [28]. This model was later upgraded to „prime-repair-restore“, where DNA compaction into chromatin is not anymore solely an obstacle to DNA repair, but chromatin components are also helping to fine-tune the DDR [29].

The chromatin organization affects genome stability maintenance. Sequencing has shown that mutation rates are different across the human genome. In multiple cancer genomes mutations accumulates at much higher rate in compact, H3K9me3-rich heterochromatin domains [30, 31]. Also, DNA repair is slower in heterochromatin [32] and specifically at telomeres, DNA damage can often be irreparable, triggering persistent DDR and cellular senescence [33].

1.3 DNA damage response at telomeres

In eukaryotic cells, telomeres help to distinguish the ends of linear chromosomes from double-stranded breaks (DSBs). Mammalian telomeres consist of arrays of TTAGGG repeats, with the complementary CCTAAA strand, ending with single stranded G-rich overhang. The length of telomeres can vary from 5 kb in human cells to 100 kb in mice. Mammalian telomeres are transcribed by RNA polymerase II into a long non-coding telomeric repeat containing RNA (TERRA)[34]. Telomeres are protected against aberrant DNA damage response by shelterin, a six-subunit protein complex (Figure 4) [35]. TRF1 and TRF2 (telomere repeat binding factor 1/2, also known as TERF1/TERF2) form homodimers, recognize the TTAGGG repeats and through their Myb-related DNA binding motifs bind the duplex DNA at telomeres [36]. TRF1 and TRF2 homodimers are bridged and stabilized on telomeres by TIN2 (TRF1-interacting nuclear factor 2) [37, 38]. TIN2 also binds TPP1 (alternatively called ACD) and therefore recruit the TPP1-POT1 (protection of telomere 1) heterodimer to telomeres [39]. POT1 coats the single stranded part of telomeres through its oligonucleotide/oligosaccharide binding (OB) fold domains [40]. Whereas most mammals (including humans) have a single POT1 gene, rodents express two POT1 paralogues that are functionally distinct. POT1a represses the DNA damage response, and POT1b controls 5′-end resection [41]. RAP1 (repressor activating protein, also called TERF2IP telomeric repeat-binding factor 2-interacting protein 1) is the most conserved shelterin component and is recruited to telomeres through interaction with TRF2 [42, 43]. In human and mouse cells, 4 proteins (TRF2, TRF1, RAP1 and TIN2) probably form the core shelterin, because they are about 10 times more abundant than

POT1 and TPP1, which is probably just in fraction of shelterin complexes [44]. Still there is about 10-fold excess of POT1, TPP1 to all the ss TTAGGG binding sites and enough core shelterin proteins to bind to all ds TTAGGG, suggesting that telomeres are mostly associated with shelterin [45].

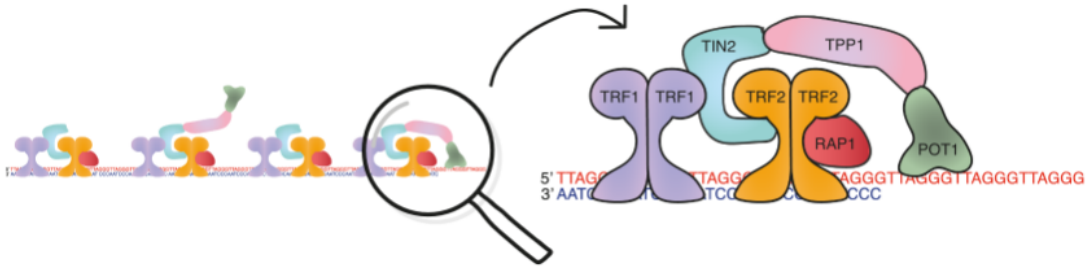

Figure 4: Scheme of shelterin complex at telomere ends
TRF2 and TRF1 homodimers bind the double stranded part of telomeres, whereas POT1 binds the single stranded, TIN2 bridges TRF1, TRF2 with TPP1-POT1 heterodimer.
Adapted from [46]

Shelterin interacts with various proteins and protein complexes (shelterin accessory factors), that contribute to its function [47]. An example of shelterin accessory factor is Apollo (SNM1B nuclease), which interacts with TRFH domain of TRF2 and helps to form the correct 3′- overhang at telomeres [48].

After every replication, telomeres have to regenerate the formation of G-rich 3′-overhang (Figure 5), which is crucial for formation of telomeric loop (t-loop) and protection of telomeres. Apollo is needed for the initial resection of the leading ends of telomeres, because those ends are presumable blunt after replication. Further resection is performed by Exo1 nuclease, which cannot cleave substrates with blunt ends. At lagging strands, Apollo seems to be dispensable, probably because DNA replication leaves 5′-recessed ends, so Exo1 can directly cleave there. Excessive resection by Apollo is blocked by POT1b [49]. In the next step, both telomeric ends are resected by Exo1. This resection seems to be unregulated, therefore leading to generation of temporarily longer 3′-overhangs in S/G2. Afterwards, the 3′-overhangs are shortened and their final length is regulated by CST-mediated fill in by Pol α/primase. In mouse, CST complex is recruited by POT1b [49].

The model for the formation of telomeric G-rich 3′-overhang was well described in mice [49](see the text above), for humans it is supposedly conserved, however there are still some uncertainties about POT1, TPP1 and their roles in CST recruitment [45].

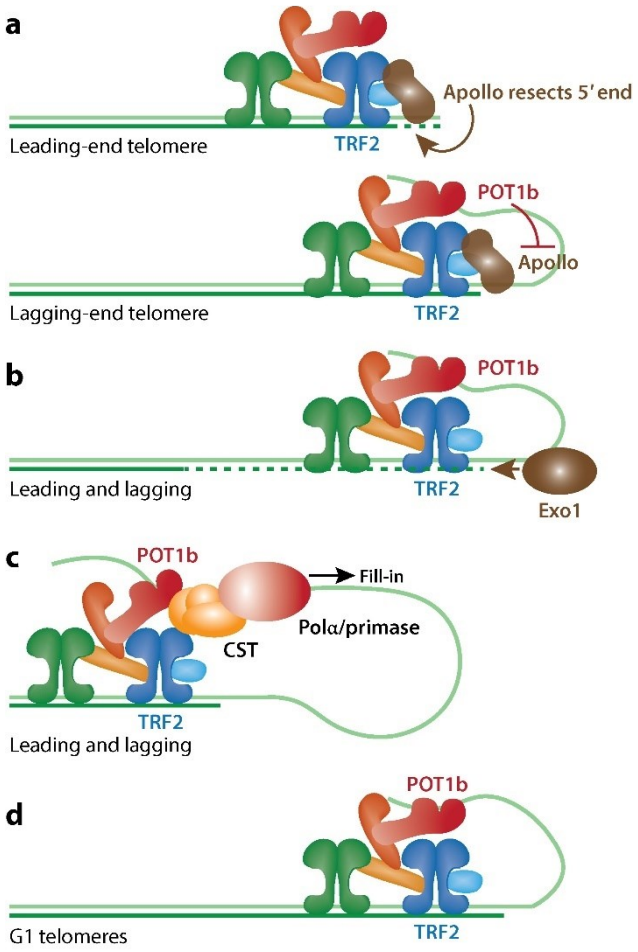

Figure 5: Telomeres have to regenerate the 3′- overhang at telomeres after every replication (The model is based on studies from mouse, in humans it is supposed to be mostly conserved. However, there might be some differences with CST which in humans in contrary to mouse binds both TPP1 and POT1 and not just POT1b as in mouse)

a) Initial resection of leading end telomere by Apollo, to prepare for cleavage by Exo1 in next step. In case of lagging end telomere Apollo is inhibited by POT1b in mouse.
b) Exo1 further resects both telomeric ends, resulting in long 3′-overhangs in S/G2
c) Ctc1, Stn1, Ten1 (CST) complex is recruited by POT1b and enables the Pol α/primase fill-in of 3′-overhangs, therefore regulating the final length of the overhangs
d) The resulting telomere with the 3′- overhang in G1 phase of cell cycle

Adapted from [45]

1.3.1 The end replication problem and cancer: telomerase vs ALT

In normal somatic human cells, the length of the double-stranded telomeric 5'-TTAGGG-3' repeat ranges from 3 to 15 kb, followed by a 30-400 nucleotide long single-stranded G-rich strand, also known as a 3'-overhang. Every cell division leads to shortening of telomeres because of incomplete replication of linear DNA by the conventional DNA polymerases. This is called the end-replication problem, which can gradually lead to critically short telomeres posing serious threats to genomic stability [50, 51]. Too short telomeres diminish the ability to load the shelterin complex. Absence of

TRF2 leads to inability to form t-loops and the exposed ends become accessible to ATM and non-homologous end-joining (NHEJ) can cause aberrant telomeric fusions. As prevention, cells can evade from the cell cycle intro replicative senescence, which stops cells from progressing into mitosis and fusion of telomeres [33, 52, 53].

Nevertheless, cells can overcome the antiproliferative checkpoints by deregulation of p53 and retinoblastoma tumor suppression pathways (Figure 6). This deregulation enhances proliferative activity, leading to further genome destabilization, by shortening and eventual fusion of telomeres, resulting in replicative telomere crisis [54, 55]. Telomere crisis can cause many genomic alterations including translocations, amplifications, deletions, polyploidization, chromothripsis, and kataegis [56]. Chromothripsis (chromosome shattering) is characterized by clusters of chromosome rearrangements that occur in a single event [57]. Kataegis describes a phenomenon of localized "hypermutation", with many base pair mutations in clusters around several hundred base pairs long [58]. To prevent the propagation of unstable genomes in the telomere crisis, most cells undergo cell death by autophagy, because pieces of broken telomeres in aberrant mitosis get into cytosol, where they activate the DNA recognizing cGAS-STING pathway. This pathway activates, through macroautophagy, machinery that systematically eradicates cells by autophagy [53, 59]. However, only small minority of cells can go through neoplastic transformation and activate the telomere maintenance mechanism (TMM) [53].

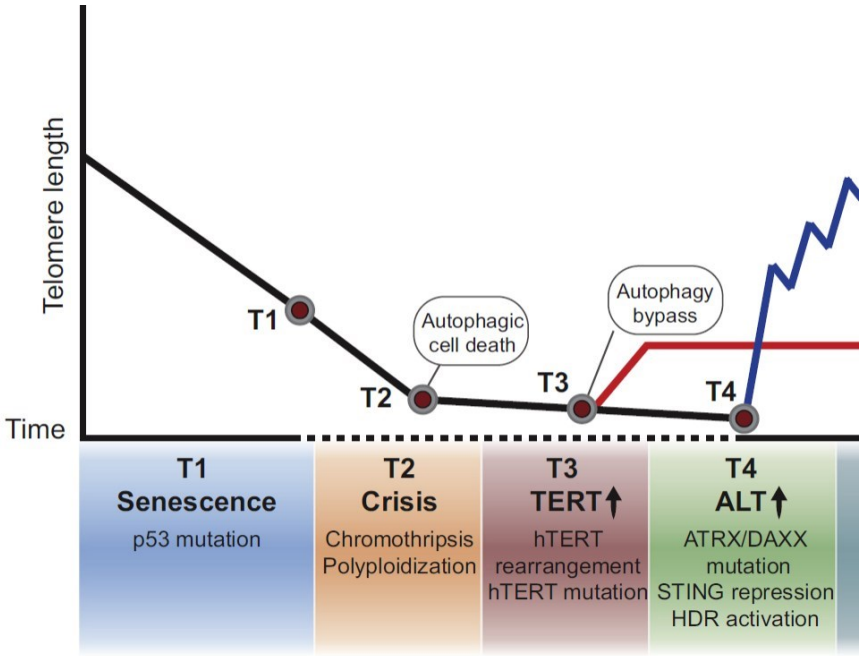

Figure 6: Telomere maintenance during cancer evolution
In normal somatic cells, telomeres shorten every cell cycle due to incomplete replication of telomeric DNA ends. Cells with too short telomeres should enter senescence at antiproliferative checkpoints (T1), however some cells manage to overcome this checkpoint by deregulation of p53 or retinoblastoma tumor suppression pathways (e.g., by p53 mutation). Critically short telomeres then often trigger telomeric fusions, chromothripsis and polyploidization, resulting in telomere crisis and autophagic cell death (T2). However, some cells manage to bypass the autophagy by activation of telomere maintenance mechanism (TMM), mostly telomerase (T3) in several cases alternative lengthening of telomeres (ALT)(T4).
Adapted from [53]

As telomere maintenance mechanism (TMM), most cells reactivate the reverse transcriptase complex called telomerase [60]. Only two constituents of telomerase complex are constitutively expressed: the noncoding telomerase template RNA (TERC) and dyskerin (protein, which is stabilizing TERC) [53, 61]. TERT promotor mutations or genomic rearrangements can elevate TERT mRNA expression and telomerase activity [62-64]. When telomerase is activated, it uses reverse transcription of telomeres to maintain the shortest telomeres, increasing the proliferation capacity and enabling the immortalization of cells [53].

In some tumors, mostly derived from mesenchymal-adrenergic lineage, cells can have permanently repressed TERT and therefore they need different mechanism to maintain telomeres. In this case, cells may exploit DNA repair pathway of homologous recombination (HR) to maintain telomeres by alternative telomere lengthening (ALT) [65]. According to clinical studies, ALT is present in approximately 5-15% of cancers, but this might be underestimated due to lack of direct clinical diagnosis for ALT [53].

ALT activity is defined as *de novo* synthesis of the telomeric DNA via other mechanism than telomerase. ALT activity of cells is often recognized by several typical molecular factors: ALT-associated PML bodies (APBs) [66], extrachromosomal telomeric repeats (ECTR) species (mostly single stranded CCCTAA C-circles and ds T-circles) [67, 68], intertelomeric tag copying [69], telomere sister chromatid exchange (t-SCE) [70], telomere dysfunction induced foci (TIFs) [71] and heterogenous telomere length [72].

ALT cells typically don't express, or express inactive protein variants, of ATRX (α-thalassemia/mental retardation syndrome X-linked) and DAXX (death-domain associated protein) [73, 74]. DAXX is an H3.3 chaperone, which in collaboration with ATRX deposits and remodels H3.3 containing nucleosomes at telomeres independently of replication [75]. Reintroduction of ATRX into ALT cancer cell lines increased H3.3

deposition to telomeres and repressed the ALT phenotype observed by decrease in telomere length, decreased APBs formation and C-circle levels [72].

1.3.2 The end protection problem

Due to its unprotected ends, the linear DNA in human cells could, trigger DNA damage response and DNA repair. Since human chromosomes are also linear, they need to have the ends protected. For this purpose, telomeres are protected by the shelterin complex and formation of t-loops [76].

The shelterin complex uses different strategies to prevent distinct DNA damage response pathways (Table 1) [45].

DDR pathway	Shelterin subunit(s)	Mechanism	General repressor
ATM kinase	TRF2 (TIN2)	t-loop	None
ATR kinase	POT1a (POT1b)	RPA exclusion	None
PARP1	TRF2, TIN2	Branched-DNA binding, ?	Ku70/80
c-NHEJ	TRF2	t-loop (iDDR, Rap1)	CYREN (S/G2)
alt-NHEJ	TRF2 (TIN2, POT1a/b)	t-loop, PARP1 repression, ?	Ku70/80
HDR	POT1a or POT1b + Rap1	?, ?	Ku70/80
Hyper-resection	POT1a/b, TRF2	Repression of ATM/ATR	53BP1/Rif1/Rev7

Table 1: Table depicting which shelterin subunits are guarding the telomeres against 7 different DDR pathways. Also, the mechanism of protection and general repressor are mentioned. Adapted from [45]

1.3.2.1 T-loops (telomere loops)

Mammalian telomeres are supposed to hide the linear DNA ends of chromosomes from DNA damage response by formation of t-loops [77]. T-loops are large lariat structures, which are formed by invasion of the 3′-telomeric overhang into the duplex telomeric array (Figure 7) [78]. The formation of t-loop resembles homologous recombination because the 3′-telomeric strand invades the homologous sequences of the ds telomeric repeats, pairs with C-rich strand and generates a D-loop (displacement loop) by displacement of G-rich strand [79].

To form the t-loops, cells need to have TRF2 [80]. Even *in vitro,* telomeric DNA can be remodeled by TRF2 into structures resembling t-loops [78]. Possible explanation for TRF2-dependent formation of t-loops might be in TRF2 ability to wrap around 90 bp of telomeric DNA around its homodimerization domain [81]. This wrapping of DNA could induce local unwinding and invasion by the 3-overhang [81]. Importantly,

expression of TRF2 mutant (Top-less) lacking the wrapping activity, reduced the number of t-loops and activated ATM, while still protected the telomeres against NHEJ [81].

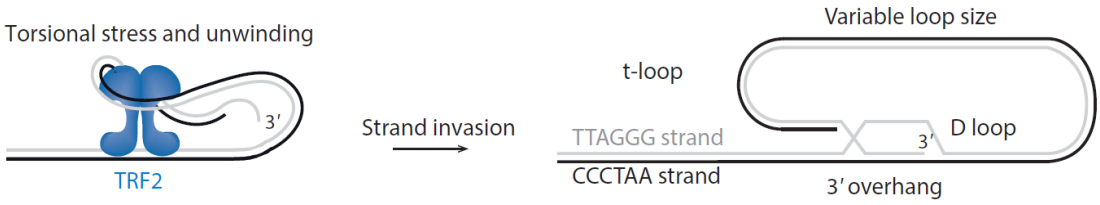

Figure 7: Scheme of t-loop formation, the strand invasion is promoted by torsional stress and unwinding created by wrapping of telomeric DNA around TRFH domains of TRF2 homodimer. Adapted from [45]

There are still many unanswered questions about t-loops: the exact percentage of telomeres forming t-loops throughout the cell cycle stages; the minimal length of telomere to form a t-loop; the possibility and potential blockage that the 3′-telomeric overhang in t-loop would be recognized as substrate for canonical DNA polymerases leading to elongation of telomeres [45]. Also, there appeared a controversial question if t-loops are really just protection mechanism or might be pathological [46].

T-loops could solve nicely the end-protection problem, but they bring different challenges. The branch migration at the base of the t-loop might lead to formation of double Holliday junction (dHJ) (Figure 8), an important intermediate in homologous recombination. To restore the t-loop structure, branch migration of dHJ might be mediated by the Bloom syndrome's mutated (BLM) helicase. Nevertheless, dHJ could be also resolved by cleavage by HJ resolvases (such as the Mus81, SLX4, SLX1, and Emi1 complex or Gen1), leading to t-loop removal and large telomeric deletions. The branched DNA binding (basic) domain of TRF2 prevents this deleterious t-loop cleavage [45, 82, 83].

Basic domain of TRF2 is limiting access of poly(ADP-ribose) polymerase (PARP1) to t-loop, by binding to the 5′ ds–ssDNA transition at the base of t-loop. PARP1 presence at t-loop promotes t-loop cleavage, probably by promoting the recruitment of HJ resolvases[84]. Apart from limiting access of PARP1 to t-loops, basic domain of TRF2 is protecting t-loops also by stabilizing Holliday junctions and preventing aberrant activity of HJ resolvases and WRN syndrome helicase on t-loops [85, 86]. Also, basic domain of TRF2 can interact with core histones to repress the t-loop cleavage [87]. Importantly, even TRF2 lacking basic branched DNA-binding domain can form t-loops and prevent telomeres from ATM activation and NHEJ [84].

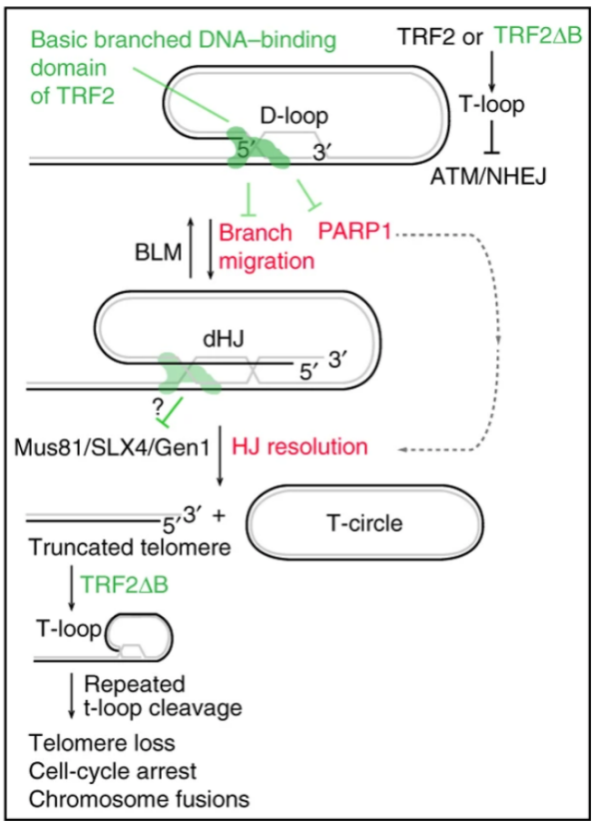

Figure 8: Scheme depicting the possible branch migration at the base of t-loop, converting the 3-way junction into 4-way double Holliday junction (dHJ). dHJ can be either restored into original t-loop structure by Bloom syndrome's mutated (BLM) helicase or it can be cleaved by HJ resolvases, resulting in truncated telomere and separated T-circle. Basic branched DNA-binding domain of TRF2 can bind both 3 and 4-way junctions and limit the access of PARP1, which would otherwise promote recruitment of HJ resolvases, leading to cleavage.
Adapted from [84]

Different type of t-loop cleavage can happen during DNA replication or elongation by telomerase. To enable access of telomerase to the 3' end of telomeres and to avoid collisions with replisome during S-phase, t-loops have to be disassembled. RTEL1 (regulator of telomere length 1) helicase is essential for removal of telomeric secondary structures (t-loops and G-quadruplexes), enabling efficient DNA replication and elongation [88, 89]. Without RTEL1, t-loops can be resolved by the SLX1-SLX4 nuclease complex, resulting in aberrant cleavage of t-loops, telomere shortening and formation of excised telomere circles (TCs)[88]. TRF2 depending on its phosphorylation at S365 can recruit RTEL1 to telomeres (Figure 9). During S-phase TRF2 S365 is dephosphorylated by the PP6C/R3 phosphatase enabling RTEL1 recruitment, outside S-phase TRF2 S365 is phosphorylated by CDK kinase. This phosphorylation is protecting t-loops against unwinding and inappropriate ATM activation [90].

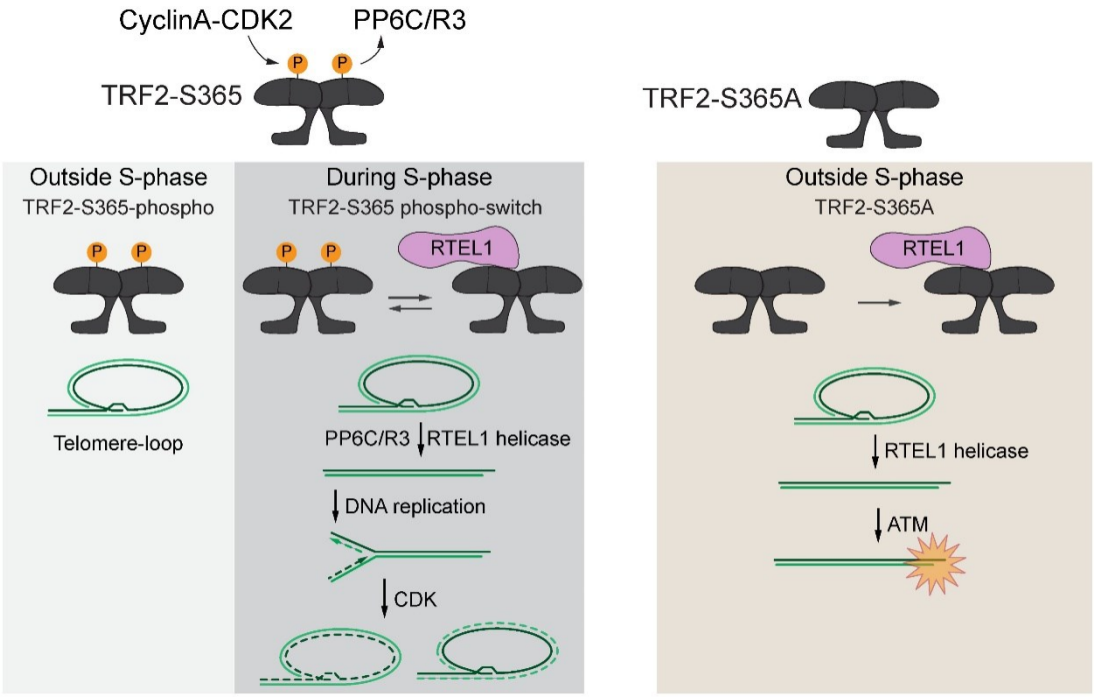

Figure 9: During S-phase to enable telomere replication RTEL1 can unwind the t-loops and secondary structures such as G-quadruplexes at telomeres. RTEL1 is recruited specifically during S-phase due to TRF2 S365 phospho-switch (during S phase is dephosphorylated by PP6C/R3 and can recruit RTEL1, outside of S-phase is phosphorylated by CDK2 kinase and cannot recruit RTEL1 to telomeres). If TRF2 is mutated at S365A, it leads to recruitment of RTEL1 to telomeres throughout the cell cycle, resulting in t-loop unwinding and inappropriate ATM activation. Adapted from [90]

1.3.2.2 Repression of ATM signalling

ATM kinase is activated by MRN complex, which recognizes double stranded breaks (DSBs) [91]. Telomeres are protected against MRN-dependent ATM activation by TRF2 [92]. TRF2 deletion increases ATM activity at telomeres. From the other shelterin components only deletion of TIN2 led to a mild increase of ATM activity [92-95]. This effect was probably caused by TIN2 ability to stabilize TRF2 [45, 96].

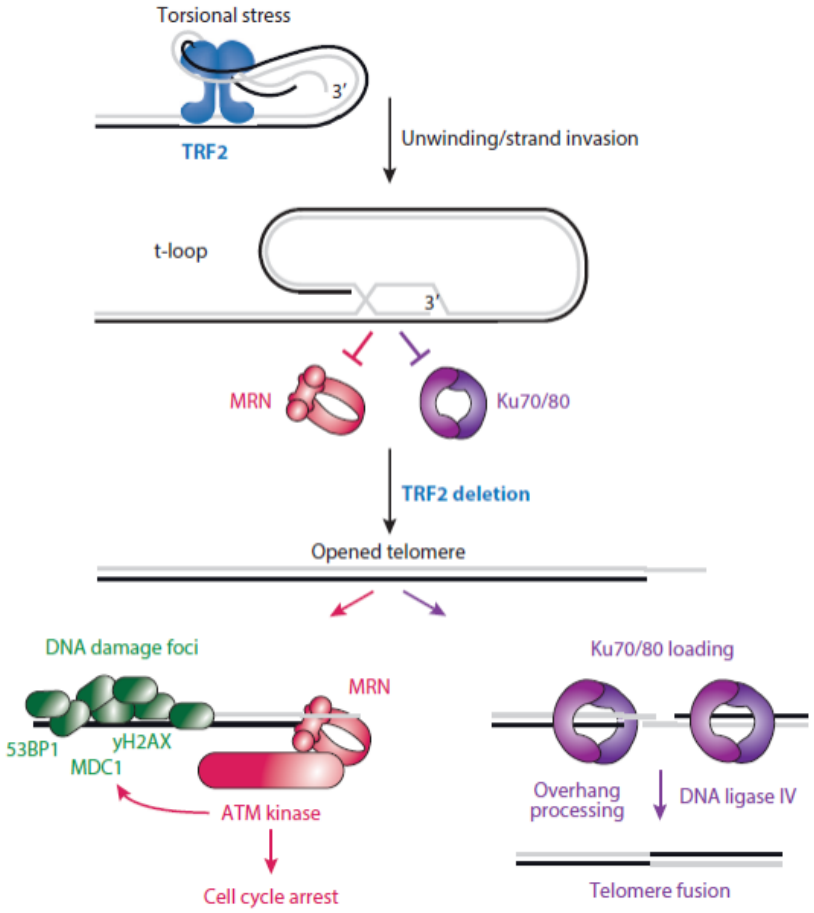

Figure 10: The TRF2 t-loop model
TRF2 can facilitate t-loop formation at telomeres, thereby block the ATM activation at the initial step by preventing MRN recognition of telomeric ends and also block classical non-homologous end joining, potentially leading to telomere fusions, by preventing Ku70/80 loading to telomeric ends. Adapted from [45].

There are several models which could explain how TRF2 prevents ATM activation. First of them suggests, that TRF2 facilitates formation of t-loops hiding the telomeric ends from MRN recognition (Figure 10). It was shown that TRF2 alone, without other shelterin components, is sufficient to form t-loops [97]. The question remains whether TRF2 can repress ATM activity also by other means. Another option would be that TRF2 (and TRF1) can mediate compaction of the telomeric chromatin and thus limit access of DNA damage factors to telomeres [98]. However, this model was not supported by other studies, which did not detect significant decompaction of telomeres after shelterin removal [99, 100]. Other study showed that TRF2 can directly associate with ATM, inhibit autophosphorylation of ATM at S1981, and thereby limit ATM activation [101]. The intriguing point is that ATM can become activated when a DSB is created inside the telomeric repeat array [102, 103]. This could not be explained

by chromatin compaction or direct association of TRF2 with ATM, those would repress ATM activity also for internal DSB at telomeres [45].

1.3.2.3 Repression of ATR signalling

ATR helps to maintain genome integrity especially in S phase, where it senses stressed replication forks and orchestrates DNA damage response to replication stress [104] . Activation of ATR starts by coating of exposed ssDNA by RPA, which enables recruitment of ATRIP-ATR complex to sites of DNA damage [105]. Once ATR is recruited to ssDNA, it is activated by two different proteins, either TopBP1 or ETAA, which both contain ATR activation domain (AAD) [106-108]. The telomeric 3'-overhang, both in linear and in t-loop configuration, has sufficient length to bind RPA and trigger ATR activation [45, 80].

To repress ATR signalling at telomeres, the shelterin complex uses POT1 (Figure 11). In human shelterin, there is only single POT1 protein whereas mice have two POT1 variants (POT1a and POT1b). At genome-wide DSBs, activation of ATR happens mostly in S phase, where ssDNA is generated as a replication and repair intermediate of stressed DNA replication forks. In contrast to that, telomeres, upon deletion of POT1, can activate ATR throughout cell cycle (in G1, S and G2) because they have ATR activation site even without resection [109]. ATR activation depends mostly on TopBP1 and not ETAA, because TopBP1 depletion prevented ATR activation [109].

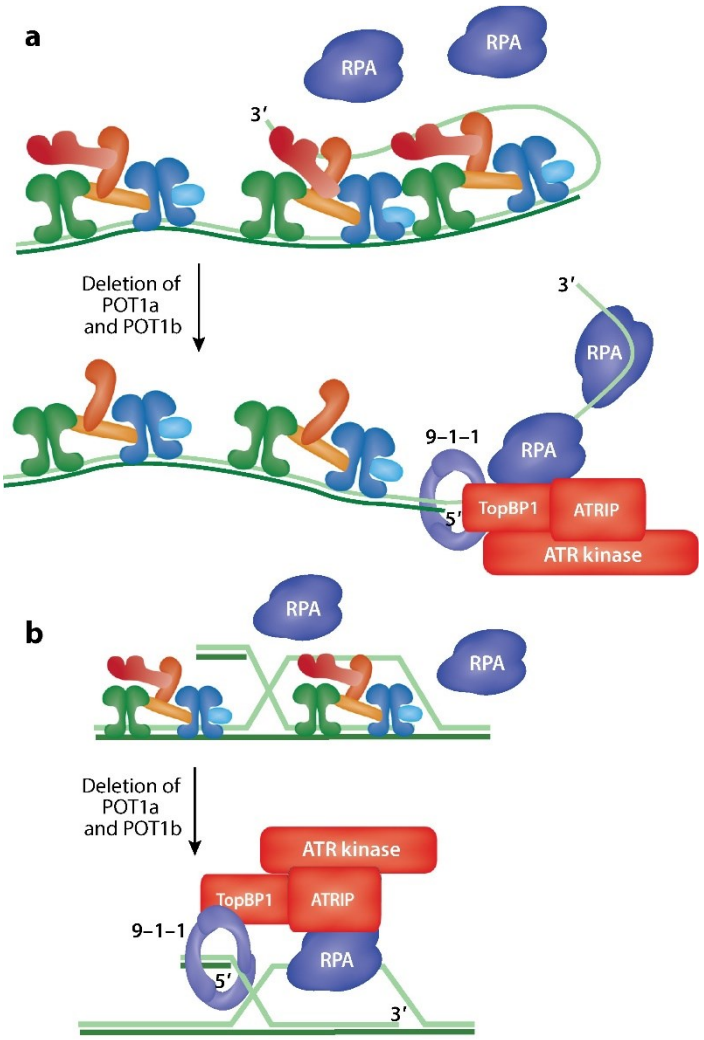

Figure 11: Model of competition between POT1 and RPA at telomeres a) in t-loop b) in linear conformation. POT1 is restricting RPA from binding to telomeres, once POT1 is deleted, the ssDNA at telomeres becomes accessible for RPA and RPA together with 9-1-1, TopBP1 and ATRIP can activate ATR. (Adapted from [45])

POT1 is supposed to prevent ATR activation by exclusion of RPA from ssDNA at telomeres [109] . When POT1 is deleted, RPA can bind telomeres throughout the cell cycle, but predominantly in S and G2 [109]. To efficiently exclude RPA from telomeres, POT1 needs to be tethered to telomeres by TIN2 in TPP1-POT1 heterodimer [96, 110, 111]. The tethering, of POT1 by shelterin to telomeres, enables POT1 to outcompete RPA, despite similar affinities of POT1 and RPA to ssDNA and higher abundancy of RPA in cells [45, 96].

It has been suggested, that heterogenous nuclear ribonucleoprotein A (hnRNPA1) can displace RPA (but not POT1) from the telomeric foci (Figure 12) [112]. The RPA displacement is inhibited by TERRA [112]. TERRA levels decrease in late S-phase and increase again after S-phase [113] . Suggesting that hnRNPA1 together with TERRA

could regulate RPA levels at telomeres throughout the cell cycle enabling RPA to transiently bind telomeric ssDNA during replication [112]. Additional help for POT1 to outcompete RPA binding at telomeres, could be the G-quadruplexes formed at G-rich telomeric strands, because POT1 binds next to some of these structures better than RPA [114].

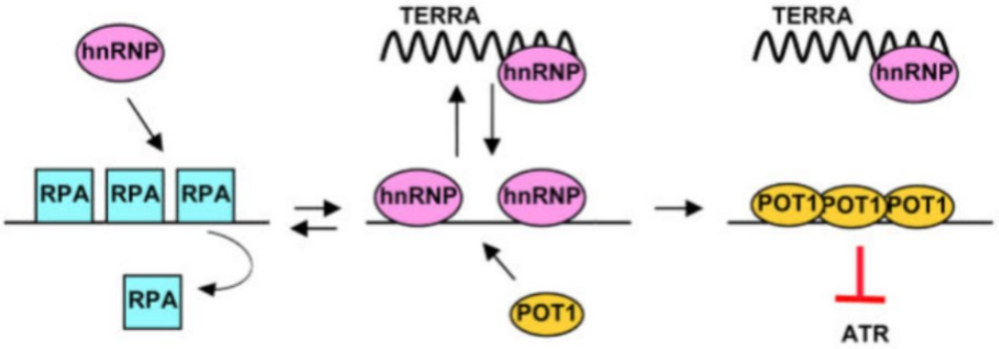

Figure 12: Model of RPA displacement from telomeres by heterogenous nuclear ribonucleoprotein (hnRNP). RPA can be displaced from telomeres by hnRNP. During early to middle S-phase, TERRA is inhibiting hnRNP displacing activity towards RPA, enabling RPA to bind telomeric ssDNA at replication forks or telomeric ends. In late S-phase, TERRA levels decline, enabling hnRNP to displace RPA. After S-phase, TERRA levels gradually increase again, establishing new dynamic balance, where hnRNP associates with TERRA leaving space on telomeric ssDNA primarily for POT1, which, in contrast to RPA, cannot be displaced by hnRNP. Adapted from [112]

1.3.2.4 Repression of classical nonhomologous end joining (c-NHEJ)

Telomeric fusions lead to dicentric chromosomes which represent a great danger to genome integrity. Resolving of dicentric chromosomes may lead to unfavourable outcomes such as: loss of heterozygosity, translocations, amplifications, chromothripsis, kataegis and tetraploidization [115]. To avoid telomeric fusions, cells repress both canonical and alternative nonhomologous end joining. Since c-NHEJ is active throughout cell cycle, it represents a constant threat to telomeres [45].

Interestingly, the presence of the natural telomeric 3' overhang does not impede c-NHEJ from occurring. However, the 3' overhang may limit telomere fusion in S and G2 phases due to CYREN [116], a small Ku70/80 binding protein that inhibits c-NHEJ for substrates with a 3' or 5' overhang. This could explain why TRF2 depletion mainly results in chromosome-type fusions instead of chromatid-type ones, as well as the higher frequency of telomere fusions in G1 rather than in S and G2 phases, once TRF2 is depleted [117].

Telomeric fusions by c-NHEJ require ATM activation [92]. Interestingly, deletion of 53BP1 in TRF2-deleted cells led very rarely c-NHEJ at telomeres [118]. Suggesting, 53BP1 as a key player for telomeric c-NHEJ due to its ability to limit hyper-resection and also due to its ability to enhance dynamic movement of DNA damage sites in the nucleus [119]. 53BP1-mediated mobility increases the likelihood of telomere fusions by allowing telomeres to move closer together. Additionally, 53BP1 promotes the clustering of unprotected telomeres, which also increases the chance of telomeric fusions[45, 99].

TRF2 is the main protein from shelterin, which prevents c-NHEJ. Deletion of Rap1 did not lead to any telomeric fusions [94], and only few telomeric fusions occur, when TRF1, TPP1 or POT1 are deleted [45]. The fusions in TPP1 or POT1 knockouts are mostly between sister chromatids and due to alt-NHEJ [120]. TIN2 deletion is causing many telomeric fusions, but the effect of TIN2 is indirect through destabilization of TRF2 [45, 96]. Reconstitution of telomeres with TRF2 alone, without other shelterin components, is sufficient to form t-loops and prevent c-NHEJ [45, 97].

TRF2 prevents c-NHEJ at telomeres mostly by t-loop formation, but it can prevent c-NHEJ also for telomeres in linear state by its region in hinge domain called iDDR (inhibitor of DDR)(Figure 13) [121]. TRF2 iDDR should limit activity of RNF168 at dysfunctional telomeres and therefore prevent 53BP1 accumulation there. Supposedly, TRF2 iDDR can, by binding to MRE11 complex, recruit BRCC3 (BRCA1/BRCA2-Containing Complex Subunit 3 also called Lys-63-Specific Deubiquitinase BRCC36), which in turn can suppress RNF168 recruitment to dysfunctional telomeres, by opposing RNF8 pathway and deubiquitinating H2A and H2AX [122]. TRF2 iDDR may limit activity of RNF168 at dysfunctional telomeres also by interaction with UBR5, ubiquitin ligase which targets RNF168 to degradation. It remains unclear if TRF2 iDDR functions similarly in human cells, as these studies were conducted using mouse embryonic fibroblasts [121, 123].

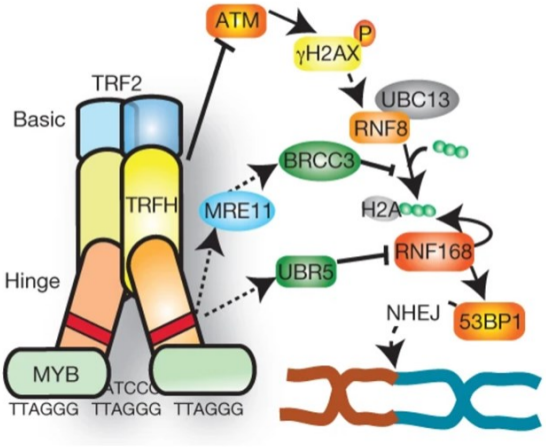

Figure 13: Proposed model for TRF2 preventing c-NHEJ and 53BP1 recruitment to telomeres. TRF2 contains TRFH homodimerization domain, which prevents ATM activation by t-loop formation. TRF2 may also limit activation downstream of ATM with TRF2 iDDR region, which is found in TRF2 hinge domain. The suggested mechanism is through BRCC3 or UBR5, but other factors might be involved. TRF2 iDDR interacts with MRE11, which can recruit BRCC3 K-63 deubiquitinase, preventing recruitment of RNF168 to dysfunctional telomeres. TRF2 iDDR can also interact with UBR5, ubiquitin ligase, which targets RNF168 to degradation.
Adapted from [121]

In addition, Rap1 may help TRF2 to prevent c-NHEJ. It is challenging to decipher the effect of Rap1 from the effect of TRF2, since Rap1 is targeted to telomeres through TRF2 in normal conditions. When TRF2 is present, Rap1 deletion does not increase amount of telomeric fusions, suggesting that Rap1 effect might be only additional prevention of telomeric fusions [94, 124]. To observe effect of Rap1 on telomeres, Sarthy et. al. used TRF2 mutant without basic and myb domain ($TRF2^{\Delta B\Delta M}$), which should heterodimerize with TRF2 and disable the binding to telomeres [125, 126]. In cells expressing $TRF2^{\Delta B\Delta M}$, they used heterologous Rap1 targeting to telomeres and observed prevention of telomeric fusions [125]. Interestingly, they did not see effect of Rap1 on ATM signalling, visualized by telomere dysfunction-induced foci (53BP1 colocalizing to telomere) [125].

1.3.2.5 Repression of alternative nonhomologous end joining (alt-NHEJ)

Cells repress alt-NHEJ at telomeres not only by shelterin components, but also by recruiting Ku70/80, that favours c-NHEJ [127]. There is still some controversy surrounding the extent to which alt-NHEJ is made up of multiple overlapping mechanisms; nevertheless, it is clear that one form of alt-NHEJ is known as microhomology-mediated end joining (MMEJ) [128]. alt-NHEJ repair begins with a

process of limited end resection that utilizes some of the same components as those found in the HR end resection machinery [128, 129].

First step of alt-NHEJ is PARP1 activation at the 5′ ds–ss transition, leading to PARylation of nearby proteins (including histones), enabling recruitment of DNA Lig3 and a DNA polymerase θ participating in the fill-in reaction, resulting in altered sequences at the fusion point [130]. alt-NHEJ is thus an error-prone end joining pathway which can cause telomeric fusions for telomeres with naturally eroded critically short telomeres [131]. alt-NHEJ requires minimal homology (one or more base pairs) and is commonly seen in telomeres, where two base pairs of telomeric repeat homology at the 3' overhangs are sufficient as microhomology template [130].

1.3.2.6 Repression of homology-directed repair (HDR)

HDR can happen between sister chromatids leading to telomere sister chromatid exchanges (T-SCEs), which can be detected by differential labeling of the leading-strand and lagging-strand DNA synthesis products [132]. The exchange can be harmless, when the telomeres have the same length. However, exchange between telomeres with unequal length can yield a daughter cell with shortened telomere, limiting the life-span of cell without telomerase [45].

HDR is repressed by Ku70/80 complex, which favors NHEJ. Only a small percentage of telomeres undergoes sister chromatid exchange in cells deficient for some shelterin components in the Ku70/80 proficient background [133]. Therefore, it would be optimal to study HDR at telomeres in cells without Ku70/80. However, human cells without Ku70/80 are not viable [134]. So, the model for repression of HDR at telomeres is based on mouse cells, where both Rap1 and one of the two POT1 proteins is needed to repress HDR at telomeres [45, 94, 135].

1.3.3 Internal DSB in telomeres and its repair

In contrast to telomere ends, where shelterin represses the DNA repair, DSBs occuring inside the telomeric repeats can be repaired. The internal telomeric DSBs activate ATM signalling and can be repaired by HR or alt-NHEJ (Figure 14) [102].

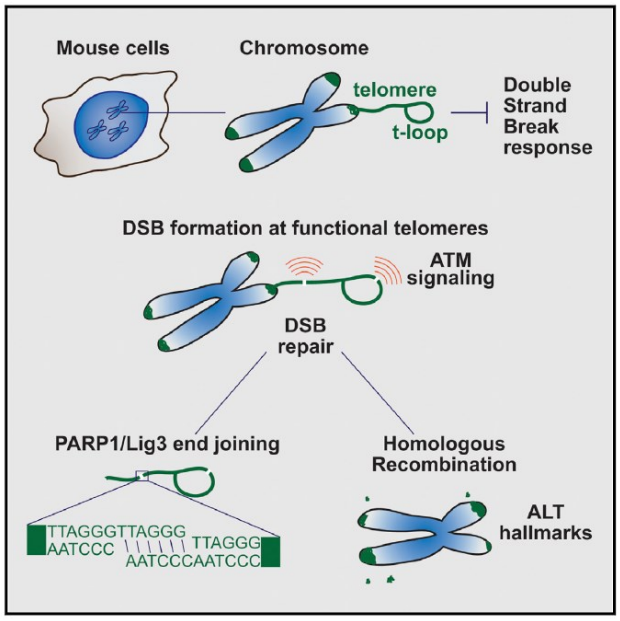

Figure 14: Double stranded breaks inside telomeres can be repaired either by HR, leading to ALT hallmarks such as increased telomere length heterogeneity and extrachromosomal telomeric signals (ECTS) or by PARP1 and Ligase 3 dependent alt-NHEJ [102].

1.4 WIP1 phosphatase (PPM1D)

In human, Wip1 phosphatase is encoded by protein phosphatase magnesium-dependent 1 delta gene (PPM1D). PPM1D was firstly described based on its increased expression after IR in p53-dependent manner and therefore named as wild-type p53 induced phosphatase 1 (Wip1) [136].

PPM1D is a nuclear serine/threonine phosphatase, which based on its homology to protein phosphatases 2C (PP2C) is also called PP2Cδ. Like other PP2C phosphatases, PPM1D functions as monomeric enzyme requiring divalent cations, such as magnesium, for its catalytic activity [136]. PPM1D is predominantly nuclear and it is tightly bound to chromatin [137]. PPM1D contains N-terminal catalytic domain (1-372 aa) and non-catalytic C-terminal part (372-605 aa)[138]. The catalytic domain contains positively charged segment called B-loop (235-268 aa), which is important for PPM1D substrate specificity [139]. B-loop is also target for allosteric Wip1 inhibitor GSK2830371 [140].

1.4.1 PPM1D substrates and its role in DDR

PPM1D can dephosphorylate targets of PI3K-like kinases (ATM, ATR) with the SQ/TQ motif (Figure 15) [139]. ATM and ATR activate DDR through a cascade of phosphorylations, with PPM1D playing an essential role in DDR termination. Notably, PPM1D can directly dephosphorylate ATM autophosphorylated at S1981. This phosphorylation is critical for ATM monomerization and activation [141]. PPM1D can inhibit by dephosphorylation checkpoint kinases: the ATR-targeted Chk1 at S345 and the ATM-targeted Chk2 at T68 [142, 143].

PPM1D is especially important for its ability to regulate p53. In unstressed cells, the degradation rate of p53 is relatively rapid, thus it does not accumulate in high concentrations [144]. Main regulator of p53 levels is Mdm2 ubiquitin ligase, which targets p53 for proteasomal degradation. MDM2 interacts with p53 at its N-terminus. DDR-induced p53 S15 phosphorylation is limiting the MDM2-p53 interaction and therefore preventing also the proteasomal degradation of p53 [145, 146]. MDM2 can also supress p53 transcriptional activity [147]. It was demonstrated that MDMX could enhance the activation of MDM2 and decrease the transcriptional activity of p53 [148]. Additionally, it was discovered that MDM2 is a transcriptional target of p53, thus creating a negative feedback loop [149]. Another negative feedback loop is between p53 and PPM1D, where PPM1D is transcriptional target of p53 and consequently PPM1D is promoting degradation of p53 and thereby helps terminate p53-dependent cell cycle arrest

[136]. PPM1D is decreasing levels of p53 by dephosphorylation of p53 at S15 and also by dephosphorylation of MDM2 at S395 and MDMX at S403 [142, 150, 151].

Recently, it has been demonstrated that PPM1D can suppress p53-dependent transactivation and cell death through inhibition of the integrated stress response (ISR) [152]. When PPM1D and MDM2 were both inhibited concurrently, an enhanced activation of the ATF4 pathway was observed, which in turn further increased transactivation of certain p53 target genes and promoted p53-dependent apoptosis. The ISR controls ATF4 expression at the translational level via eIF2α and its phosphorylation. Following diverse stress stimuli eIF2α is phosphorylated which leads to selective increased translation of ATF4 and other mRNAs. Upon PPM1D inhibition eIF2α phosphorylation at S51 was increased suggesting new way, how PPM1D inhibition contributes to ISR [152]. However, question remains whether PPM1D can dephosphorylate this site directly or the effect of PPM1D on this phosphorylation is indirect.

At chromatin regions flanking DSBs, PPM1D dephosphorylates histone H2AX at S139 (γH2AX) [137]. This phosphorylation is facilitating the recruitment and retention of factors essential for DNA repair at sites of DSBs [153] .

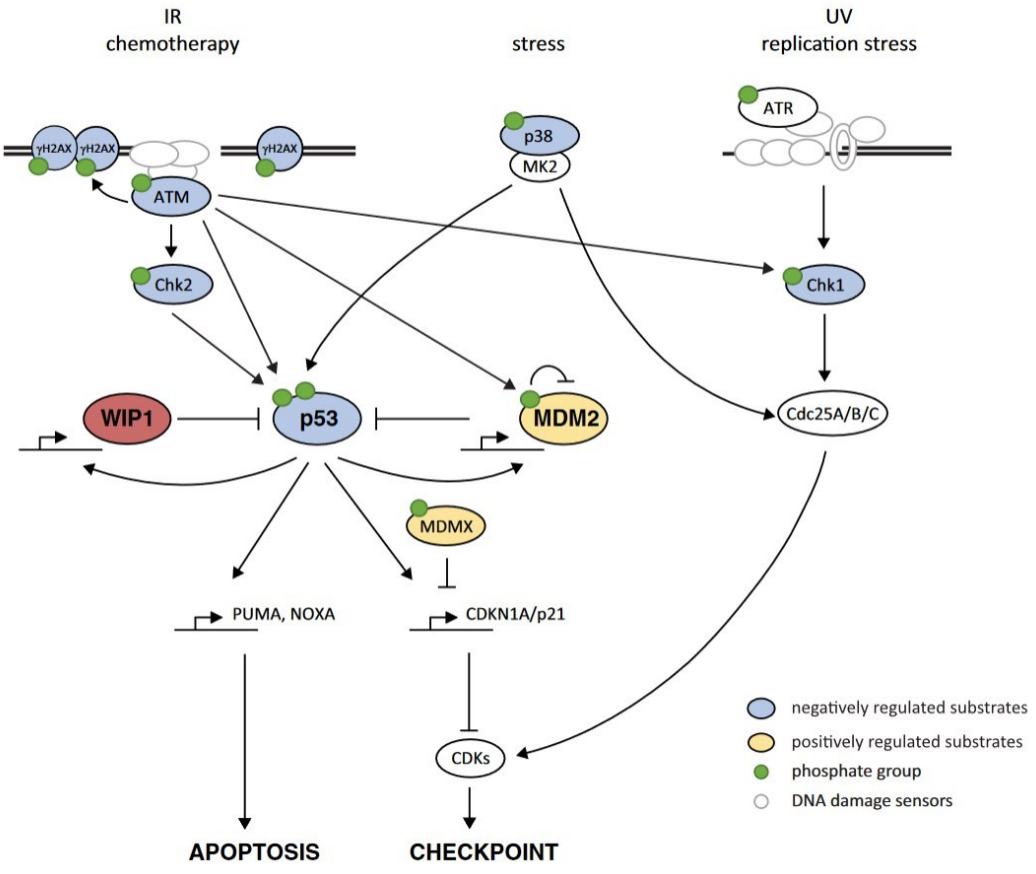

Figure 15: WIP1 plays an important role in termination of DNA damage response (DDR) by dephosphorylation of many ATM/ATR targets. Adapted from [154]

In addition to the main substrates of the DDR pathway, PPM1D has been shown to target other ATM/ATR substrates, such as the histone chaperone DAXX (S564), and the nucleotide excision repair proteins XPA (S196) and XPC (S892), which both contribute to the DDR process [155, 156] .

PPM1D has been observed to dephosphorylate the transcription intermediary factor 1-beta (KAP1) at serine 824 (S824) [157] . Under non-stressful conditions, KAP1 has been shown to suppress the expression of CDKN1/p21, which is a strong inhibitor of cyclin dependent kinases (CDKs) that is transcriptionally activated by p53, thereby allowing for the maintenance of G1 and G2 checkpoints [158]. However, ATM and CHK1/2-mediated phosphorylation of KAP1 at S824 and S473, respectively, triggered by genotoxic stress, leads to de-repression of CDKN1/p21 and thus contributes to the activation of the checkpoint [158, 159] . The dephosphorylation of KAP1 by PPM1D may potentially contribute to checkpoint recovery, though the dephosphorylation of Kap1 at S473 by PP4 appears to be more significant [160] .

By antagonizing the effect of ATM and ATR, PPM1D is enabling DDR termination and checkpoint recovery. PPM1D promotes primarily recovery from G2 checkpoint by p53 S15 dephosphorylation and is dispensable in G1 checkpoint, where PP4 phosphatase is required to dephosphorylate Kap1-S473 and thereby repress p53-dependent transcriptional activation of p21 [161].

PPM1D was also shown to dephosphorylate substrates with pTXpY motif p38 and UNG2 [162, 163] . PPM1D is supposed to dephosphorylate p38 at T180 resulting in p38 inhibition. The inhibition of p38 leads to decreased phosphorylation of p53 on its activating sites, S33 and S46. Since PPM1D is a transcriptional target of p53, this forms a regulatory negative feedback loop in the p38-p53 pathway [163]. PPM1D-dependent dephosphorylation of UNG2 may inhibit the role of UNG2 in base excision repair (BER) and impede DNA repair [162] .

All described PPM1D substrates and their cellular functions are summarized in the following table (Table 2). It is anticipated that further PPM1D substrates will be identified.

Target Protein	Site(s)	Function	References
pSQ/TQ motif			
ATM	S1981; S365	DDR	[141]
Chk1	S345	DDR	[142]
Chk2	S19; S33/35; T68; T432	DDR	[143]
DAXX	S564	DDR	[155]
H2AX	S139	DDR	[164]
MDM2	S395	regulator of p53	[150]
MDMX	S403	regulator of p53	[151]
p53	S15	DDR	[142]
p65	S536	NF-KB signalling	[165]
Ulk1	S638	Genotoxic stress induced autophagy	[166]
XPA	S196	nucleotide excision repair	[156]
XPC	S892	nucleotide excision repair	[156]
pTX/pY motif			
p38 MAPK	T180	stress response	[163]
UNG2	T6	base excision repair	[162]
Other			
LSD1	S131; S137	DDR	[167]
RBM38	S195	RNA binding protein, regulates translation of both PPM1D and p53	[168]
SMAD4	T277	TGF-β/BMP pathways, development and tissue homeostasis	[169]

Table 2: Wip1 and its published substrates

2 OBJECTIVES

The primary goal of this thesis was to assess the molecular mechanisms of DNA damage response at a deeper level. Specifically, I sought to identify new PPM1D substrates with both candidate and unbiased approaches. This analysis revealed a novel interaction between PPM1D and the shelterin complex at telomeres which I investigated in detail. Because PPM1D activity promotes cancer development and inversely PPM1D inhibition represents a potential treatment strategy, it is essential to understand its physiological roles in cells.

Aim 1 – **To decipher the role of PPM1D at telomeres**

Aim 2 – **To functionally characterize mutations in selected shelterin genes identified in cancer**

Aim 3 – **To identify novel nuclear substrates of PPM1D**

Aim 4 – **To identify new roles of PPM1D in DNA damage repair**

3 LIST OF METHODS

Experimental details can be found in reprints of publications attached to this thesis in Chapter 9.

- Tissue cultures, plasmid and siRNA transfections, preparation of stable cell lines
- Standard biochemistry techniques including SDS-PAGE and immunoblotting
- Molecular cloning and standard molecular biology techniques
- Immunoprecipitations
- Cell fractionation
- Immunocytochemistry
- Fluorescence microscopy, live-cell microscopy, confocal microscopy, high-content & high-throughput microscopy and corresponding image analysis
- Flow cytometry

4 RESULTS

Extended results can be found in reprints of publications attached to this thesis in Chapter 9.

4.1 Aim 1 – To decipher the role of PPM1D at telomeres

Data from this aim have been published in scientific article entitled:

- Storchova R, Palek M, Palkova N, Veverka P, Brom T, Hofr C, Macurek L. Phosphorylation of TRF2 promotes its interaction with TIN2 and regulates DNA damage response at telomeres. Nucleic Acids Research. 2023; 51(3):1154-1172.

Firstly, we used the promiscuous biotin ligase (BioID2) fused to PPM1D in combination with mass spectrometry to detect potential interactors of PPM1D. We observed that some of the top hits were associated to telomeres. By immunoprecipitation and proximity ligation assays we confirmed, that PPM1D can interact with shelterin components, including TRF2, Rap1 and TRF1. By confocal microscopy, we also confirmed that PPM1D can localize at telomeres. Further we focused on TRF2 that was the best scoring hit of shelterin components interacting with WIP1. We discovered that PPM1D can dephosphorylate S410 of TRF2. This phosphorylation enhanced interaction of TRF2 with TIN2. Overexpression of PPM1D resulted in reduced levels of TIN2 and TPP1 at telomeres. Conversely, inhibition of PPM1D impaired recruitment of 53BP1 to the telomeric DNA breaks. 53BP1 recruitment was rescued upon expression of TRF2 S410A mutant. Our findings suggest that TRF2 phosphorylation increases the binding of TIN2 to the shelterin complex, thereby regulating DNA repair at telomeres.

4.2 Aim 2 – To functionally characterize mutations of the shelterin components in melanoma

Data from this aim have been published in scientific article entitled:

- Stolarova L, Jelinkova S, Storchova R, Machackova E, Zemankova P, Vocka M, Kodet O, Kral J, Cerna M, Volkova Z, Janatova M, Soukupova J, Stranecky V, Dundr P, Foretova L, Macurek L, Kleiblova P, Kleibl Z. Identification of Germline Mutations in Melanoma Patients with Early Onset, Double Primary Tumors, or Family Cancer History by NGS Analysis of 217 Genes. Biomedicines. 2020 Oct 9;8(10):404.

On this aim, we collaborated with Prof. Zdeněk Kleibl (1.lf UK) and his group which mapped germline mutation in melanoma patients using next generation sequencing. In our laboratory, we focused on functional analyses of POT1 P116L mutation, which is located in the Oligonucleotide/Oligosaccharide Binding (OB) fold domain 1 of POT1. We observed that POT1 P116L mutation did not affect recruitment of POT1 to the shelterin complex through TPP1. On the other hand, POT1 P116L mutation impaired binding of POT1 to ssDNA. Therefore, we concluded that P116L is a functionally defective mutation.

4.3 Aim 3 – To identify novel substrates of PPM1D

4.3.1 Candidate approach

Data from this aim have been published in scientific article entitled:

- Storchova R, Burdova K, Palek M, Medema RH, Macurek L. A novel assay for screening WIP1 phosphatase substrates in nuclear extracts. FEBS J. 2021 Oct;288(20):6035-6051.

We developed a simple assay to validate the reported substrates of PPM1D and detect new ones. For this assay, we performed phosphatase reaction in nuclear extracts with recombinant PPM1D. We also compared results from this assay with reactions where we mixed only synthetic phosphopeptides with recombinant PPM1D. The dephosphorylation was observed on western blots with use of specific phosphoantibodies. In this way, we confirmed already established substrates with pSQ/TQ motifs including p53, Kap1 and DNA-PK. In contrast, p38 with the pTXpY motif was not dephosphorylated by the assay using nuclear extracts, only with synthetic phosphopeptides. This suggests that the assay involving nuclear extracts might be more precise and pertinent to physiological conditions, as p38 displayed a low susceptibility to PPM1D in other experiments where PPM1D was overexpressed, inhibited or knocked-out. We also discovered Deleted in Breast Cancer-1 (DBC1) T454 as a new substrate of PPM1D. DBC1 is a regulator of several transcription factors and epigenetic regulators, including SIRT1, PARP1 and HDAC3. Since we observed increased p53 acetylation after PPM1D inhibition, we wondered whether PPM1D, by DBC1 dephosphorylation, may modulate DBC1 interaction with SIRT1 deacetylase and thereby affect the levels of p53 acetylation. However, we observed that DBC1-SIRT1 interaction was stable and independent of

DBC1 T454 phosphorylation. Also, DBC1 knock down did not prevent p53 acetylation after IR or PPM1D inhibition. We found that PPM1D regulated p53 acetylation by limiting the interaction between p53 and p300 acetyltransferase.

4.3.2 Unbiased approach

- Data from this aim have not been published yet.

Using mass spectrometry, we performed unbiased screen. Firstly, we utilized U2OS PPM1D knockout cells. We treated these cells for 2 hours with etoposide 40 μM. Etoposide is a TOP2 poison, which leads to the formation of DSBs in a manner that is both transcription- and replication-dependent. [170, 171]. These nuclear extracts were further used for phosphatase reaction with PPM1D and afterwards analyzed by MS and compared to nuclear extracts without phosphatase reaction. These samples were processed in parallel, only the addition of PPM1D was omitted.

Next, we also analyzed by MS directly cell lysates enriched for phosphoproteins from U2OS, U2OS PPM1D knockout cells and U2OS with PPM1D inhibitor. All these conditions were both untreated and treated 2 hours with etoposide 40 μM. This experiment was done in collaboration with Pavel Talacko, who performed the enrichment of phosphoproteins from our cell pellets and performed the MS measurement and initial analyses.

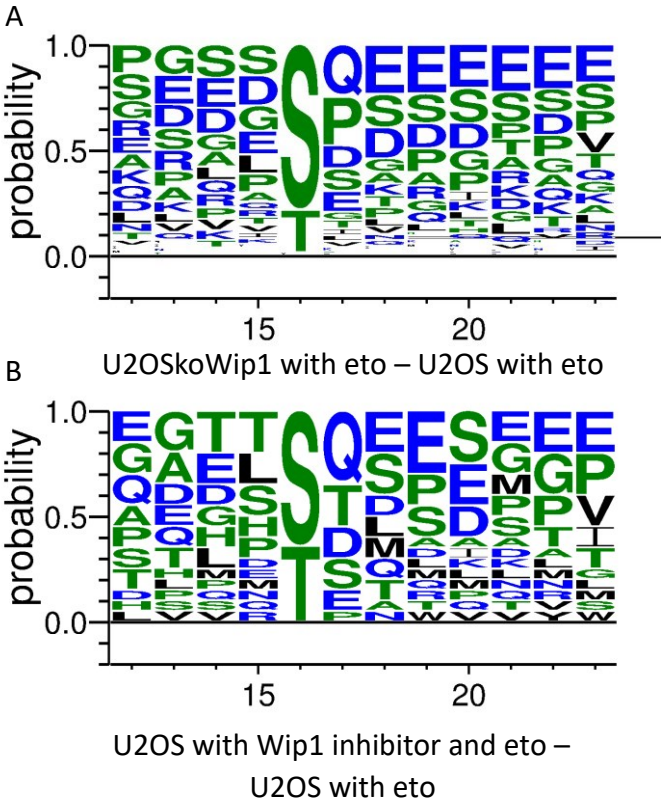

Figure 16: Sequence logo of Wip1 substrates, as expected SQ/TQ is the major motif
a) Sequence logo of significant hits enriched in U2OS koWip1 cells with etoposide compared to U2OS with etoposide (no imputation, FDR 0.05)
b) Sequence logo of significant hits enriched in U2OS cells with Wip1 inhibitor and etoposide compared to U2OS with etoposide (no imputation, FDR 0.05, difference higher than 1)

The sequence logo from U2OS cells of hits significantly enriched in Wip1 KO or after Wip1 inhibition confirmed the expected motif SQ/TQ in Wip1 substrates (Figure 16). In this unbiased screen we again confirmed known targets of Wip1 such as KAP1(TRIM28) and XPC and the novel target DBC1 (alias CCAR2) which we described in our article using candidate approach (Figure 17)[157]. We identified also many potential novel targets of Wip1 including NUMA1 S395 and UIMC S101. We further confirmed NUMA1 phosphorylation to be sensitive to Wip1 inhibition using western blotting (Figure 18).

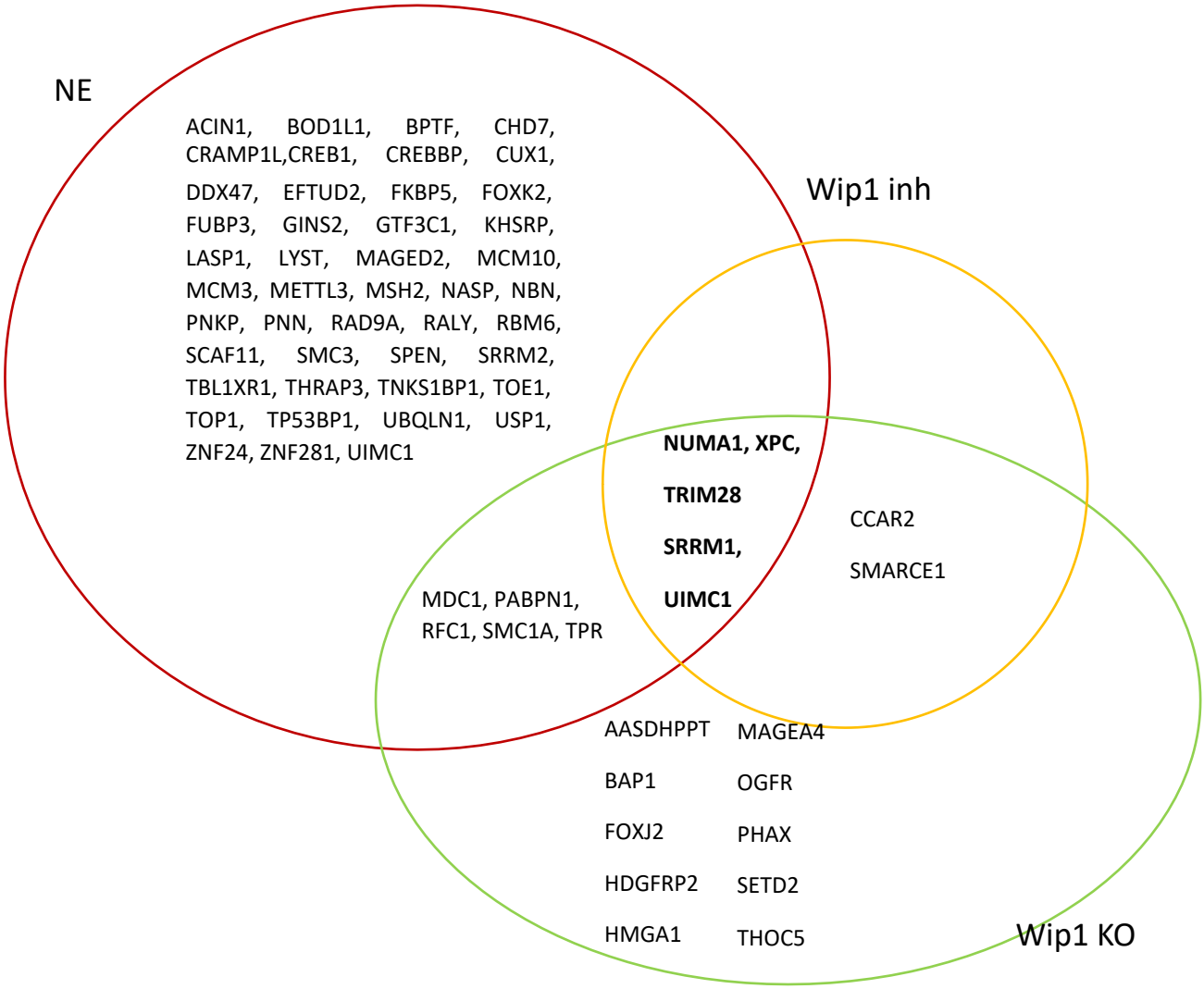

Figure 17: Venn diagram, comparing different conditions to detect Wip1 targets, overlap is shown independently of specific phosphosite that is dephosphorylated. Abbreviations: NE - nuclear extracts (U2OS koWip1 with eto minus U2OS koWip1 with eto after phosphatase reaction with Wip1), Wip1inh - U2OS cells with Wip1 inhibitor and etoposide minus U2OS cells with etoposide. Wip1 KO- U2OS koWip1 cells with etoposide minus U2OS cells with etoposide.
Selection criteria for the hits:
-NE-nuclear extracts (independent duplicate, therefore could not be evaluated for significant hits), NaN values were imputed by 18 and selection criteria were following:

- log2FC (eto –eto with Wip1 phosphatase)> 1 (is dephosphorylated by Wip1)
- log2FC (eto-NT) >0.8 (is induced by DNA damage)
- SQ or TQ site is dephosphorylated

-Wip1 inh and Wip1 KO- both from MS screen from cells, where independent quadruplicate was used, but further evaluation was done on triplicate, in Venn diagram are shown significant hits which fullfiled the following criteria:

- log2FC (eto-NT) >0.8 (is induced by DNA damage)
- SQ or TQ site is dephosphorylated
- log2FC between U2OS Wip1 inhibitor or Wip1KO with eto minus U2OS cells with eto is greater than 0.5

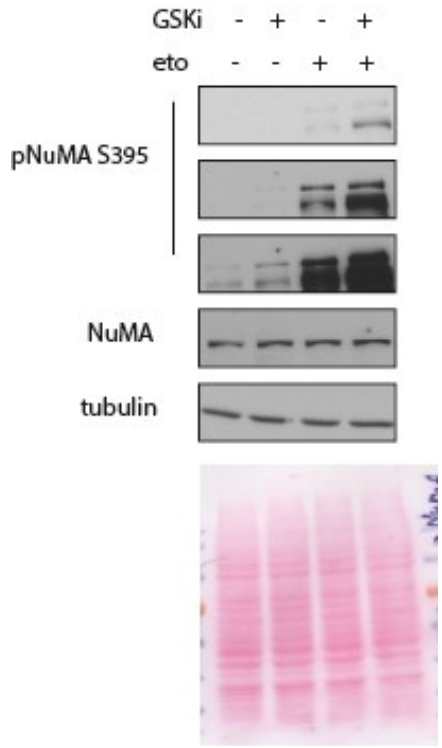

Figure 18: Confirming NUMA1 S395 to be the target of PPM1D.

4.4 Aim 4 – To identify new roles of PPM1D in DNA damage repair

Data from this aim have been published in scientific article entitled:

- Burdova K, Storchova R, Palek M, Macurek L. WIP1 Promotes Homologous Recombination and Modulates Sensitivity to PARP Inhibitors. Cells. 2019 Oct 15;8(10):1258.

In this article we used traffic light reporter system to evaluate the role of PPM1D in repair of DNA double-stranded breaks (DSBs). We observed a decreased HR/NHEJ ratio suggesting that PPM1D inhibition lowered DSB repair efficiency by homologous recombination (HR) but didn't affect NHEJ. Subsequently, we generated PPM1D knockout cell lines (U2OS and RPE) and confirmed their higher sensitivity to IR, comparable to cells with inhibited PPM1D. Also, PPM1D knockout or inhibition led to longer persistence of 53BP1 foci after IR.

The DNA repair pathway is chosen based on the balance between 53BP1/RIF and BRCA1/BARD1. Depletion of BRCA1 or BARD1 decreases HR frequency, whereas depletion of 53BP1 or RIF1 increased the HR/NHEJ ratio. This increased ratio of HR/NHEJ was rescued after Wip1 inhibition.

Thus, PPM1D might promote HR through regulation of BRCA1 /BARD1 complex. We observed that PPM1D can interact with both BRCA1 and 53BP1 and that PPM1D also dephosphorylate both of them (BRCA1 at S1524, 53BP1 at T543). The phosphorylation of 53BP1 at T543 is needed for 53BP1 interaction with Rif1. On this dephosphorylation, PPM1D is probably collaborating with phosphatase PP4C which was originally described in this process.

Since impairment of HR through mutations in BRCA1/2 leads to increased sensitivity to PARP inhibitors, we tried if PPM1D inhibition can also increase sensitivity to PARP. Indeed, we observed higher sensitivity to PARP after PPM1D inhibition or knockout. This sensitivity was even further enhanced with combined depletion of PP4C and PPM1D inhibition.

5 DISCUSSION

5.1 Aim 1 – To decipher the role of PPM1D at telomeres

PPM1D is a chromatin bound protein with poor solubility[137]. To detect new interactors of PPM1D at chromatin, we used PPM1D fused to biotin ligase BioID2 or empty BioID2 [172]. Combining immunoprecipitation of biotin tagged proteins in denaturizing conditions with MS, enabled better detection also of poorly soluble protein bound to chromatin. By this method, we identified shelterin components (specifically TRF2, TRF1 and TRF2IP) as major interactors of PPM1D. We confirmed these interactors also by co-immunoprecipitations and proximity ligation assays. Further we focused on TRF2, which out of the shelterin components scored the best in MS.

We found that PPM1D interacted with TRF2 through its basic rich loop (247-250 B-loop) localized within the catalytic domain of PPM1D. Mutants in B-loop fail to colocalize to TRF2 but still localize to nucleus because PPM1D has 2 nuclear localization signals (NLS), one in the catalytic domain in basic rich loop (247-250 B-loop) and the other one in the C-terminal domain (535-552 AA) [173]. Using confocal microscopy, we also confirmed that PPM1D can colocalize with TRF2 at approximately 60% of telomeres in both U2OS and MCF7 cells, meaning that PPM1D can associate with telomeres in various cell types with both telomerase (MCF7) or alternative lengthening of telomeres (U2OS).

Telomeres safeguard the integrity of genomes by shielding the natural ends of chromosomes from being identified as damaged DNA. When telomeres become dysfunctional, they restrict replicative lifespan and stimulate a DNA damage response that drives cells into senescence or apoptosis, thus curtailing the growth of potentially cancerous cells. On the contrary, chromosome ends without the necessary telomere protection are vulnerable to DNA repair processes that lead to end-to-end fusions and to extensive genomic instability that can contribute to the development of cancer. Telomeres are protected from aberrant DNA damage response by shelterin proteins, which were reported to be phosphorylated under different conditions. However, only a few of these events have been thoroughly studied [174, 175].

In this article, we focused on TRF2 phosphorylation at S410, which is well conserved among species, matches the consensus ATM/ATR site and is increased after

IR and genotoxic stress[139, 176]. We observed that TRF2 S410 is dephosphorylated by PPM1D and phosphorylated by ATR.

Inspiringly, other phosphorylations of TRF2 have been described as playing important roles. Particularly, phosphorylation of TRF2 at S365 was shown to be crucial phospho-switch for telomeres t-loop unwinding during S-phase [90]. TRF2 at S365 is phosphorylated by CDK throughout the cell cycle, only in S-phase dephosphorylation of TRF2 by PP6C/R3 phosphatase enables recruitment of RTEL1 helicase, which can transiently unwind the t-loops and enable telomeres replication [90, 177]. After cells were exposed to ionizing radiation, it was observed that TRF2 underwent transient phosphorylation at Thr230, allowing it to bind to DNA lesions outside of telomeres and thus promote DNA repair [178-180]. Nonetheless, the part that TRF2 modification plays in the DNA repair of telomeric lesions has yet to be elucidated.

As TRF2 S410 is phosphorylated by ATR, it is intriguing to hypothesize, that it might have a role during telomere replication. Furthermore, it is questionable whether TRF2 S410 phosphorylation may similarly to S365 phosphorylation, contribute to t-loop unwinding. Interestingly, levels of TRF2 S410 phosphorylation are low, but they increase upon DNA damage at telomeres or upon PPM1D inhibition, suggesting that S410 phosphorylation may be involved in fine-tuning response to replication stress at telomeres. However, the possible mechanism remains elusive. TRF2 S410 phosphorylation might affect recruitment of some additional factor important in overcoming replication stress, which were shown to be recruited by TRF2 including RTEL1 (helicase dismantling G4 quadruplexes and t-loop DNA) [177], Apollo (nuclease relieving topological stress) [181] and SLX4 (a multitasking protein involved in the replication stress response and the maintenance of telomere stability) [182]. Other mode how TRF2 S410 might influence replication is interaction with TIN2 which is described below.

Since the phosphorylation of S410 of TRF2 is adjacent to the TIN2-binding motif (392-408 aa, TBM motif), which is essential for interaction with TIN2, we looked closer onto this interaction. TIN2 can interact with TRF2 via 2 sites. C-terminal portion of TIN2 (TRFH binding motif, residues 256-276) can interact with TRFH domain of both TRF1 and TRF2, or the N-terminal domain of TIN2 (residues 2-202) can recognize the TIN2-binding motif (TBM, residues 392-408) of TRF2 [183]. Interestingly, the binding between N-terminal domain of TIN2 with $TRF2_{TBM}$ has almost 20 times higher affinity than the binding of TIN2 C-terminal part with $TRF2_{TRFH}$, suggesting that interaction

between TRF2 and TIN2 is mostly dependent on the N-terminal part of TIN2 and TBM motif in TRF2 [39].

The crystal structure, which has been shown to describe the TIN2-TRF2 interaction, lacks the structural information for TRF2 after residue 408 [39]. Therefore, we used Alphafold2 Colab to predict the structure of TRF2 residues 392-420 [184]. In the Alphafold2 model, S410 of TRF2 is positioned opposite to the positively charged residues of TIN2 binding motif, implying that phosphorylation of S410 might strengthen the TRF2-TIN2 interaction by formation of salt bridges between the phosphate and basic residues in the AA50-56 region of TIN2.

Indeed, we managed to confirm by many assays, that phosphorylation of TRF2 at S410 is enhancing the interaction between TRF2 and TIN2. We also observed, that the interaction between non-phosphorylatable mutant of TRF2 and TRF2 wild-type with TIN2 was comparable, which is in good agreement with published literature, where TRF2 peptide missing the phosphorylation site is still able to interact with TIN2 [39]. Therefore, we suggest that PPM1D might be fine - tuning the level of interaction between TRF2 and TIN2.

Since TIN2 is important for recruitment of TPP1-POT1 to TRF1/TRF2, we tested whether also TPP1 levels are affected by PPM1D status. Indeed, we observed an increase of TPP1 levels in TRF2 foci after PPM1D inhibition or in PPM1D knockout cells, suggesting that TRF2 S410 dephosphorylation by PPM1D may affect the shelterin assembly. This effect seems to be consistent for cells with alternative lengthening of telomeres (U2OS) and with telomerase (MCF7).

As PPM1D inhibition seems to be stabilizing the shelterin complex by increasing strength of TRF2-TIN2 interaction, we wondered if activation of PPM1D would do the opposite. Therefore, we overexpressed wildtype PPM1D, which led to decreased amount of TIN2 at telomeres. After overexpression of PPM1D-A380, which showed the strongest association to telomeres, we observed even stronger reduction of TIN2 from telomeres accompanied also by strong reduction of TRF2 staining at telomeres suggesting, that the shelterin may fall apart after dephosphorylation by PPM1D.

Since phosphorylation of TRF2 is enhanced after DSBs, we wondered what effect might the PPM1D status have on recruitment of DNA repair proteins to telomeres after DSBs. For this purpose, we induced DSBs at telomeres by Cas9 system and compared PPM1D wild type vs knockout cells. We observed no difference in NBS1 recruitment, suggesting, that DSBs are recognized by MRN complex independently of PPM1D status.

Next, we checked DDR mediator 53BP1. We could see significant reduction of 53BP1 recruitment to telomeres and 53BP1 foci formation in PPM1D knocked out cells or cells with PPM1D inhibitor. The reduction of 53BP1 foci formation and recruitment to telomeres was rescued by overexpression of PPM1D in PPM1D knocked out cells, confirming, that it is truly an effect of PPM1D. To recruit 53BP1 or BRCA1 to telomeres, histone H2A needs to be ubiquitinated [185]. Therefore, we checked ubiquitin levels with FK2 antibody and indeed we saw reduction of signal in PPM1D KO cells, which might explain the decreased levels of 53BP1. 53BP1 is essential for NHEJ (non-homologous end joining). To check, whether also the other major DSBs repair pathway, HR (homology recombination), is impaired, we focused on Rad51. Indeed, we saw reduction of Rad51 at telomeres after PPM1D inhibition or in knocked out cells, suggesting that both major DSB repair pathways are impaired at telomeres in cells lacking PPM1D. To test whether PPM1D affects the recruitment of DSB repair factors through TRF2 phosphorylation, we induced telomeric damage in cells, where we also expressed TRF2 S410A mutant vs wild type and treated with PPM1D inhibitor. Whereas TRF2-WT expression rescued only mildly the effect of decreased 53BP1 foci after PPM1D inhibition, TRF2-S410A showed significant increase of 53BP1 foci at telomeres. This suggests, that PPM1D is promoting the 53BP1 recruitment to telomeres after DSBs through dephosphorylation of TRF2 S410.

To protect DNA ends, TRF2 plays an important role in t-loop formation [80]. TIN2 was shown to promote TRF2 mediated t-loop formation *in vitro* [186]. Since loss of PPM1D is enhancing TRF2 S410 phosphorylation and TRF2-TIN2 interaction, we wondered whether it may affect t-loop formation. To check the t-loop formation, we imaged the telomeres in psoralen-crosslinked chromatin spreads using Structured Illumination Microscopy (SIM) and determined the fractions of linear and closed telomeres. Though we observed approximately 25% of telomeres were forming t-loops, which is consistent with the published literature, we didn't observe significant differences in t-loop formation between PPM1D wild-type and knocked out cells [80]. This would suggest that PPM1D is not affecting t-loop formation. Other explanation could be, that the assay is not sensitive enough to detect mild differences in t-loop formation, since approximately half of the telomeres are excluded from the analysis due to inconclusive shape. Lack of PPM1D could also promote TIN2 in facilitating TRF2 mediated higher-organization of telomeres [186].

TRF2 is supposed to suppress DNA damage via 2 modes [121]. The TRFH domain of TRF2 is essential for t-loop formation and suppression of ATM activation. TRF2 iDDR (inhibitor of DDR, residues 449-473) region in hinge domain should repress the DNA damage response at telomeres at the level of E3 ubiquitin ligase RNF168 [121]. Phosphorylation of TRF2 at S410 and iDDR motif are both in the hinge domain, which hasn't been crystallized and lacks structural information. We wondered if the TRF2 S410 phosphorylation may somehow (e.g., by allosteric modification) affect the function of iDDR motif. The iDDR motif is supposed to supress the RNF168 activity via UBR5 (E3 ubiquitin ligase) and BRCC3 (deubiquitinating enzyme) [121]. We tested whether knockdown of BRCC3, UBR5 or overexpression of RNF168 would rescue the formation of 53BP1 foci to damaged telomeres in cells with PPM1D-KO. As we didn't observe rescue, we concluded that PPM1D activity is not promoting 53BP1 foci formation at damaged telomeres through affecting ubiquitination. Possibly, lack of PPM1D might impair the recruitment of DDR factors, by enhancing the interactions between TRF2 and TIN2-TPP1-POT1 within the shelterin complex, thereby limiting the accessibility for DDR factors and also limiting the formation of possibly deleterious telomere fusions. Conversely, PPM1D activity is dephosphorylating TRF2 S410 and therefore loosening the interactions within shelterin, which might enable easier access of DDR factors to the damaged telomeres.

We found that recruitment of the truncated variant of PPM1D A380 to telomeres is greatly enhanced. Interestingly, cells reacted differently to PPM1D inhibitor, when they overexpressed truncated PPM1D and when they had just basal PPM1D levels. In cells with basal levels of PPM1D, PPM1D inhibitor did not increase telomere induced foci (TIFs), reflecting DNA damage at telomeres by co-staining 53BP1 at telomeres. Whereas when PPM1D A380 was overexpressed for 10 days, cells had more telomeric fusions and TIFs and inhibition of PPM1D in these cells increased amount of TIFs even further. This could be interesting since PPM1D is stabilized by truncation or overexpressed in some tumors, so theoretically inhibition of PPM1D could specifically enhance genome instability at telomeres in cancerous cells with truncated PPM1D whereas genome instability at telomeres in normal cells might be unaffected by PPM1D inhibitor.

There are still some tempting questions about PPM1D and its role at telomeres remaining unanswered. Firstly, PPM1D is interacting with more shelterin components than just TRF2, so it could dephosphorylate more shelterin proteins than just TRF2 probably on SQ/TQ sites. An interesting candidate could be for example the ATM/ATR

dependent phosphorylation of TRF1 at S367. This phosphorylation was observed in immortal human cells, where it leads to dissociation of TRF1 from telomeres and to enhanced telomerase assembly, pointing out the role of DNA damage transducing kinases in telomere elongation [187]. It is intriguing to test whether also PPM1D could be affecting the extent of telomeres elongation.

Another question is whether PPM1D might affect TRF2 function elsewhere than at telomeres. TRF2 was described to bind also to different locations than telomeres, specifically to heterochromatin regions which are hard to replicate such as pericentromeres, where TRF2 facilitates progression of the replication fork [188]. TRF2 can also bind to extra-telomeric G-quadruplexes and alter expression and epigenetic state of several promoters [189]. Some studies connected TRF2 with non- telomeric DNA damage response of DSBs. TRF2 was proposed to mediate strand invasion and promote HR [190, 191]. After IR TRF2 is phosphorylated by ATM at T188, however later was shown that this phosphorylation is not essential for TRF2 recruitment to DSBs [179, 192]. Future studies are needed to specify the function of TRF2 phosphorylations in DDR and to test whether TRF2 and PPM1D are connected also at nontelomeric regions.

5.2 Aim 2 – To functionally characterize mutations of the shelterin components in melanoma

POT1 (protection of telomeres) is a highly conserved shelterin protein which binds the telomeric single-stranded G-rich DNA. This single stranded G-rich DNA can be present either as 3′ overhangs at the ends of the chromosomes or in the case of formation of t-loops, where the ends of chromosomes are tucked into the double stranded part of the DNA, single stranded G-rich DNA occurs at the displaced strand [80, 193].

POT1 is recruited to telomeres by forming a functional heterodimer with another shelterin component TPP1 (also called ACD- adrenocortical dysplasia protein homolog) [96]. In this heterodimer TPP1 tethers POT1 to telomeres through interaction with TIN2-TRF1 and TIN2-TRF2 complexes [194]. POT1 has a critical role in the control of telomere length by inhibiting telomerase [40]. POT1 in collaboration with TPP1 can also prevent hyper-resection at telomeric ends by inhibiting ATR [195].

In collaboration with Zdeněk Kleibl and clinical geneticists, we have described two germline mutations in POT1. The c.703-1G>C mutation was found in a proband with melanoma, dysplastic nevi, and thyroid cancer which resulted in exon 10 skipping and a frameshift (p.V235Gfs*22). The rare missense variant c.347C>T changed the conserved

amino acid p.P116L in a patient with superficial spreading melanoma and breast cancer carrying also a germline deletion of 5395bp affecting exons 9 and 10 of the CHEK2 gene (NM_007194)[196].

For further functional analysis, we focused on P116L mutation of POT1 (Figure 19). P116L is located in the N-terminal part of POT1, which consists of 2 OB (oligosaccharide/oligonucleotide) fold domains which specifically recognize telomeric ssDNA[197]. The C-terminal part of POT1 is needed for binding of TPP1 and consists of third OB fold domain and HJRL (Holiday junction resolvase like domain) [198].

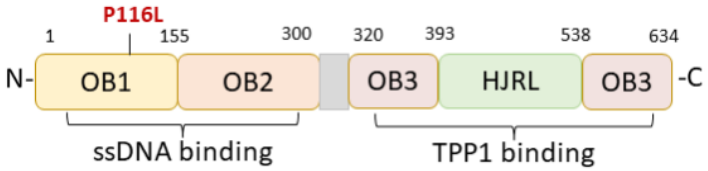

Figure 19: Domain organization of POT1 with highlighted mutation of POT1 P116L in the OB1 domain (for further description see the text above) *(numbering according to [198])*

To functionally characterize the P116L variant of POT1, we firstly performed immunoprecipitation with transiently overexpressed wildtype GFP-POT1 or GFP-POT1-P116L mutant and observed that comparable levels of TPP1 were bound by both variants. Using confocal microscopy, we also detected that both POT1 wildtype and P116L can colocalize with TRF2, suggesting that also the mutant variant of POT1 can be recruited into shelterin complex and correctly localize to telomeres. Since P116L mutation resides in OB1 fold domain which should be important for ssDNA binding, we hypothesized that it could impair binding to ssDNA. Performing pulldown with biotinylated G-rich telomeric probe, we saw that only wildtype and not the mutated variant of POT1 could bind single stranded telomeric DNA [196].

Our results are consistent with the literature and we see, that POT1 P116L mutation doesn't affect recruitment of POT1 to the shelterin complex through TPP1, for which C-terminal part of POT1 is essential. On the other hand, POT1 P116L mutation, which resides in the N-terminal part of POT1, impairs binding of POT1 to ssDNA. Therefore, we conclude that P116L is a functionally defective mutation.

Germline mutations of POT1 have been observed in various cancer types, including melanoma, chronic lymphocytic leukemia, angiosarcoma and glioma [199]. Additionally, somatic mutations of POT1 have been detected in a number of cancer types [200]. The

analysis of the correlation between the frequency of POT1 mutations and the type of tumour among cancers known to be associated with germline POT1 mutations revealed that angiosarcoma was the cancer type with the highest mutation rate (23.26%), while melanoma was associated with an average mutation rate of 3.69% [199]. Next to our studied mutation, POT1 R117C mutation was detected as causative of cardiac angiosarcomas in families with multiple tumors [201]. This study showed that R117C mutation decreased ability of POT1 to bind ssDNA and led to abnormally long telomeres with increased fragility [201]. Apart from our study, P116L mutation of POT1 has been detected also in cardiac angiosarcoma [202]. Further population studies on larger groups are necessary to assess the effect of the P116L variant on the increase in tumor risk.

5.3 Aim 3 – To identify novel substrates of PPM1D

In this part of the study, we performed candidate and unbiased screens to identify new substrates of PPM1D. To this end, we established a novel assay for screening substrates of phosphatases in nuclear extracts. We confirmed many established PPM1D substrates including p53 S15 and Kap1 S824 and identified novel substrates DBC1 T454 and DNA-PK pS2056. Interestingly, by this novel assay, we did not detect any activity of PPM1D towards its published substrate p38. p38 was originally described as PPM1D substrate using transient overexpression of PPM1D in cells, but this may have indirect effect on p38 phosphorylation either by change in transcriptional programs or by increased stress induction [163]. p38 was also described as PPM1D target using *in vitro* assays with p38 phosphopeptide [139]. We hypothesized that our novel assay is physiologically more relevant as it decreases risk of the non-specificity observed in *in vitro* assays, where phosphatase is mixed directly with a single phosphopeptide. To verify this hypothesis, we confirmed, that when p38 phosphopeptide is mixed *in vitro* with PPM1D, we see the dephosphorylation. However, we suggest that this effect is not relevant in cells, where we did not observe any dephosphorylation of p38 by PPM1D (using PPM1D inhibition or PPM1D knock-out cells). We performed subcellular fractionation and as expected, we detected PPM1D predominantly in nuclear fraction whereas p38 was present mostly in cytosol, further supporting that p38 is not a direct substrate of PPM1D.

Initial research on PPM1D knock-out mice suggested that the loss of PPM1D could suppress tumorigenesis by targeting p38, thus indirectly activating the p53 and Ink4a pathways [203, 204]. However, subsequent studies revealed that PPM1D can target p53 directly by dephosphorylating S15, as well as indirectly through its impact on ATM and

MDM2 [141, 142, 150]. We also observed that PPM1D inhibition increases p53 acetylation in p53 C-terminal domain on Lys382, which is enhancing p53 binding to DNA and stimulating transcription of its target genes [205-208].

We wondered whether PPM1D might affect p53 acetylation through its newly identified substrate DBC1 because it was published that DBC1 phosphorylation is affecting its interaction with SIRT1 deacetylase, which might affect p53 acetylation [209]. Nevertheless, we did not observe any effect of DBC1 phosphorylation on DBC1-SIRT1 interaction after PPM1D inhibition and p53 acetylation was increasing even when DBC1 was depleted by siRNA. Therefore, we hypothesized that PPM1D might regulate p53 acetylation through p300 acetyltransferase, independently of DBC1. It was published, that phosphorylations of p53 N-terminal domain, including the PPM1D known target p53 S15, are enhancing interaction between p53 and p300[210]. In agreement with this, we could see that PPM1D inhibition enhanced the p300-p53 interaction. Recent findings also suggest that ATM-induced phosphorylation of BRCA1 may facilitate the formation of the p53-p300 complex, yet the exact mechanism of this interaction has to be elucidated [211]. Indeed, we could see that PPM1D dephosphorylates BRCA1 S1524. This further supports the model that PPM1D is decreasing activity of p53 not only through p53 S15 dephosphorylation, but also by limiting p53-p300 interaction and therefore p53 K382 acetylation.

In parallel to the candidate approach, we performed also unbiased screen which unraveled many interesting potential targets of PPM1D. Unfortunately, before we managed to publish our screen, similar study with exactly same treatments (etoposide and PPM1D inhibitor) was published [212]. Etoposide, which is a TOP2 poison, is used extensively in the clinical setting as an anti-cancer agent [213]. It causes DSBs in a mode that is reliant on both transcription and replication [170, 171]. Similar to our results, they found that acute DNA damage after etoposide is counteracted by PPM1D. In etoposide-treated cells, we both noticed that PPM1D dephosphorylated mostly the SQ motif. They selected kanadaptin (SLC4A1AP) as an interesting hit which is phosphorylated after etoposide and dephosphorylated by PPM1D at S709. This phosphorylation is present in a disordered region of kanadaptin. To study the effect of the phosphorylation on structure-function and disorder functions relationship, they employed atomistic molecular dynamics simulations. They could see, that the region around S709 remained disordered even after phosphorylation and that the three nearby glutamic acids (E713, E714 and E715) were mostly solvent exposed, indicating their possible role in molecular

recognition and protein-protein interactions of the PPM1D-targeted SQ motif in the DDR[212]. In our screen, we detected phosphorylation of kanadaptin only on S712 and S312, but these phosphorylations did not change significantly in response to PPM1D.

Interestingly, Graf et al. also detected phosphorylations of the p38 (MAPK14). In U2OS, phosphorylations were found at S2, T180 and Y182 residues, while in HCT116 only S2 and Y182 were detected. Phosphorylation on S2 was located in the SQ motif and with etoposide treatment had a significant increase, without any alteration induced by PPM1Di in both cell lines. In HCT116, a mild increase of the phosphorylation at Y182 was registered upon the administration of PPM1Di when the cells had been treated with etoposide (log2FC (Eto + PPM1Di/Eto) = 0.65)). However, in U2OS, there were no changes in phosphorylations at Y182 greater than log2FC 0.5. Additionally, phosphorylation at T180 was only found in U2OS, yet there were not any significant changes observed [212]. Collectively, these results support the hypothesis that PPM1D is not directly dephosphorylating p38/MAPK14 at T180.

In our MS screen, p38(MAPK14) phosphosites were not detected at all. With regard to TRF2, we did not detect the S410 phosphosite; only the phosphosites on S365 and S421 were observed. For S421, we noted a mild increase after PPM1D inhibition. This might suggest that PPM1D additionally dephosphorylates TRF2 at S421, or that the MS analysis was not able to accurately assign which particular serine on the phosphopeptide was phosphorylated, since S421 was detected in the same peptide that also contains S410. Interestingly, similar results were observed in the screen of U2OS from Graf et. al., where they detected only 2 phosphosites of TRF2: S365 and S422. Analysis revealed that phosphorylation at S365 stayed the same under all conditions, whereas phosphorylation at S422 increased when PPM1Di was added to etoposide-treated cells (log2FC(Eto+PPM1Di/Eto) 1.7). Once again, the phosphorylation of Serine 422 located in the same peptide as Serine 410, which both share an SQ motif, raises the possibility that either MS analysis has incorrectly assigned the respective phosphosite or that PPM1D may have the ability to dephosphorylate both these residues. In HCT116, phosphorylation of TRF2 was identified exclusively at S109 with no differences between the conditions observed [212].

We detected that PPM1D can dephosphorylate TRF2 at S410 (See Results 4.1). This TRF2 phosphorylation was detected by a former screen by Kahn et. al. [214]. In this study, the authors utilized Molm13 cells carrying either a wild-type or truncated PPM1D mutation in exon 6, which enhances the stability and quantity of the PPM1D in the cells.

They observed that the PPM1D mutant cells exhibited less phosphorylation of TRF2 S410 compared to PPM1D wild-type cells and revealed that inhibiting PPM1D results in a higher level of TRF2 S410 dephosphorylation. Additionally, the authors noted an elevation in TRF2 S410 phosphorylation following the administration of cytarabine, a replication chain-terminating nucleoside analogue employed in chemotherapy for leukemias and lymphomas [215]. This increase in TRF2 S410 phosphorylation suggests a role in replication stress, which is further supported by the results of our experiment, where we observed that TRF2 S410 is phosphorylated by ATR (See Results 4.1).

Similar to Graf et. al., we detected Nuclear mitotic apparatus 1 (NUMA1 S395) as a very strong hit, which is highly induced by etoposide and dephosphorylated by PPM1D. NUMA1 was shown to be phosphorylated at S395 following oxidative damage including IR [176]. NUMA1 serves as a barrier for 53BP1 recruitment to damaged chromatin and its phosphorylation at S395 could acts as a switch. It was shown that S395A nonphosphorylatable mutant of NUMA1 is enhancing the barrier for 53BP1 recruitment to chromatin and supposedly phosphorylation of NUMA1 could enable the 53BP1 recruitment [216]. Therefore, dephosphorylation of NUMA1 at S395 could be another mechanism by which PPM1D contributes to the termination of DDR.

5.4 Aim 4 – To identify new roles of PPM1D in DNA damage repair

In this article, we showed that PPM1D inhibition decreased efficiency of HR (but not NHEJ) repair of DSBs and led to persistent DNA damage in S/G2 indicated by slower clearance of 53BP1 foci. We found that PPM1D can interact with and dephoshoprylate BRCA1 and that PPM1D can promote timely recruitment of BRCA1 to DSBs. We observed that PPM1D dephosphorylated also 53BP1 at T543, this site mediates interaction between 53BP1 and RIF1 and also promotes chromatin remodelling [217]. Even though the effect of PPM1D inhibition on 53BP1 was higher than the effect of previously described phosphatase PP4C, we did not observe any significant difference in the DNA resection upon PPM1D inhibition. Possible explanation could be, that PPM1D is affecting 53BP1 repositioning only in a small but physiologically meaningful fraction of DNA lesions depending on the chromatin background. PPM1D could also modulate HR by targeting other substrates involved in late steps of HR such as BRCA1-BARD1 complex. This complex stably interacts with PPM1D, can be phosphorylated at many sites by ATM/ATR and was shown to be important for Rad51-mediated homologous DNA pairing in HR [218]. Theoretically, PPM1D might also regulate HR through

inhibition of p53 activity because p53 can directly interact with Rad51, Rad54 and supress Rad51 expression [219-221]. Future research is still needed to determine the exact mechanism of PPM1D in HR.

Poly(ADP-ribose) polymerase (PARP) is an enzyme involved in base excision repair, a key pathway in the repair of DNA single-strand breaks [222]. Inhibition of PARP (e.g. by Olaparib) leads to the persistence of ssDNA lesions that are converted to dsDNA breaks during replication, lesions that are normally repaired by homologous recombination [222]. This is utilized in cancer treatment where inhibition of PARP combined with mutations in proteins needed for HR pathway (such as BRCA) lead to synthetic lethality [222, 223]. In line with PPM1D role in HR, we found that when PPM1D was lost, cancer cells became more sensitive to PARP inhibitors. Further, we used selective inhibitor of PPM1D (GSK2830371), which is well tolerated in normal cells. Combining olaparib with a PPM1D inhibitor caused an increase in DNA damage load in G2 cells leading to significant increase in cell death, suggesting that this combination might be advantageous for treatment of BRCA1 proficient tumors. Given that p53 is the primary target of PPM1D, it has been proposed that utilizing a PPM1D inhibitor can be effective in treating certain types of neuroblastoma, breast adenocarcinoma, and melanoma that exhibit p53 proficiency [224-227]. We propose, that combining inhibition of HR and stimulation of p53 could have synergistic effect on eradicating cells with PPM1D inhibitor.

6 CONCLUSIONS

The overall goal of this thesis was to improve understanding of the PPM1D role in DNA damage response. To elaborate on this goal, we searched for PPM1D interactors using proximity biotinylation combined with proteomic analysis. In this way, we uncovered that PPM1D can interact with shelterin components and localize at telomeres. Moreover, we observed that the truncated (but enzymatically active) variant of PPM1D A380, compared to PPM1D WT, was more efficiently recruited to telomeres, which resulted in an increased number of telomeric fusions. These discoveries could be highly relevant for some cancer types, where PPM1D is stabilized by C-terminal truncation. PPM1D inhibitor might be useful for treatment of these cancers not only because of its effect on HR but also through its effect on telomeres.

Next goal was to functionally characterize mutations of the shelterin components in melanoma, specifically focusing on the POT1 P116L mutation. My research revealed that this mutation is functionally defective due to its impaired binding of POT1 to single-stranded DNA, despite not disrupting its recruitment to the shelterin complex.

To further validate already published and detect possible new targets of PPM1D, we developed and implemented a novel screen utilizing nuclear extracts and recombinant phosphatase. We confirmed many known targets, demonstrated that p38 is not a physiological target of PPM1D and identified novel PPM1D targets including BRCA1 S1524 and DBC1 T454. Additionally, we proposed a mechanism of PPM1D inhibition leading to increased p53 acetylation.

Finally, we studied Wip1's role in DNA damage repair and discovered that it was promoting HR and not NHEJ. Our findings suggest that PPM1D inhibition in p53 proficient cells combined with HR inhibitors, such as PARP1i, could have a synergistic effect in eradicating cancer cells.

7 LIST OF PUBLICATIONS

This thesis was based on the following publications that are described in Chapter 4. The full text of the published papers can be found attached to this thesis (Chapter 9).

Storchova R*, Palek M*, Palkova N, Veverka P, Brom T, Hofr C, Macurek L. Phosphorylation of TRF2 promotes its interaction with TIN2 and regulates DNA damage response at telomeres. Nucleic Acids Research. 2023; 51(3):1154-1172.
*These authors contributed equally.

Author's contribution:
The author of this thesis contributed to the paper by performing all immunoprecipitations, substantial part of immunofluorescence experiments, statistical analysis, analysis of MS data. In addition, the author contributed extensively to the preparation of the manuscript by figure design, data analysis, and an important intellectual content.

Storchova R*, Burdova K*, Palek M, Medema RH, Macurek L. A novel assay for screening WIP1 phosphatase substrates in nuclear extracts. FEBS J. 2021 Oct;288(20):6035-6051.
*These authors contributed equally.

Author's contribution:
The author of this thesis contributed to the paper by performing phosphatase assays from nuclear extract, phosphatase assays *in vitro* with phosphopeptides, immunoprecipitations, statistical analysis, analysis of MS data. In addition, the author contributed extensively to the preparation of the manuscript by figure design, data analysis, and an important intellectual content.

Stolarova L, Jelinkova S, **Storchova R**, Machackova E, Zemankova P, Vocka M, Kodet O, Kral J, Cerna M, Volkova Z, Janatova M, Soukupova J, Stranecky V, Dundr P, Foretova L, Macurek L, Kleiblova P, Kleibl Z. Identification of Germline Mutations in Melanoma Patients with Early Onset, Double Primary Tumors, or Family Cancer History by NGS Analysis of 217 Genes. Biomedicines. 2020 Oct 9;8(10):404.

Author's contribution:
The author of this thesis contributed to the paper by performing functional assays with POT1 and POT1 P116L mutant in cells.

Burdova K, **Storchova R**, Palek M, Macurek L. WIP1 Promotes Homologous Recombination and Modulates Sensitivity to PARP Inhibitors. Cells. 2019 Oct 15;8(10):1258.

Author's contribution:
The author of this thesis contributed to the paper by performing several proliferation assays and immunofluorescence experiments.

I hereby confirm that the author of the thesis, Radka Štorchová, participated in the publications listed above to the extent specified in this chapter.

……
MUDr. Libor Macůrek, Ph.D.

8 REFERENCES

1. Jackson, S.P. and J. Bartek, *The DNA-damage response in human biology and disease.* Nature, 2009. **461**(7267): p. 1071-1078.
2. Bartek, J. and J. Lukas, *Chk1 and Chk2 kinases in checkpoint control and cancer.* Cancer Cell, 2003. **3**(5): p. 421-9.
3. Ciccia, A. and S.J. Elledge, *The DNA Damage Response: Making It Safe to Play with Knives.* Molecular Cell, 2010. **40**(2): p. 179-204.
4. Polo, S.E. and S.P. Jackson, *Dynamics of DNA damage response proteins at DNA breaks: a focus on protein modifications.* Genes Dev, 2011. **25**(5): p. 409-33.
5. Mirza-Aghazadeh-Attari, M., et al., *DNA damage response and repair in colorectal cancer: Defects, regulation and therapeutic implications.* DNA Repair (Amst), 2018. **69**: p. 34-52.
6. Ceccaldi, R., B. Rondinelli, and A.D. D'Andrea, *Repair Pathway Choices and Consequences at the Double-Strand Break.* Trends in Cell Biology, 2016. **26**(1): p. 52-64.
7. van den Berg, J., et al., *DNA end-resection in highly accessible chromatin produces a toxic break.* bioRxiv, 2019: p. 691857.
8. Krenning, L., J. van den Berg, and R.H. Medema, *Life or Death after a Break: What Determines the Choice?* Molecular Cell, 2019. **76**(2): p. 346-358.
9. van Gent, D.C. and M. van der Burg, *Non-homologous end-joining, a sticky affair.* Oncogene, 2007. **26**(56): p. 7731-7740.
10. Britton, S., J. Coates, and S.P. Jackson, *A new method for high-resolution imaging of Ku foci to decipher mechanisms of DNA double-strand break repair.* Journal of Cell Biology, 2013. **202**(3): p. 579-595.
11. Mimori, T. and J.A. Hardin, *Mechanism of interaction between Ku protein and DNA.* Journal of Biological Chemistry, 1986. **261**(22): p. 10375-10379.
12. Yin, X., et al., *Cryo-EM structure of human DNA-PK holoenzyme.* Cell Research, 2017. **27**(11): p. 1341-1350.
13. Scully, R., et al., *DNA double-strand break repair-pathway choice in somatic mammalian cells.* Nat Rev Mol Cell Biol, 2019. **20**(11): p. 698-714.
14. Gottlieb, T.M. and S.P. Jackson, *The DNA-dependent protein kinase: requirement for DNA ends and association with Ku antigen.* Cell, 1993. **72**(1): p. 131-42.
15. Jiang, W., et al., *Differential Phosphorylation of DNA-PKcs Regulates the Interplay between End-Processing and End-Ligation during Nonhomologous End-Joining.* Molecular Cell, 2015. **58**(1): p. 172-185.
16. Grawunder, U., et al., *Activity of DNA ligase IV stimulated by complex formation with XRCC4 protein in mammalian cells.* Nature, 1997. **388**(6641): p. 492-495.
17. Gu, J., et al., *Single-stranded DNA ligation and XLF-stimulated incompatible DNA end ligation by the XRCC4-DNA ligase IV complex: influence of terminal DNA sequence.* Nucleic Acids Research, 2007. **35**(17): p. 5755-5762.
18. Ochi, T., et al., *PAXX, a paralog of XRCC4 and XLF, interacts with Ku to promote DNA double-strand break repair.* Science, 2015. **347**(6218): p. 185-188.
19. Takata, M., et al., *Homologous recombination and non-homologous end-joining pathways of DNA double-strand break repair have overlapping roles in the maintenance of chromosomal integrity in vertebrate cells.* EMBO J, 1998. **17**(18): p. 5497-508.
20. Lee, J.H. and T.T. Paull, *ATM activation by DNA double-strand breaks through the Mre11-Rad50-Nbs1 complex.* Science, 2005. **308**(5721): p. 551-4.
21. Limbo, O., et al., *Ctp1 is a cell-cycle-regulated protein that functions with Mre11 complex to control double-strand break repair by homologous recombination.* Mol Cell, 2007. **28**(1): p. 134-46.
22. Daley, J.M., et al., *Enhancement of BLM-DNA2-Mediated Long-Range DNA End Resection by CtIP.* Cell Rep, 2017. **21**(2): p. 324-332.
23. Kornberg, R.D., *Structure of Chromatin.* Annual Review of Biochemistry, 1977. **46**(1): p. 931-954.

24. Luger, K., et al., *Crystal structure of the nucleosome core particle at 2.8 Å resolution.* Nature, 1997. **389**(6648): p. 251-260.
25. Hauer, M.H. and S.M. Gasser, *Chromatin and nucleosome dynamics in DNA damage and repair.* Genes & development, 2017. **31**(22): p. 2204-2221.
26. Probst, A.V., E. Dunleavy, and G. Almouzni, *Epigenetic inheritance during the cell cycle.* Nat Rev Mol Cell Biol, 2009. **10**(3): p. 192-206.
27. Li, G. and D. Reinberg, *Chromatin higher-order structures and gene regulation.* Curr Opin Genet Dev, 2011. **21**(2): p. 175-86.
28. Smerdon, M.J., *DNA repair and the role of chromatin structure.* Current Opinion in Cell Biology, 1991. **3**(3): p. 422-428.
29. Soria, G., Sophie E. Polo, and G. Almouzni, *Prime, Repair, Restore: The Active Role of Chromatin in the DNA Damage Response.* Molecular Cell, 2012. **46**(6): p. 722-734.
30. Schuster-Böckler, B. and B. Lehner, *Chromatin organization is a major influence on regional mutation rates in human cancer cells.* Nature, 2012. **488**(7412): p. 504-507.
31. Price, B.D. and A.D. D'Andrea, *Chromatin remodeling at DNA double-strand breaks.* Cell, 2013. **152**(6): p. 1344-54.
32. Goodarzi, A.A., P. Jeggo, and M. Lobrich, *The influence of heterochromatin on DNA double strand break repair: Getting the strong, silent type to relax.* DNA Repair (Amst), 2010. **9**(12): p. 1273-82.
33. Fumagalli, M., et al., *Telomeric DNA damage is irreparable and causes persistent DNA-damage-response activation.* Nat Cell Biol, 2012. **14**(4): p. 355-65.
34. Azzalin, C.M., et al., *Telomeric repeat containing RNA and RNA surveillance factors at mammalian chromosome ends.* Science, 2007. **318**(5851): p. 798-801.
35. de Lange, T., *Shelterin: the protein complex that shapes and safeguards human telomeres.* Genes Dev, 2005. **19**(18): p. 2100-10.
36. Broccoli, D., et al., *Human telomeres contain two distinct Myb-related proteins, TRF1 and TRF2.* Nat Genet, 1997. **17**(2): p. 231-5.
37. Ye, J.Z., et al., *TIN2 binds TRF1 and TRF2 simultaneously and stabilizes the TRF2 complex on telomeres.* J Biol Chem, 2004. **279**(45): p. 47264-71.
38. Houghtaling, B.R., et al., *A dynamic molecular link between the telomere length regulator TRF1 and the chromosome end protector TRF2.* Curr Biol, 2004. **14**(18): p. 1621-31.
39. Hu, C., et al., *Structural and functional analyses of the mammalian TIN2-TPP1-TRF2 telomeric complex.* Cell Res, 2017. **27**(12): p. 1485-1502.
40. Loayza, D. and T. De Lange, *POT1 as a terminal transducer of TRF1 telomere length control.* Nature, 2003. **423**(6943): p. 1013-8.
41. Hockemeyer, D., et al., *Recent expansion of the telomeric complex in rodents: Two distinct POT1 proteins protect mouse telomeres.* Cell, 2006. **126**(1): p. 63-77.
42. Lazzerini-Denchi, E. and A. Sfeir, *Stop pulling my strings - what telomeres taught us about the DNA damage response.* Nat Rev Mol Cell Biol, 2016. **17**(6): p. 364-78.
43. Li, B., S. Oestreich, and T. de Lange, *Identification of human Rap1: implications for telomere evolution.* Cell, 2000. **101**(5): p. 471-83.
44. Takai, K.K., et al., *In vivo stoichiometry of shelterin components.* J Biol Chem, 2010. **285**(2): p. 1457-67.
45. de Lange, T., *Shelterin-Mediated Telomere Protection.* Annu Rev Genet, 2018. **52**: p. 223-247.
46. Ruis, P. and S.J. Boulton, *The end protection problem-an unexpected twist in the tail.* Genes Dev, 2021. **35**(1-2): p. 1-21.
47. Diotti, R. and D. Loayza, *Shelterin complex and associated factors at human telomeres.* Nucleus, 2011. **2**(2): p. 119-35.
48. Wu, P., et al., *Apollo contributes to G overhang maintenance and protects leading-end telomeres.* Mol Cell, 2010. **39**(4): p. 606-17.
49. Wu, P., H. Takai, and T. de Lange, *Telomeric 3' overhangs derive from resection by Exo1 and Apollo and fill-in by POT1b-associated CST.* Cell, 2012. **150**(1): p. 39-52.
50. Lingner, J., J.P. Cooper, and T.R. Cech, *Telomerase and DNA end replication: no longer a lagging strand problem?* Science, 1995. **269**(5230): p. 1533-4.

51. Maestroni, L., S. Matmati, and S. Coulon, *Solving the Telomere Replication Problem.* Genes (Basel), 2017. **8**(2).
52. d'Adda di Fagagna, F., et al., *A DNA damage checkpoint response in telomere-initiated senescence.* Nature, 2003. **426**(6963): p. 194-8.
53. Hoang, S.M. and R.J. O'Sullivan, *Alternative Lengthening of Telomeres: Building Bridges To Connect Chromosome Ends.* Trends Cancer, 2020. **6**(3): p. 247-260.
54. Hayashi, M.T., et al., *A telomere-dependent DNA damage checkpoint induced by prolonged mitotic arrest.* Nat Struct Mol Biol, 2012. **19**(4): p. 387-94.
55. Hayashi, M.T., et al., *Cell death during crisis is mediated by mitotic telomere deprotection.* Nature, 2015. **522**(7557): p. 492-6.
56. Maciejowski, J., et al., *Chromothripsis and Kataegis Induced by Telomere Crisis.* Cell, 2015. **163**(7): p. 1641-54.
57. von Morgen, P. and J. Maciejowski, *The ins and outs of telomere crisis in cancer.* Genome Med, 2018. **10**(1): p. 89.
58. Nik-Zainal, S., et al., *Mutational processes molding the genomes of 21 breast cancers.* Cell, 2012. **149**(5): p. 979-93.
59. Nassour, J., et al., *Autophagic cell death restricts chromosomal instability during replicative crisis.* Nature, 2019. **565**(7741): p. 659-663.
60. Kim, N.W., et al., *Specific association of human telomerase activity with immortal cells and cancer.* Science, 1994. **266**(5193): p. 2011-5.
61. Montanaro, L., et al., *Relationship between dyskerin expression and telomerase activity in human breast cancer.* Cell Oncol, 2008. **30**(6): p. 483-90.
62. Akincilar, S.C., et al., *Long-Range Chromatin Interactions Drive Mutant TERT Promoter Activation.* Cancer Discov, 2016. **6**(11): p. 1276-1291.
63. Chiba, K., et al., *Mutations in the promoter of the telomerase gene TERT contribute to tumorigenesis by a two-step mechanism.* Science, 2017. **357**(6358): p. 1416-1420.
64. Peifer, M., et al., *Telomerase activation by genomic rearrangements in high-risk neuroblastoma.* Nature, 2015. **526**(7575): p. 700-4.
65. Bryan, T.M., et al., *Evidence for an alternative mechanism for maintaining telomere length in human tumors and tumor-derived cell lines.* Nat Med, 1997. **3**(11): p. 1271-4.
66. Draskovic, I., et al., *Probing PML body function in ALT cells reveals spatiotemporal requirements for telomere recombination.* Proc Natl Acad Sci U S A, 2009. **106**(37): p. 15726-31.
67. Henson, J.D., et al., *DNA C-circles are specific and quantifiable markers of alternative-lengthening-of-telomeres activity.* Nat Biotechnol, 2009. **27**(12): p. 1181-5.
68. Cesare, A.J. and J.D. Griffith, *Telomeric DNA in ALT cells is characterized by free telomeric circles and heterogeneous t-loops.* Mol Cell Biol, 2004. **24**(22): p. 9948-57.
69. Dunham, M.A., et al., *Telomere maintenance by recombination in human cells.* Nat Genet, 2000. **26**(4): p. 447-50.
70. Londono-Vallejo, J.A., et al., *Alternative lengthening of telomeres is characterized by high rates of telomeric exchange.* Cancer Res, 2004. **64**(7): p. 2324-7.
71. Cesare, A.J., et al., *Spontaneous occurrence of telomeric DNA damage response in the absence of chromosome fusions.* Nat Struct Mol Biol, 2009. **16**(12): p. 1244-51.
72. Sobinoff, A.P. and H.A. Pickett, *Alternative Lengthening of Telomeres: DNA Repair Pathways Converge.* Trends Genet, 2017. **33**(12): p. 921-932.
73. Mason-Osann, E., et al., *Identification of a novel gene fusion in ALT positive osteosarcoma.* Oncotarget, 2018. **9**(67): p. 32868-32880.
74. Lovejoy, C.A., et al., *Loss of ATRX, genome instability, and an altered DNA damage response are hallmarks of the alternative lengthening of telomeres pathway.* PLoS Genet, 2012. **8**(7): p. e1002772.
75. Lewis, P.W., et al., *Daxx is an H3.3-specific histone chaperone and cooperates with ATRX in replication-independent chromatin assembly at telomeres.* Proc Natl Acad Sci U S A, 2010. **107**(32): p. 14075-80.
76. de Lange, T., *How telomeres solve the end-protection problem.* Science, 2009. **326**(5955): p. 948-52.

77. de Lange, T., *T-loops and the origin of telomeres.* Nat Rev Mol Cell Biol, 2004. **5**(4): p. 323-9.
78. Griffith, J.D., et al., *Mammalian telomeres end in a large duplex loop.* Cell, 1999. **97**(4): p. 503-14.
79. Doksani, Y. and T. de Lange, *The role of double-strand break repair pathways at functional and dysfunctional telomeres.* Cold Spring Harb Perspect Biol, 2014. **6**(12): p. a016576.
80. Doksani, Y., et al., *Super-resolution fluorescence imaging of telomeres reveals TRF2-dependent T-loop formation.* Cell, 2013. **155**(2): p. 345-356.
81. Benarroch-Popivker, D., et al., *TRF2-Mediated Control of Telomere DNA Topology as a Mechanism for Chromosome-End Protection.* Mol Cell, 2016. **61**(2): p. 274-86.
82. Wang, R.C., A. Smogorzewska, and T. de Lange, *Homologous recombination generates T-loop-sized deletions at human telomeres.* Cell, 2004. **119**(3): p. 355-68.
83. Saint-Leger, A., et al., *The basic N-terminal domain of TRF2 limits recombination endonuclease action at human telomeres.* Cell Cycle, 2014. **13**(15): p. 2469-74.
84. Schmutz, I., et al., *TRF2 binds branched DNA to safeguard telomere integrity.* Nat Struct Mol Biol, 2017. **24**(9): p. 734-742.
85. Nora, G.J., N.A. Buncher, and P.L. Opresko, *Telomeric protein TRF2 protects Holliday junctions with telomeric arms from displacement by the Werner syndrome helicase.* Nucleic Acids Res, 2010. **38**(12): p. 3984-98.
86. Poulet, A., et al., *TRF2 promotes, remodels and protects telomeric Holliday junctions.* EMBO J, 2009. **28**(6): p. 641-51.
87. Konishi, A., T. Izumi, and S. Shimizu, *TRF2 Protein Interacts with Core Histones to Stabilize Chromosome Ends.* J Biol Chem, 2016. **291**(39): p. 20798-810.
88. Vannier, J.B., et al., *RTEL1 dismantles T loops and counteracts telomeric G4-DNA to maintain telomere integrity.* Cell, 2012. **149**(4): p. 795-806.
89. Uringa, E.J., et al., *RTEL1 contributes to DNA replication and repair and telomere maintenance.* Mol Biol Cell, 2012. **23**(14): p. 2782-92.
90. Sarek, G., et al., *CDK phosphorylation of TRF2 controls t-loop dynamics during the cell cycle.* Nature, 2019. **575**(7783): p. 523-527.
91. Stracker, T.H. and J.H. Petrini, *The MRE11 complex: starting from the ends.* Nat Rev Mol Cell Biol, 2011. **12**(2): p. 90-103.
92. Denchi, E.L. and T. de Lange, *Protection of telomeres through independent control of ATM and ATR by TRF2 and POT1.* Nature, 2007. **448**(7157): p. 1068-71.
93. Celli, G.B. and T. de Lange, *DNA processing is not required for ATM-mediated telomere damage response after TRF2 deletion.* Nat Cell Biol, 2005. **7**(7): p. 712-8.
94. Sfeir, A., et al., *Loss of Rap1 induces telomere recombination in the absence of NHEJ or a DNA damage signal.* Science, 2010. **327**(5973): p. 1657-61.
95. Sfeir, A., et al., *Mammalian telomeres resemble fragile sites and require TRF1 for efficient replication.* Cell, 2009. **138**(1): p. 90-103.
96. Takai, K.K., et al., *Telomere protection by TPP1/POT1 requires tethering to TIN2.* Mol Cell, 2011. **44**(4): p. 647-59.
97. Timashev, L.A. and T. De Lange, *Characterization of t-loop formation by TRF2.* Nucleus, 2020. **11**(1): p. 164-177.
98. Bandaria, J.N., et al., *Shelterin Protects Chromosome Ends by Compacting Telomeric Chromatin.* Cell, 2016. **164**(4): p. 735-46.
99. Timashev, L.A., et al., *The DDR at telomeres lacking intact shelterin does not require substantial chromatin decompaction.* Genes Dev, 2017. **31**(6): p. 578-589.
100. Vancevska, A., et al., *The telomeric DNA damage response occurs in the absence of chromatin decompaction.* Genes Dev, 2017. **31**(6): p. 567-577.
101. Karlseder, J., et al., *The telomeric protein TRF2 binds the ATM kinase and can inhibit the ATM-dependent DNA damage response.* PLoS Biol, 2004. **2**(8): p. E240.
102. Doksani, Y. and T. de Lange, *Telomere-Internal Double-Strand Breaks Are Repaired by Homologous Recombination and PARP1/Lig3-Dependent End-Joining.* Cell Rep, 2016. **17**(6): p. 1646-1656.

103. Tang, J., et al., *Acetylation limits 53BP1 association with damaged chromatin to promote homologous recombination.* Nat Struct Mol Biol, 2013. **20**(3): p. 317-25.
104. Saldivar, J.C., D. Cortez, and K.A. Cimprich, *The essential kinase ATR: ensuring faithful duplication of a challenging genome.* Nat Rev Mol Cell Biol, 2017. **18**(10): p. 622-636.
105. Zou, L. and S.J. Elledge, *Sensing DNA damage through ATRIP recognition of RPA-ssDNA complexes.* Science, 2003. **300**(5625): p. 1542-8.
106. Thada, V. and D. Cortez, *Common motifs in ETAA1 and TOPBP1 required for ATR kinase activation.* J Biol Chem, 2019. **294**(21): p. 8395-8402.
107. Achuthankutty, D., et al., *Regulation of ETAA1-mediated ATR activation couples DNA replication fidelity and genome stability.* J Cell Biol, 2019. **218**(12): p. 3943-3953.
108. Kumagai, A., et al., *TopBP1 activates the ATR-ATRIP complex.* Cell, 2006. **124**(5): p. 943-55.
109. Gong, Y. and T. de Lange, *A Shld1-controlled POT1a provides support for repression of ATR signaling at telomeres through RPA exclusion.* Mol Cell, 2010. **40**(3): p. 377-87.
110. Frescas, D. and T. de Lange, *Binding of TPP1 protein to TIN2 protein is required for POT1a,b protein-mediated telomere protection.* J Biol Chem, 2014. **289**(35): p. 24180-7.
111. Hockemeyer, D., et al., *Telomere protection by mammalian Pot1 requires interaction with Tpp1.* Nat Struct Mol Biol, 2007. **14**(8): p. 754-61.
112. Flynn, R.L., et al., *TERRA and hnRNPA1 orchestrate an RPA-to-POT1 switch on telomeric single-stranded DNA.* Nature, 2011. **471**(7339): p. 532-6.
113. Porro, A., et al., *Molecular dissection of telomeric repeat-containing RNA biogenesis unveils the presence of distinct and multiple regulatory pathways.* Mol Cell Biol, 2010. **30**(20): p. 4808-17.
114. Ray, S., et al., *G-quadruplex formation in telomeres enhances POT1/TPP1 protection against RPA binding.* Proc Natl Acad Sci U S A, 2014. **111**(8): p. 2990-5.
115. Maciejowski, J. and T. de Lange, *Telomeres in cancer: tumour suppression and genome instability.* Nat Rev Mol Cell Biol, 2017. **18**(3): p. 175-186.
116. Arnoult, N., et al., *Regulation of DNA repair pathway choice in S and G2 phases by the NHEJ inhibitor CYREN.* Nature, 2017. **549**(7673): p. 548-552.
117. Konishi, A. and T. de Lange, *Cell cycle control of telomere protection and NHEJ revealed by a ts mutation in the DNA-binding domain of TRF2.* Genes Dev, 2008. **22**(9): p. 1221-30.
118. Dimitrova, N., et al., *53BP1 promotes non-homologous end joining of telomeres by increasing chromatin mobility.* Nature, 2008. **456**(7221): p. 524-8.
119. Lottersberger, F., et al., *53BP1 and the LINC Complex Promote Microtubule-Dependent DSB Mobility and DNA Repair.* Cell, 2015. **163**(4): p. 880-93.
120. Rai, R., et al., *The function of classical and alternative non-homologous end-joining pathways in the fusion of dysfunctional telomeres.* EMBO J, 2010. **29**(15): p. 2598-610.
121. Okamoto, K., et al., *A two-step mechanism for TRF2-mediated chromosome-end protection.* Nature, 2013. **494**(7438): p. 502-5.
122. Shao, G., et al., *The Rap80-BRCC36 de-ubiquitinating enzyme complex antagonizes RNF8-Ubc13-dependent ubiquitination events at DNA double strand breaks.* Proc Natl Acad Sci U S A, 2009. **106**(9): p. 3166-71.
123. Gudjonsson, T., et al., *TRIP12 and UBR5 suppress spreading of chromatin ubiquitylation at damaged chromosomes.* Cell, 2012. **150**(4): p. 697-709.
124. Kabir, S., D. Hockemeyer, and T. de Lange, *TALEN gene knockouts reveal no requirement for the conserved human shelterin protein Rap1 in telomere protection and length regulation.* Cell Rep, 2014. **9**(4): p. 1273-80.
125. Sarthy, J., et al., *Human RAP1 inhibits non-homologous end joining at telomeres.* EMBO J, 2009. **28**(21): p. 3390-9.
126. van Steensel, B., A. Smogorzewska, and T. de Lange, *TRF2 protects human telomeres from end-to-end fusions.* Cell, 1998. **92**(3): p. 401-13.
127. Sfeir, A. and T. de Lange, *Removal of shelterin reveals the telomere end-protection problem.* Science, 2012. **336**(6081): p. 593-7.

128. Sfeir, A. and L.S. Symington, *Microhomology-Mediated End Joining: A Back-up Survival Mechanism or Dedicated Pathway?* Trends Biochem Sci, 2015. **40**(11): p. 701-714.
129. Truong, L.N., et al., *Microhomology-mediated End Joining and Homologous Recombination share the initial end resection step to repair DNA double-strand breaks in mammalian cells.* Proc Natl Acad Sci U S A, 2013. **110**(19): p. 7720-5.
130. Mateos-Gomez, P.A., et al., *Mammalian polymerase theta promotes alternative NHEJ and suppresses recombination.* Nature, 2015. **518**(7538): p. 254-7.
131. Capper, R., et al., *The nature of telomere fusion and a definition of the critical telomere length in human cells.* Genes Dev, 2007. **21**(19): p. 2495-508.
132. Bailey, S.M., et al., *Strand-specific postreplicative processing of mammalian telomeres.* Science, 2001. **293**(5539): p. 2462-5.
133. Wu, L., et al., *Pot1 deficiency initiates DNA damage checkpoint activation and aberrant homologous recombination at telomeres.* Cell, 2006. **126**(1): p. 49-62.
134. Wang, Y., G. Ghosh, and E.A. Hendrickson, *Ku86 represses lethal telomere deletion events in human somatic cells.* Proc Natl Acad Sci U S A, 2009. **106**(30): p. 12430-5.
135. Palm, W., et al., *Functional dissection of human and mouse POT1 proteins.* Mol Cell Biol, 2009. **29**(2): p. 471-82.
136. Fiscella, M., et al., *Wip1, a novel human protein phosphatase that is induced in response to ionizing radiation in a p53-dependent manner.* Proc Natl Acad Sci U S A, 1997. **94**(12): p. 6048-53.
137. Macurek, L., et al., *Wip1 phosphatase is associated with chromatin and dephosphorylates [gamma]H2AX to promote checkpoint inhibition.* Oncogene, 2010. **29**(15): p. 2281-2291.
138. Lammers, T. and S. Lavi, *Role of type 2C protein phosphatases in growth regulation and in cellular stress signaling.* Crit Rev Biochem Mol Biol, 2007. **42**(6): p. 437-61.
139. Yamaguchi, H., et al., *The Wip1 phosphatase PPM1D dephosphorylates SQ/TQ motifs in checkpoint substrates phosphorylated by PI3K-like kinases.* Biochemistry, 2007. **46**(44): p. 12594-603.
140. Gilmartin, A.G., et al., *Allosteric Wip1 phosphatase inhibition through flap-subdomain interaction.* Nat Chem Biol, 2014. **10**(3): p. 181-7.
141. Shreeram, S., et al., *Wip1 phosphatase modulates ATM-dependent signaling pathways.* Mol Cell, 2006. **23**(5): p. 757-64.
142. Lu, X., B. Nannenga, and L.A. Donehower, *PPM1D dephosphorylates Chk1 and p53 and abrogates cell cycle checkpoints.* Genes Dev, 2005. **19**(10): p. 1162-74.
143. Fujimoto, H., et al., *Regulation of the antioncogenic Chk2 kinase by the oncogenic Wip1 phosphatase.* Cell Death Differ, 2006. **13**(7): p. 1170-80.
144. Maltzman, W. and L. Czyzyk, *UV irradiation stimulates levels of p53 cellular tumor antigen in nontransformed mouse cells.* Mol Cell Biol, 1984. **4**(9): p. 1689-94.
145. Haupt, Y., et al., *Mdm2 promotes the rapid degradation of p53.* Nature, 1997. **387**(6630): p. 296-9.
146. Shieh, S.Y., et al., *DNA damage-induced phosphorylation of p53 alleviates inhibition by MDM2.* Cell, 1997. **91**(3): p. 325-34.
147. Pei, D., Y. Zhang, and J. Zheng, *Regulation of p53: a collaboration between Mdm2 and Mdmx.* Oncotarget, 2012. **3**(3): p. 228-35.
148. Wang, X., J. Wang, and X. Jiang, *MdmX protein is essential for Mdm2 protein-mediated p53 polyubiquitination.* J Biol Chem, 2011. **286**(27): p. 23725-34.
149. Barak, Y., et al., *mdm2 expression is induced by wild type p53 activity.* EMBO J, 1993. **12**(2): p. 461-8.
150. Lu, X., et al., *The Wip1 Phosphatase acts as a gatekeeper in the p53-Mdm2 autoregulatory loop.* Cancer Cell, 2007. **12**(4): p. 342-54.
151. Zhang, X., et al., *Phosphorylation and degradation of MdmX is inhibited by Wip1 phosphatase in the DNA damage response.* Cancer Res, 2009. **69**(20): p. 7960-8.
152. Andrysik, Z., et al., *PPM1D suppresses p53-dependent transactivation and cell death by inhibiting the Integrated Stress Response.* Nat Commun, 2022. **13**(1): p. 7400.
153. Kinner, A., et al., *Gamma-H2AX in recognition and signaling of DNA double-strand breaks in the context of chromatin.* Nucleic Acids Res, 2008. **36**(17): p. 5678-94.

154. Pechackova, S., K. Burdova, and L. Macurek, *WIP1 phosphatase as pharmacological target in cancer therapy.* J Mol Med (Berl), 2017. **95**(6): p. 589-599.
155. Brazina, J., et al., *DNA damage-induced regulatory interplay between DAXX, p53, ATM kinase and Wip1 phosphatase.* Cell Cycle, 2015. **14**(3): p. 375-87.
156. Nguyen, T.A., et al., *The oncogenic phosphatase WIP1 negatively regulates nucleotide excision repair.* DNA Repair (Amst), 2010. **9**(7): p. 813-23.
157. Storchova, R., et al., *A novel assay for screening WIP1 phosphatase substrates in nuclear extracts.* FEBS J, 2021. **288**(20): p. 6035-6051.
158. Lee, Y.K., et al., *Doxorubicin down-regulates Kruppel-associated box domain-associated protein 1 sumoylation that relieves its transcription repression on p21WAF1/CIP1 in breast cancer MCF-7 cells.* J Biol Chem, 2007. **282**(3): p. 1595-606.
159. Blasius, M., et al., *A phospho-proteomic screen identifies substrates of the checkpoint kinase Chk1.* Genome Biol, 2011. **12**(8): p. R78.
160. Donehower, L.A., *Phosphatases reverse p53-mediated cell cycle checkpoints.* Proc Natl Acad Sci U S A, 2014. **111**(20): p. 7172-3.
161. Shaltiel, I.A., et al., *Distinct phosphatases antagonize the p53 response in different phases of the cell cycle.* Proc Natl Acad Sci U S A, 2014. **111**(20): p. 7313-8.
162. Lu, X., et al., *The p53-induced oncogenic phosphatase PPM1D interacts with uracil DNA glycosylase and suppresses base excision repair.* Mol Cell, 2004. **15**(4): p. 621-34.
163. Takekawa, M., et al., *p53-inducible wip1 phosphatase mediates a negative feedback regulation of p38 MAPK-p53 signaling in response to UV radiation.* Embo j, 2000. **19**(23): p. 6517-26.
164. Macurek, L., et al., *Wip1 phosphatase is associated with chromatin and dephosphorylates gammaH2AX to promote checkpoint inhibition.* Oncogene, 2010. **29**(15): p. 2281-91.
165. Chew, J., et al., *WIP1 phosphatase is a negative regulator of NF-kappaB signalling.* Nat Cell Biol, 2009. **11**(5): p. 659-66.
166. Torii, S., et al., *Identification of PPM1D as an essential Ulk1 phosphatase for genotoxic stress-induced autophagy.* EMBO Rep, 2016. **17**(11): p. 1552-1564.
167. Peng, B., et al., *Modulation of LSD1 phosphorylation by CK2/WIP1 regulates RNF168-dependent 53BP1 recruitment in response to DNA damage.* Nucleic Acids Res, 2015. **43**(12): p. 5936-47.
168. Zhang, M., et al., *PPM1D phosphatase, a target of p53 and RBM38 RNA-binding protein, inhibits p53 mRNA translation via dephosphorylation of RBM38.* Oncogene, 2015. **34**(48): p. 5900-11.
169. Park, D.S., et al., *Wip1 regulates Smad4 phosphorylation and inhibits TGF-beta signaling.* EMBO Rep, 2020. **21**(5): p. e48693.
170. Tammaro, M., et al., *Replication-dependent and transcription-dependent mechanisms of DNA double-strand break induction by the topoisomerase 2-targeting drug etoposide.* PLoS One, 2013. **8**(11): p. e79202.
171. Gothe, H.J., et al., *Spatial Chromosome Folding and Active Transcription Drive DNA Fragility and Formation of Oncogenic MLL Translocations.* Mol Cell, 2019. **75**(2): p. 267-283 e12.
172. Kim, D.I., et al., *An improved smaller biotin ligase for BioID proximity labeling.* Mol Biol Cell, 2016. **27**(8): p. 1188-96.
173. Chuman, Y., et al., *Characterization of the active site and a unique uncompetitive inhibitor of the PPM1-type protein phosphatase PPM1D.* Protein Pept Lett, 2008. **15**(9): p. 938-48.
174. Peuscher, M.H. and J.J. Jacobs, *Posttranslational control of telomere maintenance and the telomere damage response.* Cell Cycle, 2012. **11**(8): p. 1524-34.
175. Walker, J.R. and X.D. Zhu, *Post-translational modifications of TRF1 and TRF2 and their roles in telomere maintenance.* Mech Ageing Dev, 2012. **133**(6): p. 421-34.
176. Matsuoka, S., et al., *ATM and ATR substrate analysis reveals extensive protein networks responsive to DNA damage.* Science, 2007. **316**(5828): p. 1160-6.
177. Sarek, G., et al., *TRF2 recruits RTEL1 to telomeres in S phase to promote t-loop unwinding.* Mol Cell, 2015. **57**(4): p. 622-635.

178. Tanaka, H., et al., *DNA damage-induced phosphorylation of the human telomere-associated protein TRF2.* Proc Natl Acad Sci U S A, 2005. **102**(43): p. 15539-44.
179. Huda, N., et al., *DNA damage-induced phosphorylation of TRF2 is required for the fast pathway of DNA double-strand break repair.* Mol Cell Biol, 2009. **29**(13): p. 3597-604.
180. Bradshaw, P.S., D.J. Stavropoulos, and M.S. Meyn, *Human telomeric protein TRF2 associates with genomic double-strand breaks as an early response to DNA damage.* Nat Genet, 2005. **37**(2): p. 193-7.
181. van Overbeek, M. and T. de Lange, *Apollo, an Artemis-related nuclease, interacts with TRF2 and protects human telomeres in S phase.* Curr Biol, 2006. **16**(13): p. 1295-302.
182. Wan, B., et al., *SLX4 assembles a telomere maintenance toolkit by bridging multiple endonucleases with telomeres.* Cell Rep, 2013. **4**(5): p. 861-9.
183. Chen, Y., et al., *A shared docking motif in TRF1 and TRF2 used for differential recruitment of telomeric proteins.* Science, 2008. **319**(5866): p. 1092-6.
184. Jumper, J., et al., *Highly accurate protein structure prediction with AlphaFold.* Nature, 2021. **596**(7873): p. 583-589.
185. Fradet-Turcotte, A., et al., *53BP1 is a reader of the DNA-damage-induced H2A Lys 15 ubiquitin mark.* Nature, 2013. **499**(7456): p. 50-4.
186. Kaur, P., et al., *TIN2 is an architectural protein that facilitates TRF2-mediated trans- and cis-interactions on telomeric DNA.* Nucleic Acids Res, 2021. **49**(22): p. 13000-13018.
187. Tong, A.S., et al., *ATM and ATR Signaling Regulate the Recruitment of Human Telomerase to Telomeres.* Cell Rep, 2015. **13**(8): p. 1633-46.
188. Mendez-Bermudez, A., et al., *Genome-wide Control of Heterochromatin Replication by the Telomere Capping Protein TRF2.* Mol Cell, 2018. **70**(3): p. 449-461.e5.
189. Mukherjee, A.K., et al., *Telomere repeat-binding factor 2 binds extensively to extra-telomeric G-quadruplexes and regulates the epigenetic status of several gene promoters.* J Biol Chem, 2019. **294**(47): p. 17709-17722.
190. Mao, Z., et al., *TRF2 is required for repair of nontelomeric DNA double-strand breaks by homologous recombination.* Proc Natl Acad Sci U S A, 2007. **104**(32): p. 13068-73.
191. Kong, X., et al., *Biphasic recruitment of TRF2 to DNA damage sites promotes non-sister chromatid homologous recombination repair.* J Cell Sci, 2018. **131**(23).
192. Huda, N., et al., *Recruitment of TRF2 to laser-induced DNA damage sites.* Free Radic Biol Med, 2012. **53**(5): p. 1192-7.
193. Baumann, P. and T.R. Cech, *Pot1, the putative telomere end-binding protein in fission yeast and humans.* Science, 2001. **292**(5519): p. 1171-5.
194. Liu, D., et al., *PTOP interacts with POT1 and regulates its localization to telomeres.* Nat Cell Biol, 2004. **6**(7): p. 673-80.
195. Kibe, T., M. Zimmermann, and T. de Lange, *TPP1 Blocks an ATR-Mediated Resection Mechanism at Telomeres.* Mol Cell, 2016. **61**(2): p. 236-46.
196. Stolarova, L., et al., *Identification of Germline Mutations in Melanoma Patients with Early Onset, Double Primary Tumors, or Family Cancer History by NGS Analysis of 217 Genes.* Biomedicines, 2020. **8**(10).
197. Lei, M., E.R. Podell, and T.R. Cech, *Structure of human POT1 bound to telomeric single-stranded DNA provides a model for chromosome end-protection.* Nat Struct Mol Biol, 2004. **11**(12): p. 1223-9.
198. Chen, C., et al., *Structural insights into POT1-TPP1 interaction and POT1 C-terminal mutations in human cancer.* Nat Commun, 2017. **8**: p. 14929.
199. Shen, E., et al., *POT1 mutation spectrum in tumour types commonly diagnosed among POT1-associated hereditary cancer syndrome families.* J Med Genet, 2020. **57**(10): p. 664-670.
200. Wu, Y., R.C. Poulos, and R.R. Reddel, *Role of POT1 in Human Cancer.* Cancers (Basel), 2020. **12**(10).
201. Calvete, O., et al., *A mutation in the POT1 gene is responsible for cardiac angiosarcoma in TP53-negative Li-Fraumeni-like families.* Nat Commun, 2015. **6**: p. 8383.
202. Calvete, O., et al., *The wide spectrum of POT1 gene variants correlates with multiple cancer types.* Eur J Hum Genet, 2017. **25**(11): p. 1278-1281.

203. Bulavin, D.V., et al., *Amplification of PPM1D in human tumors abrogates p53 tumor-suppressor activity.* Nat Genet, 2002. **31**(2): p. 210-5.
204. Bulavin, D.V., et al., *Inactivation of the Wip1 phosphatase inhibits mammary tumorigenesis through p38 MAPK-mediated activation of the p16(Ink4a)-p19(Arf) pathway.* Nat Genet, 2004. **36**(4): p. 343-50.
205. Tang, Y., et al., *Acetylation is indispensable for p53 activation.* Cell, 2008. **133**(4): p. 612-26.
206. Luo, J., et al., *Acetylation of p53 augments its site-specific DNA binding both in vitro and in vivo.* Proc Natl Acad Sci U S A, 2004. **101**(8): p. 2259-64.
207. Barlev, N.A., et al., *Acetylation of p53 activates transcription through recruitment of coactivators/histone acetyltransferases.* Mol Cell, 2001. **8**(6): p. 1243-54.
208. Gu, W. and R.G. Roeder, *Activation of p53 sequence-specific DNA binding by acetylation of the p53 C-terminal domain.* Cell, 1997. **90**(4): p. 595-606.
209. Zannini, L., et al., *DBC1 phosphorylation by ATM/ATR inhibits SIRT1 deacetylase in response to DNA damage.* J Mol Cell Biol, 2012. **4**(5): p. 294-303.
210. Jenkins, L.M., et al., *Two distinct motifs within the p53 transactivation domain bind to the Taz2 domain of p300 and are differentially affected by phosphorylation.* Biochemistry, 2009. **48**(6): p. 1244-55.
211. Li, Q., et al., *PP2Cdelta inhibits p300-mediated p53 acetylation via ATM/BRCA1 pathway to impede DNA damage response in breast cancer.* Sci Adv, 2019. **5**(10): p. eaaw8417.
212. Graf, J.F., et al., *Substrate spectrum of PPM1D in the cellular response to DNA double-strand breaks.* iScience, 2022. **25**(9): p. 104892.
213. Nitiss, J.L., *Targeting DNA topoisomerase II in cancer chemotherapy.* Nat Rev Cancer, 2009. **9**(5): p. 338-50.
214. Kahn, J.D., et al., *PPM1D-truncating mutations confer resistance to chemotherapy and sensitivity to PPM1D inhibition in hematopoietic cells.* Blood, 2018. **132**(11): p. 1095-1105.
215. Faruqi, A. and P. Tadi, *Cytarabine*, in *StatPearls*. 2023: Treasure Island (FL).
216. Salvador Moreno, N., et al., *The nuclear structural protein NuMA is a negative regulator of 53BP1 in DNA double-strand break repair.* Nucleic Acids Res, 2019. **47**(6): p. 2703-2715.
217. Chapman, J.R., et al., *RIF1 is essential for 53BP1-dependent nonhomologous end joining and suppression of DNA double-strand break resection.* Mol Cell, 2013. **49**(5): p. 858-71.
218. Zhao, W., et al., *BRCA1-BARD1 promotes RAD51-mediated homologous DNA pairing.* Nature, 2017. **550**(7676): p. 360-365.
219. Linke, S.P., et al., *p53 interacts with hRAD51 and hRAD54, and directly modulates homologous recombination.* Cancer Res, 2003. **63**(10): p. 2596-605.
220. Arias-Lopez, C., et al., *p53 modulates homologous recombination by transcriptional regulation of the RAD51 gene.* EMBO Rep, 2006. **7**(2): p. 219-24.
221. Gatz, S.A. and L. Wiesmuller, *p53 in recombination and repair.* Cell Death Differ, 2006. **13**(6): p. 1003-16.
222. Farmer, H., et al., *Targeting the DNA repair defect in BRCA mutant cells as a therapeutic strategy.* Nature, 2005. **434**(7035): p. 917-21.
223. Bryant, H.E., et al., *Specific killing of BRCA2-deficient tumours with inhibitors of poly(ADP-ribose) polymerase.* Nature, 2005. **434**(7035): p. 913-7.
224. Pechackova, S., et al., *Inhibition of WIP1 phosphatase sensitizes breast cancer cells to genotoxic stress and to MDM2 antagonist nutlin-3.* Oncotarget, 2016. **7**(12): p. 14458-75.
225. Sriraman, A., et al., *Cooperation of Nutlin-3a and a Wip1 inhibitor to induce p53 activity.* Oncotarget, 2016. **7**(22): p. 31623-38.
226. Chen, Z., et al., *Wip1 inhibitor GSK2830371 inhibits neuroblastoma growth by inducing Chk2/p53-mediated apoptosis.* Sci Rep, 2016. **6**: p. 38011.
227. Wu, C.E., et al., *Targeting negative regulation of p53 by MDM2 and WIP1 as a therapeutic strategy in cutaneous melanoma.* Br J Cancer, 2018. **118**(4): p. 495-508.

9 REPRINTS OF PUBLICATIONS

1154–1172 *Nucleic Acids Research, 2023, Vol. 51, No. 3* *Published online 18 January 2023*
https://doi.org/10.1093/nar/gkac1269

Phosphorylation of TRF2 promotes its interaction with TIN2 and regulates DNA damage response at telomeres

Radka Storchova[1,†], Matous Palek[1,†], Natalie Palkova[1], Pavel Veverka[2], Tomas Brom[2], Ctirad Hofr[2] and Libor Macurek[1,*]

[1]Cancer Cell Biology, Institute of Molecular Genetics of the Czech Academy of Sciences, Prague CZ-14220, Czech Republic and [2]LifeB, Functional Genomics and Proteomics, National Centre for Biomolecular Research, Faculty of Science, Masaryk University, Brno CZ-62500, Czech Republic

Received July 11, 2022; Revised November 25, 2022; Editorial Decision December 21, 2022; Accepted December 23, 2022

ABSTRACT

Protein phosphatase magnesium-dependent 1 delta (PPM1D) terminates the cell cycle checkpoint by dephosphorylating the tumour suppressor protein p53. By targeting additional substrates at chromatin, PPM1D contributes to the control of DNA damage response and DNA repair. Using proximity biotinylation followed by proteomic analysis, we identified a novel interaction between PPM1D and the shelterin complex that protects telomeric DNA. In addition, confocal microscopy revealed that endogenous PPM1D localises at telomeres. Further, we found that ATR phosphorylated TRF2 at S410 after induction of DNA double strand breaks at telomeres and this modification increased after inhibition or loss of PPM1D. TRF2 phosphorylation stimulated its interaction with TIN2 both in vitro and at telomeres. Conversely, induced expression of PPM1D impaired localisation of TIN2 and TPP1 at telomeres. Finally, recruitment of the DNA repair factor 53BP1 to the telomeric breaks was strongly reduced after inhibition of PPM1D and was rescued by the expression of TRF2-S410A mutant. Our results suggest that TRF2 phosphorylation promotes the association of TIN2 within the shelterin complex and regulates DNA repair at telomeres.

INTRODUCTION

Genome instability is one of the hallmarks of cancer cells (1). DNA damage response driven by Ataxia telangiectasia mutated (ATM) and Ataxia telangiectasia and Rad3-related protein (ATR) kinases represents a surveillance mechanism that protects genome integrity by orchestrating a temporal cell cycle arrest and DNA repair (2–4). DNA double strand breaks (DSBs) are repaired either by non-homologous end joining (NHEJ) or by homologous recombination (HR). Protein phosphatase magnesium-dependent 1 delta (PPM1D, also known as WIP1) promotes recovery from the G2 checkpoint by counteracting activities of the tumour suppressor p53 and KRAB-interacting protein 1 (KAP1) (5,6). In addition, PPM1D terminates DNA damage response by directly targeting ATM, histone H2AX, BRCA1 and other proteins at the chromatin flanking the DNA lesions (7–10). Amplification of the *PPM1D* locus or gain-of-function mutations in the last exon of PPM1D have been reported to promote tumorigenesis by inhibiting p53 pathway and are commonly found in various solid tumours and haematological malignancies (11–14).

Although essential for preventing global genome instability, DNA repair at the ends of chromosomes needs to be actively suppressed to prevent the fusion of telomeric DNA (15). Integrity of the telomeres is protected by the shelterin complex comprising of telomeric repeat-binding factor 1 (TRF1), telomeric repeat-binding factor 2 (TRF2), TRF2-interacting telomeric protein 1 (TERF2IP; further referred to as RAP1), TRF1-interacting nuclear protein 2 (TIN2; also known as TINF2), protection of telomeres protein 1 (POT1), and Adrenocortical dysplasia protein homolog (ACD, hereafter referred to as TPP1) (16). TRF1 and TRF2 form homodimers through the TRFH domains, and they bind the TTAGGG repeats in the double-stranded telomeric DNA through their C-terminal Myb domains (17). In addition, the N-terminal basic domain of TRF2 can bind branched DNA structures and the double stranded DNA also wraps around the TRFH domain of TRF2 (18–20). The heterodimer comprising of TPP1 and POT1 associates with the single-stranded DNA through two oligonucleotide/oligosaccharide-binding (OB) folds of POT1 (21,22). In addition, TPP1 also promotes the recruitment of the telomerase (23). TIN2 bridges the TRF1 and TRF2 homodimers with TPP1 and prevents activation of

*To whom correspondence should be addressed. Tel: +420 241063210; Email: macurek@img.cas.cz
†The authors wish it to be known that, in their opinion, the first two authors should be regarded as Joint First Authors.

ATR by stabilizing TPP1-POT1 at telomeric ssDNA (24–26). Similarly, TIN2 promotes TRF2 binding to telomeres thus protecting telomeric DNA from uncapping and from activation of ATM (26–29). Structural studies have revealed that TIN2 interacts with the TRFH domains of TRF1 and TRF2, and with a short motif between the residues 392–408 of TRF2 (hereafter referred to as a TIN2-binding motif, TBM) (30,31). Due to its unique DNA-binding ability, TRF2 promotes the folding of the telomeric DNA into a lasso-like structure referred to as a t-loop that prevents activation of ATM (15,32,33). In addition, the basic domain of TRF2 has been reported to prevent unwinding of the t-loops whereas recruitment of the Regulator of telomere elongation helicase 1 (RTEL1) by TRF2 promotes telomere unwinding during the replication (20,34,35). Loss of TRF2 leads to exposure of the DNA end, causing activation of ATM followed by ubiquitination-dependent recruitment of 53BP1 (forming nuclear patches termed Telomere dysfunction-Induced Foci (TIFs)) and subsequent fusion of telomeres by NHEJ (36–38). In contrast to TRF2, TRF1 is required for replication of the telomeric DNA and its loss leads to telomeric fragility (39). Single-molecule imag-ing revealed the ability of TIN2 and TRF2 to compact the telomeric DNA *in vitro*; however, the importance of DNA de-compaction for DNA repair at telomeres still remains unclear (40–43).

Here, we aimed to identify new substrates of PPM1D at chromatin. Using proximity biotinylation assay and immunoprecipitation, we identified the shelterin complex as a major interacting partner of PPM1D in human cells. Confocal microscopy confirmed a close association between PPM1D and shelterin at telomeres in various cell types. Since PPM1D directly interacted with TRF2 *in vitro*, we evaluated the ability of PPM1D to dephosphorylate TRF2 in cells. We found that ATR phosphorylated TRF2 at S410 upon CRISPR Cas9-mediated induction of DNA breaks at telomeres. Inhibition or loss of PPM1D significantly increased the level of TRF2-S410 phosphorylation. In addition, PPM1D dephosphorylated TRF2 *in vitro*. Importantly, increased phosphorylation of TRF2-S410 in cells treated with PPM1D inhibitor promoted the association of TIN2 with the damaged telomeres and prevented recruitment of the DNA repair factor 53BP1. Inversely, the expression of a non-phosphorylatable mutant TRF2-S410A rescued the recruitment of 53BP1 to DSBs at telomeres in cells treated with PPM1D inhibitor. Furthermore, overexpression of PPM1D impeded with assembly of the shelterin at telomeres and promoted telomeric fusions. We conclude that ATR and PPM1D control the binding of TIN2 at telomeres by inversely regulating the phosphorylation of TRF2 at S410.

MATERIALS AND METHODS

Cells

Human hTERT-immortalized RPE1 cells (here referred to as RPE), HEK293, human breast adenocarcinoma MCF7 or human osteosarcoma U2OS cells were grown in DMEM supplemented with 6% FBS (Gibco), Penicillin and Streptomycin. U2OS-PPM1D-KO cells with a knock-out of PPM1D were described previously (44). HeLa cells with doxycycline-inducible knock-down of TRF2 were described previously (45). HeLa-shTRF2 cells were transfected by pEGFP-TRF2 or pEGFP-TRF2-S410A and selected with geneticin followed by single cell clone expansion. RPE1 cells transfected with pCW57-GFP-P2A-PPM1D-A380 plasmid were selected by geneticin for 3 weeks followed by single clone expansion and expression of the catalytic domain of PPM1D was induced by doxycycline. All cells were regularly tested for mycoplasma infection using MycoAlert kit (Lonza). Plasmid DNA transfection was performed using polyethylenimine in ratio 1:6. Stable cell lines were generated by transfection of HEK293 cells with plasmid pBIOID2-HA or pBIOID2-PPM1D-D314A followed by 3 weeks selection with geneticin and expansion of single cell clones. Silencer Select siRNAs were transfected using RNAiMAX (both Thermo Scientific) at final concentration 5 nM and cells were analyzed after 2 days. Alternatively, two subsequent rounds of siRNA transfection were performed and cells were analyzed after 4 days. Expression of Cas9 was induced in iCut-RPE1 cells by overnight treatment with doxycycline and Shield-1 (1 mM, Aobious) and telomeric DNA damage was generated by transfection of the synthetic sgRNA TTAGGGTTAGGGTTAGGGTT (Sigma) as described previously (46,47). sgRNA was transfected by Lipofectamine RNAiMAX (Thermofisher) at final concentration 5 nM.

Plasmids

Coding sequence of human TRF2 was PCR amplified from pLPC-NMyc-TRF2 (Addgene ID: 16066) (48) and inserted in frame into pEGFP plasmid. Mutagenesis of TRF2 was performed using PCR amplification followed by ligation of DNA fragments into pEGFP backbone by Gibson assembly kit (NEB). Correct mutagenesis was confirmed by sequencing. Numbering of the human TRF2 residues is based on reference sequence NP_005643. Phosphatase dead mutant PPM1D-D314A was cloned in frame into MCS-BioID2-HA (Addgene ID:74224). Constructs pEJS477-pHAGE-TO-Spy-dCas9-3Xm Cherry-SgRNA-Telomere-All-in-one (Addgene ID:85717) and pEJS469-pLK.O1-SpyS gRNA-DTS13-Telomere (Addgene ID: 85715) were used for visualization of telomeres. DNA double strand breaks at telomeres were induced by transfecting cells with pSpCas9(BB)-2A-GFP (PX458, Addgene ID:48138) containing the telomeric sgRNA, whereas the empty plasmid served as a negative control. DNA fragments corresponding to the full length human PPM1D, its deletion mutants lacking the Pro loop (*1*Pro loop) or B loop (*1*B loop), fragment coding for unstructured C-terminal region (amino acids 370–605, CT) or fragment coding the catalytic domain (amino acids 1–380, A380) were ligated in frame into pEGFP or in pCW57-GFP-2A-MCS (Addgene ID: 71783) plasmids.

Antibodies and reagents

The following antibodies were used in this study: TRF2 (ab108997, for WB), TIN2 (ab197894, for WB) from Abcam; TRF2 (NB110-57130, for IF), TIN2 (NBP2-55709, for IF), RAP1 (NBP1-82433, for IF), 53BP1 (NB100-305, for IF) from Novus Biologicals; TRF2 (sc271710,

for IF), TIN2 (sc73177, for IF), TPP1 (sc100597, for IF and WB), RAP1 (sc53434, for WB), PPM1D (sc376257, for IF and WB), PPM1D (sc20712, for IF) from Santa Cruz Biotechnology; Phospho-Histone H2A.X (Ser139) (clone D7T2V, #80312), KAP1-S824 (#4127) and PPM1D (clone D4F7, 11901 for WB) from Cell Signaling Technology; gH2AX (05-636, for WB), GFP (11814460001, for WB), FLAG (F1804, for IF), Fk2 (04-263, for IF) from Roche. A custom-made pTRF2-S410 antibody was generated by immunization of rabbits with KLH-conjugated phospho-peptide RLVLEEDpSQSTEPSA corresponding to amino acids 403–417 of the human TRF2 (according to the numbering in reference sequence NP_005643.2) (Davids Biotechnologie). Subsequently, immune sera was affinity purified using negative and positive selection with non-phosphorylated and phosphorylated peptides, respectively. PPM1D inhibitor GSK2830371 was from MedChemExpress and was validated previously (44,49). Validated small molecule inhibitors of ATM (KU-55933), ATR (VE-821) and DNA-PK (NU7026) were from MedChemExpress and were used at final concentrations 10, 10 and 5 mM, respectively.

Immunofluorescence microscopy

Cells grown on coverslips were washed in PBS, fixed by 4% PFA for 15 min and permeabilized with 0.2% Triton-X100 for 5 min. Where indicated, cells were pre-extracted prior fixation in 25 mM HEPES pH 7.4, 50 mM NaCl, 1 mM EDTA, $MgCl_2$, 300 mM Sucrose, 0.5% Triton X-100 for 5 min. After washing in PBS, coverslips were blocked with 1% BSA in PBS for 30 min, incubated with primary antibodies for 2 h at room temperature and subsequently with Alexa Fluor secondary antibodies (Thermo Scientific) for 1 h. After incubation with DAPI for 2 min, coverslips were washed with water and mounted with Vectashield. For proximity ligation assay (PLA), coverslips were stained with the indicated primary antibodies followed by incubation with PLA probes (Merck, Duolink In Situ PLA Probe Anti-Rabbit PLUS and MINUS, DUO92002, DUO92004) for 1 h at 37 °C, ligation for 30 min at 37 °C, and polymerase reaction for 2 h at 37 °C according to the manufacturer's protocol (Merck, Duolink In Situ Detection Reagents Red, DUO92008). For immunofluorescence-FISH, coverslips were fixed, permeabilized, and blocked as described above. After dehydration with 70%, 95% and 100% ethanol for 3 min each, the coverslips were incubated for 10 min at 80°C face down on a slide with 20 ml of hybridization solution (10 mM Tris–HCl pH 7.2, 60% formamide, 0.4 mM TelC-Cy5 PNA probe (Panagene), and 0.5% blocking reagent (Roche, 10% stock in 100 mM maleic acid pH 7.5 and 150 mM NaCl). Hybridization was performed for 2 h at room temperature in a humidified chamber in dark. The coverslips were then washed twice for 10 min in wash buffer 1 (10 mM Tris–HCl pH 7.2, 70% formamide) and twice for 5 min in PBS. Incubation with primary antibodies was performed overnight at 4°C, followed with PBS wash and incubation with secondary antibodies for 1 h at room temperature. The coverslips were then stained with DAPI, rinsed in water and mounted using Vectashield. For the high content microscopy, images were acquired using Olympus ScanR equipped with 60×/1.42 OIL objective and analyzed using ScanR analysis software. Confocal imaging was performed using Leica DMi8 equipped with HC PL APO 63×/1.40 OIL CS2 objective. Images were acquired as Z-stacks of five planes with voxel size 44 × 44 × 129.7 nm and 3D-deconvolved using Huygens Professional (Scientific Volume Imaging) based on the theoretical point spread function. Metaphase spreads were imaged using Leica DM6000 equipped with a HCX PL APO 63×/1.40 OIL objective and a sCMOS Leica DFC 900 camera.

Metaphase FISH

Cells were synchronised in late G2 phase by treatment with 9 mM R0-3306 (MedChemExpress) for 16 h. After washing with PBS, cells were released into media supplemented with 0.1 ug/ml colcemid (Sigma) and incubated for 3 h. Subsequently, cells were trypsinised, pelleted at 300 g for 5 min and resuspended in 5 ml of warm 75 mM KCl. After incubation for 30 min at 37°C, cell suspension was mixed with 1.25 ml of fixative solution (methanol:acetic acid, 3:1) while vortexing. After centrifugation, cells were 3× washed with fixative solution. Finally, cells were resuspended in 200–800 ml of fixative solution to achieve concentration 4×10^6 cells/ml, and dropped onto frozen slides from distance of 30 cm. Slides were air dried overnight, washed 3 × 5 min in PBS and hybridisation was performed as described above. After washing in wash buffer 1 and three times 10 min in wash buffer 2 (100 mM Tris–HCl pH 7.2, 150 mM NaCl, 0.08% Tween 20), slides were stained with DAPI, PBS washed, dehydrated with 70%–95%–100% ethanol series, and mounted in Vectashield.

Sample preparation for imaging of telomeric loops

For super-resolution imaging of telomeric loops, we used modified protocol from Doksani et al. Parental U2OS and PPM1D KO cells were trypsinized, washed with PBS and resuspended in 5 volumes of ice-cold nuclei extraction (NE) buffer (10 mM HEPES–KOH pH 7.9, 10 mM KCl, 1.5 $MgCl_2$, 0.5 mM DTT, 0.5 mM PMSF) supplemented with cOmplete protease inhibitor cocktail (Roche). After 5 min of incubation, cells were pelleted at 500 g for 5 min at 4°C and resuspended in 2 volumes on NE buffer. Nuclei were released from cells using Dounce homogeniser and collected with centrifugation at 800 g for 5 min at 4°C. Nuclei were resuspended in nuclei wash (NW) buffer (10 mM Tris–HCl pH 7.4, 15 mM NaCl, 60 mM KCl, 5 mM EDTA) in concentration 1–2 × 10^7 nuclei/ml, and incubated with 100 mg/ml of Trioxalen (Sigma) on ice while stirring in the dark for 5 min. Crosslinking was performed by exposing 2 ml of nuclei suspension at a 6-well plate to 365 nm light for 30 min on ice. Cross-linked nuclei were centrifuged at 800 g for 5 min at 4°C, washed with ice-cold NW buffer, and resuspended at 1 × 10^7 nuclei/ml. The nuclei suspension was diluted 10× in spreading buffer (10 mM Tris–HCl pH 7.4, 10 mM EDTA, 0.05% SDS, 1 M NaCl) pre-warmed at 37°C, and 100 ml of the suspension was immediately dispersed on 13 mm round 1.5H coverslips using cytospin at 600 rpm for 2 min. Coverslips were dried at room temperature for 1 h and fixed

in methanol:acetic acid (3:1) for 1h. Coverslips were dehydrated with 70%–95%–100% ethanol series and hybridized with TelC-Cy5 PNA probe overnight at 4°C in a humidified chamber protected from light. After washing with wash buffer 1 and wash buffer 2, coverslips were washed in water, air-dried and mounted with Vectashield.

Structured illumination imaging

Three dimensional-structured illumination microscopy (3D-SIM) was performed using DeltaVision OMX™ V4 equipped with Blaze Module (GE Healthcare) and a PLAN APO N 60×/1.42 OIL objective. A 568 nm OPSL laser was used for excitation and a pco.edge 5.5 sCMOS camera for signal detection. Raw images were acquired in a z-stack with 125 nm step, 8 z slices, 15 images per slice, pixel size 80 nm. The image reconstruction was performed using SoftWorX software (GE Healthcare). Blinded analysis of telomeres in maximal projection images was done as previously described (33). Only telomere without gaps in telomere staining >500 nm were scored. Branched and overlapping telomeres (30–60% of molecules) were excluded from analysis.

Proximity biotinylation assay and mass spectrometry

HEK293 stably transfected with empty pBIOID2 or pBIOID2-PPM1D-D314A were grown in media supplemented with 50 mM biotin for 5 h, then cells were collected, washed in cold PBS and lysed under denaturating conditions in lysis buffer (50 mM Tris pH 7.4, 1.0% SDS, 1 mM dithiothreitol, supplemented with cOmplete protease inhibitor). Protein lysates were diluted with four volumes of PBS and sonicated 3× for 30 s. Cell lysates were cleared by centrifugation at 15 000 g for 10 min and biotinylated proteins were pulled down by incubation with Dynabeads M-280 Streptavidin for 90 min. After washing twice in lysis buffer and twice with PBS, on-bead trypsin digestion was performed and peptides were analyzed by mass spectrometry using Orbitrap Fusion instrument (Q-OT- qIT, Thermo Scientific). All data were analyzed and quantified using MaxQuant (version 1.6.2.1) and Perseus softwares (50,51). Three biological replicates were analyzed and median peptide intensities were compared. Statistical significance was calculated using Student's t-test and hits with FDR <0.05 were considered significant.

Immunoprecipitation

HEK293 cells were transfected with pEGFP, pEGFP-TRF2 or pEGFP-TRF1 and collected after 48 h. Cells were extracted by IP buffer (50 mM Tris pH 8.0, 150 mM NaCl, 1% Tween20, 0.1% NP-40, 10% glycerol, 2 mM EDTA, 3 mM EGTA, 10 mM $MgCl_2$) supplemented with PhosSTOP and protease inhibitors (Roche), sonicated and DNA was digested by Bensonase. Cell extracts were incubated with GFP Trap beads (Chromotek) for 1 h and after washing, proteins were eluted by Laemli buffer and analyzed by immunoblotting.

In vitro phosphatase assay

Expression and purification of human His-PPM1D was described previously (52). EGFP-TRF2 was purified from transiently transfected U2OS cells using GFP trap and a high salt IP buffer (50 mM Tris pH 8.0, 1 M NaCl, 1% Tween20, 0.1% NP-40, 10% glycerol, 2 mM EDTA, 3 mM EGTA, 10 mM $MgCl_2$) supplemented with PhosSTOP and protease inhibitors. Beads were washed with a phosphatase buffer and incubated with mock or with 150 ng of the purified His-PPM1D for 20 min at 37°C. Reaction was stopped by addition of 4× concentrated Laemli buffer.

Peptide pull down

Biotin-Ahx-ISRLVLEEDpSQSTEPSAGLN-amide (TRF2-pS410) and Biotin-Ahx-ISRLVLEEDSQSTEPSAGLN-amide (TRF2-CTRL) peptides were synthesized (Genscript), dissolved in ammonia water and then diluted to 1 mg/ml in TBST (150 mM NaCl, 3 mM KCl, 25 mM Tris pH 8.0, 10% glycerol, 1 mM DTT, 0.1% Tween20). Peptide pull down was performed as described (53). Dynabeads M-280 Streptavidin (Thermo Fisher Scientific) were incubated with peptides (20 mg) in TBST for 60 min and then beads were washed 3 times with TBST. Coupled beads were incubated with Hela nuclear extract (6 mg/ml, IpraCell) for 90 min at 4°C and then were washed 3 times with TBST and once with PBS. Proteins bound to the beads were digested by trypsin and peptides were analyzed by mass spectrometry. Three independent experiments were compared in one MS measurement.

Fluorescence anisotropy assay

Purification of human TIN2 was described previously (54). TRF2-pS410 and TRF2-CTRL peptides fluorescently labelled at N-terminus with carboxyfluorescein (FAM; λ_{ex} 494 nm, λ_{em} 518 nm) were synthesized by GenScript. Peptides (3 nM) in a 1.5 ml quartz-glass cuvette with a magnetic stirrer were titrated with TIN2 to a final concentration of 500 nM in 50 mM NaCl in 50 mM phosphate buffer, pH 7.0 at 25°C. Fluorescence anisotropy change upon addition of TIN2 was measured at λ_{ex} 490 nm, λ_{em} 520 nm with excitation and emission slits 9 nm. Fluorescence anisotropy was measured three times, and averaged with a relative standard deviation always lower than 3%. The value of the dissociation constant was determined by non-linear least square fits according to the equation: $r = r^{MAX} c / (K_D + c)$ using OriginPro 2022 (OriginLab Corporation) (20).

Cell proliferation assay

Cell survival assay was performed as described (10). Briefly, cells were seeded to 96-well plates at 100–130 cells/well, and treated as indicated. Seven days after treatment, resazurin was added in fresh media at final concentration 30 mg/ml. Fluorescence at excitation wavelength 560 nm and emission 590 nm was measured using Envision plate reader (PerkinElmer, Waltham, MA, USA) after 2 h incubation.

Statistical analysis

Statistic was calculated using PRISM 5 (GraphPad Software). Only two-tailed test were used. Student's t-test were performed under the assumption of normality. As a non-parametric test, we used Mann–Whitney statistics. All experiments were reproduced with similar results at least two times.

RESULTS

PPM1D interacts with components of the shelterin complex

Protein phosphatase magnesium-dependent 1 delta (PPM1D) is a chromatin-bound protein with poor solubility making analysis of its interacting partners a major challenge (8). To identify proteins forming a complex with PPM1D, we established a stable HEK293 cell line expressing a phosphatase-dead PPM1D-D314A fused with a proximity-dependent biotin identification (BioID2) tag and control cells expressing empty BioID2 (55,56). After incubating with biotin, cells were extracted under denaturating conditions and biotinylated proteins were isolated using streptavidin beads and subsequently identified by mass spectrometry (Figure 1A, Supplementary Table S1). This analysis revealed that three components of the shelterin complex (namely TRF2, TRF1 and RAP1) and telomere-associated exonuclease DCLRE1B (also known as Apollo) were significantly enriched in complex with PPM1D-D314A-BioID2 fusion protein. To confirm the results from the proximity biotin labelling assay, we performed immunoprecipitation from HEK293 cells expressing EGFP-PPM1D or empty EGFP. We found that EGFP-PPM1D specifically interacted with TRF2 and RAP1 (Figure 1B). In addition, EGFP-TRF2 and EGFP-TRF1 pulled down endogenous PPM1D from MCF7 cells indicating that PPM1D interacts with shelterin in various cell types (Figure 1C). To map the interaction between PPM1D and the shelterin, we performed immunoprecipitation with the full length EGFP-PPM1D, a mutant containing the catalytic domain of PPM1D (PPM1D-A380) or a mutant comprising of the unstructured C-terminal region of PPM1D (PPM1D-CT) (Figure 1D, E). Due to the presence of two NLS sequences located at the C-terminal region and within the B-loop, respectively, the catalytic domain of PPM1D as well as the C-terminal fragment of PPM1D localized in the nucleus (Figure 1F) (57). However, only the catalytic domain of PPM1D but not the C-terminal tail co-immunoprecipitated with TRF2 (Figure 1E). Moreover, isolated EGFP-TRF2 (but not EGFP alone) was able to pull down purified His-PPM1D *in vitro,* suggesting that the interaction between TRF2 and PPM1D is direct (Supplementary Figure S1A).

Finally, we tested the interaction between PPM1D and shelterin in cells using a proximity ligation assay (43). We observed distinct nuclear foci in MCF7 cells when probing for PPM1D and RAP1 (Figure 1G). Similarly, two distinct sets of antibodies directed against PPM1D and TRF2 showed a strong nuclear PLA signal in MCF7 and U2OS cells (Figure 1H, Supplementary Figure S1B). Importantly, the specificity of the observed PLA signal was confirmed by a strong reduction caused by treating cells with GSK2830371 (further referred to as PPM1Di) that promotes a proteasomal degradation of PPM1D (Figure 1G, Supplementary Figure S1C) (44,49). Similarly, depletion of TRF2 by RNA interference suppressed the PLA signal thus supporting our conclusion that PPM1D and TRF2 interact in the cell nuclei (Figure 1H).

Taken together, we conclude that PPM1D interacts through its catalytic domain with several components of the shelterin complex in various cell types regardless of the type of telomere maintenance, including telomerase proficient MCF7 cells and alternative telomere lengthening (ALT)-dependent U2OS cells.

PPM1D is present at telomeres

Apart from functions at telomeres, TRF2 and TRF1 were reported to localize also to other chromatin compartments (58–61). Therefore, we wondered where the interaction between PPM1D and the shelterin complex occurred at subcellular level. To this end, we transfected U2OS cells with a plasmid expressing an enzymatically inactive dCas9-mCherry reporter together with a telomere-specific sgRNA and we visualized telomeres by confocal microscopy (62). In parallel, we probed cells with validated antibodies against PPM1D and TRF2 (Supplementary Figure S1D, E) (8). As expected, signal from the dCas9-mCherry telomeric reporter overlapped with the staining for TRF2 (Figure 2A). As expected, we observed a dotted nuclear pattern reflecting the localization of PPM1D to the chromatin (Figure 2A) (8). In addition, we noticed that a fraction of spots recognized by PPM1D antibody localized at telomeres (Figure 2A). To investigate possible contribution of the stochastic cluster overlap, we randomized PPM1D signal distribution using Interaction Factor package in ImageJ and compared random overlap with non-random values (63). We confirmed that the experimentally observed overlap between PPM1D and the telomeric staining in U2OS cells was statistically significant (Figure 2B). In addition, we observed that PPM1D was present at approximately 60% of telomeres probably reflecting a dynamic interaction between PPM1D and the shelterin complex (Figure 2B). Finally, we used an identical experimental approach to determine PPM1D distribution in MCF7 cells (Figure 2C). We noted that TRF2 foci in MCF7 cells were smaller than in U2OS cells probably reflecting shorter telomeres in MCF7 cells compared to the ALT-positive U2OS cells. Nevertheless, we found that a fraction of endogenous PPM1D localized at telomeres recognized by TRF2 staining in MCF7 cells (Figure 2D). Interestingly, the fraction of telomeres positive for PPM1D was comparable in MCF7 and U2OS cells (Figure 2D). In summary, we conclude that PPM1D can associate with telomeres in various cell types.

To identify the regions in PPM1D that are necessary for its localization at telomeres, we transfected cells with plasmids expressing EGFP-tagged PPM1D or its deletion mutants. We found that the wild-type EGFP-PPM1D, a deletion mutant lacking the Proline-rich region (referred to as *1*Pro) and a PPM1D-A380 mutant comprising of the catalytic domain between amino acids 1–380 all were enriched in TRF2 foci (Figure 2E, Supplementary Figure S1F, G). In contrast, the unstructured C-terminal fragment

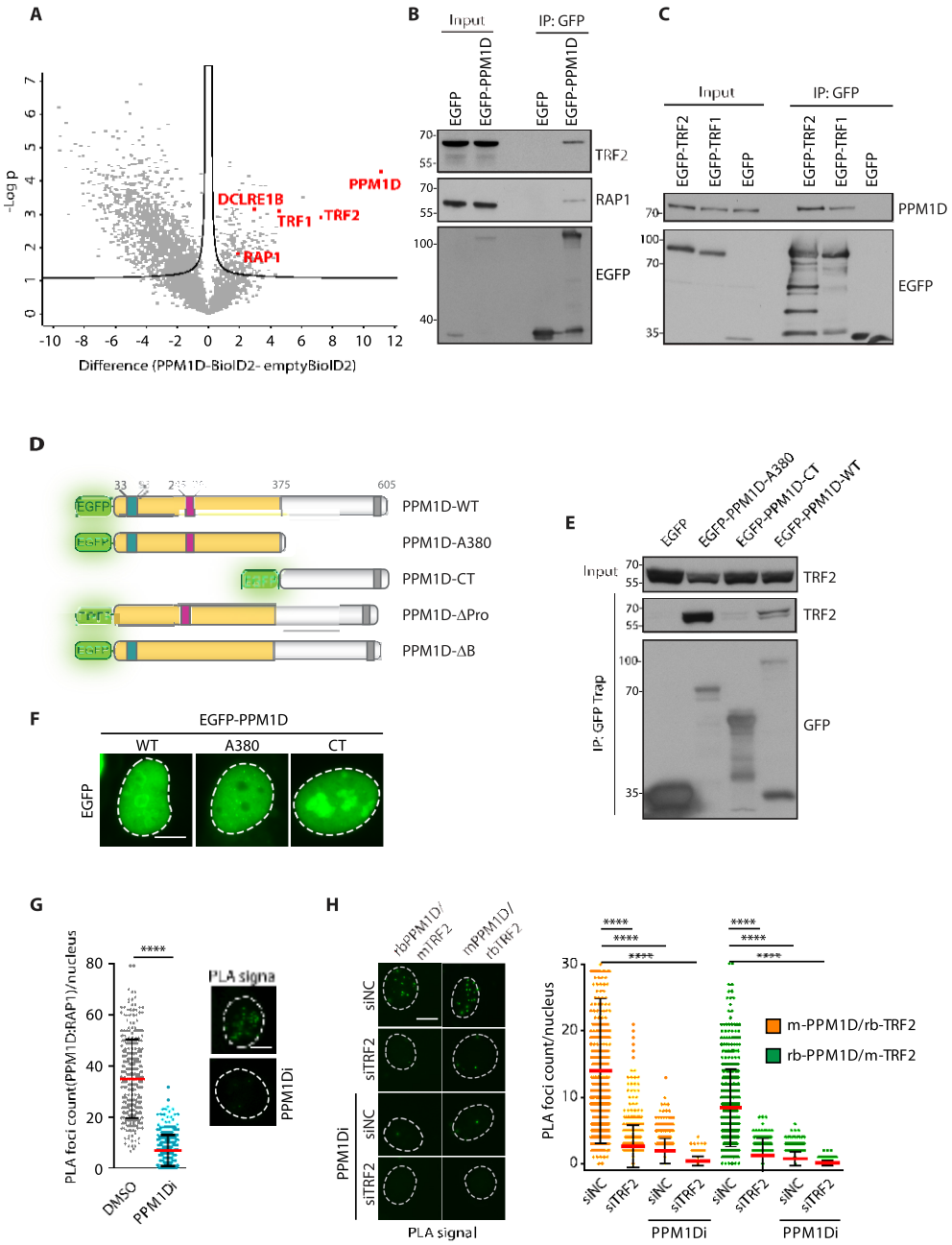

Figure 1. PPM1D interacts with component of the shelterin complex. (**A**) HEK293 cells stably expressing PPM1D-D314A-BioID2 or empty BioID2 were lysed 5h after treatment with biotin. Biotinylated proteins were pulled down by streptavidin beads and bound proteins were analyzed by MS ($n = 3$). Volcano plot shows –log P values for proteins enriched or reduced in PPM1D-BioID2 sample. Line delineates the statistical significance (FDR < 0.05). (**B**) HEK293 cells were lysed 24 h after transfection with plasmids expressing EGFP or EGFP-PPM1D and cell extracts supplemented with bensonase were incubated with GFP trap. Bound proteins were analyzed by immunoblotting. (**C**) MCF7 cells were transfected with plasmids expressing EGFP, EGFP-TRF1, or EGFP-TRF2. Cell extracts supplemented with bensonase were incubated with GFP trap. Binding of PPM1D was probed by immunoblotting. (**D**) Scheme of EGFP-tagged PPM1D constructs used in the study. Shown are the catalytic domain in yellow, the basic loop in magenta, the Proline-rich loop in cyan and the NLS in grey. Note that an additional NLS is located within the B loop. (**E**) HEK293 cells were transfected with plasmids expressing EGFP, the wild type EGFP-PPM1D, EGFP-PPM1D-A380 corresponding to the catalytic domain, or EGFP-PPM1D-CT corresponding to the unstructured C-terminal tail of PPM1D. Cell extracts were incubated with GFP trap and binding of TRF2 was evaluated by immunoblotting. (**F**) U2OS were transfected with plasmids coding for EGFP-PPM1D variants. Cells were fixed and visualized by wide-field microscopy, the scale bar represents 10 mm. Representative images are shown. (**G**) MCF7 cells were fixed and probed for interaction of PPM1D with RAP1 by PLA assay. Where indicated, cells were treated with PPM1D inhibitor for 24 h. Mean count on nuclear PLA foci is plotted ± SD, $n = 300$. Statistical significance was evaluated using Mann–Whitney test, (****$P <$ 0.0001). Representative experiment is shown from two independent repeats. The scale bar in representative images corresponds to 10 mm. (**H**) MCF7 cells were transfected twice with control siRNA (siNC) or siRNA to TRF2. After 6 days, cells were fixed and probed for interaction of PPM1D with TRF2 by PLA assay using two different pairs of antibodies (rabbit rb-PPM1D/mouse m-TRF2, mouse m-PPM1D/rabbit rb-TRF2). Where indicated, cells were treated with PPM1D inhibitor for 18 h prior fixation. Mean count of the nuclear PLA foci is plotted ± SD, $n = 500$. Statistical significance was evaluated using Mann–Whitney test (****$P <$ 0.0001). Representative experiment is shown from two independent repeats. The scale bar in representative images corresponds to 10 mm.

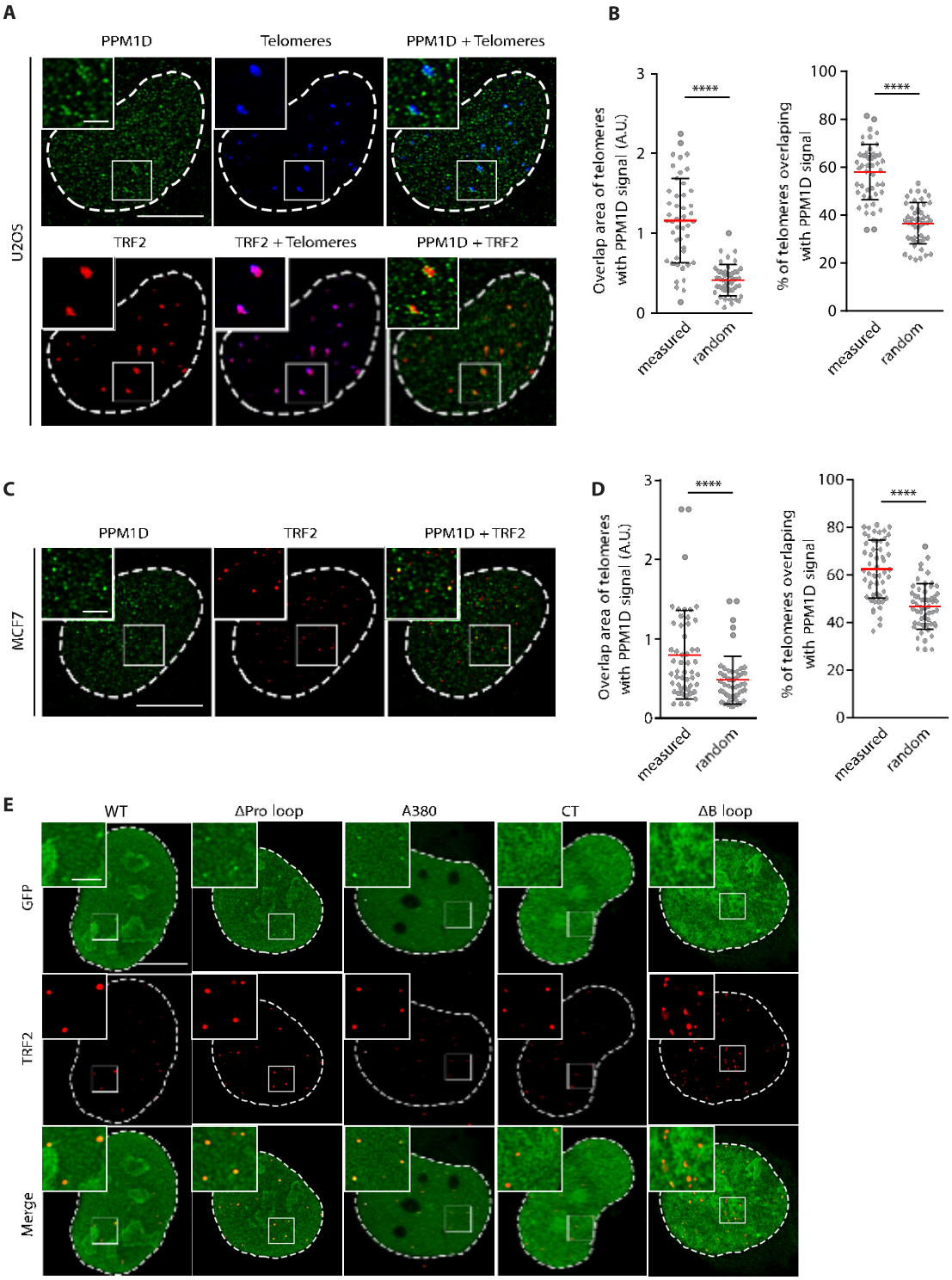

Figure 2. PPM1D is present at telomeres. (**A**) U2OS cells were co-transfected with plasmids coding for mCherry-dCas9 and telomeric repeat-targeting sgRNA. After 24h, cells were fixed and stained for PPM1D and TRF2. Images show a single confocal plane processed with deconvolution. The scale bars represent 10 mm or 2 mm, respectively. (**B**) Quantification of A. Area of the overlapping PPM1D and TRF2 signal was determined using Interaction Factor package in ImageJ. Subsequently, PPM1D signal was randomized for each image. Means of 20 randomizations are plotted together with experimentally observed values (left). Shown is also a fraction of telomeres that contain PPM1D signal (right). Values for 46 cells form two independent experiments are plotted with means ± SD. Statistical significance was evaluated using paired *t*-test (*****P* < 0.0001). (**C**) MCF7 cells were stained for PPM1D and TRF2 and imaged by confocal microscopy. A representative single deconvolved planes are shown. The scale bar represents 10 mm or 2 mm respectively. (**D**) PPM1D and TRF2 signals from (C) were analyzed as in (B). Values for 51 cells form two independent experiments are plotted with means ± SD. Statistical significance was evaluated using paired *t*-test (*****P* < 0.0001). (**E**) U2OS cells were transfected with plasmids coding for individual EGFP-PPM1D variants. Cells were fixed, stained for TRF2 and imaged by confocal microscopy. A representative single deconvolved planes are shown. The scale bar represents 10 or 2 mm, respectively.

of PPM1D failed to accumulate in TRF2-positive foci although it showed a strong nuclear staining (Figure 2E). Finally, a deletion mutant lacking amino acids 246–251 of the B loop (referred to as *1*B) localized to the nucleus but it failed to co-localize with TRF2 (Figure 2E, Supplementary Figure S1F, G). Thus, the microscopic analysis revealed that the B loop in the catalytic domain of PPM1D mediates its localization at telomeres, which is in good agreement with the data from immunoprecipitation (Figure 1E). In addition, the observed difference between intensities of the wild-type EGFP-PPM1D and the EGFP-PPM1D-A380 mutant suggests that the C-terminal tail of PPM1D may be involved in negative regulation of PPM1D localization at telomeres.

PPM1D counteracts ATR-dependent phosphorylation of TRF2 at S410

As PPM1D localizes at telomeres, we wondered if it could regulate the phosphorylation of the shelterin components either in context of the cell cycle progression or following DNA damage at telomeres. Since PPM1D has been implicated in termination of the global DNA damage response, we have focused on the phosphorylations triggered by exposure of cells to genotoxic stress. Unfortunately, commercial antibodies raised against several phosphopeptides in TRF2 and TRF1 did not show sufficient level of sensitivity and specificity preventing us from testing the effect of PPM1D activity (data not shown). Therefore, we generated an affinity purified rabbit polyclonal antibody against the phosphorylated S410 of TRF2 that is conserved across species, matches a consensus motif for ATM/ATR and PPM1D and has previously been detected in cells exposed to ionizing radiation or to treatment with cytarabine (Supplementary Figure S1H) (64–66). First, we tested the reactivity of pTRF2-S410 antibody using the wild-type EGFP-TRF2 or the EGFP-TRF2-S410A mutant immunopurified from HEK293 cells. Importantly, we observed a strong reduction of the signal in the alanine mutant, confirming that the pTRF2-S410 antibody predominantly recognizes the phosphorylated form of TRF2 in immunoblotting (Figure 3A). In addition, we found that the basal level of pTRF2-S410 signal that was increased by treatment of the cells with hydroxyurea and/or PPM1D inhibitor which is consistent with the DNA damage-induced phosphorylation of TRF2 that is counteracted by PPM1D (Figure 3B). In agreement with this possibility, we found that purified His-PPM1D dephosphorylated the purified TRF2 at S410 *in vitro* (Figure 3C). Next, we used control HeLa cells or cells with doxycycline-induced knock-down of TRF2 and exposed them to ionizing radiation (60 Gy) (45). In non-treated cells, the phosphorylation of endogenous TRF2 was below the detection limit in the nuclear extracts. On the other hand, the extensive DNA damage induced the signal of pTRF2-S410 antibody and importantly, the specificity was confirmed by depletion of the TRF2 (Figure 3D). As expected, treatment of cells with PPM1Di decreased the level of PPM1D protein and induced γH2AX staining (8,44,49). In addition, we found that inhibition of PPM1D further increased the pTRF2-S410 signal suggesting that PPM1D might dephosphorylate pTRF2-S410 (Figure 3D). To validate specificity of the pTRF2-S410 antibody in immunofluorescence microscopy, we depleted endogenous TRF2 in U2OS cells by RNAi and treated them or not with PPM1D inhibitor (Figure 3E). As expected, we observed a strong induction of the pTRF2-S410 signal at telomeres upon treatment of control cells with PPM1D inhibitor. Importantly, the signal was lost upon depletion of TRF2, thus confirming specificity of the antibody (Figure 3E). Further, we observed an increase in pTRF2-S410 phosphorylation in U2OS-PPM1D-KO cells and the signal was significantly reduced by expression of the FLAG-PPM1D confirming that the observed phenotype was indeed caused by the loss of PPM1D (Figure 3F). We conclude that PPM1D counteracts the TRF2-S410 phosphorylation at telomeres.

As the basal level of pTRF2-S410 signal in non-treated cells was relatively low, we searched for conditions that would stimulate the phosphorylation of TRF2. Upon exposure to ionizing radiation, DSBs are randomly generated across the genome making interpretation of events observed at telomeres difficult. To induce DSBs specifically at telomeres, we transfected cells with a plasmid expressing Cas9 and a sgRNA targeting the telomeric repeats (67). Consistent with previous reports, we observed formation of the telomeric dysfunction-induced foci (TIFs) defined by recruitment of 53BP1 and by phosphorylation of H2AX at S139 (called γH2AX) (Figure 3G, H, Supplementary Figure S1I) (68). As expected, DSBs induction eventually resulted in telomere clustering that we observed as reduced telomere count and increased area of the foci (Supplementary Figure S2A–C) (69). In addition, we noted an increased γH2AX signal in cells lacking PPM1D, which is in agreement with the previously described role of PPM1D in dephosphorylating H2AX at chromatin (Figure 3H, Supplementary Figure S1I) (8). Importantly, telomeric DNA damage also strongly induced the TRF2-S410 phosphorylation at telomeres and the signal was further increased in U2OS-PPM1D-KO cells (Figure 3I, Supplementary Figure S2D). Of note, pTRF2-S410 signal was significantly enriched at telomeres in U2OS-PPM1D-KO cells without any induction of telomeric damage suggesting that PPM1D may constantly dephosphorylate TRF2 at telomeres (Figure 3I, Supplementary Figure S2D).

Finally, we induced DSBs at telomeres in cells treated with small molecule inhibitors of the major protein kinases responding to DNA damage and assayed the impact on protein phosphorylation at telomeres. Similarly to DSBs induced by TRF1-FokI, we observed that inhibition of ATM reduced the level of γH2AX at telomere breaks induced by Cas9 (Figure 3J) (70). In contrast, pTRF2-S410 phosphorylation was insensitive to the inhibition of ATM but was reduced upon treatment with ATR inhibitor (Figure 3K, Supplementary Figure S2E). Similarly, we observed that RNAi-mediated depletion of ATR (but not ATM) supressed the level of pTRF2-S410 phosphorylation (Supplementary Figure S2F–H). We conclude that following induction of DSBs at telomeres, TRF2 phosphorylation at S410 is inversely regulated by ATR and PPM1D.

TRF2 phosphorylation at S410 increases its binding to TIN2

Several recent studies have identified regions within individual shelterin components that mediate protein–protein

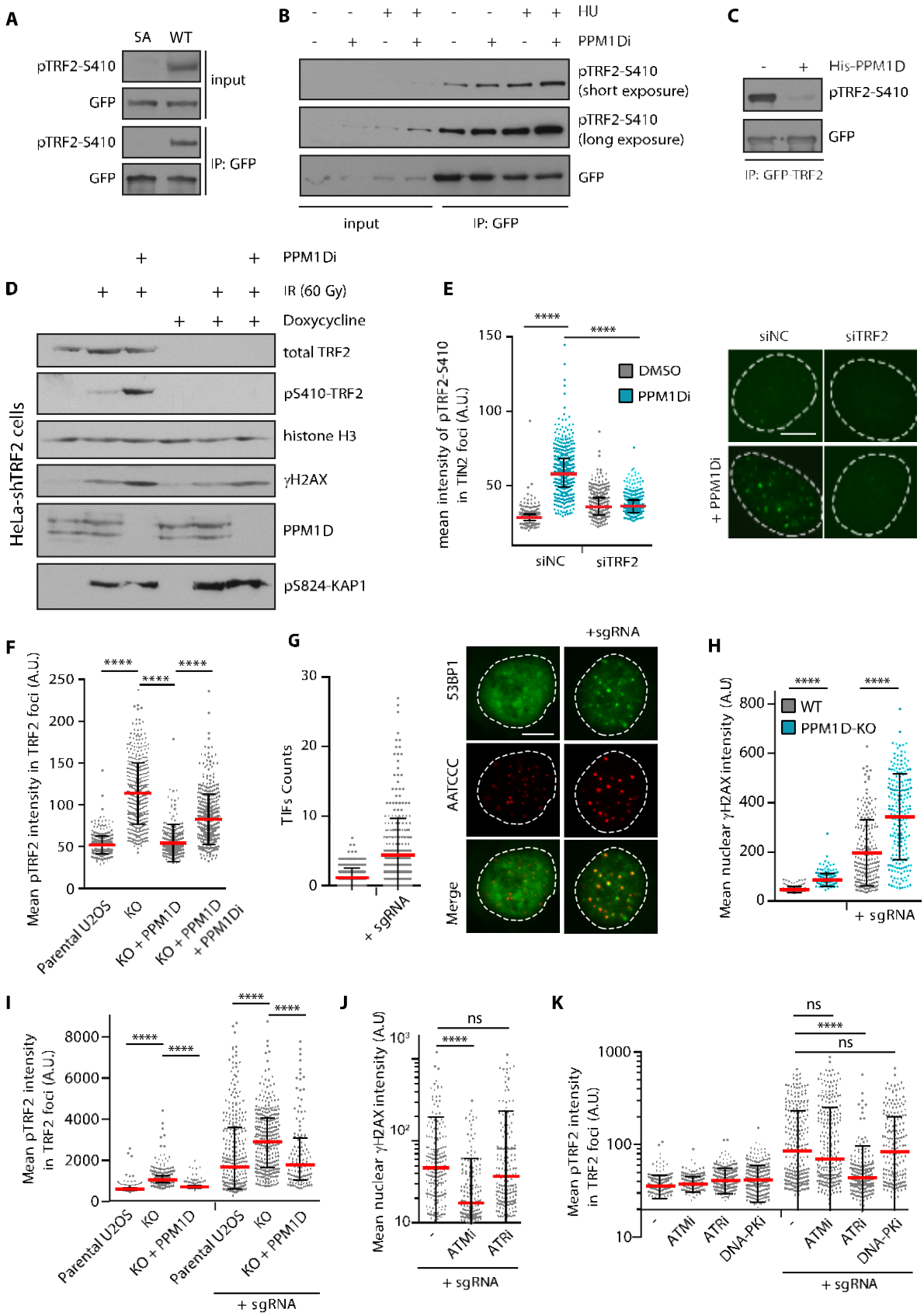

Figure 3. TRF2 is phosphorylated at S410 by ATR and dephosphorylated by PPM1D. (**A**) HEK293 cells were transfected with the wild-type EGFP-TRF2 (WT) or EGFP-TRF2-S410A (SA) mutant and incubated with PPM1Di for 18 h prior harvesting. Cell extracts were incubated with GFP trap

interactions and are critically needed for folding of the shelterin complex (16,25,30,31,71). For instance, the TRF1$_{TRFH}$ (residues 58–268) and TRF2 $_{TRFH}$ (residues 84–287) domains interact with a TRFH-binding motif (TBM) of TIN2 (residues 256–276) (30). In addition, TRFH domain of TIN2 interacts with a recently described TBM2 region of TRF2 (residues 392–408) (31). As the published crystal structure of TIN2$_{TRFH}$-TRF2$_{TBM}$2 interaction interface lacks the structural information for S410, we used Alphafold2 Colab to predict the position of residues 392–420 of TRF2 (30). The structural alignment of Alphafold2 model showed a perfect overlap with the crystal structure (with RMSD 0.252 Å) (Supplementary Figure S3A). In this model, S410 of TRF2 is positioned opposite the positively charged residues of TIN2$_{TRFH}$ suggesting that phosphorylation of S410 might strengthen the TRF2-TIN2 interaction by formation of salt bridges between the phosphate and basic residues in the AA50–56 region of TIN2 (Supplementary Figure S3A). To experimentally test the impact of TRF2$_{TBM}$2 phosphorylation on TRF2-TIN2 interaction, we designed several independent assays. First, we performed a pull down from the nuclear extracts using biotinylated phosphorylated or non-phosphorylated peptides of TRF2 as baits. Mass spectrometry analysis revealed that the phosphorylated but not the non-phosphorylated TRF2 peptide specifically pulled down TIN2, TPP1 and POT1 (Figure 4A, Supplementary Table S2). Second, we quantified the binding affinities of the purified TIN2 with short, fluorescently labelled TRF2 oligopeptides containing phosphorylated or non-phosphorylated S410 (Figure 4B). Analysis of the binding isotherms showed that the binding affinity for unmodified TRF2-S410 oligopeptide was K_D = 240 ± 80 nM that corresponded well to the previously reported affinity for TRF2-TIN2 binding (71). When S410 was phosphorylated, we observed a significant increase of the binding affinity with the corresponding K_D = 180 ± 30 nM. To confirm the data from the *in vitro* assays, we tested the interaction between TRF2 and TIN2 in cells by immunoprecipitation (Figure 4C). Consistent with the previous reports, we observed that the wild-type EGFP-TRF2 interacted with TIN2 (25). In addition, the non-phosphorylatable EGFP-TRF2-S410A mutant pulled down a reduced but still detectable level of TIN2, suggesting that modification of S410 is not absolutely required for the basal interaction between TRF2-TIN2 (Figure 4C). This finding is in agreement with the previous report where interaction was observed with a TRF2$_{TBM}$2 fragment (residues 392–408) lacking the S410 site (72). Interestingly, however, we observed an increased interaction between the phosphorylation mimicking EGFP-TRF2-S410E mutant, which is consistent with increased binding affinity between TRF2 and TIN2 upon phosphorylation (Figure 4C).

To test if the TRF2 interaction with TIN2 is regulated by PPM1D, we performed the PLA assay in parental U2OS cells, U2OS-PPM1D-KO and U2OS cells treated with PPM1D inhibitor. We observed that loss or inhibition of PPM1D significantly increased the interaction between TRF2 and TIN2 (Figure 4D, E, Supplementary Figure S3B). Consistent with this, we found that TIN2 was enriched at telomeres in U2OS cells treated with PPM1D inhibitor compared to the non-treated cells (Figure 4F). Similarly, intensity of the TIN2 signal at telomeres was increased in U2OS-PPM1D-KO cells compared to the parental U2OS cells and the level was rescued by expression of the wild-type EGFP-PPM1D (Figure 4G). Importantly, total protein levels of TRF2 and TIN2 remained unchanged in U2OS-PPM1D-KO cells thus excluding the possibility that the observed enrichment of TIN2 at telomeres is a consequence of altered protein expression (Figure 4H). In contrast to TIN2, we did not observe any increase in TRF2 accumulation at telomeres in cells lacking PPM1D suggesting that the increased recruitment of TIN2 depends on phosphorylation status of TRF2 rather than a change of its total levels at the telomere (Figure 4I). As TIN2 mediates the recruitment of

←----------

and bound proteins were analyzed by immunoblotting. (**B**) HEK293 stably expressing EGFP-TRF2 were treated with DMSO, HU (2 mM), PPM1Di (1 mM) or combination of both for 18 h. Cell extracts were incubated with GFP trap and bound proteins were analyzed by immunoblotting. (**C**) *In vitro* phosphatase assay. EGFP-TRF2 was isolated from cells by GFP Trap in a buffer containing 1 M NaCl. Beads were washed with a phosphatase buffer and incubated with mock or with the purified His-PPM1D for 20 min at 37°C. Level of TRF2-S410 phosphorylation was analyzed by immunoblotting. (**D**) HeLa cells stably transfected with inducible TRF2 shRNA were treated with mock or with doxycycline (2 mg/ml) for 7 days and were exposed or not to IR (60 Gy). Where indicated, cells were incubated with PPM1Di for the last 12 h. Nuclear extracts were separated on 4–20% SDS-PAGE gel and analyzed by immunoblotting. (**E**) U2OS cells after two consecutive transfections of control or TRF2 siRNA were treated or not with PPM1D inhibitor (2 mM, 4 h), fixed and co-stained for TIN2 (telomeric marker) and pTRF2-S410. Plotted is the mean pTRF2-S410 intensity in TIN2-positive foci, each dot represents a single cell (n = 500). Bars indicate mean ± SD, statistical significance was evaluated using Mann–Whitney test (****P < 0.0001). Representative experiment is shown from two independent repeats. The scale bar in representative images corresponds to 10 mm. (**F**) Parental U2OS, U2OS-PPM1D-KO and U2OS-PPM1D-KO cells stably expressing FLAG-PPM1D were treated or not with PPM1D inhibitor for 24 h. Cells were pre-extracted, fixed and stained for TRF2 and pTRF2-S410. Plotted is the mean pTRF2-S410 intensity in TRF2-positive foci, each dot represents a single cell (n = 300). Bar indicates mean ± SD, statistical significance was evaluated using Mann–Whitney test (****P < 0.0001). Representative experiment is shown from two independent repeats. (**G**) U2OS cells were transfected with plasmids coding for Cas9-EGFP with or without the telomeric repeat-targeting sgRNA. After 24 h, cells were fixed, hybridized with telomeric FISH probe, and stained for 53BP1 (TIF marker). The scale bar represent 10 mm). Bar indicates mean ± SD, n = 300. (**H**) Parental U2OS or U2OS-PPM1D-KO cells were transfected with plasmids coding for Cas9-EGFP with or without telomeric repeat-targeting sgRNA. After 24 h, cells were fixed and stained for γH2AX. Mean nuclear intensity is plotted ± SD, n ≥ 208. Statistical significance was evaluated using Mann–Whitney test (****P < 0.0001). Representative experiment is shown from three independent repeats. (**I**) U2OS cells were transfected as in H and were stained for TRF2 and pTRF2-S410. Plotted is the mean pTRF2-S410 intensity in TRF2-positive foci. Bars indicate mean ± SD, n ≥ 150. Statistical significance was evaluated using Mann–Whitney test (****P < 0.0001). Representative experiment is shown from two independent repeats. (**J**) U2OS cells were transfected with plasmids coding for Cas9-EGFP with or without the telomeric repeat-targeting sgRNA and were treated with indicated inhibitors for 20 h. After fixation, the intensity of γH2AX signal in TRF2 foci was determined by ScanR microscopy. Bars indicate median ± SD, n ≥ 161. Statistical significance was evaluated using Mann–Whitney test (****P < 0.0001). Representative experiment is shown from two independent repeats. (**K**) U2OS cells were treated as in (J) and were probed with TRF2 and pTRF2-S410 antibodies. Plotted is the mean pTRF2-S410 intensity in TRF2 foci. Bars indicate median ± SD, n ≥ 249. Statistical significance was evaluated using Mann–Whitney test (****P < 0.0001). Representative experiment is shown from two independent repeats.

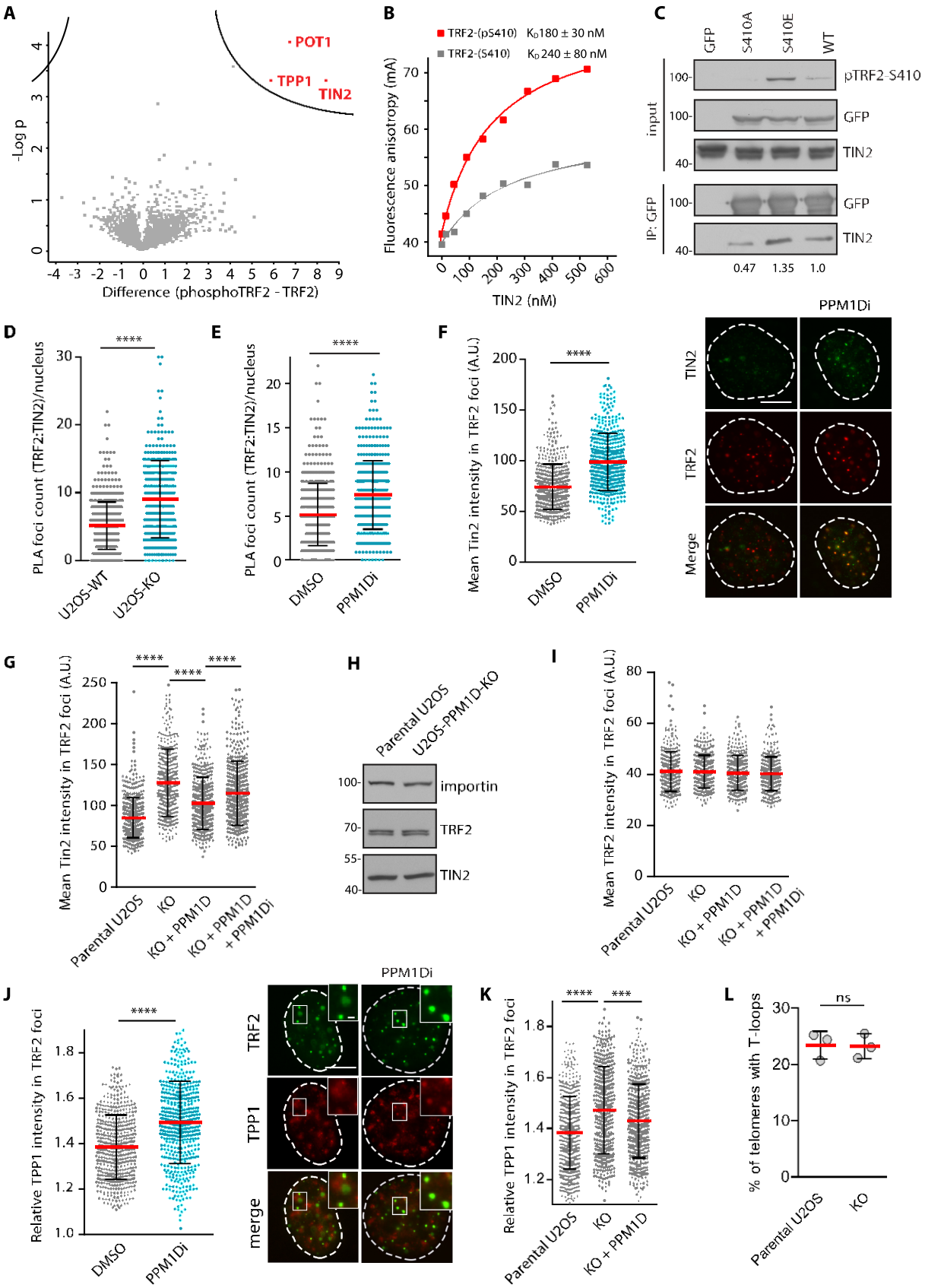

Figure 4. TRF2 phosphorylation at S410 increases its binding to TIN2. (**A**) Biotin-Ahx-ISRLVLEEDpSQSTEPSAGLN (TRF2-pS410) and Biotin-Ahx–SRLVLEEDSQSTEPSAGLN (TRF-CTRL) peptides were incubated with nuclear extracts and pulled down by streptavidin beads. Bound proteins were

TPP1-POT1 to TRF1/2 we also evaluated the amount of TPP1 at telomeres. We observed that inhibition or loss of PPM1D increased the level of TPP1 at telomeres confirming that the activity of PPM1D may regulate assembly of the shelterin complex at telomeres (Figure 4J, K). Similarly to U2OS cells, we observed that inhibition of PPM1D increased the phosphorylation of TRF2-S410 as well as the levels of TIN2 and TPP1 at telomeres in MCF7 cells, suggesting that the impact of PPM1D activity on recruitment of shelterin components to telomeres is not restricted to cells with alternative lengthening of telomeres (Supplementary Figure S3C, D and E).

TRF2 and TIN2 jointly protect telomeric ends by promoting formation of t-loop and therefore we asked if manipulation with the strength of TRF2:TIN2 binding by removing PPM1D activity could affect t-loop formation. To this end, we prepared chromatin spreads from the parental U2OS and U2OS-PPM1D-KO cells and determined fractions of the linear or looped chromosome ends by 3D-SIM microscopy as previously described (33). Consistent with published literature, we observed t-loops in about 25% of chromosomes (33,73). However, we did not find any significant differences between parental U2OS and U2OS-PPM1D-KO cells (Figure 4L, Supplementary Figure S3F) suggesting that PPM1D activity does not interfere with formation of the t-loop. On the other hand, we cannot exclude that differences in organisation of the chromosome ends caused by loss of PPM1D are below the sensitivity of the assay because we were unable to conclusively categorize about a half of the imaged telomeres.

Increased PPM1D activity impairs assembly of the shelterin complex

As the interaction of TRF2 and TIN2 responded to the inhibition of PPM1D, we asked if increased activity of PPM1D might interfere with function of the shelterin complex at telomeres. Indeed, we found that overexpression of the wild-type PPM1D decreased the amount of TIN2 at telomeres (Figure 5A). In addition, we observed that expression of the A380 fragment of PPM1D (that showed the strongest targeting to the telomeres in Figure 2E) efficiently stripped TIN2 from the telomeres (Figure 5A). Of note, expression of the A380 fragment of PPM1D also reduced the intensity of TRF2 staining at telomeres suggesting that assembly of the shelterin may be impaired after dephosphorylation by PPM1D (Figure 5B).

To study consequences of the increased PPM1D expression, we developed a doxycycline-inducible RPE1-PPM1D-A380 cells (Supplementary Figure S4A), and followed formation of TIFs upon treatment with doxycycline for 10 days (Figure 5C). Although the fraction of cells with > 3 TIFs was slightly higher in cells treated with doxycycline compared to control cells, the difference was not statistically significant (Figure 5C). As PPM1D can target γH2AX and ATM, we hypothesised that failure to form TIFs could be caused by overall suppression of DDR by PPM1D activity (8,74). Therefore, we treated RPE1-PPM1D-A380 cells for 10 days to allow formation of potential telomeric damage and then treated cells with PPM1D inhibitor just before fixation to allow activation of DDR. Indeed, transient PPM1D inhibition increased activity of ATM as documented by increased level of KAP1-S824 phosphorylation (Figure 5C). Consistently, upon transient inhibition of PPM1D, we observed a significant increase of TIF formation in cells expressing PPM1D-A380 suggesting that these cells experienced telomeric damage (Figure 5C). Next, we analyzed telomeric damage in RPE1-PPM1D-A380 cells by telomeric FISH in metaphase spreads (Figure 5D). We noted that the fraction of telomeric fusions was doubled in RPE1-PPM1D-A380 cells treated with doxycycline compared to control cells Figure 5D) confirming that increased PPM1D activity in cells promotes damage of the telomeric DNA.

Finally, we asked if the phosphorylation of TRF2 is required for cell proliferation. To this end, we used HeLa cells

←

identified by mass spectrometry (n = 3). Plotted are –log P values of proteins enriched or reduced in condition with TRF2-pS410 peptide. The line delineates the statistical significance (FDR < 0.1). (**B**) Fluorescently-labelled TRF2-pS410 and TRF2-CTRL peptides were titrated with purified TIN2 to a final concentration of 500 nM. Fluorescence anisotropy change was measured and dissociation constant values for unmodified and modified oligopeptides were calculated as described in Methods. (**C**) HEK293 cells stably expressing EGFP-TRF2 were treated with DMSO or with PPM1D inhibitor for 4 h. EGFP-TRF2 was immunoprecipitated from cell extracts with GFP Trap. Proteins were separated by SDS-PAGE and binding of TIN2 was determined by immunoblotting. Numbers at the bottom indicate the TIN2 signal relative to the total immunoprecipitated TRF2 and normalized to the wild-type TRF2. Representative result from three experiments is shown. (**D**) TRF2:TIN2 interaction was determined in parental U2OS and U2OS-PPM1D-KO cells by PLA. Mean PLA foci count is plotted ± SD, n = 500. Statistical significance was evaluated using Mann–Whitney test (****P < 0.0001). Representative experiment is shown from two independent repeats. (**E**) TRF2:TIN2 interaction was determined in U2OS cells treated with DMSO or PPM1Di by PLA. Mean PLA foci count is plotted ± SD, n = 500. Statistical significance was evaluated using Mann–Whitney test (****P < 0.0001). Representative experiment is shown from two independent repeats. (**F**) U2OS cells were treated or not with PPM1Di for 24 h, pre-extracted, fixed and stained with TRF2 (m-Santa Cruz) and TIN2 (Rb-Novus) antibodies. Mean TIN2 intensity in TRF2 foci is plotted ± SD, n = 300. Statistical significance was evaluated using Mann–Whitney test (****P < 0.0001). Representative experiment is shown from two independent repeats. The scale bar represents 10 mm. (**G**) Parental U2OS, U2OS-PPM1D-KO and U2OS-PPM1D-KO stably expressing FLAG-PPM1D cells were treated or not with PPM1Di for 24 h. Cells were pre-extracted, fixed and stained for TIN2 and TRF2. Mean TIN2 intensity in TRF2 foci ± SD is plotted, n = 300. Statistical significance was evaluated using Mann–Whitney test (****P < 0.0001). Representative experiment is shown from two independent repeats. (**H**) Levels of TRF2 and TIN2 were analyzed in whole cell extracts from the parental U2OS and U2OS-PPM1D-KO cells by immunoblotting. Importin staining was used as a loading control. (**I**) Cells from G were analysed for TRF2 intensity in TRF2 foci. Plotted is mean ± SD, n = 300. (**J**) U2OS cells were treated or not with PPM1Di for 24 h, pre-extracted, fixed and stained with TRF2 and TPP1 antibodies. Mean TPP1 intensity in TRF2 foci normalized to the mean nuclear TPP1 intensity ± SD is plotted, n > 300. Statistical significance was evaluated using Mann–Whitney test (****P < 0.0001). The scale bars in representative images corresponds to 10 mm and 1 mm respectively. (**K**) Parental U2OS, U2OS-PPM1D-KO cells and U2OS-PPM1D-KO stably expressing FLAG-PPM1D cells were pre-extracted, fixed and stained for TPP1 and TRF2. Mean TPP1 intensity in TRF2 foci normalized to the mean nuclear TPP1 intensity ± SD is plotted, n > 300. Statistical significance was evaluated using Mann–Whitney test (****P < 0.0001, ***P < 0.001). (**L**) Chromosome spreads from parental U2OS and U2OS-PPM1D-KO cells were hybridized with TAACCC FISH-probe and imaged by 3D-SIM. Plotted is a fraction of telomeres that formed t-loops. More than 203 telomeres were quantified per condition in each experiment (n = 3). Significance was determined by unpaired t-test.

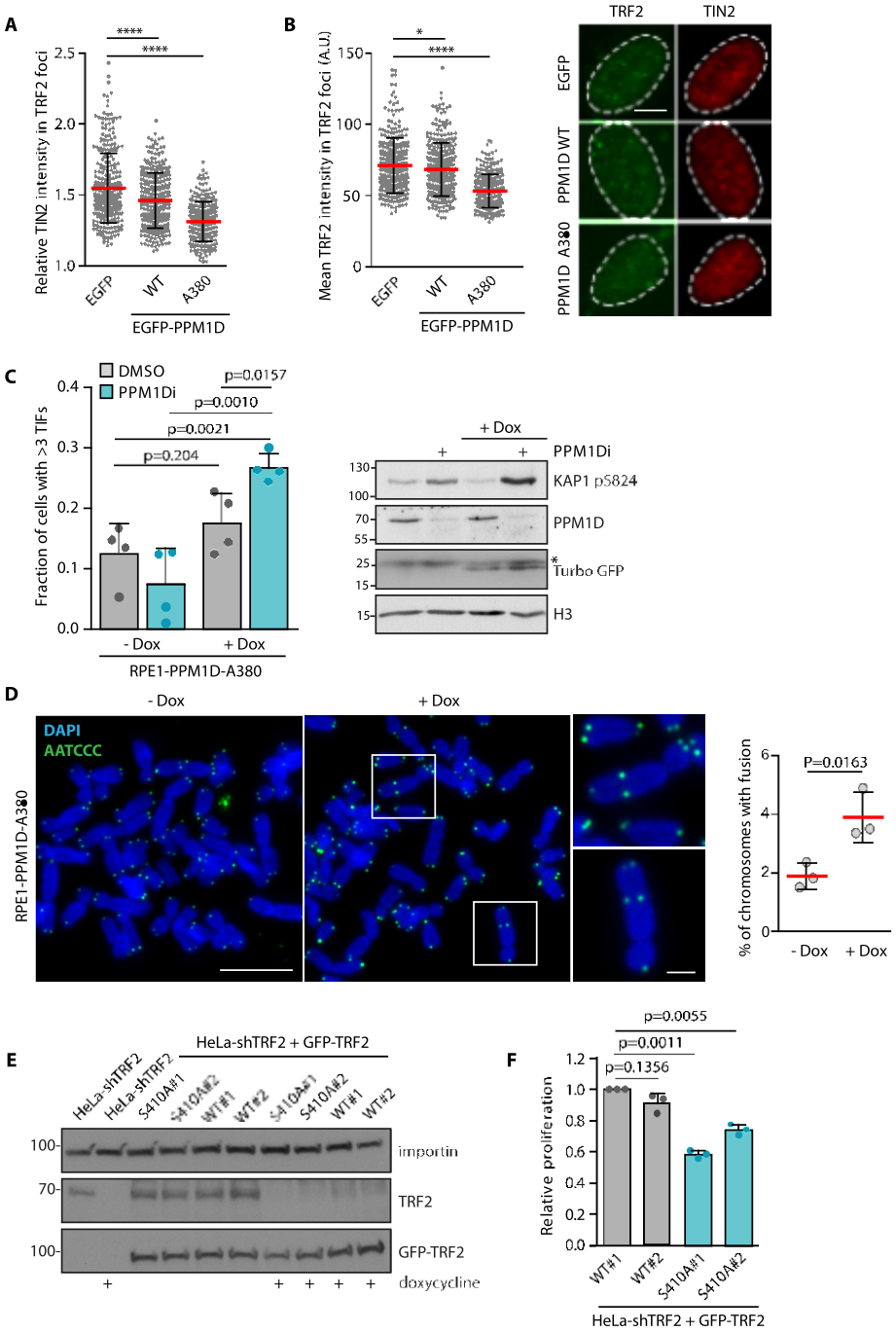

Figure 5. Increased PPM1D activity at telomere impairs shelterin function. (**A**) U2OS cells were fixed 24 h after transfection with the wild type or A380 mutant of PPM1D, and were stained with TRF2 and TIN2 antibodies. Relative TIN2 intensity in TRF2 foci is plotted ± SD, $n \geq 286$. Statistical significance was evaluated using Mann–Whitney test (****$P < 0.0001$). (**B**) Plotted is the mean intensity of TRF2 staining in nuclear foci ± SD in cells from K. Statistical significance was evaluated using Mann–Whitney test (*$P < 0.05$, ****$P < 0.0001$), $n \geq 286$. The scale bar in representative images corresponds to 10 mm. (**C**) Expression of the catalytic domain of PPM1D was induced or not in RPE1-PPM1D-A380 cells by addition of doxycycline for 10 days and where indicated, PPM1D inhibitor was added to the media 1 h prior fixation. Cells were hybridized with TAACCC FISH-probe, stained for 53BP1, and formation of TIFs was quantified by ScanR microscopy. Plotted is a fraction of cells with more than three TIFs. Mean ± SD is shown, statistical significance was evaluated by unpaired *t*-test ($n = 4$). Whole cell lysates were evaluated by immunoblotting, phosphorylation of KAP1 at S824 is a marker of ATM activity, TurboGFP is a marker of PPM1D-A380 expression, the asterisk indicates a non-specific band. Note that PPM1D (Santa Cruz) recognizes only the endogenous full length PPM1D. (**D**) Quantification of chromosome fusions in RPE1-PPM1D-A380 cells treated or not with doxycycline for 10 days. More than 1246 chromosomes per condition was analyzed in each of the three independent experiments. Mean ± SD is shown, statistical significance was evaluated by paired *t*-test. The scale bars in the representative images corresponds to 10 or 2 mm, respectively. (**E**) HeLa cells with tetracycline-inducible knock down of endogenous TRF2 were stably reconstituted with the wild type or S410A mutant GFP-TRF2 and single cell clones were cultured in the absence or presence of doxycycline for 5 days. Whole cell lysates were analyzed by immunoblotting. (**F**) Cells from E were seeded into 96 wells at 100 cells/well, and cultured for additional 7 days. Relative cell proliferation was determined by resazurin assay. Statistical significance was determined by unpaired *t*-test, $n = 3$.

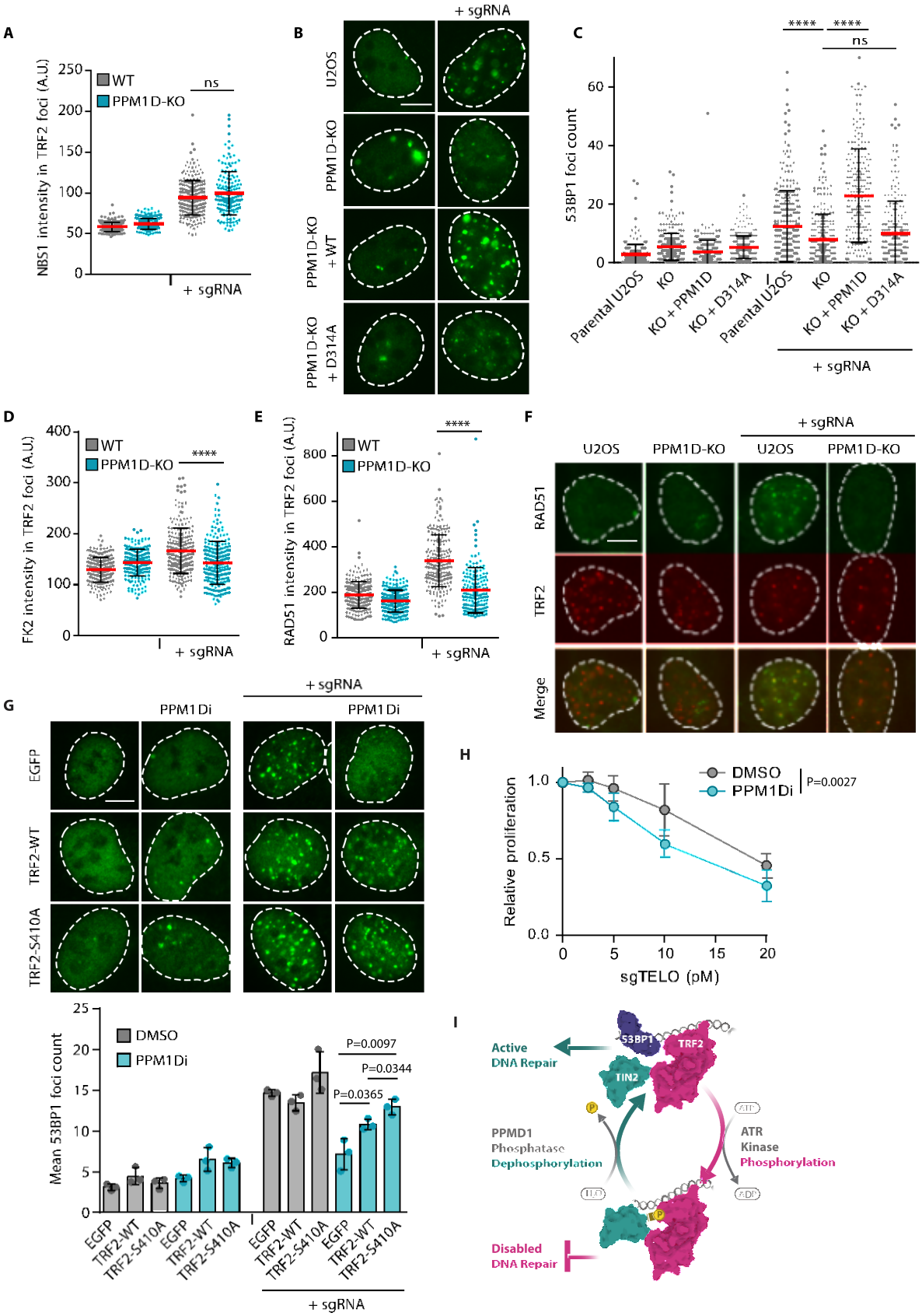

Figure 6. Loss of PPM1D affects recruitment of DNA repair factors to telomeric breaks. (**A**) Parental and U2OS-PPM1D-KO cells were transfected with plasmids coding for Cas9-EGFP with or without the telomere-targeting sgRNA. After 24 h, cells were fixed and stained for NBS1 and TRF2. Plotted

with inducible knock down of endogenous TRF2 and stably reconstituted them with the wild-type or S410A mutant TRF2 (Figure 5E). After 12 days of doxycycline treatment, we compared relative proliferation and found that two independent clones expressing S410A TRF2 proliferated significantly worse than the cells expressing the wild-type TRF2 (Figure 5F) suggesting that impaired phosphorylation of TRF2 leads to suppression of cell proliferation.

Loss of PPM1D supresses recruitment of DNA repair proteins to the DSBs at telomeres

Finally, we investigated the consequence of altered PPM1D activity for DNA repair at telomeres. We induced DSBs at telomeres by Cas9 and compared recruitment of various DNA repair factors in control cells and in PPM1D-KO cells. We found no difference in recruitment of NBS1 suggesting that recognition of the DNA break by MRN complex was unaffected by the loss of PPM1D (Figure 6A, Supplementary Figure S4B). In contrast, we observed that recruitment of 53BP1 protein to telomeric DSBs was significantly reduced in U2OS-PPM1D-KO cells (Figure 6B, C). Similarly, formation of the 53BP1 foci upon Cas9-mediated DNA damage at telomeres was impaired in MCF7 and RPE1 cells treated with PPM1D inhibitor (Supplementary Figure S4C, D). Importantly, recruitment of 53BP1 to damaged telomeres was rescued in U2OS-PPM1D-KO cells by expression of the wild type EGFP-PPM1D (but not with the phosphatase dead D314A mutant) confirming that the phenotype was indeed caused by a loss of PPM1D activity (Figure 6B, C). We also noted that the level of protein ubiquitination detected by FK2 antibody was reduced at damaged telomeres in U2OS-PPM1D-KO cells (Figure 6D, Supplementary Figure S4E). Histone H2A ubiquitination is required for recruitment of 53BP1 and BRCA1 to DNA damage foci, and thus the lack of ubiquitination at telomeres may explain the decreased level of 53BP1 in cells treated with PPM1D inhibitor (75). As the mouse TRF2 has previously been shown to recruit a deubiquitinating enzyme BRCC3 through a so-called iDDR region (36), we tested if the observed defect of 53BP1 binding upon inhibition of PPM1D could be rescued by depletion of BRCC3. However, we did not observe any difference in 53BP1 recruitment to the telomeric DSBs suggesting that the phosphorylation of TRF2 at S410 suppresses 53BP1 recruitment through a distinct molecular mechanism than the iDDR region (Supplementary Figure S4F).

Besides impaired formation of 53BP1 foci, we also observed strongly reduced recruitment of RAD51 to the telomeric breaks suggesting that the repair through homologous recombination is also impaired (Figure 6E, F). To investigate if the effect of PPM1D inhibition on TRF2 phosphorylation and reduced recruitment of 53BP1 are functionally linked, we co-expressed Cas9 together with the telomeric sgRNA and various forms of TRF2 in cells treated or not with PPM1D inhibitor. Whereas expression of the wild-type EGFP-TRF2 did not fully rescue recruitment of 53BP1 to damaged telomeres, expression of the EGFP-TRF2-S410A mutant significantly increased the level of 53BP1 at damaged telomeres (Figure 6G). This result suggests that PPM1D promotes recruitment of 53BP1 to DNA breaks at telomeres by dephosphorylating TRF2.

To evaluate the functional outcome of PPM1D inhibition at damaged telomeres, we determined the relative proliferation of RPE1-iCut cells upon induction of a mild telomeric DNA damage achieved by titrating down of the amount of telomeric sgRNA (46) (Figure 6H, Supplementary Figure S4G). We found that PPM1D inhibition significantly suppressed proliferation of the RPE1-iCut cells that experienced telomeric DNA damage (Figure 6H). We conclude that PPM1D activity is needed for the cell response to telomeric DNA damage although the precise molecular defect in DNA repair remains to be addressed by future research.

In the summary, we show that TRF2 is phosphorylated at S410 upon DNA damage at telomeres by ATR which promotes its interaction with TIN2 and limits recruitment of 53BP1 to the breaks. Phosphorylation of TRF2 is reversed by the activity of PPM1D phosphatase that promotes recruitment of 53BP1 to telomeres (Figure 6I). Physiological levels of TRF2 phosphorylation are required for cell survival as increased TRF2 phosphorylation does not allow efficient repair, while impaired TRF2 phosphorylation su-

←----------

is the mean NBS1 signal in TRF2 foci ± SD, $n \geq 171$. Statistical significance was evaluated using Mann–Whitney test. Representative experiment is shown from two independent repeats. (**B**) Parental, U2OS-PPM1D-KO cells and U2OS-PPM1D-KO cells stably expressing FLAG-PPM1D variants were transfected with plasmids coding for Cas9-EGFP with or without the telomere-targeting sgRNA. After 24 h, cells were fixed and stained for 53BP1, the scale bar represents 10 mm. (**C**) Quantification of (B). Plotted is the mean of 53BP1 foci count ± SD, $n \geq 221$. Statistical significance was evaluated using Mann–Whitney test (****$P < 0.0001$). Representative experiment is shown. (**D**) Cells were treated as in A and were stained for TRF2 and conjugated ubiquitin using Fk2 antibody. Plotted is the mean FK2 signal in TRF2 foci ± SD, $n \geq 205$. Statistical significance was evaluated using Mann–Whitney test (****$P < 0.0001$). Representative experiment is shown from two independent repeats. (**E**) Parental and U2OS-PPM1D-KO cells were transfected as in (A), fixed, and stained for RAD51 and TRF2. Plotted is mean RAD51 intensity in TRF2 foci ± SD, $n \geq 161$. Statistical significance was evaluated using Mann–Whitney test (****$P < 0.0001$). Representative experiment is shown from two independent repeats. (**F**) Representative images for (E), the scale bar represents 10 mm. (**G**) Parental and U2OS-PPM1D-KO cells were co-transfected with plasmids coding for GFP or GFP-TRF2 variants, and FLAG-Cas9 with or without the telomere-targeting sgRNA, and treated or not with PPM1Di for 24 h. Cells were fixed and stained for 53BP1 and FLAG. Only FLAG and GFP double positive cells were analyzed. Means of three independent experiments are plotted ± SD. Statistical significance was evaluated using unpaired *t*-test. Representative images are shown, the scale bar represents 10 mm. (**H**) RPE1-iCut cells were treated overnight with doxycycline and Shield-1 and telomeric DNA damage was induced by transfection of indicated amounts of telomeric sgRNA. Cells were incubated with DMSO or PPM1D inhibitor for 7 days. Relative proliferation was determined by resazurin assay and was normalized to non-treated cells ($n = 3$). (**I**) Model of pTRF2-S410 function at telomere. Under basal conditions, non-phosphorylated TRF2 interacts with TIN2 through its TRFH domain and with telomeric DNA through its Myb domain. Induction of DSBs at telomeres leads to recruitment of DNA repair factors including 53BP1. Upon activation of ATR, TRF2 is phosphorylated at S410, which promotes tight binding of TIN2 and protects the broken telomere from recruitment of 53BP1. Loss of PPM1D activity leads to hyper-phosphorylation of TRF2 and prevents recruitment of 53BP1 to the telomeric DSBs, possibly decreasing the risk of the telomere fusion.

presses shelterin complex assembly and may lead to telomeric fusions.

DISCUSSION

Several components of the shelterin complex were reported to undergo phosphorylation at various conditions, however only some of these events were thoroughly characterized (76). Most importantly, CDK-dependent phosphorylation of TRF2 at Ser365 prevents recruitment of the helicase RTEL1 to telomeres (35). During S phase, TRF2-Ser365 is dephosphorylated by PP6 phosphatase that promotes recruitment of RTEL1, unwinding the t-loops and telomere replication (34,35). Following exposure of cells to ionizing radiation, TRF2 was reported to be transiently phosphorylated at Thr230 allowing its association with DNA lesions outside the telomeres and promoting DNA repair (77–79). However, the role of TRF2 modification in DNA repair of the telomeric lesions has remained unclear.

Here, we report a new phosphorylation of TRF2 at S410 that is strongly induced by Cas9-mediated DSBs at telomeres. Using specific small-molecule inhibitors and RNA interference, we identify ATR as the major kinase responsible for TRF2-S410 modification at damaged telomeres. Further, we show that the level of TRF2-S410 phosphorylation is tightly regulated by PPM1D phosphatase that associates with TRF2 and localizes at the telomeres. Loss of PPM1D or inhibition of its enzymatic activity strongly induced TRF2-S410 phosphorylation at telomeres and promoted recruitment of TIN2 and TPP1 to the telomeres. Since the S410 is located close to the TBM2 region responsible for the interaction with TIN2, we tested the impact of TRF2-S410 phosphorylation on this interaction. An unbiased proteomic approach revealed that the phosphorylated peptide spanning residues 403–417 of TRF2 (but not the non-phosphorylated counterpart), pulled down the TIN2-TPP1-POT1 trimer from the nuclear extract. Subsequently, a fluorescence anisotropy assay performed with synthetic peptides and with purified TIN2 confirmed that TRF2 phosphorylation at S410 increases the affinity between TRF2 and TIN2. When expressed in cells, the non-phosphorylatable TRF2-S410A mutant was able to interact with TIN2, which suggests that phosphorylation is not critically needed for mediating the interaction. On the other hand, the PLA assay revealed a stronger interaction between TRF2 and TIN2 upon inhibition of PPM1D that increases the level of TRF2 phosphorylation at S410. As TRF2 and TIN2 protect the ends of telomeres by promoting t-loop formation, we tested if the activity of PPM1D affects the architecture of the telomeric ends through regulating the shelterin complex assembly. To address this, we imaged the telomeres in psoralen-crosslinked chromatin spreads using Structured Illumination Microscopy and determined the fractions of linear and closed telomeres. Consistent with the published literature, we observed t-loops in about 25% of telomeres in parental cells (33). Nevertheless, fraction of the t-loops was comparable in U2OS-PPM1D-KO cells suggesting that PPM1D activity may not affect the t-loop formation. As approximately half of the imaged telomeres is excluded from the analysis due to inconclusive shape, we also cannot rule out the possibility that the assay is not sensitive enough to detect mild differences in the t-loop formation. Alternatively, the activity of PPM1D may impact a higher-order organization of the telomeres mediated in cis and trans by TRF2 and TIN2 (40).

The main finding of this study is that PPM1D is needed for DNA damage response at telomeric DSBs (Figure 6I). When PPM1D activity was present, cells recruited DNA repair factors to the DSBs located at telomeres. Conversely, loss or inhibition of PPM1D impaired recruitment of the DNA repair factors 53BP1 and RAD51 to the broken telomeres. As the non-phosphorylatable TRF2-S410A mutant rescued the recruitment of 53BP1 significantly better than the wild-type TRF2, we concluded that phosphorylation of TRF2 inhibits DNA damage response at telomeres. The dimerization domain and the iDDR region (corresponding to residues 449–473 of human TRF2) within the hinge domain of TRF2 were previously shown to supress the DNA damage response at telomeres by preventing activation of ATM and by inhibiting the RNF168-dependent ubiquitination, respectively (36). We found that the formation of 53BP1 foci at telomeric DSBs was not rescued by depletion of the BRCC3 or UBR5 in U2OS-PPM1D-KO cells suggesting that PPM1D affects DDR independently of the iDDR region in TRF2. We hypothesize that DSB-induced phosphorylation of TRF2 may allow cells to re-establish the telomere organization by promoting TRF2 association with TIN2-TPP1-POT1. An increased assembly of the shelterin may then interfere with the recruitment of 53BP1 to the break, thus limiting the risk of telomeric fusions. In contrast, dephosphorylation of TRF2 and weakening its interaction with TIN2-TPP1-POT1 could make the telomere more accessible to the recruitment of the DNA repair proteins.

We also noted that overexpression of PPM1D decreased the levels of TRF2 at telomeres which is in line with the disassembly of the shelterin after dephosphorylation of its components. However, we did not observe the formation of the TIFs upon overexpression of PPM1D, possibly due to the ability of PPM1D to efficiently suppress the activity of ATM (7,80). We propose that PPM1D activity needs to be tightly balanced at telomeres to allow the recruitment of DNA repair proteins to DSBs while preventing disassembly of the shelterin from the telomeres. Of note, high levels of active PPM1D are commonly present in cancer cells due to amplification of the chromosomal locus 17q23 or due to gain-of-function mutations in the last exon of *PPM1D* (11,12,65,81,82). It is tempting to speculate that besides the established role of the overexpressed PPM1D in overriding the cell cycle checkpoint, the increased activity of PPM1D could promote genome instability in cancer cells by interfering with the telomere functions.

DATA AVAILABILITY

Data from the mass spectrometry analysis were uploaded to the PRIDE database (accession numbers PXD035268 and PXD035273) and are also provided as source data in the supplementary material.

SUPPLEMENTARY DATA

Supplementary Data are available at NAR Online.

ACKNOWLEDGEMENTS

We are grateful to Kyle Roux, Feng Zhang, Joachim Lingner, Renė H. Medema, Adam Karpf and Titia de Lange for providing reagents, Ivan Novotny for technical assistance with microscopy, Pavel Talacko and Marek Vrbacky for mass spectrometric analysis, Kamila Burdova for help with data analysis, and to Pavel Janscak for critical reading of the manuscript.

FUNDING

Czech Science Foundation [19-15962S]; National Institute for Cancer Research [Programme EXCELES, ID Project No. LX22NPO5102] funded by the EU; P.V. and C.H. were supported by Ministry of Education, Youth and Sports of the Czech Republic [LTAUSA19024]; T.B. by Brno Ph.D. Talent Scholarship; microscopic analysis was performed in the core facility of IMG ASCR supported by MEYS [LM2018129, CZ.02.1.01/0.0/0.0/ 18_046/0016045, RVO 68378050-KAV-NPUI]; proteomic analysis was performed in Laboratory of Mass Spectrometry in BIOCEV, Charles University and in Proteomics Service Laboratory at IPHYS and IMG (supported by RVO) [67985823 and 68378050]. Funding for open access charge: institutional budget of the corresponding author.

Conflict of interest statement. None declared.

REFERENCES

1. Hanahan,D. and Weinberg,RobertA. (2011) Hallmarks of cancer: the next generation. *Cell*, **144**, 646–674.
2. Jackson,S.P. and Bartek,J. (2009) The DNA-damage response in human biology and disease. *Nature*, **461**, 1071–1078.
3. Ciccia,A. and Elledge,S.J. (2010) The DNA damage response: making it safe to play with knives. *Mol. Cell.*, **40**, 179–204.
4. Bartek,J. and Lukas,J. (2007) DNA damage checkpoints: from initiation to recovery or adaptation. *Curr. Opin. Cell. Biol.*, **19**, 238–245.
5. Lindqvist,A., de Bruijn,M., Macurek,L., Bras,A., Mensinga,A. and Bruinsma,W. (2009) Wip1 confers G2 checkpoint recovery competence by counteracting p53-dependent transcriptional repression. *EMBO J.*, **28**, 3196–3206.
6. Jaiswal,H., Benada,J., Müllers,E., Akopyan,K., Burdova,K., Koolmeister,T., Helleday,T., Medema,R.H., Macurek,L. and Lindqvist,A. (2017) ATM/Wip1 activities at chromatin control Plk1 re-activation to determine G2 checkpoint duration. *EMBO J.*, **36**, 2161–2176.
7. Shreeram,S., Demidov,O., Hee,W., Yamaguchi,H., Onishi,N. and Kek,C. (2006) Wip1 phosphatase modulates ATM-dependent signaling pathways. *Mol. Cell.*, **23**, 757–764.
8. Macurek,L., Lindqvist,A., Voets,O., Kool,J., Vos,H. and Medema,R. (2010) Wip1 phosphatase is associated with chromatin and dephosphorylates gammaH2AX to promote checkpoint inhibition. *Oncogene*, **15**, 2281–2291.
9. Moon,S., Lin,L., Zhang,X., Nguyen,T., Darlington,Y., Waldman,A., Lu,X. and LA.,D. (2010) Wildtype p53-induced phosphatase 1 dephosphorylates histone variant gamma-H2AX and suppresses DNA double strand break repair. *J. Biol. Chem.*, **23**, 12935–12947.
10. Burdova,K., Storchova,R., Palek,M. and Macurek,L. (2019) WIP1 promotes homologous recombination and modulates sensitivity to PARP inhibitors. *Cells*, **8**, 1258.
11. Le Guezennec,X. and Bulavin,D.V. (2010) WIP1 phosphatase at the crossroads of cancer and aging. *Trends Biochem. Sci.*, **35**, 109–114.
12. Bulavin,D.V., Demidov,O.N., Saito,S.i., Kauraniemi,P., Phillips,C., Amundson,S.A., Ambrosino,C., Sauter,G., Nebreda,A.R., Anderson,C.W. *et al.* (2002) Amplification of PPM1D in human tumors abrogates p53 tumor-suppressor activity. *Nat. Genet.*, **31**, 210.
13. Husby,S., Hjermind Justesen,E. and Grønbæk,K. (2021) Protein phosphatase, Mg(2+)/Mn(2+)-dependent 1D (PPM1D) mutations in haematological cancer. *Br. J. Haematol.*, **192**, 697–705.
14. Pecháčková,S., Burdová,K. and Macurek,L. (2017) WIP1 phosphatase as pharmacological target in cancer therapy. *J. Mol. Med.*, **95**, 589–599.
15. Denchi,E.L. and de Lange,T. (2007) Protection of telomeres through independent control of ATM and ATR by TRF2 and POT1. *Nature*, **448**, 1068.
16. de Lange,T. (2018) Shelterin-mediated telomere protection. *Annu. Rev. Genet.*, **52**, 223–247.
17. Broccoli,D., Smogorzewska,A., Chong,L. and de Lange,T. (1997) Human telomeres contain two distinct Myb-related proteins, TRF1 and TRF2. *Nat. Genet.*, **17**, 231–235.
18. Schmutz,I., Timashev,L., Xie,W., Patel,D.J. and de Lange,T. (2017) TRF2 binds branched DNA to safeguard telomere integrity. *Nat. Struct. Mol. Biol.*, **24**, 734–742.
19. Benarroch-Popivker,D., Pisano,S., Mendez-Bermudez,A., Lototska,L., Kaur,P., Bauwens,S., Djerbi,N., Latrick,C.M., Fraisier,V., Pei,B. *et al.* (2016) TRF2-mediated control of telomere DNA topology as a mechanism for chromosome-end protection. *Mol. Cell.*, **61**, 274–286.
20. Necasova,I., Janoušková,E., Klumpler,T. and Hofr,C. (2017) Basic domain of telomere guardian TRF2 reduces D-loop unwinding whereas Rap1 restores it. *Nucleic Acids Res.*, **45**, 12170–12180.
21. Baumann,P. and Cech,T.R. (2001) Pot1, the putative telomere end-binding protein in fission yeast and humans. *Science*, **292**, 1171–1175.
22. Lei,M., Podell,E.R. and Cech,T.R. (2004) Structure of human POT1 bound to telomeric single-stranded DNA provides a model for chromosome end-protection. *Nat. Struct. Mol. Biol.*, **11**, 1223–1229.
23. Xin,H., Liu,D., Wan,M., Safari,A., Kim,H., Sun,W., O'Connor,M.S. and Songyang,Z. (2007) TPP1 is a homologue of ciliate TEBP-beta and interacts with POT1 to recruit telomerase. *Nature*, **445**, 559–562.
24. Takai,K.K., Kibe,T., Donigian,J.R., Frescas,D. and de Lange,T. (2011) Telomere protection by TPP1/POT1 requires tethering to TIN2. *Mol. Cell.*, **44**, 647–659.
25. Ye,J.Z., Donigian,J.R., van Overbeek,M., Loayza,D., Luo,Y., Krutchinsky,A.N., Chait,B.T. and de Lange,T. (2004) TIN2 binds TRF1 and TRF2 simultaneously and stabilizes the TRF2 complex on telomeres. *J. Biol. Chem.*, **279**, 47264–47271.
26. Frescas,D. and de Lange,T. (2014) Binding of TPP1 protein to TIN2 protein is required for POT1a,b protein-mediated telomere protection. *J. Biol. Chem.*, **289**, 24180–24187.
27. Kim,S.H., Davalos,A.R., Heo,S.J., Rodier,F., Zou,Y., Beausejour,C., Kaminker,P., Yannone,S.M. and Campisi,J. (2008) Telomere dysfunction and cell survival: roles for distinct TIN2-containing complexes. *J. Cell. Biol.*, **181**, 447–460.
28. O'Connor,M.S., Safari,A., Xin,H., Liu,D. and Songyang,Z. (2006) A critical role for TPP1 and TIN2 interaction in high-order telomeric complex assembly. *Proc. Natl. Acad. Sci. U.S.A.*, **103**, 11874–11879.
29. Frescas,D. and de Lange,T. (2014) TRF2-tethered TIN2 can mediate telomere protection by TPP1/POT1. *Mol. Cell. Biol.*, **34**, 1349–1362.
30. Chen,Y., Yang,Y., van Overbeek,M., Donigian,J.R., Baciu,P., de Lange,T. and Lei,M. (2008) A shared docking motif in TRF1 and TRF2 used for differential recruitment of telomeric proteins. *Science*, **319**, 1092–1096.
31. Hu,C., Rai,R., Huang,C., Broton,C., Long,J., Xu,Y., Xue,J., Lei,M., Chang,S. and Chen,Y. (2017) Structural and functional analyses of the mammalian TIN2-TPP1-TRF2 telomeric complex. *Cell. Res.*, **27**, 1485–1502.
32. Griffith,J.D., Comeau,L., Rosenfield,S., Stansel,R.M., Bianchi,A., Moss,H. and de Lange,T. (1999) Mammalian telomeres end in a large duplex loop. *Cell*, **97**, 503–514.
33. Doksani,Y., Wu,J.Y., de Lange,T. and Zhuang,X. (2013) Super-resolution fluorescence imaging of telomeres reveals TRF2-dependent T-loop formation. *Cell*, **155**, 345–356.
34. Sarek,G., Vannier,J.B., Panier,S., Petrini,J.H.J. and Boulton,S.J. (2015) TRF2 recruits RTEL1 to telomeres in S phase to promote t-loop unwinding. *Mol. Cell.*, **57**, 622–635.
35. Sarek,G., Kotsantis,P., Ruis,P., Van Ly,D., Margalef,P., Borel,V., Zheng,X.F., Flynn,H.R., Snijders,A.P., Chowdhury,D. *et al.* (2019) CDK phosphorylation of TRF2 controls t-loop dynamics during the cell cycle. *Nature*, **575**, 523–527.

36. Okamoto,K., Bartocci,C., Ouzounov,I., Diedrich,J.K., Yates,J.R. 3rd and Denchi,E.L. (2013) A two-step mechanism for TRF2-mediated chromosome-end protection. *Nature*, **494**, 502–505.
37. Dimitrova,N., Chen,Y.C., Spector,D.L. and de Lange,T. (2008) 53BP1 promotes non-homologous end joining of telomeres by increasing chromatin mobility. *Nature*, **456**, 524–528.
38. van Steensel,B., Smogorzewska,A. and de Lange,T. (1998) TRF2 protects human telomeres from end-to-end fusions. *Cell*, **92**, 401–413.
39. Sfeir,A., Kosiyatrakul,S.T., Hockemeyer,D., MacRae,S.L., Karlseder,J., Schildkraut,C.L. and de Lange,T. (2009) Mammalian telomeres resemble fragile sites and require TRF1 for efficient replication. *Cell*, **138**, 90–103.
40. Kaur,P., Barnes,R., Pan,H., Detwiler,A., Liu,M., Mahn,C., Hall,J., Messenger,Z., You,C., Piehler,J. *et al.* (2021) TIN2 is an architectural protein that facilitates TRF2-mediated trans- and cis-interactions on telomeric DNA. *Nucleic Acids Res.*, **49**, 13000–13018.
41. Bandaria,J.N., Qin,P., Berk,V., Chu,S. and Yildiz,A. (2016) Shelterin protects chromosome ends by compacting telomeric chromatin. *Cell*, **164**, 735–746.
42. Timashev,L.A., Babcock,H., Zhuang,X. and de Lange,T. (2017) The DDR at telomeres lacking intact shelterin does not require substantial chromatin decompaction. *Genes Dev.*, **31**, 578–589.
43. Vancevska,A., Douglass,K.M., Pfeiffer,V., Manley,S. and Lingner,J. (2017) The telomeric DNA damage response occurs in the absence of chromatin decompaction. *Genes Dev.*, **31**, 567–577.
44. Pechackova,S., Burdova,K., Benada,J., Kleiblova,P., Jenikova,G. and Macurek,L. (2016) Inhibition of WIP1 phosphatase sensitizes breast cancer cells to genotoxic stress and to MDM2 antagonist nutlin-3. *Oncotarget*, **7**, 14458–14475.
45. Grolimund,L., Aeby,E., Hamelin,R., Armand,F., Chiappe,D., Moniatte,M. and Lingner,J. (2013) A quantitative telomeric chromatin isolation protocol identifies different telomeric states. *Nat. Commun.*, **4**, 2848.
46. van den Berg,J., A,G.M., Kielbassa,K., Feringa,F.M., Freire,R. and Medema,R.H. (2018) A limited number of double-strand DNA breaks is sufficient to delay cell cycle progression. *Nucleic Acids Res.*, **46**, 10132–10144.
47. Friskes,A., Koob,L., Krenning,L., Severson,T.M., Koeleman,E.S., Vergara,X., Schubert,M., van den Berg,J., Evers,B., Manjoń,A.G. *et al.* (2022) Double-strand break toxicity is chromatin context independent. *Nucleic Acids Res.*, **50**, 9930–9947.
48. Smogorzewska,A. and de Lange,T. (2002) Different telomere damage signaling pathways in human and mouse cells. *EMBO J.*, **21**, 4338–4348.
49. Gilmartin,A.G., Faitg,T.H., Richter,M., Groy,A., Seefeld,M.A., Darcy,M.G., Peng,X., Federowicz,K., Yang,J., Zhang,S.-Y. *et al.* (2014) Allosteric Wip1 phosphatase inhibition through flap-subdomain interaction. *Nat. Chem. Biol.*, **10**, 181–187.
50. Cox,J., Hein,M.Y., Luber,C.A., Paron,I., Nagaraj,N. and Mann,M. (2014) Accurate proteome-wide label-free quantification by delayed normalization and maximal peptide ratio extraction, termed MaxLFQ. *Mol. Cell. Proteomics*, **13**, 2513–2526.
51. Tyanova,S., Temu,T., Sinitcyn,P., Carlson,A., Hein,M.Y., Geiger,T., Mann,M. and Cox,J. (2016) The Perseus computational platform for comprehensive analysis of (prote)omics data. *Nat. Methods*, **13**, 731–740.
52. Storchova,R., Burdova,K., Palek,M., Medema,R.H. and Macurek,L. (2021) A novel assay for screening WIP1 phosphatase substrates in nuclear extracts. *FEBS J.*, **288**, 6035–6051.
53. Chapman,J.R. and Jackson,S.P. (2008) Phospho-dependent interactions between NBS1 and MDC1 mediate chromatin retention of the MRN complex at sites of DNA damage. *EMBO Rep.*, **9**, 795–801.
54. Janovič,T., Stojaspal,M., Veverka,P., Horaťková,D. and Hofr,C. (2019) Human telomere repeat binding factor TRF1 replaces TRF2 bound to shelterin core hub TIN2 when TPP1 is absent. *J. Mol. Biol.*, **431**, 3289–3301.
55. Kim,D., Jensen,S., Noble,K., Roux,K., Motamedchaboki,K. and Roux,K. (2016) An improved smaller biotin ligase for BioID proximity labeling. *Mol. Biol. Cell.*, **27**, 1188–1196.
56. Roux,K.J., Kim,D.I., Raida,M. and Burke,B. (2012) A promiscuous biotin ligase fusion protein identifies proximal and interacting proteins in mammalian cells. *J. Cell Biol.*, **196**, 801–810.
57. Chuman,Y., Kurihashi,W., Mizukami,Y., Nashimoto,T., Yagi,H. and Sakaguchi,K. (2009) PPM1D430, a novel alternative splicing variant of the human PPM1D, can dephosphorylate p53 and exhibits specific tissue expression. *J. Biochem.*, **145**, 1–12.
58. Mendez-Bermudez,A., Lototska,L., Bauwens,S., Giraud-Panis,M.J., Croce,O., Jamet,K., Irizar,A., Mowinckel,M., Koundrioukoff,S., Nottet,N. *et al.* (2018) Genome-wide control of heterochromatin replication by the telomere capping protein TRF2. *Mol. Cell.*, **70**, 449–461.
59. Wilson,F.R., Ho,A., Walker,J.R. and Zhu,X.D. (2016) Cdk-dependent phosphorylation regulates TRF1 recruitment to PML bodies and promotes C-circle production in ALT cells. *J. Cell. Sci.*, **129**, 2559–2572.
60. Hussain,T, PurohitG,S.D., Kar,A, Kishore Mukherjee,A, Sharma,S, Sengupta,S, Dhapola,P, Maji,B, Vedagopuram,S, Horikoshi,NT *et al.* (2017) Transcription regulation of CDKN1A (p21/CIP1/WAF1) by TRF2 is epigenetically controlled through the REST repressor complex. *Sci. Rep.*, **7**, 11541.
61. Imran,S.A.M., Yazid,M.D., Cui,W. and Lokanathan,Y. (2021) The intra- and extra-telomeric role of TRF2 in the DNA damage response. *Int. J. Mol. Sci.*, **22**, 9900.
62. Pawluk,A., Amrani,N., Zhang,Y., Garcia,B., Hidalgo-Reyes,Y., Lee,J., Edraki,A., Shah,M., Sontheimer,E.J., Maxwell,K.L. *et al.* (2016) Naturally occurring off-switches for CRISPR-Cas9. *Cell*, **167**, 1829–1838.
63. Bermudez-Hernandez,K., Keegan,S., Whelan,D.R., Reid,D.A., Zagelbaum,J., Yin,Y., Ma,S., Rothenberg,E. and Fenyo¨,D. (2017) A method for quantifying molecular interactions using stochastic modelling and super-resolution microscopy. *Sci. Rep.*, **7**, 14882.
64. Matsuoka,S., Ballif,B.A., Smogorzewska,A., McDonald,E.R. 3rd, Hurov,K.E., Luo,J., Bakalarski,C.E., Zhao,Z., Solimini,N., Lerenthal,Y. *et al.* (2007) ATM and ATR substrate analysis reveals extensive protein networks responsive to DNA damage. *Science*, **316**, 1160–1166.
65. Kahn,J.D., Miller,P.G., Silver,A.J., Sellar,R.S., Bhatt,S., Gibson,C., McConkey,M., Adams,D., Mar,B., Mertins,P. *et al.* (2018) PPM1D truncating mutations confer resistance to chemotherapy and sensitivity to PPM1D inhibition in hematopoietic cells. *Blood*, **132**, 1095.
66. Yamaguchi,H., Durell,S.R., Chatterjee,D.K., Anderson,C.W. and Appella,E. (2007) The Wip1 phosphatase PPM1D dephosphorylates SQ/TQ motifs in checkpoint substrates phosphorylated by PI3K-like kinases. *Biochemistry*, **46**, 12594–12603.
67. Chen,B., Gilbert,L.A., Cimini,B.A., Schnitzbauer,J., Zhang,W., Li,G.W., Park,J., Blackburn,E.H., Weissman,J.S., Qi,L.S. *et al.* (2013) Dynamic imaging of genomic loci in living human cells by an optimized CRISPR/Cas system. *Cell*, **155**, 1479–1491.
68. Takai,H., Smogorzewska,A. and de Lange,T. (2003) DNA damage foci at dysfunctional telomeres. *Curr. Biol.*, **13**, 1549–1556.
69. Mao,P., Liu,J., Zhang,Z., Zhang,H., Liu,H., Gao,S., Rong,Y.S. and Zhao,Y. (2016) Homologous recombination-dependent repair of telomeric DSBs in proliferating human cells. *Nat. Commun.*, **7**, 12154.
70. Doksani,Y. and de Lange,T. (2016) Telomere-internal double-strand breaks are repaired by homologous recombination and PARP1/Lig3-dependent end-joining. *Cell Rep.*, **17**, 1646–1656.
71. Veverka,P., Janovič,T. and Hofr,C. (2019) Quantitative biology of human shelterin and telomerase: searching for the weakest point. *Int. J. Mol. Sci.*, **20**, 3186.
72. Hu,C., Rai,R., Huang,C., Broton,C., Long,J., Xu,Y., Xue,J., Lei,M., Chang,S. and Chen,Y. (2017) Structural and functional analyses of the mammalian TIN2-TPP1-TRF2 telomeric complex. *Cell. Res.*, **27**, 1485–1502.
73. Van Ly,D., Low,R.R.J., Frölich,S., Bartolec,T.K., Kafer,G.R., Pickett,H.A., Gaus,K. and Cesare,A.J. (2018) Telomere loop dynamics in chromosome end protection. *Mol. Cell.*, **71**, 510–525.
74. Shreeram,S., Demidov,O.N., Hee,W.K., Yamaguchi,H., Onishi,N., Kek,C., Timofeev,O.N., Dudgeon,C., Fornace,A.J., Anderson,C.W. *et al.* (2006) Wip1 phosphatase modulates ATM-dependent signaling pathways. *Mol. Cell*, **23**, 757–764.
75. Fradet-Turcotte,A., Canny,M.D., Escribano-Diaz,C., Orthwein,A., Leung,C.C.Y., Huang,H., Landry,M.-C., Kitevski-LeBlanc,J., Noordermeer,S.M., Sicheri,F. *et al.* (2013) 53BP1 is a reader of the DNA-damage-induced H2A Lys 15 ubiquitin mark. *Nature*, **499**, 50–54.

76. Walker,J.R. and Zhu,X.D. (2012) Post-translational modifications of TRF1 and TRF2 and their roles in telomere maintenance. *Mech. Ageing. Dev.*, **133**, 421–434.
77. Tanaka,H., Mendonca,M.S., Bradshaw,P.S., Hoelz,D.J., Malkas,L.H., Meyn,M.S. and Gilley,D. (2005) DNA damage-induced phosphorylation of the human telomere-associated protein TRF2. *PNAS*, **102**, 15539–15544.
78. Huda,N., Tanaka,H., Mendonca,M.S. and Gilley,D. (2009) DNA damage-induced phosphorylation of TRF2 is required for the fast pathway of DNA double-strand break repair. *Mol. Cell. Biol.*, **29**, 3597–3604.
79. Bradshaw,P.S., Stavropoulos,D.J. and Meyn,M.S. (2005) Human telomeric protein TRF2 associates with genomic double-strand breaks as an early response to DNA damage. *Nat. Genet.*, **37**, 193–197.
80. Shreeram,S., Hee,W., Demidov,O., Kek,C., Yamaguchi,H. and Fornace,A. (2006) Regulation of ATM/p53-dependent suppression of myc-induced lymphomas by Wip1 phosphatase. *J. Exp. Med.*, **203**, 2793–2799.
81. Hsu,J.I., Dayaram,T., Tovy,A., De Braekeleer,E., Jeong,M., Wang,F., Zhang,J., Heffernan,T.P., Gera,S., Kovacs,J.J. *et al.* (2018) PPM1D mutations drive clonal hematopoiesis in response to cytotoxic chemotherapy. *Cell. Stem. Cell.*, **23**, 700–713.
82. Kleiblova,P., Shaltiel,I.A., Benada,J., Sevcik,J., Pechackova,S., Pohlreich,P., Voest,E.E., Dundr,P., Bartek,J., Kleibl,Z. *et al.* (2013) Gain-of-function mutations of PPM1D/Wip1 impair the p53-dependent G1 checkpoint. *J. Cell. Biol.*, **201**, 511–521.

biomedicines

MDPI

Article

Identification of Germline Mutations in Melanoma Patients with Early Onset, Double Primary Tumors, or Family Cancer History by NGS Analysis of 217 Genes

Lenka Stolarova [1,2,y], Sandra Jelinkova [1,y], Radka Storchova [2], Eva Machackova [3], Petra Zemankova [1], Michal Vocka [4], Ondrej Kodet [5,6,7], Jan Kral [1], Marta Cerna [1], Zuzana Volkova [1], Marketa Janatova [1], Jana Soukupova [1], Viktor Stranecky [8], Pavel Dundr [9], Lenka Foretova [3], Libor Macurek [2], Petra Kleiblova [10] and Zdenek Kleibl [1,*]

1 Institute of Biochemistry and Experimental Oncology, First Faculty of Medicine, Charles University, 128 53 Prague, Czech Republic; lenka.stolarova@lf1.cuni.cz (L.S.); sandra.jelinkova@lf1.cuni.cz (S.J.); petra.zemankova@lf1.cuni.cz (P.Z.); jan.kral@lf1.cuni.cz (J.K.); marta.cerna@lf1.cuni.cz (M.C.); zuzana.klusonova@lf1.cuni.cz (Z.V.); marketa.janatova@lf1.cuni.cz (M.J.); jana.soukupova@lf1.cuni.cz (J.S.)

2 Laboratory of Cancer Cell Biology, Institute of Molecular Genetics of the Czech Academy of Sciences, 142 20 Prague, Czech Republic; radka.storchova@img.cas.cz (R.S.); libor.macurek@img.cas.cz (L.M.)

3 Department of Cancer Epidemiology and Genetics, Masaryk Memorial Cancer Institute, 656 53 Brno, Czech Republic; emachack@mou.cz (E.M.); foretova@mou.cz (L.F.)

4 Department of Oncology, First Faculty of Medicine, Charles University and General University Hospital in Prague, 128 08 Prague, Czech Republic; michal.vocka@vfn.cz

5 Department of Dermatology and Venereology, First Faculty of Medicine, Charles University and General University Hospital in Prague, 128 08 Prague, Czech Republic; ondrej.kodet@vfn.cz

6 Institute of Anatomy, First Faculty of Medicine, Charles University, 128 00 Prague, Czech Republic

7 BIOCEV, First Faculty of Medicine, Charles University, 252 50 Vestec, Czech Republic

8 Research Unit for Rare Diseases, Department of Paediatrics and Inherited Metabolic Disorders, First Faculty of Medicine, Charles University and General University Hospital in Prague, 121 00 Prague, Czech Republic; Viktor.Stranecky@lf1.cuni.cz

9 Department of Pathology, First Faculty of Medicine, Charles University and General University Hospital in Prague, 128 00 Prague, Czech Republic; pavel.dundr@vfn.cz

10 Institute of Biology and Medical Genetics, First Faculty of Medicine, Charles University and General University Hospital in Prague, 128 00 Prague, Czech Republic; petra.kleiblova@lf1.cuni.cz

* Correspondence: zdenek.kleibl@lf1.cuni.cz; Tel.: +420-22496-5745

y These authors equally contributed to this work.

Received: 31 August 2020; Accepted: 5 October 2020; Published: 9 October 2020

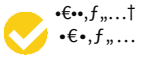

Abstract: Cutaneous melanoma is the deadliest skin malignity with a rising prevalence worldwide. Patients carrying germline mutations in melanoma-susceptibility genes face an increased risk of melanoma and other cancers. To assess the spectrum of germline variants, we analyzed 264 Czech melanoma patients indicated for testing due to early melanoma (at <25 years) or the presence of multiple primary melanoma/melanoma and other cancer in their personal and/or family history. All patients were analyzed by panel next-generation sequencing targeting 217 genes in four groups: high-to-moderate melanoma risk genes, low melanoma risk genes, cancer syndrome genes, and other genes with an uncertain melanoma risk. Population frequencies were assessed in 1479 population-matched controls. Selected POT1 and CHEK2 variants were characterized by functional assays. Mutations in clinically relevant genes were significantly more frequent in melanoma patients than in controls (31/264; 11.7% vs. 58/1479; 3.9%; p = 2.0 10 ^{6}). A total of 9 patients (3.4%) carried mutations in high-to-moderate melanoma risk genes (CDKN2A, POT1, ACD) and 22 (8.3%) patients in other cancer syndrome genes (NBN, BRCA1/2, CHEK2, ATM, WRN, RB1). Mutations in high-to-moderate melanoma risk genes (OR = 52.2; 95%CI 6.6–413.1; p = 3.2 10 ^{7}) and in other cancer syndrome genes (OR = 2.3; 95%CI 1.4–3.8; p = 0.003) were significantly associated with melanoma risk.

We found an increased potential to carry these mutations (OR = 2.9; 95%CI 1.2–6.8) in patients with double primary melanoma, melanoma and other primary cancer, but not in patients with early age at onset. The analysis revealed aected genes in Czech melanoma patients and identified individuals who may benefit from genetic testing and future surveillance management of mutation carriers.

Keywords: melanoma; familial melanoma; hereditary cancer predisposition; germline mutations; panel sequencing; NGS

1. Introduction

With 287,723 newly diagnosed cases and 60,712 fatalities in 2018, cutaneous melanoma remains the deadliest skin malignity globally. The highest standardized melanoma incidence occurs in Australia and New Zealand; however, European and US patients account for more than 75% of new melanoma cases annually [1]. The GLOBOCAN cancer registry ranks the Czech Republic as 18th among 185 countries in the world in terms of age-standardized melanoma incidence rates (between the USA and Canada) [2].

The risk of melanoma is largely modified by factors influencing individual sensitivity to UV radiation and sunlight exposure, and sunburns during childhood in particular are a major behavioral risk factor [3]. Other individual host factors include the amount, type, and arrangement of cutaneous melanin, the presence of multiple atypical moles (the most frequent precancerous melanoma lesions), and a family history of melanoma [4].

The hereditary component of melanoma development has been assessed in a large prospective study of twins from Nordic countries revealing melanoma heritability with a familial cancer risk of 19.6% and 6.1% for monozygotic and dizygotic twins, respectively, compared with 1.2% for the overall population [5]. The proportion of familial melanoma cases is approximately 5–10%; however, pathogenic germline mutation carriers have been identified in only a minority of the analyzed familial melanoma cases [6].

The major melanoma-susceptibility gene is CDKN2A, coding for two alternatively transcribed mRNAs translated into the cyclin-dependent kinase inhibitor $p16^{INK4}$ and the tumor suppressor $p14^{ARF}$ participating in p53 activation, respectively [7]. Germline CDKN2A mutations have been found in about 20–40% of melanoma-prone families (with 3 melanoma cases), but in only 0.2–3% of non-familial melanoma cases [8,9]. Other high-risk but extremely rare germline mutations aect cyclin-dependent kinase 4 (CDK4) and BRCA1-associated protein 1 (BAP1) genes [10,11]. Germline CDK4 mutations cluster in exon 2, coding for a domain interacting with $p16^{INK4}$ [12]. The BAP1 protein codes for deubiquitinase, counteracting BRCA1-BARD1 ubiquitin ligase activity [13]. Hereditary BAP1 mutations predispose people to hypopigmented skin melanoma, uveal melanoma, mesothelioma, renal cell carcinoma, and other cancers [13]. Other potential high- to moderate-risk genes include ACD (also known as TPP1), POT1, and TER2IP coding for shelterin proteins forming a telomere-protecting complex [14]. Rare promoter mutations in telomerase (TERT gene) coding for an enzyme-maintaining telomere length have been found in familial melanoma [15]. An increased melanoma risk has been documented in carriers of germline mutations causing other cancer syndromes, including hereditary breast and ovarian cancer (BRCA1/BRCA2), retinoblastoma (RB1), or xeroderma pigmentosum (XPs) [16]. The low-risk group includes variants in genes coding for proteins involved in melanogenesis (MC1R, MITF, OCA2, SLC45A2, TYR, TYRP1) and other processes (ASIP, CASP8, MTAP, OBFC1), revealed dominantly by genome-wide association studies (GWAS) [17–19]. The identification of individuals carrying germline mutations in melanoma-predisposition genes enables their tailored surveillance with an early detection of melanoma and other associated tumors, and with genetic counselling for their relatives.

The Czech national cancer registry has recorded nearly doubled melanoma incidence during the past 25 years (from 7.55 cases per 100,000 inhabitants in 1994 to 13.47 in 2018), and melanoma has become the most rapidly growing malignant tumor among children and teenagers [20,21]. However, an analysis of genetic factors contributing to its development has not been performed in the Czech Republic to date.

Our study aimed primarily to characterize the spectrum and prevalence of germline mutations influencing melanoma risk. We have analyzed 264 high-risk Czech melanoma patients by panel next generation sequencing (NGS) targeting 217 genes that included eight high-to-moderate melanoma risk genes, 26 low melanoma risk genes, 37 other cancer-predisposing genes and 146 genes altered in melanoma but not associated with increased familial risk. Another task of our study was to identify melanoma patients who may benefit from genetic testing by comparing clinicopathological data from the carriers and non-carriers of germline mutations.

2. Materials and Methods

2.1. Study Population

We analyzed genomic DNA obtained from the peripheral blood of 264 unrelated melanoma patients indicated for a genetic analysis by medical geneticists based on individual or family criteria (Table 1). All patients were Caucasians of a Czech origin and provided written informed consent with the analysis approved by Ethics Committee of the General University Hospital in Prague (No.: 56/15 Grant VES 2016 AZV 1.LFUK from 2015/06/18). The patients included a subgroup of 129 individuals (97 females/32 males) indicated at the General University Hospital in Prague and 135 individuals (96 females/39 males) indicated at the Masaryk Memorial Cancer Institute in Brno. Known clinicopathological characteristics are provided in Supplementary Table S1.

Table 1. Characteristic of subgroups combining personal cancer history (rows) and family cancer history (FCH; columns) criteria in 264 melanoma (M.) patients enrolled in the study.

Criteria	Posit. FCH incl. M.	Posit. FCH incl. Other Cancers	Negative FCH	Unknown FCH	Patients; N (%)	Mean Age; yrs (Range)
Multiple primary M. & other cancer	0	4	0	2	6 (2.3)	45.0 (38–58)
Multiple primary M.	5	8	3	1	17 (6.4)	37.3 (24–75)
M. & other cancer	9	45	9	8	71 (26.9)	47.3 (14–83)
M. only, dg at < 25 yrs	5	17	11	3	36 (13.6)	20.0 (9–24)
M. only, dg at 25 yrs	41	62	24	7	134 (50.8)	37.1 (25–69)
Patients; N (% of all)	60 (22.7)	136 (51.5)	47 (17.8)	21 (8.0)	264 (100)	37.7 (9–83)
Mean age; yrs (range)	38.9 (9–69)	37.8 (14–83)	33.0 (15–66)	44.2 (14–75)	-	-

The control population included germline variants in targeted genes obtained from whole exome sequencing (WES) performed for various non-cancer conditions in 1479 unselected, adult, anonymized, ethnically matched controls (1014 males, mean age 55.5 years, range 18–88 years and 465 females, mean age 56.8 years, range 18–84). These anonymized genotypes of population-matched controls were provided by the National Center for Medical Genomics (http://ncmg.cz).

2.2. CZMELAC Sequence Capture Panel

The CZMELAC panel (CZech MELAnoma panel for Cancer predisposition) targeted 217 genes including (i) high-to-moderate and (ii) low melanoma risk genes, (iii) hereditary cancer syndrome genes with an uncertain melanoma risk, (iv) genes associated with "melanoma" in the Phenopedia database with at least two entries (assessed June 16, 2016; Table 2) [6,9,14,16,22–25].

The primary gene target for probe coverage was represented by all coding exons, including 10 bases from adjacent intronic regions, and it was designed using the NimbleDesign software (Roche) as

described previously [26,27]. The final CZMELAC panel target reached 563,471 bases. Because of the strict design conditions, some repeats and homologous regions were left untargeted (Supplementary Table S2).

Table 2. Analyzed genes in CZEMELAC (CZech MELAnoma panel for Cancer predisposition) panel. Detailed information, including full names of analyzed genes, is provided in Supplementary Table S2.

High-to-moderate melanoma risk genes	ACD, BAP1, CDK4, CDKN2A, MITF, POT1, TERF2IP, TERT
Low melanoma risk genes	AGR3, ARNT, ASIP, CASP8, CCND1, CDKN2B, CLPTM1L, FTO, HERC2, IRF4, MC1R, MGMT, MTAP, MX2, OBFC1, OCA2, PARP1, PLA2G6, SETDB1, SLC24A4, SLC45A2, TERF1, TERF2, TINF2, TYR, TYRP1
Hereditary cancer syndrome genes with uncertain melanoma risk	APC, ATM, BARD1, BMPR1A, BRCA1, BRCA2, BRIP1, CDH1, FH, CHEK2, KIT, MET, MSH2, MSH3, MSH6, NBN, NF1, NF2, PALB2, PMS2, POLD1, POLE, PTEN, RAD51C, RAD51D, RB1, RET, SDHA, SDHB, SDHC, SDHD, SMAD4, STK11, TP53, VHL, WRN, WT1
Genes with unknown impact on hereditary melanoma development	ABLIM1, APEX1, ATRN, AURKA, BBC3, BLM, BRAF, BRMS1, CASP10, CBL, CCAR2, CCNH, CDK10, CDK7, CDKN1A, CDKN1B, CDKN1C, CEBPA, COX8A, CTLA4, CTNNB1, CYP11A1, CYP17A1, CYP19A1, CYP1A1, CYP1A2, CYP3A5, DAB2IP, DCAF4, DDB1, DDB2, EDNRB, EGF, EGFR, EIF1AX, EPCAM, ERBB2, ERBB4, ERCC1, ERCC2, ERCC3, ERCC4, ERCC5, ERCC6, ERCC8, EXOC2, EZH2, FANCC, FANCL, FANCM, FAS, FASLG, FGFR2, FGFR4, FLCN, FLT1, FOXP3, GATA2, GATA4, GC, GNA11, GNAQ, GPC3, GSTM1, GSTM3, GSTP1, GSTT1, H2AFY, HRAS, IDH1, IDH2, IFIH1, IFNA1, IFNG, IL10, IL2RA, IL4, IL6, IL8, ING4, KAT6A, KIAA1967, KMT2A, KRAS, LRIG1, MAP2K1, MDM2, MLH1, MLH3, MMP1, MMP3, MUTYH, MYH7B, NCOA6, NFKB1, NFKBIE, NOD2, NOTCH3, NRAS, PAX5, PDGFRA, PIGU, PIK3CA, PIK3R1, PIK3R4, PMAIP1, PMS1, POLH, POMC, PPM1D, PPP6C, PRF1, PTGS2, PTCH1, PTPN11, PTPN22, RAC1, RAD23A, RAD23B, RASEF, RECQL, RECQL4, RHOBTB2, RUNX1, SBDS, SF3B1, SH2B3, SLX4, SMARCB1, SNX31, STAG2, STK19, SUZ12, TACC1, TERC, TLR3, TRPM1, TSC1, TSC2, VDR, XAB2, XPA, XPC, XRCC1, XRCC3, ZNF365

2.3. Targeted NGS Analysis

Genomic DNA was isolated from peripheral blood and 200–500 ng was used to prepare the NGS library. DNA was diluted in low TE buer [10 mM Tris-HCl (pH 8.0) with 0.1 mM EDTA] and sheared by ultrasound (Covaris E220; Covaris, Chicago, IL, USA) to approximately 200 bp fragments checked using Agilent High Sensitivity DNA Kit on the 2100 Bioanalyzer (Agilent, Santa Clara, CA, USA). The subsequent end-repair, A-tailing, and ligation of adapters were performed using the KAPA HTP Library Preparation kit (Roche, Basel, Switzerland) according to the manufacturer with in-house prepared adapters. The processed fragments were size-selected (targeting 250–450 bp fragments) and primed with barcodes (identical to Illumina TruSeq HT index i7 and i5) by ligation-mediated PCR (LM-PCR), using in-house prepared double-indexing primers, to distinguish individual samples in subsequent pooling. The size and quality of fragments after the dual size selection and LM-PCR were controlled using Agilent High Sensitivity DNA Kit. Thirty individual samples (33 ng each) were pooled for enrichment and hybridized for 72 h with the CZMELAC panel probes (SeqCap EZ Choice Library; Roche, Basel, Switzerland). The enriched targeted sequences were amplified by post-capture PCR to create the final sequencing library. The enrichment was controlled using qPCR (NimbleGen SeqCap EZ Library SR User's Guide). The final 15 M library was sequenced on MiSeq using MiSeq Reagent Kit v. 3 (150 cycles; Illumina, San Diego, CA, USA) targeting 100 mean coverage per sample.

2.4. Bioinformatics

The CZMELAC panel sequencing data generated in FASTQ files were analyzed as described previously [27]. Novoalign was used for mapping FASTQ files to hg19 reference. The variant-call format (VCF) files were processed by the GATK pipeline (https://software.broadinstitute.org/gatk/) from BAM files. The VCF files were annotated using SnpE. We identified medium-size indels (insertions or duplications >35bp) using Pindel (http://gmt.genome.wustl.edu/packages/pindel/) and copy number variations (CNV) using CNVkit (https://pypi.python.org/pypi/CNVkit), using the settings that we described in detail recently [26,27].

2.5. Variant Filtration and Prioritization

The primary list of annotated sequences was filtered in successive steps that included the elimination of: (i) low quality variants (quality < 150); (ii) out of bait variants (intergenic/deep intronic/UTR variants); (iii) intronic variants out of canonical splicing sites (1–2 nucleotides in introns); (iv) variants with a minor allele frequency (MAF) > 0.003 in any of the ExAC/ESP6500/1000Genomes databases; (v) variants with MAF > 0.001 (n > 2) in 1479 population-matched controls; (vi) synonymous variants; (vii) variants referred to as benign or likely benign (B/LB) in ClinVar; (viii) variants located in the repeat masking track from the UCSC Genome Browser; (ix) frameshift/stop-gain variants in the last exon. Filtration steps ii-ix were not applied if the found variants were referred to as pathogenic/likely pathogenic (P/LP) in ClinVar or "deleterious" in our functional analyses. The dataset of the control population was filtered identically. The final set of P/LP variants included only frameshift, stop-gain, frameshifting CNV, canonical splicing, ClinVar P/LP variants, and variants classified as "deleterious" by our functional analyses. All P/LP variants (variants with very strong and strong evidence of pathogenicity according to the ACMG guidelines [28] denoted throughout this text also as "mutations") were in melanoma patients manually inspected in IGV and, when uncertain, confirmed by Sanger sequencing. The CNV P/LP variants were confirmed by multiplex ligation-dependent probe amplification (MLPA; for CHEK2) or by quantitative PCR (for SLC45A2 and TRPM1; Supplementary Figure S1).

2.6. Analysis of Splicing Alterations

All RNA samples obtained from peripheral blood or from expanded leukocytes (with/without nonsense-mediated decay inhibitor) were analyzed for splicing alterations using targeted RNA NGS with the CZMELAC panel, as described recently [29].

2.7. Statistical Analysis

The dierences between the analyzed groups and subgroups were calculated by ^{2} or Fischer exact tests.

2.8. Functional Assays for Selected Germline Variants

2.8.1. CHEK2 Functional Analysis

A functional analysis of CHEK2 VUS was performed as described recently [30]. Human RPE1-CHEK2-knock-out cells were transfected with wild-type or mutant EGFP-CHK2 and the level of KAP1-S473 phosphorylation was determined by immunofluorescence microscopy using ScanR station (Olympus, Tokyo, Japan).

2.8.2. POT1 Functional Analysis

Cell lines and plasmids. MCF-7 and HEK293 cells (generously provided by Rene Medema, NKI, Amsterdam) were grown in DMEM containing 6% FBS, penicillin (100 U/mL) and streptomycin (0.1 mg/mL). The cells were regularly tested for mycoplasma contamination using the MycoAlert kit (Lonza, Basel, Switzerland). A DNA fragment corresponding to human POT1 was PCR-amplified from pLPC-myc-hPOT1 (Addgene, ID:12387, Watertown, MA, USA) and inserted in frame into the XhoI/XmaI sites of pEGFP-C3. Plasmid pCDNA-3xFLAG-NLS-TPP1 was obtained from Addgene (ID: 53585, Watertown, MA, USA). Cells were transfected with plasmid DNA using polyethylenimine 40K (Polysciences, Warrington, PA, USA).

Immunofluorescence microscopy. To evaluate the localization of POT1 at telomeres, MCF-7 cells grown on coverslips were transfected with EGFP-POT1 or EGFP-POT1-P116L and analyzed by immunofluorescence microscopy. Cells were pre-extracted with 0.5% Triton-X 100 in ice-cold PBS for 5 min and fixed with 4% PFA for 15 min in room temperature (RT). Cells were blocked in 1% BSA for 30 min. Coverslips were incubated with TRF2 antibody (clone B-5, Santa Cruz, Dallas, TX, USA) for

2 h in RT, washed 3 in PBS, incubated with secondary antibody for 1h in RT. After washing in PBS and DAPI, coverslips were mounted with Vectashield and images were acquired using the confocal microscope Leica (Wetzlar, Germany) TCS SP8 equipped with a 63x/1.40 objective.

Immuno-precipitation. The ability of POT1 to interact with the shelterin complex was evaluated by immuno-precipitation. HEK293 cells were co-transfected with FLAG-TPP1 and EGFP, EGFP-POT1 or EGFP-POT1-P116L. Cells were extracted in IP buer (50 mM Tris pH 8.0, 120 mM NaCl, 1% Tween-20, 0.1% NP-40, 1.0% glycerol, 2 mM EDTA, 3 mM EGTA, 10 mM $MgCl_2$, protease inhibitors (Roche, Basel, Switzerland) and EtBr (50 g/mL)) and sonicated 3 20 sec. Clarified cell extracts were incubated with GFP-Trap beads (Chromotek, Planegg, Germany) for 1 h. After washing 4 with IP buer, bound proteins were eluted with Laemli buer and separated by SDS-PAGE.

Telomeric DNA binding assay. POT1 binding to telomeric DNA was tested in vitro as described [31,32]. HEK293 cells transfected with EGFP, EGFP-POT1 or EGFP-POT1-P116L were extracted in IP buffer, sonicated and centrifuged for 20 min at 4 C. Cell extracts were precleared with streptavidin sepharose beads for 1 h. Supernatants were then incubated with 2 g of biotinylated telomeric DNA (ssG: biotin-TATATA(TTAGGG)8) or (tel5: biotin-GCAAGCTTTACCGATACA GC(TTAGGG)5) [31,32], or control DNA (ssC: biotin-TATATA(CCCTAA)8), for 12 h and Streptavidin beads were added for 1 h before washing with IP buer. Bound proteins were eluted with Laemli buer and analyzed by Western blotting (WB) using antibody against GFP (clone 7.1, Roche, Basel, Switzerland).

3. Results

3.1. Germline Variants in Analyzed Genes

The overall mean coverage for all samples reached 116.7 with a good coverage uniformity across 217 analyzed genes (mean percent of target bases with coverage 20, 50, and 100 was 99.3%, 96.9%, and 79.2%, respectively). Panel NGS in 264 patients yielded 16,359 unique germline variants. Five hundred and sixteen of them remained after the application of variant filtration rules (described in the Methods section). Variants of uncertain significance (VUS) represented a majority (87%) of them and were excluded from further analyses as clinically inconclusive at the moment. The final 83 pathogenic/likely pathogenic (P/LP) germline variants (66 unique) in 71/264 (26.8%) melanoma patients were detected in 42/217 targeted genes (Supplementary Table S3) and included five copy number variants (CNV; two in CHEK2 and SLC45A2, respectively, and one in TRPM1; Supplementary Figure S1). Using the identical prioritization procedure, we identified 225 P/LP variants in 204/1479 (13.8%) controls in 82/217 targeted genes, including two CNV (both in the CHEK2 gene). Overall, 43/264 (16.3%) patients (Table 3) and 87/1479 (5.9%) controls carried a mutation in a gene previously associated with melanoma or other cancer.

Table 3. Germline P/LP (pathogenic/likely pathogenic) variants in melanoma patients.

(a)	Gene: Coding Sequence (Protein) Change - Concomitant Mutation	Mel Site (Age) (b)	Other Tumors in Proband (Age)	Family Cancer History Tumor Type (N) (c)
	High-to-moderate risk genes			
F	CDKN2A: c.16_20del5 (p.G6Qfs*7)	TR (38)	none	BC (1), Leu (1), Mel (1), other 3 relatives with unknown tumors
F	CDKN2A: c.71G>C (p.R24P)	TR (24)	Mel (35)	CRC (1), Mel (1), UrC(1)
F	CDKN2A: c.71G>C (p.R24P)	TR (28)	Mel (38)	Mel (2)
F	CDKN2A: c.95_112del (p.L32_L37del)	LE (28)	GC (48)	BC (2), CRC(1), GC (1), LC (1), Mel (2)
M	CDKN2A: c.334C>G (p.R112G)	HE (43)	none	Mel (1), PaC(1)
F	CDKN2A: c.457+4_457+5delAG (p.Y129Hfs*11)	TR (29)	Mel (34)	BT (1)
F	POT1: c.347C>T (p.P116L); - CHEK2: c.909-2028_1095+330del5395 (p.M304Lfs*15)	UE (41)	Mel (41,42,44); BC (47)	RC (1)
F	POT1: c.703-1G>C (p.V235Gfs*22)	n.a. (37)	TC (34); BT (47)	BC (1), CRC (1), LC(1), SgT (1), TC (1)
M	ACD: c.755delA (p.D255Afs*9)	UE (39)	none	negative

Table 3. Cont.

(a)	Gene: Coding Sequence (Protein) Change - Concomitant Mutation	Mel Site (Age) (b)	Other Tumors in Proband (Age)	Family Cancer History Tumor Type (N) (c)
Low-risk genes				
F	OCA2: c.1211C>T (p.T404M); - KAT6A: c.1138G>T (p.E380*)	n.a. (29)	none	Mel(1)
M	OCA2: c.1327G>A (p.V443I)	TR (15)	none	negative
F	OCA2: c.1327G>A (p.V443I)	TR (43)	none	BC (3), CRC (3), PaC (1)
F	OCA2: c.1327G>A (p.V443I)	LE (52)	Ly (38); SkC (49)	Leu (1), Unknown (1)
M	OCA2: c.2037G>C (p.W679C)	n.a. (50)	none	negative
M	OCA2: c.2037G>C (p.W679C)	n.a. (68)	SkC (68)	n.a.
M	TYRP1: c.1054_1057del4 (p.N353Vfs*31); - TRPM1: De2-7 (p.?)	TR (36)	none	Mel (2)
M	SLC45A2: De1-2 (p.?); - GSTM3: c.393C>A (p.Y131*)	EY (25)	none	n.a.
F	SLC45A2: De1-4 (p.?)	TR (42)	BC (41)	PrC (1)
M	TYR: c.650G>A (p.R217Q)	TR (37)	none	negative
F	TYR: c.1037-7T>A (p.?); - FANCC: c.455dupA (p.N152Kfs*9)	HE (66)	BC (52); CRC (66)	BC (2), HCC (1),
F	TINF2: c.796C>T (p.R266*)	UE (48)	none	CRC (2), GbC (1), Mel (1), PrC (2), RC (1), Sarcoma (1)
Hereditary cancer syndrome genes				
F	NBN: c.657_661del5 (p.K219Nfs*16)	TR (24)	none	BC (1), BT (1), Mel (1)
F	NBN: c.657_661del5 (p.K219Nfs*16)	EY (25)	none	negative
M	NBN: c.657_661del5 (p.K219Nfs*16)	TR (37)	none	n.a.
F	NBN: c.657_661del5 (p.K219Nfs*16)	HE (45)	Mel (68); OC (56)	n.a.
F	NBN: c.657_661del5 (p.K219Nfs*16)	TR (65)	OC (67)	negative
M	NBN: c.1126delG (p.D376Ifs*2)	n.a. (47)	none	LC (2), Mel (1),
F	NBN: c.1723G>T (p.E575*); - NFKBIE: c.165_169dup5 (p.E57Afs*51)	LE (9)	none	Mel (1)
M	BRCA2: c.475G>A (p.V159M)	UE (45)	RC (46)	HL (1)
F	BRCA2: c.1389_1390delAG (p.V464Gfs*3)	LE (47)	BC (59,59)	GC (2)
F	BRCA2: c.5682C>G (p.Y1894*)	n.a. (67)	BT (59); BC (56)	3 sisters with gynecological tumors, LC (1), retinoblastoma (1)
M	BRCA2: c.7007G>A (p.R2336H); - IFIH1: c.2464C>T (p.R822*)	HE (22)	none	BT (1), PrC (2), TC (1)
M	BRCA2: c.8168_8172ins4 (p.Y2726Mfs*10); - TYRP1: c.1254C>A (p.Y418*)	n.a. (40)	Mel (36); NHL (38)	LC (2)
F	BRCA1: c.68_69delAG (p.E23Vfs*17)	TR (47)	UrC (56); OC (57)	n.a.
F	BRCA1: c.1687C>T (p.Q563*)	EY (54)	BC (46)	OC (1)
F	BRCA1: c.4214delT (p.I1405Kfs*10); - ATM: c.7630-2A>C (p.?); - MUTYH c.1187G>A (p.G396D)	LE (46)	OC (46); BC (49)	BC (3), OC (2)
F	BRCA1: c.5266dupC (p.Q1756Pfs*74)	TR (53)	BC (54)	negative
M	CHEK2:c.909-2028_1095+330del5395 (p.M304Lfs*15)	UE (28)	none	CRC(1), Ly (1), Mel (1), MMT (1)
M	CHEK2: c.846+4_846+7del4 (p.D265-H282del)	TR (38)	none	BC (1), CRC (2)
F	ATM: c.381delA (p.V128*) - WRN: c.1105C>T (p.R369*)	TR (41)	Mel (50)	BC (2), PaC (1)
F	ATM: c.5932G>T (p.E1978*)	TR (35)	none	LC (1), UrC (1)
F	RAD51D: c.405+2T>C (p.?); - CHEK2: c.917G>C (p.G306A)	TR (26)	none	CC (1)
F	RB1: c.608-1G>T (p.?)	TR (32)	BC (45)	GbC (1), LC (1)

(a) gender: M—male; F—female. (b) Melanoma localization: EY—eye; HE—head; LE—lower extremity; TR—trunk; UE—upper extremity. (c) BC—breast cancer; BT—brain tumor; CC—cervix cancer; CRC—colorectal cancer; GC—gastric cancer; GbC—gallbladder cancer, HCC—hepatocellular cancer; (n)HL—(non)Hodgkin lymphoma; LC—lung cancer; Leu—leukemia; Ly—lymphoma; Mel—melanoma; MMT—malignant mesenchymal tumor; OC—ovarian cancer; PaC—pancreatic cancer; PrC—prostate cancer; RC—renal cancer; SgT—salivary gland tumor; SkC—skin cancer; TC—thyroid cancer; UrC—urinary cancer. The reference numbers for genes listed in this table are provided in Supplementary Table S1.

3.1.1. Mutations in High-to-Moderate Melanoma Risk Genes

The highest prevalence in a subgroup of high-to-moderate melanoma risk genes was found in CDKN2A (NM_000077). Disease-causing variants identified in six patients included ClinVar P/LP missense variants c.71G>C (p.R24P; in two patients) and c.334C>G (p.R112G), frameshift c.16_20delGGGAG (p.G6Qfs*7), in-frame c.95_112del18 (p.L32_L37del; shortening C-terminal part of

ankyrin 1 domain and adjacent -hairpin loop), and the novel splicing alteration c.457+4_457+5delAG, resulting in the activation of an aberrant splicing site (r.384_457del74) and a frameshift (p.Y129Hfs*11; Figure 1).

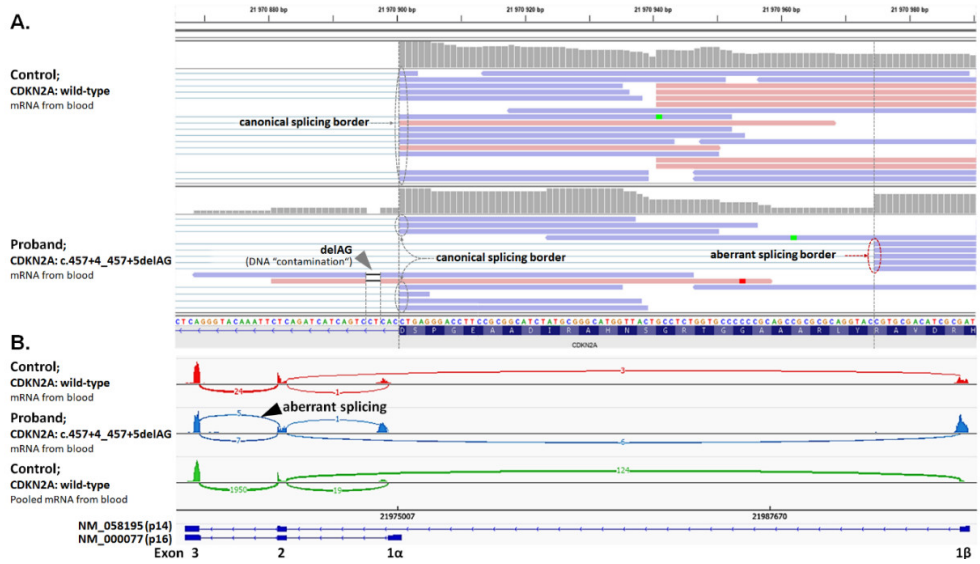

Figure 1. Characterization of splicing aberrations in CDKN2A. (**A**) NGS analysis of RNA isolated from blood lymphocytes identified aberrant splicing in a proband carrying the c.457+4_457+5delAG variant (visible as two reads originated from DNA "contamination"; grey arrowhead). The variant causes the elimination of the canonical splice site and activation of the cryptic splice site within exon 2, resulting in the deletion of 74 nts (r.384_457del74) and premature protein termination (p.Y129Hfs*11). (**B**) The sashimi plot shows the presence of aberrant splicing in 5/12 reads in a proband's sample, absent in 24 reads of a control with wild-type CDKN2A, and another 1950 reads of 100 pooled controls.

Two germline mutations were also found in POT1 (NM_015450). The c.703-1G>C mutation found in a proband with melanoma, dysplastic nevi, and thyroid cancer (Figure 2A) aected the canonical acceptor splice site of intron 10 resulting in exon 10 skipping at the mRNA level (r.703_869del167) and a frameshift (p.V235Gfs*22; Figure 2B). The rare missense variant c.347C>T changed the conserved amino acid p.P116L [33] in a patient with superficial spreading melanoma and breast cancer carrying also a germline deletion of 5395bp aecting exons 9 and 10 of the CHEK2 gene (NM_007194) (Figure 2C). To dissect the functional consequences of the POT1 missense variant inherited from the maternal branch of the family, we performed a functional analysis. First, we immuno-precipitated wild-type EGFP-POT1 or mutant EGFP-POT1-P116L from transiently transfected cells and found that both variants bound comparable levels of TPP1 (alias ACD) protein which mediates the binding of POT1 to the shelterin complex (Figure 2D). Confocal microscopy revealed that EGFP-POT1-P116L colocalized with TRF2, suggesting that it can assemble into the shelterin complex and correctly localize to telomeres (Figure 2E). Since the p.P116L mutation resides within the oligosaccharide/oligonucleotide-binding (OB1) domain [34], we hypothesized that it may impair the binding of POT1 to ssDNA. Indeed, we found that only the wild-type POT1 (but not POT1-P116L) mutant bound to the biotinylated telomeric G strand eciently (Figure 2F). We concluded that although the p.P116L isoform can localize to telomeric dsDNA through its interaction with ACD, it fails to bind telomeric ssDNA, which makes it a functionally deleterious mutation contributing to melanoma risk.

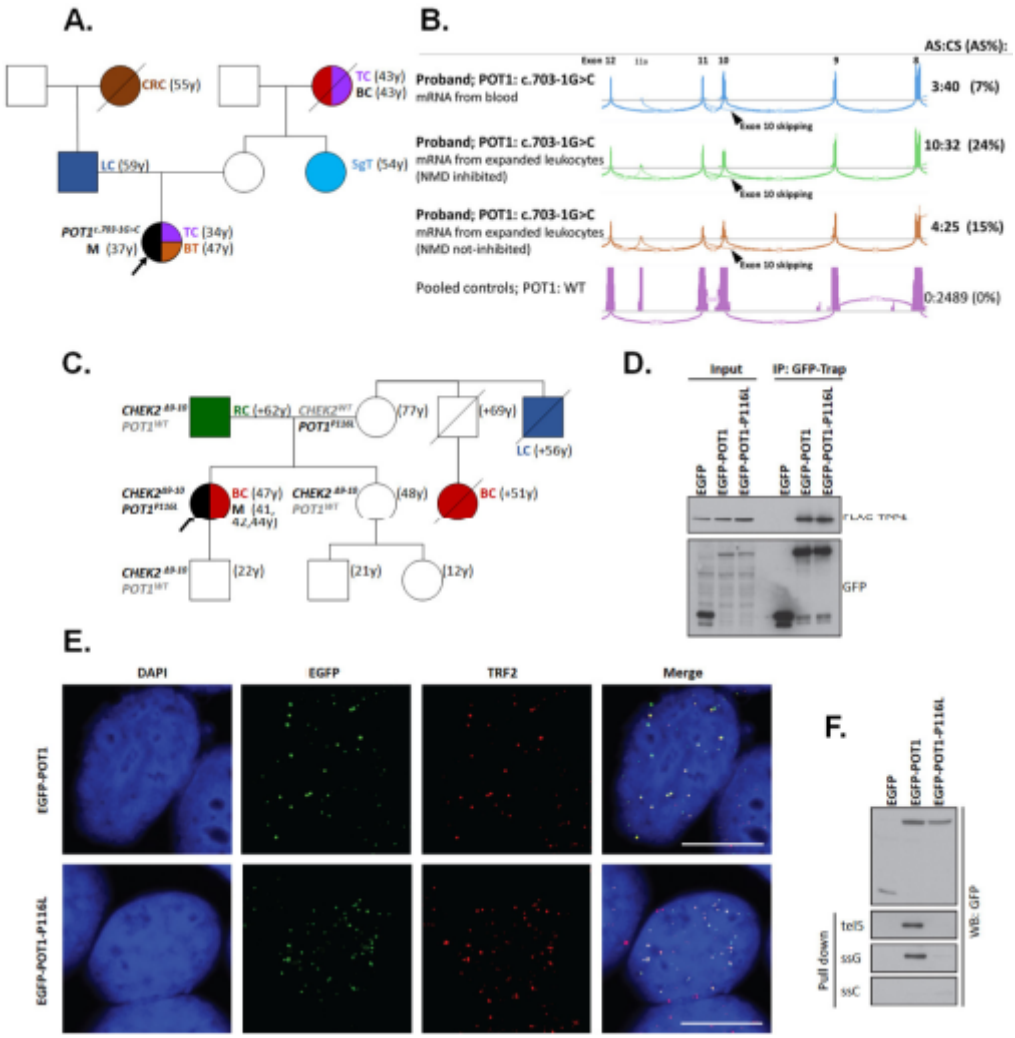

Figure 2. Characterization of POT1 germline variants. (**A**) Family of a patient carrying c.703-1G>C. (**B**) The variant causes aberrant splicing (AS) with exon 10 skipping (r.703_869del167; arrowhead; resulting in a frameshift at the protein level: p.V235Gfs*22) that was never observed in an analysis of wild-type POT1 samples (compared in blue and purple sashimi plots). However, AS mRNA is mostly subjected to nonsense-mediated decay (NMD). The number of NGS reads of non-degraded AS products in comparison with reads from canonical splicing (CS) products increased upon the cultivation of the patient's lymphocytes with puromycin (an NMD inhibitor; compared as green and brown plots). (**C**) Segregation of germline mutations in a family with missense p.P116L POT1 and CNV CHEK2 (c.909-2028_1095+330del5395) germline mutations. (**D**–**F**) Functional characterization was performed for the p.P116L POT1 mutation. (**D**) POT1-P116L interacts with shelterin components. Extracts from cells transfected with FLAG-TPP1 (alias ACD) and EGFP, EGFP-POT1 or EGFP-POT1-P116L were immuno-precipitated using GFP-Trap. Bound proteins were analyzed with EGFP and FLAG antibodies. (**E**) POT1-P116L is able to localize to telomeres. Cells transfected with EGFP-POT1 or EGFP-POT1-P116L were fixed and stained with TRF2 antibody and analyzed using confocal microscopy. A representative image of a single plane is shown. Bar indicates 10 m. (**F**) POT1-P116L mutant does not bind telomeric ssDNA. Extracts from cells transfected with EGFP, EGFP-POT1 or EGFP-POT1-P116L were incubated with biotinylated oligonucleotides corresponding to telomeric ssDNA (tel5 and ssG) or control DNA (ssC) and pulled down with streptavidin beads. The bound proteins were analyzed by immunoblotting using anti-GFP antibody. Abbreviations: BC—breast cancer; BT—brain tumor; CRC—colorectal cancer; LC—lung cancer; M—melanoma; RC—renal cancer; SgT—salivary gland tumor; TC—thyroid cancer.

One patient carried the c.755delA (p.D255Afs*9) mutation in ACD (NM_001082486), another shelterin complex gene associated with high melanoma risk [35]. This mutation results in the truncation of the POT1-binding domain of the ACD protein. Another ACD mutation, c.617dupT (p.H206Qfs*26), was the only P/LP variant from the category of high-to-moderate risk genes found in the control group. Although we did not find mutations in TERT, BAP1, or CDK4, germline mutations in the high-to-moderate risk category were present in 3.4% of patients (Table 4).

Table 4. Frequency of pathogenic/likely pathogenic (P/LP) germline variants in melanoma-susceptibility subgroups classified according to the risk of hereditary/familial melanoma risk. Eleven carriers of more than one P/LP variant were excluded from the analysis.

Melanoma Susceptibility Class	P/LP Variants; N (%)		OR (95%CI); p
	264 Patients	1479 Controls	
Multiple Mutation Carriers INCLUDED *			
High-to-moderate risk melanoma genes	9 (3.4)	1 (0.1)	52.2 (6.6–413.1); $3.2\ 10^{-7}$
Low-risk melanoma genes	12 (4.5)	35 (2.4)	1.9 (1.0–3.8); 0.06
Hereditary cancer syndrome genes	22 (8.3)	57 (3.9)	2.3 (1.4–3.8); 0.003
Genes with unknown familial melanoma risk	28 (10.6)	132 (8.9)	1.2 (0.8–1.8); 0.4
Multiple Mutation Carriers EXCLUDED			
High-to-moderate risk melanoma genes	8 (3.2)	1 (0.1)	48.1 (6.4–2116.9); $1.5\ 10^{-6}$
Low-risk melanoma genes	8 (3.2)	35 (2.4)	1.3 (0.5–3.0); 0.51
Hereditary cancer syndrome genes	16 (6.3)	57 (3.9)	1.7 (0.9–3.0); 0.09
Genes with unknown familial melanoma risk	28 (10.6)	132 (8.9)	1.2 (0.8–1.8); 0.4

*If carriers of concomitant mutations pertained to more than one risk group, they were assigned to a group with a higher risk as shown in Table 3: High-risk melanoma genes > Hereditary cancer syndrome genes > Low-risk melanoma genes > Genes with unknown familial melanoma risk.

3.1.2. Mutations in Low-Risk Melanoma Genes

The low-risk melanoma gene group revealed 12 carriers of mutations in 5 genes (Table 3; another TYRP1 carrier also had a pathogenic BRCA2 mutation). Hereditary melanoma risk was not increased in carriers of low-risk gene mutations (Table 4); however, we found a higher frequency in patients vs. controls for mutations in TYRP1 (0.8 vs. 0%; p = 0.02) and OCA2 (2.3 vs. 0.5%; OR = 4.3; 95%CI 1.2–14.2; p = 0.01); Supplementary Table S4.

3.1.3. Mutations in Genes Associated with Hereditary Cancer Syndromes

Altogether, 22/264 (8.3%) patients (Table 3) and 57/1479 controls (3.9%) carried a P/LP variant in genes associated with hereditary cancer syndromes. Overrepresentation of mutations in patients indicated an increased melanoma risk in carriers of mutations in hereditary cancer syndrome genes (OR = 2.27; 95%CI = 1.36–3.78; p = 0.003); however, melanoma risk lost its significance after the exclusion of six patients carrying other concomitant mutations (Table 4). The mutations in NBN (OR = 10.0; 95%CI 2.5–47.0; $p = 3.2\ 10^{-4}$) and BRCA2 (OR = 9.5; 95%CI 1.8–61.4; p = 0.003) were the most frequent and significantly associated with hereditary melanoma. The frequencies of germline mutations in CHEK2 gene (Supplementary Figures S1 and S2), BRCA1, and MUTYH were three times higher in patients over controls but marginally insignificant (all p = 0.051; Supplementary Table S4).

3.1.4. Mutations in Other Genes with Unknown Familial Melanoma Risk

Mutations in 23 other genes with unknown familial melanoma risk were found in 28/264 (10.7%) patients and in a similar proportion of controls (132/1479; 8.9%). Neither the genes individually (Supplementary Table S5) nor the entire group of these genes (Table 4) were associated with a significant increase in melanoma risk.

3.2. Clinicopathological Characteristics of Melanoma Patients Carrying Germline Mutations

A total of 11 carriers of more than one P/LP variant were excluded from the comparison of clinicopathological characteristics performed in the remaining 60 carriers of P/LP variants and 193 non-carriers (Figure 3A).

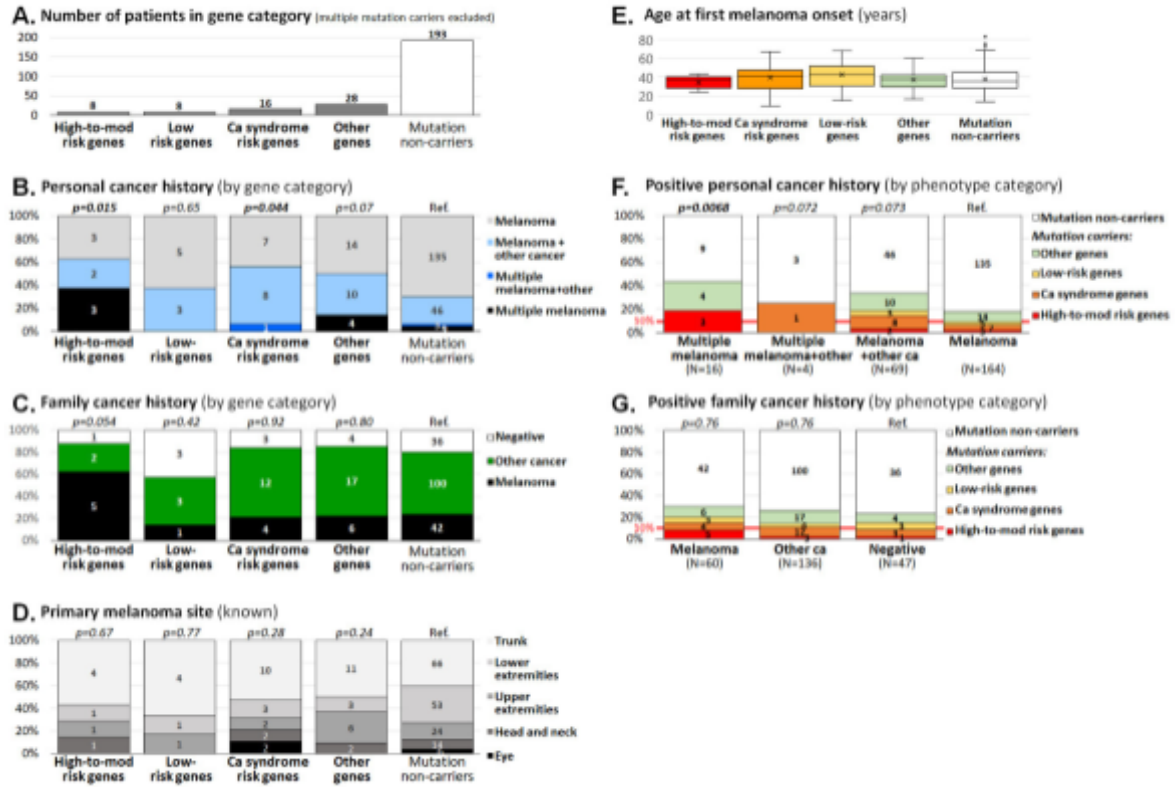

Figure 3. Clinicopathological characteristics of melanoma patients based on the presence of germline mutations. Panel **A** overviews the number of melanoma patients in the gene categories displayed in panels **B** to **E**. The p-values express significance of the dierences in distribution of variables between particular category of mutation carriers and non-carriers (considered as the reference). Panel **F** and **G** display proportion of mutation carriers in analyzed gene categories in individuals with positive personal cancer history (**F**); excluding 11 multiple mutation carriers) and in individuals with known positive family cancer history (**G**); excluding 21 individuals with unknown family cancer history). Dierences in proportions of carriers and non-carriers (p-values) in particular subgroups were calculated in patients with positive personal history (**F**) against patients with melanoma only (Ref.) and in patients with positive family cancer history (**G**) against patients with negative cancer history (Ref.).

Classification according to the presence of mutations in melanoma susceptibility classes (shown in Table 4) revealed an increased frequency of patients with multiple melanoma or double primary tumors among the carriers of mutations in high-to-moderate melanoma risk genes (5/8; 63% patients) and in cancer syndrome genes (9/16; 56% of patients), respectively, when compared with non-carriers (58/193; 30% of patients; Figure 3B). On the other hand, no dierence was found in the presence of melanoma or other cancers in patients' relatives, anatomical localization of melanoma, or age at melanoma onset (Figure 3C–E). The importance of personal cancer history for the potential to carry a mutation was confirmed when we calculated the proportion of patients with germline mutations in particular personal cancer history categories (Figure 3F). We noticed a significantly increased proportion of mutation carriers among patients with multiple melanoma (7/16; 44% of patients), compared with patients with single melanoma (29/164; 18% patients; p = 0.021). It is noteworthy that 14/89 (16%) patients with more than one tumor in personal history (i.e., patients with multiple melanoma, multiple

melanoma plus other cancer, and melanoma plus other cancer) carried a mutation in a clinically relevant gene (a high-to-moderate risk melanoma gene or a cancer syndrome gene), compared with 10/164 carriers (6%) among patients with single melanoma only (p = 0.023). Thus, tumor multiplicity (not restricted to melanoma multiplicity) in probands increased the risk that they will carry a mutation (OR = 2.9; 95%CI 1.2–6.8). A positive family cancer history did not increase the risk of being a mutation carrier (Figure 3G); however, the prevalence of mutations in patients with a positive family cancer history (24/196 carriers, 12%) surpassed the 10% threshold justifying genetic testing in this group (in contrast to 4/47; 8.5% positively tested patients without family cancer history; p = 0.6).

Altogether, 7/11 double mutation carriers (excluded from the analysis of clinicopathological data) carried at least one mutation in high-risk melanoma (POT1/CHEK2) or syndromic (ATM/WRN, BRCA1, BRCA2 (2x), CHEK2/RAD51D, NBN) genes (Table 3). Melanoma or tumor multiplicity in personal cancer history was present in four (36%) of these patients and all of them had a positive family cancer history, indicating that personal or family cancer history positivity was also more frequent among double mutation carriers.

4. Discussion

Our analysis demonstrated that 31/264 (11.7%) high-risk Czech melanoma patients (compared with 35/1479 or 2.3% controls) carried a mutation in some of the clinically important high-to-moderate melanoma risk genes (9 patients; 3.4%) or other cancer syndrome-associated genes (22 patients; 8.3%). As expected, CDKN2A was the most frequently mutated gene in the high-to-moderate risk gene group (in six analyzed patients; 2.3%). Four out of six CDKN2A mutation carriers developed >1 melanoma (3 patients) or other cancer (1 patient); all six carriers had a positive family cancer history and five of them had at least one relative with melanoma. The progressively rising probability of CDKN2A mutation prevalence with an increasing number of aected relatives with melanoma was described by Goldstein and colleagues in their study analyzing families of a European descent with at least three melanoma patients [36]. The frequency of CDKN2A mutation carriers rose from <40% for patients with three relatives with melanoma to >90% for those with more than six relatives with melanoma. In line with this observation, we have noticed three CDKN2A mutation carriers among 50 patients with one melanoma relative (6%) and two CDKN2A carriers among 10 patients with two melanoma relatives (20%). Goldstein et al. also observed an increased prevalence of pancreatic cancer patients in families with CDKN2A mutations (found in one p.R112G mutation carrier in our study). Germline mutations in high-risk melanoma susceptibility genes convey an increased risk of other cancers modifying genetic counselling in mutation carriers [24]. The spectrum of tumors in relatives diagnosed with cancer in the families of six CDKN2A mutation carriers included melanoma (7), breast cancer (3), rectal cancer (2), and gastric, pancreatic, lung, and endometrial cancer, brain tumor, and leukemia (one each).

The three remaining patients with germline mutations in high-to-moderate melanoma risk genes carried a P/LP variant in genes coding for shelterin complex proteins. The protection of telomeres protein 1 (POT1) is essential for the control of telomere length by inhibiting telomerase [32]. In addition, POT1 prevents hyper-resection at telomeric ends by inhibiting ATR [37]. The function of POT1 at telomeres is determined by its interaction with the telomeric single-stranded 5'-TTAGGG-3' repeats and with the TRF1/2 subunits of the shelterin complex through TPP1 (ACD) protein. Interaction with telomeric G-strand DNA is mediated by the two N-terminal OB domains of POT1, whereas the C-terminal part of POT1 interacts with TPP1 (ACD) [38]. Previous in silico and functional studies identified unstable binding and defective interaction with ssDNA for the p.R117C missense variant [33,39]. We found the adjacent p.P116L variant, described previously in a patient with sporadic cardiac sarcoma [33], in a patient with multiple melanoma and breast cancer, who also carried a large pathogenic CHEK2 deletion. A functional analysis of the P116L isoform demonstrating its normal interaction with TPP1 (ACD) protein but impaired ssDNA binding led us to conclude that p.P116L is a functionally defective mutation. Germline POT1 mutations have been initially described as increasing the risk of melanoma, but later studies indicate a broader cancer spectrum associated with these

mutations. Notably, POT1 mutations have recently been associated with familial non-medullary thyroid cancer [40–42]. A duplicity of thyroid cancer with melanoma has been identified in a patient with a newly characterized splicing POT1 mutation (thyroid cancer was present in the patient's untested mother's mother). In a single melanoma patient with a negative family cancer history, we identified a mutation in the ACD gene truncating the C-terminal proportion of the protein containing POT1- and TINF2-interacting domains required for the localization of ACD protein into the shelterin complex. Overall, high-to-moderate risk germline mutations aecting shelterin complex genes were found in three (1.1%) analyzed patients in our study. We also detected another shelterin gene truncating mutation aecting the TINF2 gene that we included in the low-risk gene category; however, another TINF2 truncation has recently been described to segregate with multiple thyroid cancer and melanoma in one family [43]. A higher prevalence of mutations in ACD, TERF2IP, and POT1 was identified in 12/132 (9.1%) high-risk CDKN2A/CDK4/TERT/BAP1 wild-type European and Australian patients with multiple melanoma (3) [44]. A higher prevalence of germline mutations in BAP1 (not identified in our patients) and POT1 was also reported in a recent study by Pastorino and colleagues who identified seven carriers (2.6%) of mutations in each of these two genes among 273 Italian melanoma patients [45]. The enrollment of 22 melanoma patients with atypical Spitz nevi with relatives developing BAP1-related tumors can explain an increased prevalence of BAP1 mutation carriers in this Italian study. Germline BAP1 mutations were rarely identified in Czech patients so far, dominantly in probands with uveal melanoma or Spitz nevi [46,47].

The highest prevalence of germline mutations in our melanoma patients was found in the NBN gene (in 7/264 patients; 2.7%), coding for nibrin, a protein contributing to a MRN complex formation, sensing for DNA double strand breaks. We found the most frequent, Slavic founder germ-line hypomorphic variant c.657del5 in five patients [48]. Two of them also developed ovarian cancer, which was associated with NBN germline mutations in our population [49]. An increased melanoma prevalence among NBN c.657del5 mutation carriers was reported from Poland (with a frequency comparable to our patients) and southern Germany (with lower prevalence) [50–52]. Two of our melanoma patients (diagnosed with melanoma at 9 and 47 years, respectively; both with a melanoma-positive family cancer history) carried other rare NBN truncations. Gass and colleagues [53] reported a female carrier of the c.698_701del4 germline mutation developing melanoma, squamous cell carcinoma, and breast cancer with a sister suering from melanoma and other relatives aected by various cancer types, indicating that other NBN truncations increase melanoma risk. Analyses of NBN in other cancers demonstrated a highly variable population-specific prevalence of its germline mutations. Current NCCN guidelines report an association of NBN mutations with an increased breast cancer risk (https://www.nccn.org/professionals/physician_gls/pdf/genetics_bop.pdf), but further studies of unselected cancer patients with carefully population-matched controls are required to determine cancer risk associated with other cancer types, including melanoma. The prevalence of NBN mutations but also BRCA2 mutations was significantly (nine-fold) higher in patients than in controls. P/LP variants in BRCA1 and CHEK2 were less enriched in patients over controls and statistically insignificant ($p = 0.051$; Supplementary Table S5). The role of germline mutations in the breast-ovarian cancer predisposition genes BRCA1 and BRCA2 in the risk of familial melanoma development is still a matter of debate [54] and the exact melanoma risk increase (if any) in mutation carriers is uncertain. The same could be said of CHEK2 as documented in a recent meta-analysis evaluating the association of germline CHEK2 mutations with melanoma [55]. Large studies utilizing large gene panels to analyze patients with unselected melanoma or, even better, unselected cancer, will be required to dissect the risk of melanoma associated with hereditary cancer syndrome genes. However, we would like to emphasize that 4/9 BRCA1 or BRCA2 pathogenic mutation carriers and all CHEK2 P/LP variant carriers would not be eligible for germline genetic testing according to the current guidelines, despite the fact that all other mutation carriers (except for one patient with the founder c.5266dupC BRCA1 mutation) had a positive family cancer history and four also developed secondary tumors alongside solitary or

multiple melanoma (Table 3). The genetic counselling was oered to all carriers of mutations in high and moderate cancer risk genes.

An analysis of clinicopathological characteristics shows not only that multiple primary melanoma patients carry an increased risk of mutations in melanoma-predisposition genes, but also that the presence of melanoma and other non-melanoma cancer in the proband increased the potential to carry a clinically meaningful mutation in a melanoma predisposition or hereditary cancer syndrome gene.

We are aware of some limitations of our study. Most melanoma patients analyzed in our study were referred to the analysis by medical geneticists. This fact explains the enrichment of patient population in early-onset, multiple cancer, and family cancer-positive cases and incomplete clinicopathological data that lack phenotypic characteristics (eye and hair color, skin phototype according to Fitzpatrick, total number of nevi, the presence of clinically atypical nevi, freckle density, iris pigmentation), lifetime history of sunburns, and specific melanoma characteristics (histological subtype, Breslow thickness, clinical staging) in most of the patients. We are also aware that the gene selection in our CZMELAC panel would omit potentially clinically important gene(s). However, we would like to emphasize that we aimed to evaluate the importance of known melanoma/other cancer predisposition genes and candidate genes for clinical purposes in our melanoma patients rather than to identify genes that have not been associated with hereditary melanoma so far. Furthermore, only P/LP mutations were considered for subsequent statistical analyses. We excluded all VUS (except those in CHEK2 and POT1 that we functionally classified as deleterious) as currently clinically inconclusive, being aware that some of them may represent potentially important variants in both patient and control datasets. The presence of VUS substantially hampers the clinical utility of NGS diagnostics. Classifications of VUS frequently require demanding and time-consuming functional analyses that are beyond the expertise available in most of diagnostic laboratories. Therefore, VUS classifications, which are critically important for appropriate clinical interpretations of variants in cancer predisposition genes, are an opportunity for a collaborative eort of international consortia bringing together experts from various disciplines, who may provide substantial capacity for in vitro testing of VUS characterized by the co-operating laboratories.

In conclusion, we comprehensively assessed the prevalence of germline variants aecting currently known or candidate melanoma-predisposition genes in Czech melanoma patients and in the general population. Our analysis demonstrated that high-to-moderate risk genes, including genes coding for shelterin complex proteins, should be targeted in the multicancer panel NGS analysis. An analysis of clinicopathological characteristics indicated that patients eligible for such an analysis should not be restricted to multiple primary melanoma patients or patients with a positive familial melanoma cancer history, but they should also include melanoma patients with other primary cancer and melanoma patients with a positive family cancer history.

Supplementary Materials: The following are available online at http://www.mdpi.com/2227-9059/8/10/404/s1, Table S1: Clinicopathological characteristics of analyzed melanoma patients, Table S2: List of 217 targeted genes in CZMELAC panel, Table S3: List of 83 P/LP variants found in melanoma patients (column H) and 225 P/LP variants identified in controls, Table S4: Frequency of pathogenic/likely pathogenic germline mutations in 89 out of 217 analyzed genes identified in 264 high-risk melanoma patients or in 1479 population-matched controls, Table S5: Found germline P/LP variants in genes with unknown association to familial melanoma, Figure S1: Intragenic deletions and duplications from technical control samples with known alterations and in samples from analyzed patients. Figure S2: New CHEK2 germline variants (p.T133A and p.Y297D) identified in two melanoma patients were functionally classified as neutral in RPE1-CHEK2-KO cell-based assay.

Author Contributions: Conceptualization: Z.K., L.M.; methodology: Z.K., L.M., P.K.; software: P.Z., L.S., V.S.; validation: L.S., S.J., J.K., M.C., P.K.; formal analysis: L.S., S.J., R.S., M.V.; investigation: L.S., S.J., R.S., J.K., M.C., Z.V., M.J., J.S.; resources: E.M., M.V., O.K., P.D., V.S., L.F., L.M.; data curation: E.M., M.V., O.K., L.F.; writing—original draft preparation: L.S., Z.K.; writing—review and editing: all authors; visualization: Z.K., P.Z., P.K.; funding acquisition: P.D., L.M., Z.K., P.K. All authors have read and agreed to the published version of the manuscript.

Funding: This research was funded by the Ministry of Health of the Czech Republic (grant numbers NV16-30954A, NV18-03-00024, NV19-03-00279), by Charles University projects (SVV 260516, PROGRES Q28/LF1) and by the Academy of Sciences of the Czech Republic project Strategie AV21, Qualitas. We would like to thank the National Center for Medical Genomics (LM2018132) for providing allelic frequencies in ethnically matched populations (project CZ.02.1.01/0.0/0.0/18_046/0015515).

Acknowledgments: We would like to thank all patients and their families for their participation in this study.

Conflicts of Interest: The authors declare no conflict of interest.

References

1. Ferlay, J.; Colombet, M.; Soerjomataram, I.; Mathers, C.; Parkin, D.; Piñeros, M.; Znaor, A.; Bray, F. Estimating the global cancer incidence and mortality in 2018: GLOBOCAN sources and methods. Int. J. Cancer **2018**, 144, 1941–1953. [CrossRef]
2. Bray, F.; Me, J.F.; Soerjomataram, I.; Siegel, R.L.; Torre, L.A.; Jemal, A. Global cancer statistics 2018: GLOBOCAN estimates of incidence and mortality worldwide for 36 cancers in 185 countries. CA Cancer J. Clin. **2018**, 68, 394–424. [CrossRef] [PubMed]
3. Narayanan, D.L.; Saladi, R.N.; Fox, J.L. Review: Ultraviolet radiation and skin cancer. Int. J. Dermatol. **2010**, 49, 978–986. [CrossRef] [PubMed]
4. Shain, A.H.; Bastian, B.C. From melanocytes to melanomas. Nat. Rev. Cancer **2016**, 16, 345–358. [CrossRef]
5. Mucci, L.A.; Hjelmborg, J.B.; Harris, J.R.; Czene, K.; Havelick, D.J.; Scheike, T.; Gra, R.E.; Holst, K.; Möller, S.; Unger, R.H.; et al. Familial Risk and Heritability of Cancer Among Twins in Nordic Countries. JAMA **2016**, 315, 68–76. [CrossRef] [PubMed]
6. Hawkes, J.E.; Truong, A.; Meyer, L.J. Genetic predisposition to melanoma. Semin. Oncol. **2016**, 43, 591–597. [CrossRef]
7. Maggi, L.B.; Winkeler, C.L.; Miceli, A.P.; Apicelli, A.J.; Brady, S.N.; Kuchenreuther, M.J.; Weber, J.D. ARF tumor suppression in the nucleolus. Biochim. Biophys. Acta **2014**, 1842, 831–839. [CrossRef]
8. Gruis, N.A.; Van Der Velden, P.A.; Sandkuijl, L.A.; Prins, D.E.; Weaver-Feldhaus, J.; Kamb, A.; Bergman, W.; Frants, R.R. Homozygotes for CDKN2 (p16) germline mutation in Dutch familial melanoma kindreds. Nat. Genet. **1995**, 10, 351–353. [CrossRef]
9. Hill, V.K.; Gartner, J.J.; Samuels, Y.; Goldstein, A.M. The Genetics of Melanoma: Recent Advances. Annu. Rev. Genom. Hum. Genet. **2013**, 14, 257–279. [CrossRef]
10. Sargen, M.R.; Pfeier, R.; Yang, X.R.; Tucker, M.A.; Goldstein, A.M. Variation in Cutaneous Patterns of Melanomagenesis According to Germline CDKN2A/CDK4 Status in Melanoma-Prone Families. J. Investig. Dermatol. **2020**, 140, 174–181.E3. [CrossRef]
11. Betti, M.; Aspesi, A.; Biasi, A.; Casalone, E.; Ferrante, D.; Ogliara, P.; Gironi, L.C.; Giorgione, R.; Farinelli, P.; Grosso, F.; et al. CDKN2A and BAP1 germline mutations predispose to melanoma and mesothelioma. Cancer Lett. **2016**, 378, 120–130. [CrossRef]
12. Zuo, L.; Weger, J.; Yang, Q.; Goldstein, A.M.; Tucker, M.A.; Walker, G.J.; Hayward, N.; Dracopoli, N.C. Germline mutations in the p16INK4a binding domain of CDK4 in familial melanoma. Nat. Genet. **1996**, 12, 97–99. [CrossRef] [PubMed]
13. Carbone, M.; Yang, H.; Pass, H.I.; Krausz, T.; Testa, J.R.; Gaudino, G. BAP1 and Cancer. Nat. Rev. Cancer **2013**, 13, 153–159. [CrossRef]
14. Goldstein, A.M.; Xiao, Y.; Sampson, J.; Rotunno, M.; Bennett, H.; Wen, Y.; Jones, K.; Vogt, A.; Burdette, L.; Luo, W.; et al. Rare germline variants in known melanoma susceptibility genes in familial melanoma. Hum. Mol. Genet. **2017**, 26, 4886–4895. [CrossRef] [PubMed]
15. Harland, M.; Petljak, M.; Robles-Espinoza, C.D.; Ding, Z.; Gruis, N.A.; Van Doorn, R.; Pooley, K.A.; Dunning, A.M.; Aoude, L.G.; Wadt, K.A.W.; et al. Germline TERT promoter mutations are rare in familial melanoma. Fam. Cancer **2015**, 15, 139–144. [CrossRef] [PubMed]
16. Leachman, S.A.; Lucero, O.M.; Sampson, J.E.; Cassidy, P.; Bruno, W.; Queirolo, P.; Ghiorzo, P. Identification, genetic testing, and management of hereditary melanoma. Cancer Metastasis Rev. **2017**, 36, 77–90. [CrossRef]
17. Chatzinasiou, F.; Lill, C.M.; Kypreou, K.; Stefanaki, I.; Nicolaou, V.; Spyrou, G.; Evangelou, E.; Roehr, J.T.; Kodela, E.; Katsambas, A.; et al. Comprehensive Field Synopsis and Systematic Meta-analyses of Genetic Association Studies in Cutaneous Melanoma. J. Natl. Cancer Inst. **2011**, 103, 1227–1235. [CrossRef] [PubMed]

18. Law, M.H.; GenoMEL, consortium; Bishop, D.T.; Lee, J.E.; Brossard, M.; Martin, N.G.; Moses, E.K.; Song, F.; Barrett, J.H.; Kumar, R.; et al. Genome-wide meta-analysis identifies five new susceptibility loci for cutaneous malignant melanoma. Nat. Genet. **2015**, 47, 987–995. [CrossRef]
19. Roberts, M.; Asgari, M.; Toland, A. Genome-wide association studies and polygenic risk scores for skin cancer: Clinically useful yet? Br. J. Dermatol. **2019**, 181, 1146–1155. [CrossRef]
20. Dušek, L.; Mužík, J.; Malúšková, D.; Májek, O.; Pavlík, T.; Koptíková, J.; Melichar, B.; Buchler, T.; Fínek, J.; Cibula, D.; et al. Cancer incidence and mortality in the Czech Republic. Klin. Onkol. **2014**, 27, 406–423. [CrossRef]
21. Krejci, D.; Zapletalova, M.; Svobodova, I.; Pehalova, L.; Muzik, J.; Klimes, D.; Snajdrova, L.; Bajciova, V.; Mudry, P.; Kodytkova, D.; et al. Epidemiological Trends for Childhood and Adolescent Cancers in the Period 1994–2016 in the Czech Republic. Klin. Onkol. **2019**, 32, 10. [CrossRef]
22. Soura, E.; Eliades, P.J.; Shannon, K.; Stratigos, A.J.; Tsao, H. Hereditary melanoma: Update on syndromes and management. J. Am. Acad. Dermatol. **2016**, 74, 395–407. [CrossRef] [PubMed]
23. Soura, E.; Eliades, P.J.; Shannon, K.M.; Stratigos, A.J.; Tsao, H. Hereditary melanoma: Update on syndromes and management: Emerging melanoma cancer complexes and genetic counseling. J. Am. Acad. Dermatol. **2016**, 74, 411–420. [CrossRef] [PubMed]
24. Read, J.; Wadt, K.; Hayward, N.K. Melanoma genetics. J. Med Genet. **2015**, 53, 1–14. [CrossRef] [PubMed]
25. Yu, W.; Clyne, M.; Khoury, M.J.; Gwinn, M. Phenopedia and Genopedia: Disease-centered and gene-centered views of the evolving knowledge of human genetic associations. Bioinformatics **2009**, 26, 145–146. [CrossRef] [PubMed]
26. Lhota, F.; Zemankova, P.; Kleiblova, P.; Soukupova, J.; Vocka, M.; Stranecky, V.; Janatova, M.; Hartmannová, H.; Hodaňová, K.; Kmoch, S.; et al. Hereditary truncating mutations of DNA repair and other genes in BRCA1/BRCA2/PALB2 -negatively tested breast cancer patients. Clin. Genet. **2016**, 90, 324–333. [CrossRef]
27. Soukupova, J.; Zemankova, P.; Lhotova, K.; Janatova, M.; Borecka, M.; Stolarova, L.; Lhota, F.; Foretova, L.; Machackova, E.; Stranecky, V.; et al. Validation of CZECANCA (CZEch CAncer paNel for Clinical Application) for targeted NGS-based analysis of hereditary cancer syndromes. PLoS ONE **2018**, 13, e0195761. [CrossRef] [PubMed]
28. Richards, S.; Aziz, N.; Bale, S.; Bick, D.; Das, S.; Gastier-Foster, J.; Grody, W.W.; Hegde, M.; Lyon, E.; Spector, E.; et al. Standards and guidelines for the interpretation of sequence variants: A joint consensus recommendation of the American College of Medical Genetics and Genomics and the Association for Molecular Pathology. Genetics **2015**, 17, 405–424. [CrossRef]
29. Walker, L.C.; Lattimore, V.L.; Kvist, A.; Kleiblova, P.; Zemankova, P.; De Jong, L.; Wiggins, G.A.R.; Hakkaart, C.; Cree, S.L.; Behar, R.; et al. Comprehensive Assessment of BARD1 Messenger Ribonucleic Acid Splicing with Implications for Variant Classification. Front. Genet. **2019**, 10, 10. [CrossRef] [PubMed]
30. Kleiblova, P.; Stolarova, L.; Krizova, K.; Lhota, F.; Hojny, J.; Zemankova, P.; Havranek, O.; Vocka, M.; Cerna, M.; Lhotova, K.; et al. Identification of deleterious germline CHEK2 mutations and their association with breast and ovarian cancer. Int. J. Cancer **2019**, 145, 1782–1797. [CrossRef] [PubMed]
31. Zhou, J.; Chan, J.; Lambelé, M.; Yusufzai, T.; Stump, J.; Opresko, P.L.; Thali, M.; Wallace, S.S. NEIL3 Repairs Telomere Damage during S Phase to Secure Chromosome Segregation at Mitosis. Cell Rep. **2017**, 20, 2044–2056. [CrossRef] [PubMed]
32. Loayza, D.; De Lange, T. POT1 as a terminal transducer of TRF1 telomere length control. Nat. Cell Biol. **2003**, 423, 1013–1018. [CrossRef] [PubMed]
33. Calvete, O.; Lázaro, C.; Domínguez, F.; Bougeard, G.; Kunze, K.; Braeuninger, A.; Teule, A.; Lasa, A.; Cajal, T.R.Y.; Llort, G.; et al. The wide spectrum of POT1 gene variants correlates with multiple cancer types. Eur. J. Hum. Genet. **2017**, 25, 1278–1281. [CrossRef] [PubMed]
34. Lei, M.; Podell, E.R.; Cech, T.R. Structure of human POT1 bound to telomeric single-stranded DNA provides a model for chromosome end-protection. Nat. Struct. Mol. Biol. **2004**, 11, 1223–1229. [CrossRef] [PubMed]
35. Aoude, L.G.; Wadt, K.; Pritchard, A.L.; Hayward, N.K. Genetics of familial melanoma: 20 years after CDKN2A. Pigment. Cell Melanoma Res. **2015**, 28, 148–160. [CrossRef] [PubMed]
36. Goldstein, A.M.; Chan, M.; Harland, M.; Hayward, N.K.; Demenais, F.; Bishop, D.T.; Azizi, E.; Bergman, W.; Bianchi-Scarrà, G.; Bruno, W.; et al. Features associated with germline CDKN2A mutations: A GenoMEL study of melanoma-prone families from three continents. J. Med Genet. **2006**, 44, 99–106. [CrossRef]

37. Kibe, T.; Zimmermann, M.; De Lange, T. TPP1 Blocks an ATR-Mediated Resection Mechanism at Telomeres. Mol. Cell **2016**, 61, 236–246. [CrossRef]
38. Kendellen, M.F.; Barrientos, K.S.; Counter, C.M. POT1 Association with TRF2 Regulates Telomere Length. Mol. Cell. Biol. **2009**, 29, 5611–5619. [CrossRef]
39. Calvete, O.; Martínez, P.; García-Pavía, P.; Benitez-Buelga, C.; Paumard, B.; Fernandez, V.; Domínguez, F.; Salas, C.; Romero-Laorden, N.; García-Donás, J.; et al. A mutation in the POT1 gene is responsible for cardiac angiosarcoma in TP53-negative Li–Fraumeni-like families. Nat. Commun. **2015**, 6, 8383. [CrossRef]
40. Richard, M.A.; Lupo, P.J.; Morton, L.M.; Yasui, Y.A.; Sapkota, Y.A.; Arnold, M.A.; Aubert, G.; Neglia, J.P.; Turcotte, L.M.; Leisenring, W.M.; et al. Genetic variation in POT1 and risk of thyroid subsequent malignant neoplasm: A report from the Childhood Cancer Survivor Study. PLoS ONE **2020**, 15, e0228887. [CrossRef]
41. Srivastava, A.; Miao, B.; Skopelitou, D.; Kumar, V.; Kumar, A.; Paramasivam, N.; Bonora, E.; Hemminki, K.; Försti, A.; Bandapalli, O.R. A Germline Mutation in the POT1 Gene Is a Candidate for Familial Non-Medullary Thyroid Cancer. Cancers **2020**, 12, 1441. [CrossRef] [PubMed]
42. Wilson, T.L.-S.; Hattangady, N.; Lerario, A.M.; Williams, C.; Koeppe, E.; Quinonez, S.; Osborne, J.; Else, T.; Cha, K.B. A new POT1 germline mutation—Expanding the spectrum of POT1-associated cancers. Fam. Cancer **2017**, 53, 1–566. [CrossRef] [PubMed]
43. He, H.; Li, W.; Comiskey, J.D.F.; Liyanarachchi, S.; Nieminen, T.T.; Wang, Y.; DeLap, M.K.E.; Brock, P.; De La Chapelle, A. A Truncating Germline Mutation of TINF2 in Individuals with Thyroid Cancer or Melanoma Results in Longer Telomeres. Thyroid **2020**, 30, 204–213. [CrossRef]
44. Aoude, L.G.; Pritchard, A.L.; Robles-Espinoza, C.D.; Wadt, K.; Harland, M.; Choi, J.; Gartside, M.; Quesada, V.; A Johansson, P.; Palmer, J.M.; et al. Nonsense Mutations in the Shelterin Complex Genes ACD and TERF2IP in Familial Melanoma. J. Natl. Cancer Inst. **2015**, 107, dju408. [CrossRef] [PubMed]
45. Pastorino, L.; Andreotti, V.; Dalmasso, B.; Vanni, I.; Ciccarese, G.; Mandalà, M.; Spadola, G.; Pizzichetta, M.A.; Ponti, G.; Tibiletti, M.G.; et al. Insights into Genetic Susceptibility to Melanoma by Gene Panel Testing: Potential Pathogenic Variants in ACD, ATM, BAP1, and POT1. Cancers **2020**, 12, 1007. [CrossRef] [PubMed]
46. Macháčková, E.; Házová, J.; Hrabincová, E.S.; Vašíčková, P.; Navrátilová, M.; Svoboda, M.; Foretová, L. Retrospective NGS Study in High-risk Hereditary Cancer Patients at Masaryk Memorial Cancer Institute. Klin. Onkol. **2016**, 29 (Suppl. S1), S35–S45. [CrossRef]
47. Foretová, L.; Navrátilová, M.; Svoboda, M.; Házová, J.; Vašíčková, P.; Sťahlová, E.H.; Fabian, P.; Schneiderová, M.; Macháčková, E.; Hrabincová, E.S. BAP1 Syndrome—Predisposition to Malignant Mesothelioma, Skin and Uveal Melanoma, Renal and Other Cancers. Klin. Onkol. **2019**, 32, 118–122. [CrossRef] [PubMed]
48. Fiévet, A.; Bellanger, D.; Zahed, L.; Burglen, L.; Derrien, A.; D'Enghien, C.D.; Lespinasse, J.; Parfait, B.; Pedespan, J.; Rieunier, G.; et al. DNA repair functional analyses of NBN hypomorphic variants associated with NBN-related infertility. Hum. Mutat. **2020**, 41, 608–618. [CrossRef]
49. Lhotova, K.; Stolarova, L.; Zemankova, P.; Vočka, M.; Janatova, M.; Borecka, M.; Cerna, M.; Jelinkova, S.; Kral, J.; Volkova, Z.; et al. Multigene Panel Germline Testing of 1333 Czech Patients with Ovarian Cancer. Cancers **2020**, 12, 956. [CrossRef]
50. Dębniak, T.; Górski, B.; Cybulski, C.; Jakubowska, A.; Kurzawski, G.; Lener, M.; Mierzejewski, M.; Masojć, B.; Mędrek, K.; Kładny, J.; et al. Germline 657del5 mutation in the NBS1 gene in patients with malignant melanoma of the skin. Melanoma Res. **2003**, 13, 365–370. [CrossRef]
51. Steen, J.; Varon, R.; Mosor, M.; Maneva, G.; Maurer, M.; Stumm, M.; Nowakowska, D.; Rubach, M.; Kosakowska, E.; Ruka, W.; et al. Increased cancer risk of heterozygotes withNBS1 germline mutations in poland. Int. J. Cancer **2004**, 111, 67–71. [CrossRef] [PubMed]
52. Meyer, P.; Stapelmann, H.; Frank, B.; Varon, R.; Burwinkel, B.; Schmitt, C.; Boettger, M.B.; Klaes, R.; Sperling, K.; Hemminki, K.; et al. Molecular genetic analysis of NBS1 in German melanoma patients. Melanoma Res. **2007**, 17, 109–116. [CrossRef] [PubMed]
53. Gass, J.M.; Jackson, J.; Macklin, S.; Blackburn, P.; Hines, S.; Atwal, P.S. A case of contralateral breast cancer and skin cancer associated with NBN heterozygous pathogenic variant c.698_701delAACA. Fam. Cancer **2017**, 2013, 551–553. [CrossRef] [PubMed]
54. Adams, D.J.; Bishop, D.T.; Robles-Espinoza, C.D. Melanoma predisposition—A limited role for germline BRCA1 and BRCA2 variants. Pigment. Cell Melanoma Res. **2019**, 33, 6–7. [CrossRef] [PubMed]

55. Bui, A.-T.N.; Leboeuf, N.R.; Nambudiri, V.E. Skin cancer risk in CHEK2 mutation carriers. J. Eur. Acad. Dermatol. Venereol. **2020**. [CrossRef]

The FEBS Journal

FEBS PRESS science publishing by scientists

A novel assay for screening WIP1 phosphatase substrates in nuclear extracts

Radka Storchova[1,2], Kamila Burdova[1], Matous Palek[1], René H. Medema[3] and Libor Macurek[1]

1 Cancer Cell Biology, Institute of Molecular Genetics of the Czech Academy of Sciences, Prague, Czech Republic
2 Faculty of Science, Charles University, Prague, Czech Republic
3 Division of Cell Biology, Netherlands Cancer Institute, Amsterdam, The Netherlands

Keywords
acetylation; DNA damage response; p53; protein phosphatase

Correspondence
L. Macurek, Cancer Cell Biology, Institute of Molecular Genetics of the Czech Academy of Sciences, Videnska 1083, 14200 Prague, Czech Republic
Tel: +420241063210
E-mail: libor.macurek@img.cas.cz

Radka Storchova and Kamila Burdova contributed equally to this work

(Received 26 February 2021, revised 13 April 2021, accepted 10 May 2021)

doi:10.1111/febs.15965

Upon exposure to genotoxic stress, cells activate DNA damage response (DDR) that coordinates DNA repair with a temporal arrest in the cell cycle progression. DDR is triggered by activation of ataxia telangiectasia mutated/ataxia telangiectasia and Rad3-related protein kinases that phosphorylate multiple targets including tumor suppressor protein tumor suppressor p53 (p53). In addition, DNA damage can activate parallel stress response pathways [such as mitogen-activated protein kinase p38 alpha (p38)/MAPK-activated protein kinase 2 (MK2) kinases] contributing to establishing the cell cycle arrest. Wild-type p53-induced phosphatase 1 (WIP1) controls timely inactivation of DDR and is needed for recovery from the G2 checkpoint by counteracting the function of p53. Here, we developed a simple *in vitro* assay for testing WIP1 substrates in nuclear extracts. Whereas we did not detect any activity of WIP1 toward p38/MK2, we confirmed p53 as a substrate of WIP1. Inhibition or inactivation of WIP1 in U2OS cells increased phosphorylation of p53 at S15 and potentiated its acetylation at K382. Further, we identified Deleted in breast cancer gene 1 (DBC1) as a new substrate of WIP1 but surprisingly, depletion of DBC1 did not interfere with the ability of WIP1 to regulate p53 acetylation. Instead, we have found that WIP1 activity suppresses p53-K382 acetylation by inhibiting the interaction between p53 and the acetyltransferase p300. Newly established phosphatase assay allows an easy comparison of WIP1 ability to dephosphorylate various proteins and thus contributes to identification of its physiological substrates.

Introduction

DNA damage response (DDR) pathway protects cells from genome instability by coordinating DNA repair with a temporal arrest in the cell cycle progression [1,2]. Various types of DNA lesions activate kinases of PIK3-like family, comprising of ataxia telangiectasia mutated (ATM) and DNA-dependent protein kinase (DNA-PK) activated by DNA double-strand breaks and ataxia telangiectasia and Rad3-related protein (ATR) activated by single stranded DNA [3]. Proteomic screens identified thousands of various phosphorylations mediated by these kinases in the proximity of DNA lesions [such as histone H2A.X (H2AX)-S139, breast cancer type 1

Abbreviations
ATM, ataxia telangiectasia mutated; ATR, ataxia telangiectasia and Rad3-related protein; BRCA1, breast cancer type 1 susceptibility protein; CHK1, checkpoint kinase 1; DBC1, deleted in breast cancer gene 1; DDR, DNA damage response; DNA-PK, DNA-dependent protein kinase; EGFP, enhanced green fluorescent protein; H2AX, histone H2A.X; KAP1, KRAB-associated protein 1; MK2, MAPK-activated protein kinase 2; NE, nuclear extract; p38, mitogen-activated protein kinase p38 alpha; p53, tumor suppressor p53; SIRT1, NAD-dependent protein deacetylase sirtuin-1; WIP1, wild-type p53-induced phosphatase 1.

susceptibility protein (BRCA1)-pS1524, and other DNA repair proteins] and also diffusely throughout the nucleus [such as the checkpoint kinases 1/2 (CHK1/2), KRAB-associated protein 1 (KAP1), and the tumor suppressor protein p53] [4,5]. Progression through the cell cycle is arrested by induction of the cyclin-dependent kinase inhibitors p21 and $p27^{Kip1}$, and by inactivation of CDC25 phosphatases [6,7]. In addition to the canonical DDR, some forms of genotoxic stress (such as UVC radiation and doxorubicin) activate a general stress response pathway mitogen-activated protein kinase p38 alpha (p38)/MAPK-activated protein kinase 2 (MK2) that contributes to establishing the cell cycle arrest [8–10]. Following DNA repair, massive protein phosphorylation induced by DDR is removed by protein phosphatases allowing cells to reinitiate the proliferation program. Although overlap among protein substrates likely exists among various phosphatases, PP4 phosphatase was implicated in recovery from the G1 checkpoint, whereas wild-type (WT) p53-induced phosphatase 1 (WIP1) promotes recovery from the G2 checkpoint [11].

WIP1 is a serine/threonine protein phosphatase encoded by *PPM1D* gene and is commonly overexpressed or mutated in human cancers. Basal expression of WIP1 is low, and it increases following stabilization of p53 after DNA damage [12]. WIP1 was reported to target numerous proteins of the DDR pathway including ATM, H2AX, BRCA1, CHK1, CHK2, KAP1, p53, $p27^{Kip1}$, and many others [6,13–18]. However, several lines of evidence suggest that inhibition of p53 pathway is the major function of WIP1. Firstly, sustained activity of p53 prevents checkpoint recovery in WIP1-depleted cells after combined inhibition of ATM, CHK1/2, and p38 kinases [19]. Secondly, inhibition of WIP1 can lead to the loss of recovery competence caused by p53-p21-dependent activation of APC/C^{Cdh1} followed by degradation of essential cell cycle regulators [20,21]. Finally, amplification of *PPM1D* locus or gain-of-function mutations in *PPM1D* occur mostly in cancers that retain the WT p53 [22–25]. Subsequently, inhibition of WIP1 has been proposed as a possible strategy for treatment of human cancers carrying WT p53 including neuroblastoma and medulloblastoma [26,27].

Based on reactivity of the recombinant WIP1 with synthetic phosphopeptides, two types of consensus motifs were described, namely pS/pTQ and pTXpY [28,29]. The first motif corresponds to the sequence commonly phosphorylated by ATM/ATR explaining the overlap between the substrates of ATM/ATR and WIP1 [30]. A phosphoproteomic analysis of cells treated or not with cytarabine and with WIP1 inhibitor later confirmed the presence of WIP1 consensus motif comprising of pS/pTQ flanked by acidic residues [31]. p38 is the only reported substrate of WIP1 carrying the pTXpY consensus site. The threonine residue within the doubly phosphorylated peptide pT180-pY182 of the active p38 is dephosphorylated by WIP1 *in vitro* and overexpression of WIP1 was reported to suppress the activity of p38 induced by UV irradiation [32].

Here, we aimed to validate the reported targets of WIP1 phosphatase as many of them were identified before a routine use of RNA interference and CRISPR/Cas9-mediated gene editing preventing their thorough validation in cellular models. To this end, we developed a simple phosphatase assay in nuclear extracts (NEs) that allows assaying WIP1 activity in context of whole proteins instead of the commonly used synthetic phosphopeptides. This assay confirmed the ability of purified full-length WIP1 to dephosphorylate multiple targets in DDR pathway and identified deleted in breast cancer gene 1 (DBC1)-pT454 and DNA-PK-pS2056 as new substrates of WIP1. In contrast, we found that pCHK1 and p38 are poor substrates of WIP1. Findings obtained by the *in vitro* assay were confirmed in WIP1 knock-out cells and in cells treated with a selective WIP1 inhibitor GSK2830371. In addition to protein dephosphorylation, WIP1 activity also suppressed acetylation of p53. Contrary to our expectations, we found that DBC1 was not involved in control of p53 acetylation. Instead, we observed that WIP1 activity counteracted the interaction of p53 with the acetyltransferase p300.

Fig. 1. WIP1 phosphatase assay in NEs. (A) A diagram showing the preparation of cell lysates used for *in vitro* phosphatase assay. U2OS-WIP1-KO cells were treated with DMSO (NT) or etoposide (20 μM for 45 or 120 min), or were exposed to UVC (10 $J{\cdot}m^{-2}$). After dounce homogenization, suspension was spinned down at 500 ***g*** for 5 min. Cell nuclei in in the pellet were extracted by hypertonic buffer, spinned down at 16 000 ***g*** for 15 min, and the supernatant formed a NE subsequently used for *in vitro* phosphatase assays. (B) NE from A was incubated with or without purified His-WIP1 for 15 min at 37 °C. Where indicated, WIP1 inhibitor or ATM inhibitor was added to the reaction. Samples were analyzed by immunoblotting. (C) NEs isolated from nontreated U2OS-WIP1-KO cells, cells treated for indicated times with etoposide or cells 45 min after exposure to UVC (10 $J{\cdot}m^{-2}$) were incubated with mock or purified His-WIP1 for 15 min at 37 °C. Protein phosphorylation was evaluated by immunoblotting using indicated phosphospecific antibodies. (D) Indicated synthetic phosphopeptides (100 μM) were incubated with His-WIP1 (100 ng) for 60 min at 37 °C. Where indicated, WIP1 inhibitor was added to the reaction. Released phosphate was detected by PiPer Phosphatase Assay Kit. Shown is mean ± SD ($n = 3$).

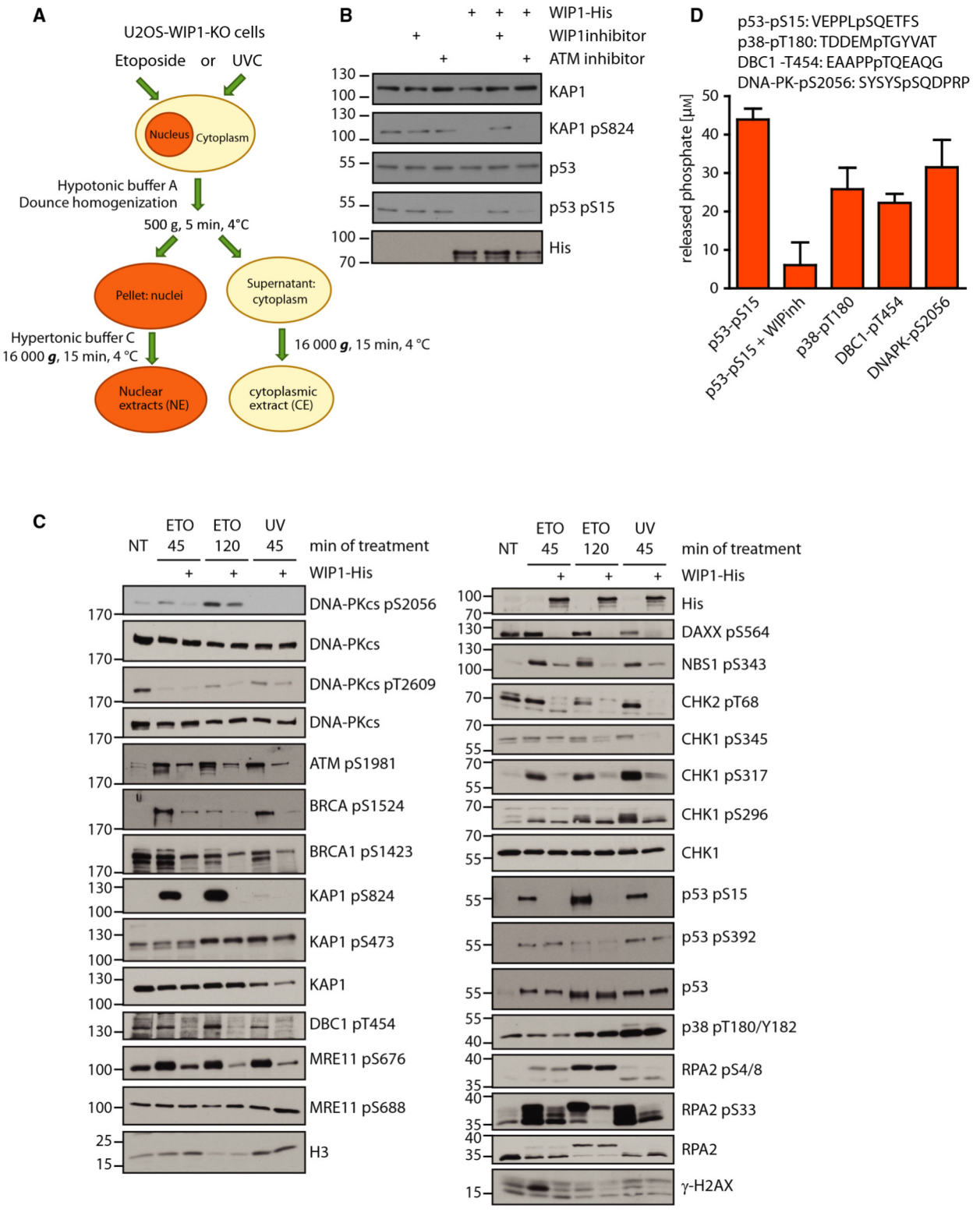

Phosphatase assay reported here allows an easy validation and identification of new substrates of WIP1.

Results

WIP1 phosphatase assay in nuclear extracts

WIP1 has been reported to dephosphorylate multiple targets in DDR and p38/MK2 pathways. Some of these data relayed mostly on the ability of recombinant WIP1 to dephosphorylate synthetic phosphopeptides *in vitro* and were not sufficiently validated in cellular models. We hypothesized that accessibility of the phosphorylated residues might be different in context of the whole proteins and protein complexes and in the presence of competitive substrates. To test the enzymatic activity of WIP1 in more physiological conditions, we developed an assay where we use NE isolated from U2OS-WIP1-KO cells after DNA damage as a complex substrate mixture for recombinant His-WIP1 and detect the level of protein phosphorylation by phospho-specific antibodies (Fig. 1A). To validate the assay, we first incubated the NE with purified WIP1 in the presence of DMSO or WIP1 inhibitor and tested the level of KAP1-pS824 phosphorylation, an established target of WIP1 [16]. As expected, modification of KAP1 was efficiently removed by WIP1, but it persisted in the sample treated with WIP1 inhibitor (Fig. 1B). The phosphatase assay was performed in the absence of ATP to minimize the effect of active protein kinases present in NE on protein phosphorylation. Importantly, inhibition of ATM did not affect the level of KAP1-pS824 modification, indicating that ATM was not active during the phosphatase assay (Fig. 1B). Next, we used a panel of previously validated phospho-specific antibodies to evaluate the ability of WIP1 to target the corresponding phosphorylated residues (Fig. 1C). In good agreement with previous reports, we observed that WIP1 efficiently dephosphorylated p53-pS15 [18], γ-H2AX [14], ATM-pS1981 [13], BRCA1-pS1524 [15], KAP1-pS824 [16], DAXX-pS564 [33], pCHK2-T68 [17], and pCHK1-pS317 [18]. All these residues matched the pSQ/TQ consensus motif previously reported for WIP1 phosphatase [29]. In addition, we identified several new putative substrates of WIP1 including MRE11-pS676, RPA2-pS33, DNA-PK-pS2056, and DBC1-pT454. In contrast, WIP1 did not target all phosphopeptides as exemplified by KAP1-pS473, RPA2-pS4/8, and p53-pS392 that remained fully phosphorylated despite the presence of active WIP1. Finally, we found that purified WIP1 failed to dephosphorylate p38-pT180 in the NE although it dephosphorylated a synthetic phosphopeptide corresponding to the activating phosphorylation of p38 (Fig. 1C,D). This surprising observation suggests that active p38 is a poor substrate of WIP1 compared to multiple other phosphoproteins. We conclude that dephosphorylation of the NEs is an easy assay that allows testing of WIP1 activity in complex protein mixture.

Activity of p38/MK2 pathway is not affected by inhibition or overexpression of WIP1

In the next step, we wished to confirm the findings from the *in vitro* assay in cellular context. To this end, we compared protein phosphorylation in parental U2OS cells, U2OS treated with a specific WIP1 inhibitor GSK2830371 and in U2OS-WIP1-KO cells [21,27]. To compare the dynamics of protein phosphorylation, we collected whole cell lysates (WCLs) prior to or 1, 4, and 8 h postexposure to ionizing radiation (Fig. 2A). As expected, we observed an increased and prolonged phosphorylation of γH2AX, p53-pS15, and KAP1-pS824 in cells with inhibition or loss of WIP1 confirming that these proteins are good substrates of WIP1 [14,16,18,34]. In addition, inhibition of WIP1 increased the level of DNA-PK-pS2056 and DBC1-pT454 in the early time points after exposure of cells to ionizing radiation suggesting that DNA-PK and DBC1 could be new substrates of WIP1. Specificity of DBC1-pT454 and DNA-PK-pS2056 antibodies was validated by depletion of DBC1 and DNA-PK, respectively (Fig. 2B,C). In contrast, phosphorylation of RPA32-

Fig. 2. Validation of WIP1 phosphatase substrates in cells. (A) Parental U2OS or U2OS-WIP1-KO cells were exposed to ionizing radiation (3 Gy) and WCLs were collected at indicated times. Where indicated, cells were incubated with WIP1 inhibitor. Levels of protein phosphorylation were detected by immunoblotting. Loading controls were performed on every protein gel. For simplicity, only one representative staining of TFIIH is shown. (B) U2OS transfected with control or DNA-PK siRNA were treated with mock or etoposide and WCLs were probed for total DNA-PK and DNA-PK-pS2056 using immunoblotting. Staining for importin served as a loading control. (C) U2OS transfected with control or DBC1 siRNA were treated with WIP1 inhibitor, etoposide or combination of both and WCLs were probed for total DBC1 and DBC1-pT454 using immunoblotting. Staining for histone H3 served as a loading control. (D) Parental U2OS or U2OS-WIP1-KO cells were exposed to UVC radiation (10 $J \cdot m^{-2}$) and WCLs were collected at indicated times. Where indicated, cells were incubated with WIP1 inhibitor. Levels of protein phosphorylation were detected by immunoblotting. (E) Parental U2OS or U2OS-WIP1-KO cells were treated as in D, and WCLs were collected at 1, 2, 6 and 24 h after exposure to UVC.

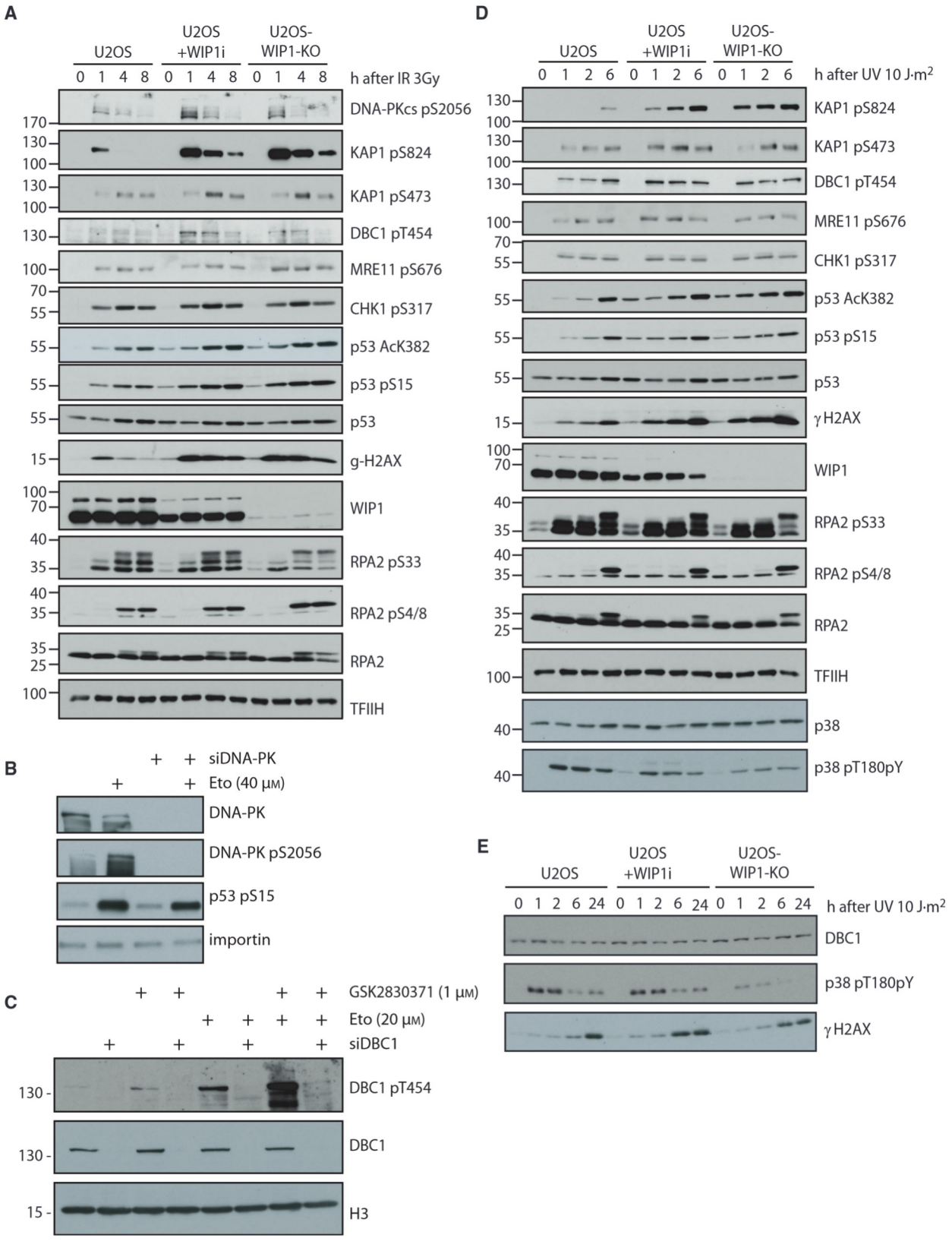

pS33, MRE11-pS676, and CHK1-pS317 showed comparable dynamics in WIP1 deficient and control cells, suggesting that these proteins are not physiological substrates of endogenous WIP1 although they can be dephosphorylated *in vitro* (Figs 1B and 2A). Similar pattern of WIP1-dependent dephosphorylation was observed in cells after induction of genotoxic stress by UVC radiation, only the DNA-PK-pS2056 autophosphorylation was below the detection limit reflecting the poor activation of DNA-PK by UVC (Fig. 2D). As expected, exposure of parental U2OS cells to UVC induced phosphorylation of p38 at T180/Y182 corresponding to its activation. Surprisingly, we observed a slight reduction (rather than expected increase) of p38 phosphorylation in cells treated with WIP1 inhibitor or in WIP1 knock-out cells following exposure to UVC (Fig. 2D). Importantly, inhibition or deletion of WIP1 did not increase p38 phosphorylation even after 24 h exposure to UVC, suggesting that WIP1 does not affect the late p38/MK2 response triggered by genotoxic stress (Fig. 2E) [35]. The lack of effect of WIP1 on the level of phosphorylated p38 in cells is consistent with the *in vitro* assay and suggests that p38 is not a physiological substrate of WIP1.

To exclude the possibility that WIP1 may target p38 only after specific type of stress, we tested activation of p38 also after treatment of cells with a topoisomerase II inhibitor doxorubicin or after induction of hyperosmotic stress. As expected, extended incubation of U2OS cells with doxorubicin activated p38/MK2 pathway [8]; however, inhibition of WIP1 did not lead to further induction of the p38-pT180-pY182 signal (Fig. 3A). Similarly, incubation of cells in hypertonic media containing 350 mM NaCl caused comparable stimulation of p38/MK2 pathway in RPE cells and RPE-WIP1-KO cells (Fig. 3B). Inhibition of WIP1 did not affect the activation of p38 also in MCF7 cells, suggesting that the inability of WIP1 to target p38 represents a general phenomenon and cannot be explained by a cell type specific defect (Fig. 3C). Finally, we tested the ability of WIP1 to dephosphorylate p38 in cells with tetracycline-inducible expression of FLAG-WIP1 [19]. Whereas high overexpression of the WT WIP1, but not of the phosphatase-dead D314A mutant, decreased p53-pS15 phosphorylation in cells exposed to UVC, we did not observe any effect on the level of active p38 and its downstream target MK2-pT334 (Fig. 3D).

One of the possibilities why WIP1 fails to dephosphorylate p38 in cells could be a lack of protein-protein interactions between WIP1 and p38. To test this, we immunoprecipitated overexpressed enhanced green fluorescent protein (EGFP) or EGFP-WIP1 using GFP trap in the presence of EtBr and Benzonase to efficiently extract WIP1 from the chromatin. Notably, we did not observe co-immunoprecipitation between EGFP-WIP1 and p38 (Fig. 3E). In contrast, EGFP-WIP1 formed a complex with its previously described substrate KAP1 and with DBC1, a new putative substrate identified in this study (Fig. 3E). We speculated that distinct subcellular localization might be a contributing factor for the lack of interaction between WIP1 and p38. We fractionated cells into cytosolic, nuclear soluble, and chromatin fractions and probed for subcellular distribution of both proteins. As expected, WIP1 was dominantly enriched at chromatin (Fig. 3F) [14]. In contrast, p38 was enriched in the cytosol and nucleoplasm but was not present in the chromatin fraction (Fig. 3F). We conclude that WIP1 does not regulate the activity of p38/MK2 pathway in cells.

WIP1 stably interacts with DBC1

Next, we aimed to independently confirm the identified interaction between DBC1 and WIP1 using a proximity ligation assay (PLA) [36]. Indeed, we observed a nuclear PLA signal between DBC1 and WIP1 in basal conditions that was not further enhanced after exposure of cells to etoposide, suggesting that DBC1 and WIP1 stably interact even in the absence of DNA damage (Fig. 4A). The specificity of the PLA signal was confirmed using WIP1-KO cells where PLA signal was dramatically reduced (Fig. 4A). Similarly, depletion of DBC1 by RNAi reduced the immunofluorescence signal confirming the specificity of the antibody (Fig. 4B). In addition, we observed a strong PLA signal between p53 and WIP1 in etoposide treated cells (Fig. 4C,D). Specificity of the signal was confirmed in p53-KO and WIP1-KO cells (Fig. 4C,D). In contrast to the WIP1-DBC1 interaction, we observed only low level of PLA signal for p53 and WIP1 in basal conditions but it was strongly enhanced upon induction of DNA damage (Fig. 4C,D). Finally, we tested the PLA between WIP1 and p38 but we did not observe any specific signal under basal conditions or after DNA damage (data not shown), which is in agreement with the lack of interaction observed by immunoprecipitation.

WIP1 regulates p53 acetylation independently of DBC1

DBC1 was previously implicated in acetylation of p53 at K382 through inhibition of the NAD-dependent protein deacetylase sirtuin-1 (SIRT1) deacetylase [37–39]. Interaction between DBC1 and SIRT1 deacetylase

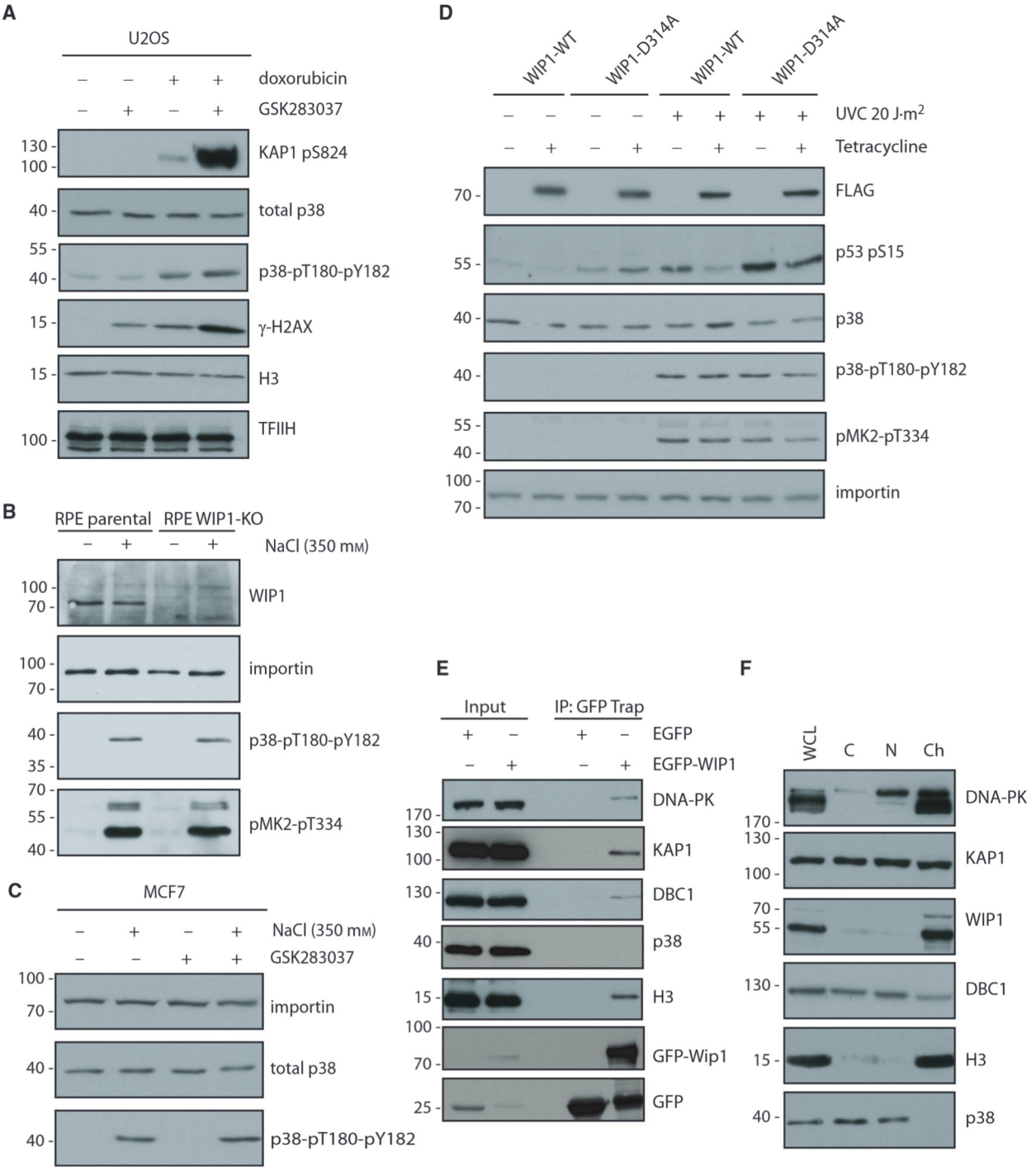

Fig. 3. p38 is not dephosphorylated by WIP1. (A) U2OS cells were treated with mock or WIP1 inhibitor and incubated with doxorubicin (0.5 μM) for 24 h. WCLs were analyzed by immunoblotting with indicated antibodies. (B) Parental RPE and RPE-WIP1-KO cells were incubated in media containing 350 mM NaCl for 15 min. WCLs were analyzed by immunoblotting with indicated antibodies. (C) MCF7 cells were pretreated with mock or with WIP1 inhibitor and incubated in media containing 350 mM NaCl for 15 min. WCLs were analyzed by immunoblotting with indicated antibodies. (D) U2OS cells with Tet-ON inducible WT or phosphatase dead (D314A) FLAG-WIP1 were treated or not with tetracycline for 12 h. Cells were harvested 1 h after exposure to mock or UVC (20 $J \cdot m^{-2}$) and analyzed by immunoblotting. (E) EGFP or EGFP-WIP1 was immunoprecipitated from transfected HEK293 cells and bound proteins were analyzed by immunoblotting. (F) U2OS cells were fractionated to cytosolic (C), nuclear soluble (N) and chromatin (Ch) fractions and distribution of proteins was analyzed by immunoblotting. H3 is a marker of chromatin. WCL of U2OS cells is shown as control.

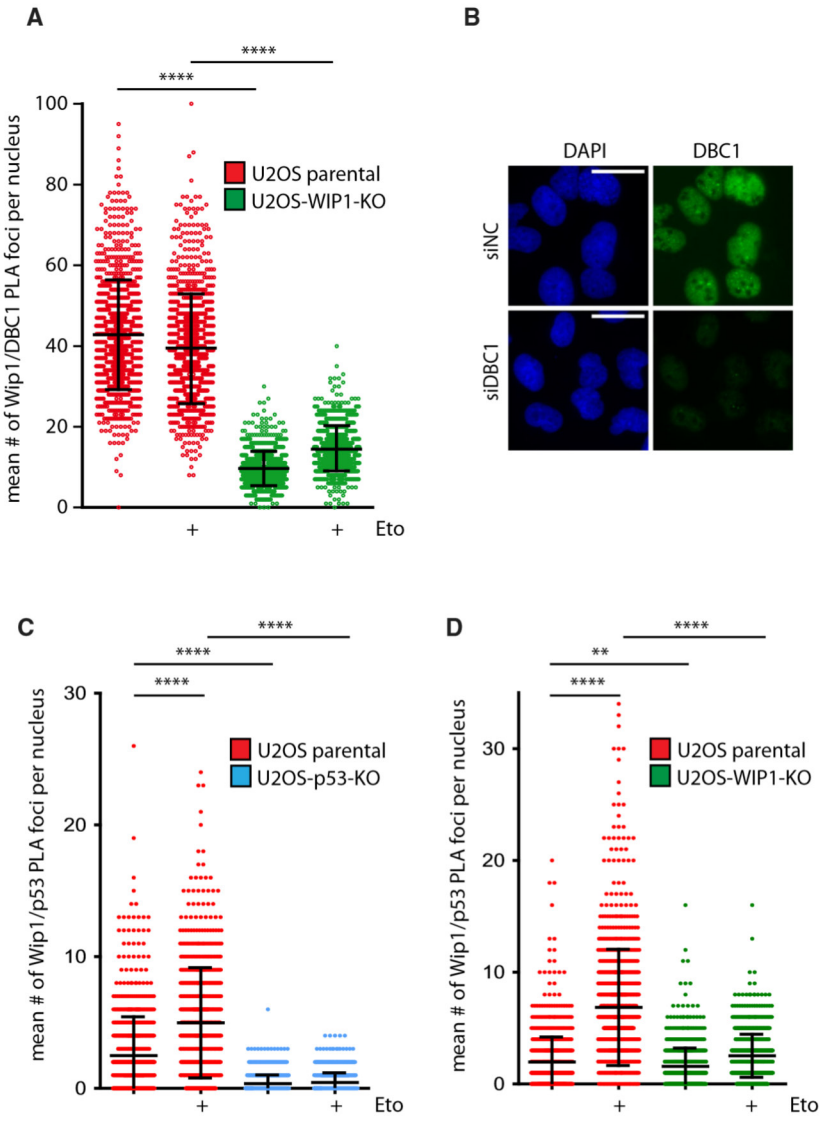

Fig. 4. DBC1 stably interacts with WIP1. (A) Parental U2OS or U2OS-WIP1-KO cells were treated or not with etoposide for 2 h, fixed, and probed for interaction between WIP1 and DBC1 by PLA using mouse monoclonal antibody to WIP1 and rabbit polyclonal antibody to DBC1. Shown is mean number of nuclear PLA foci ± SD. Every dot represents a single cell (n = 900). Statistical significance was determined using Mann–Whitney test (****P < 0.0001). (B) U2OS transfected with control or DBC1 siRNA were fixed and probed with antibody to DBC1. Scale bar indicates 30 μm. (C) Parental U2OS or U2OS-p53-KO cells were treated or not with etoposide for 2 h, fixed and probed for interaction between WIP1 and p53 by PLA using mouse monoclonal antibody to p53 and rabbit polyclonal antibody to WIP1. Shown is mean number of nuclear PLA foci ± SD. Every dot represents a single cell (n = 500). Statistical significance was determined using Mann–Whitney test (****P < 0.0001). (D) Parental U2OS or U2OS-WIP1-KO cells were treated or not with etoposide for 2 h, fixed and probed for interaction between WIP1 and p53 by PLA using mouse monoclonal antibody to p53 and rabbit polyclonal antibody to WIP1. Shown is mean number of nuclear PLA foci ± SD. Every dot represents a single cell (n = 500). Statistical significance was determined using Mann–Whitney test (**P < 0.01, ****P < 0.0001).

was reported to be regulated through an ATM-dependent phosphorylation of DBC1 at T454 [37]. Here, we noted increased p53 K382 acetylation in WIP1 knockout cells and after WIP1 inhibition in unchallenged conditions as well as after exposure to ionizing radiation or UVC (Fig. 2A,B). Based on the

Fig. 5. DBC1-pT454 is a new substrate of WIP1. (A) EGFP and WT EGFP-DBC1 were immunoprecipitated from stably transfected HEK293 cells using GFP trap and bound proteins were analyzed by MS (n = 3). Hits showing FDR < 0.05 are shown. (B) EGFP, WT EGFP-DBC1 and mutant EGFP-DBC1-T454A (TA) were immunoprecipitated from stably transfected HEK293 cells 2 h after treatment with mock (NT) or etoposide (40 μM, eto) and bound proteins were analyzed by MS (n = 3). Shown are $\log_2$ intensities of DBC1 and SIRT1 ± SD. (C) EGFP, WT EGFP-DBC1-WT, EGFP-DBC1-T454A, or EGFP-DBC1-T454D was immuno-precipitated from HEK293 cells using GFP trap and bound SIRT1 was analyzed by immunoblotting. (D) Endogenous DBC1 was immunoprecipitated from U2OS cells treated with mock, etoposide or combination of etoposide and WIP1 inhibitor. IgG was used as negative control. Proteins were analyzed by immunoblotting with indicated antibodies. (E) HEK293 cells were transfected with empty plasmid or myc-SIRT1, were treated with mock or WIP1 inhibitor, and were exposed to ionizing radiation (10 Gy, upper panel). Cell extracts were immunoprecipitated using anti-myc antibody and proteins were analyzed by immunoblotting. Alternatively, immunoprecipitation was performed from cells that were not exposed to IR (lower panel). (F) U2OS cells were transfected with a control siRNA or siRNA to DBC1. Cells were treated with mock or WIP1 inhibitor and were exposed or not to ionizing radiation (3 Gy). After 4 h, cells were lysed and analyzed by immunoblotting.

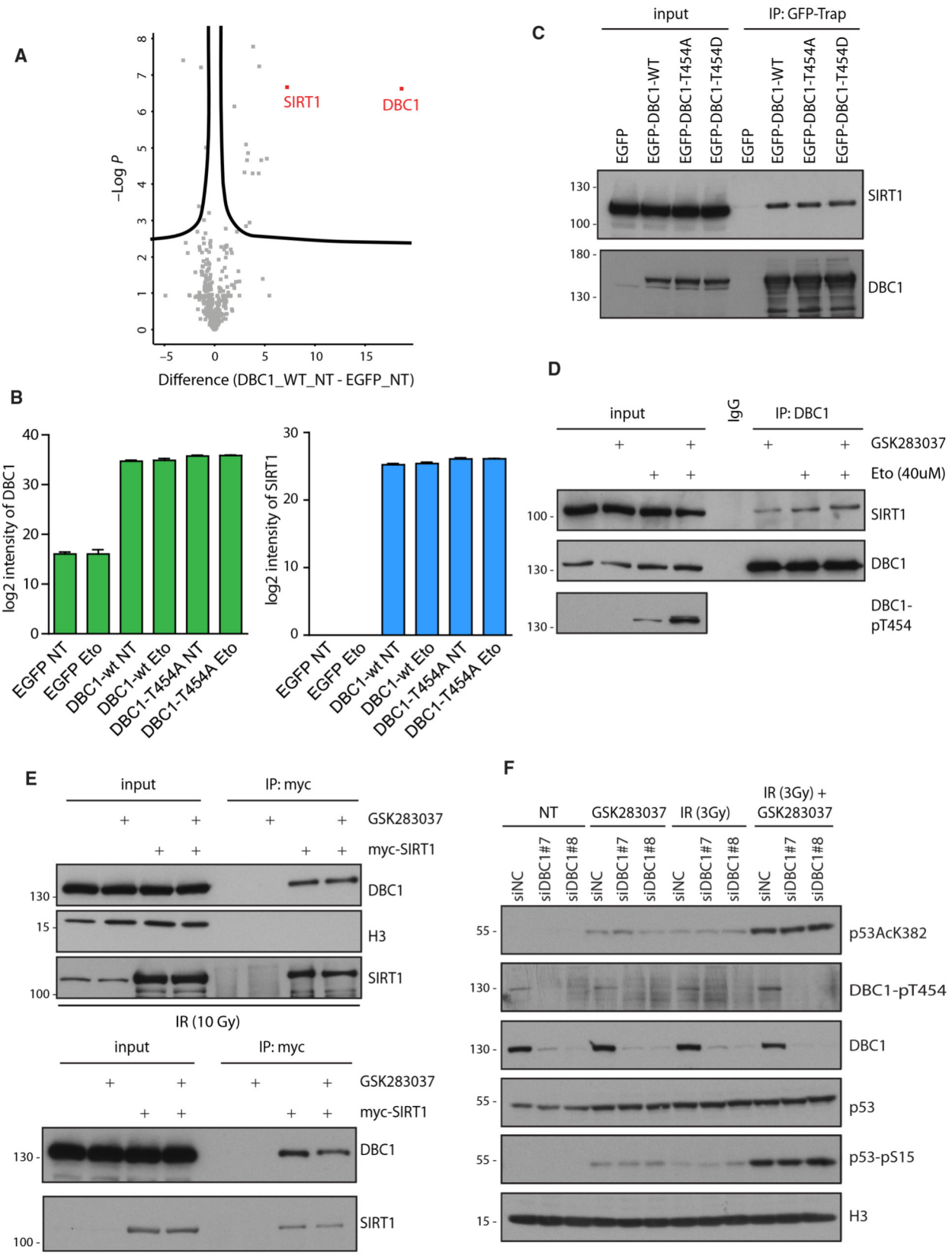

published data, we hypothesized that WIP1 might control p53 acetylation through regulating the interaction between SIRT1 and its inhibitor DBC1. Using mass spectrometry analysis of immunoprecipitated EGFP or EGFP-DBC1-WT from stably transfected HEK293 cells, we confirmed that SIRT1 was a major interacting partner of DBC1 (Fig. 5A). However, the proteomic analysis did not show any induction of the interaction between DBC1-WT and SIRT1 after exposure of cells to etoposide (Fig. 5B). In addition, the interaction between SIRT1 and DBC1-WT or DBC1-T454A mutant was comparable suggesting that the two proteins formed a stable complex and the interaction did not require phosphorylation of DBC1 (Fig. 5B). In agreement with this possibility, we observed a comparable interaction of the nonphosphorylable EGFP-DBC1-T454A and phospho-mimicking EGFP-DBC1-T454D mutant with endogenous SIRT1 (Fig. 5C). In addition, we found that endogenous SIRT1 interacted with DBC1 under basal conditions in U2OS cells when phosphorylation of T454 was not detected (Fig. 5D). This interaction was only slightly increased after induction of genotoxic stress by etoposide, but it did not further increase in the presence of WIP1 inhibitor despite a dramatic induction of DBC1 phosphorylation at T454 (Fig. 5D). Conversely, myc-SIRT1 co-immunoprecipitated comparable levels of endogenous DBC1 from cells exposed to ionizing radiation and treated or not with WIP1 inhibitor (Fig. 5E). In addition, DBC1 co-immunoprecipitated with SIRT1 also in cell extracts from cells that were not exposed to IR (Fig. 5E). Our data are thus consistent with the formation of a stable complex between SIRT1 and DBC1 that is not controlled through phosphorylation of DBC1 by ATM. Finally, we noted that depletion of DBC1 did not prevent induction of p53 acetylation by ionizing radiation and also that WIP1 potentiated p53-K382 acetylation regardless the presence or absence of DBC1 (Fig. 5F). As we did not find any evidence for the role of WIP1 in p53 de-acetylation through DBC1-SIRT1, we asked if WIP1 could control p53 acetylation through the acetyltransferase p300/CBP. Indeed, we found that depletion of p300 reduced the effect of WIP1 inhibition on p53-K382 acetylation (Fig. 6A). In addition, the level of p53-K382 acetylation induced by ionizing radiation was further increased by inhibition of WIP1 and this effect was suppressed upon depletion of p300 (Fig. 6A).

To address a potential mechanism of action, we tested the interaction between p53 and p300 by a PLA assay. First, we validated two sets of antibodies to p53 and p300 by RNAi (Fig. 6B,C). Next, we performed PLA after treating cells with GSK2830371, etoposide, or combination of both. Treatment with etoposide increased the PLA signal between p53 and p300, suggesting that this interaction is induced by DNA damage (Fig. 7A,B). Similarly, we observed that WIP1 inhibition increased the interaction between p53 and p300 (Fig. 7A,B). Importantly, the interaction between the p53 and p300 further increased after combined treatment with etoposide and WIP1 inhibitor (Fig. 7A,B). The same phenotype was confirmed by using another combination of antibodies to p53 and p300 (Fig. 7C,D). Conversely, tetracycline-induced expression of the active WIP1 reduced the interaction between p53 and p300 (Fig. 7E). We conclude that WIP1 activity counteracts the acetylation of p53 at K382 by counteracting the interaction of p53 with the acetyltransferase p300.

Discussion

Here, we established a phosphatase assay for testing the substrates of WIP1 in NEs isolated from cells after exposure to genotoxic stress. Many of the previously reported targets of WIP1 were independently confirmed using this technique whereas others were identified as poor substrates. In particular, we have found that WIP1 fails to dephosphorylate p38 *in vitro* and to suppress p38 activity in various cell types. This finding challenges the current view of WIP1 as a direct negative regulator of p38/MK2 pathway. We find that high overexpression of active WIP1 does not prevent activation of the p38 pathway in response to acute exposure to UVC. Similarly, inhibition or loss of WIP1 did not increase the level of p38 activation after UVC or other forms of stress. Most of the studies describing the effect of WIP1 on p38 pathway relied on shRNA-mediated depletion of WIP1 in the stable cell lines or on prolonged treatment with WIP1 inhibitor [40]. For instance, Deng *et al.* [40] reported that treatment of A549 cells with GSK2830371 for 24–48 h increased the level of active p38. In the short treatment with an efficient dose of GSK2830371, we did not observe any effect on the basal level of active p38. Extended inhibition of WIP1 may lead to changes in the transcriptional program and thus increased p38 phosphorylation observed under such conditions could be caused indirectly. In addition, fractionation of cells revealed that WIP1 and p38 were distributed in distinct subcellular compartments and we failed to detect interaction between WIP1 and p38 by co-immunoprecipitation from whole-cell extracts. As expected, we found that the majority of WIP1 was present at chromatin, whereas p38 distributed to the soluble fraction. Based on these observations, we propose that p38 is not a direct substrate of WIP1 phosphatase.

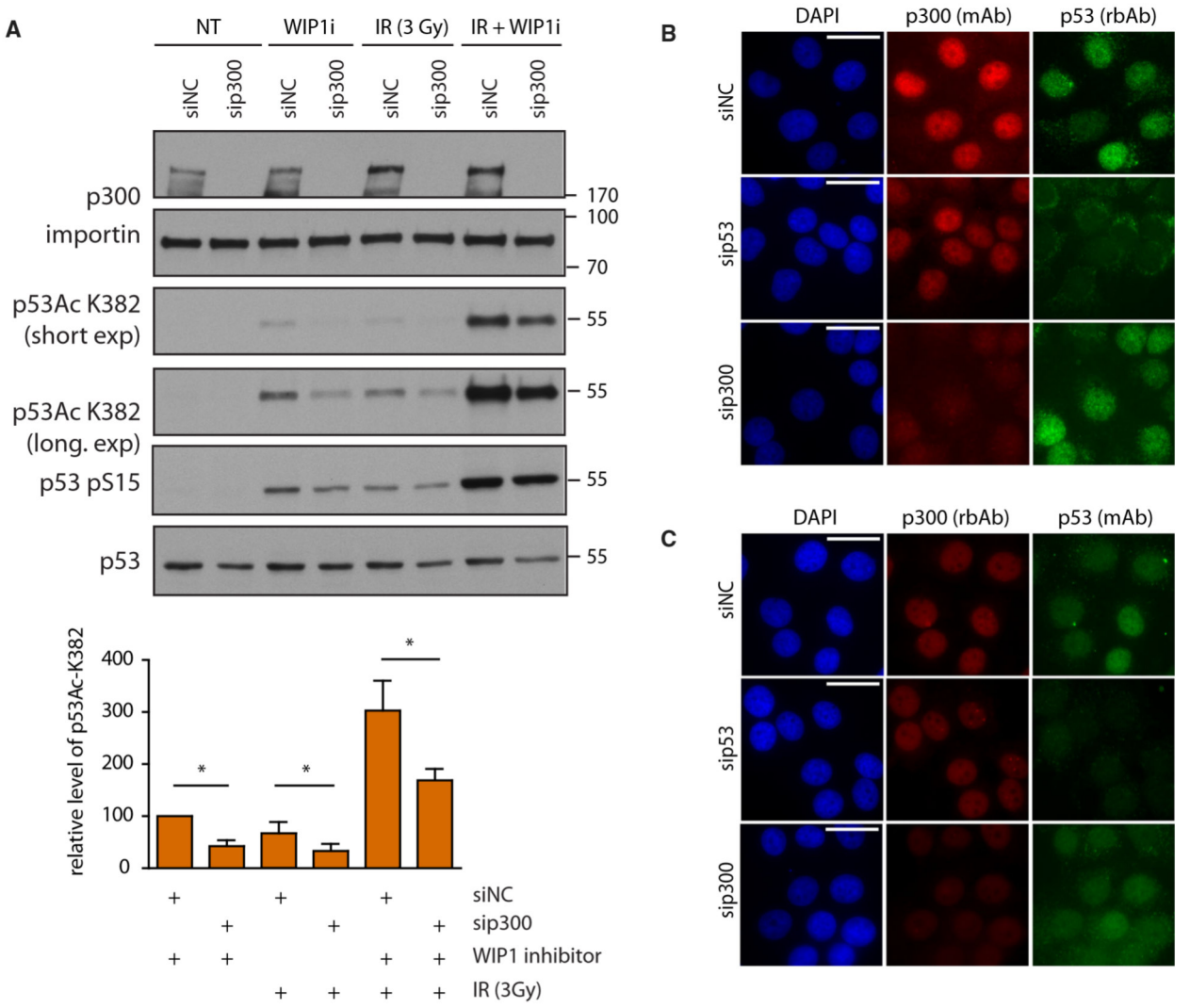

Fig. 6. WIP1 activity counteracts p53 acetylation at K382. (A) U2OS cells were transfected with control siRNA or siRNA to p300. Cells were treated with mock or WIP1 inhibitor and were exposed or not to ionizing radiation (3 Gy). After 4 h, cells were lysed and analyzed by immunoblotting. Level of p53 acetylation was quantified and normalized to importin (loading control) and to control siRNA-transfected cells treated with WIP1 inhibitor. Statistical significance was determined by *t*-test ($n = 3$, $*P < 0.05$). (B) MCF7 cells were transfected with control siRNA or siRNA to p300 or to p53. Cells were fixed after 48 h and probed with a mouse monoclonal antibody against p300 and a rabbit polyclonal antibody to p53. Representative images are shown, scale bar indicates 30 μm. (C) MCF7 cells were transfected with control siRNA or siRNA to p300 or to p53. Cells were fixed after 48 h and probed with a rabbit polyclonal antibody to p300 and a mouse monoclonal antibody to p53. Representative images are shown, and scale bar indicates 30 μm.

Based on the pioneering work in WIP1 knock-out mice, loss of WIP1 was originally believed to suppress tumorigenesis through targeting p38 leading to indirect induction of p53 and Ink4a pathways [23,41]. Formation of the mammary tumors induced by Errb2 and WIP1 expression was suppressed by the presence of a constitutively active MKK6 acting as an upstream activator of p38 [42]. On the other hand, WIP1 was later demonstrated to target p53 directly through dephosphorylating S15 and also indirectly through its effect on ATM and MDM2 [18,43,44]. In addition, WIP1 activity interferes with acetylation of the C-terminal part of p53 that is involved in DNA-binding and stimulating transcription of the target genes [45–48]. Here we tested the possibility that WIP1 may control p53 acetylation through its newly recognized substrate DBC1. However,

we did not observe any differences between T454A, T454D, and WT DBC1 in the ability to form a complex with SIRT1 deacetylase. Further, we noted that depletion of DBC1 did not prevent an increased acetylation of p53 upon treatment with WIP1 inhibitor. Our data thus favor a DBC1-independent impact of WIP1 on p53. Indeed, we found that WIP1 controls formation of the complex between p53 and p300 acetyltransferase. The N-terminal region of p53 has been reported to interact with Taz1 and Taz2 domains of p300 and this interaction is positively regulated by phosphorylation of the transactivation domain of p53, including S15 and other residues [49–53]. As expected, we find that WIP1 efficiently dephosphorylates S15 of p53 *in vitro* and *in vivo*. In addition, ATM-induced modification of BRCA1 has recently been implicated in facilitating p53-p300 complex formation, although the precise mechanism underlying this interaction remains to be described. In agreement with recent reports, we observe that WIP1 efficiently dephosphorylates S1524 of BRCA1 [15,54]. We propose a model in which WIP1 counteracts acetylation of p53 through dephosphorylating its N-terminal domain and BRCA1-pS1524 jointly leading to dissociation of the p53-p300 complex (Fig. 7F).

In summary, we have developed a simple assay for testing of WIP1 phosphatase substrates in NEs. Besides validation of several established targets of WIP1, we report DBC1 as novel substrate of WIP1. Contrary to our expectations, we did not observe any impact of DBC1 on p53 acetylation and the function of DBC1 phosphorylation remains to be addressed by future research. As the T454 residue locates within the newly described Nudix domain implicated in NAD^+ binding [], it will be interesting to investigate a potential impact of DBC1 phosphorylation on NAD^+ metabolism. Finally, we report the ability of WIP1 to interact with and dephosphorylate DNA-PK. Autophosphorylation of DNA-PK was originally proposed to facilitate NHEJ repair by regulating the dynamics of DNA-PK at DNA double-strand breaks [56]. Whereas importance of phosphorylation of the T2609 cluster for classical nonhomologous end-joining has recently been confirmed, function of DNA-PK-pS2056 remains elusive [57–59]. Development of novel assays will be necessary for addressing a functional relevance of DNA-PK phosphorylation mediated by ATM and removed by WIP1.

Materials and methods

Cell lines

U2OS, U2OS-WIP1-KO, Hek293, MCF-7 and RPE cells were grown at 37 °C and 5% CO_2 in DMEM containing 6% FBS, Penicillin (100 $U{\cdot}mL^{-1}$), and Streptomycin (0.1 $mg{\cdot}mL^{-1}$). U2OS-WIP1-KO and RPE-WIP1-KO cell lines with inactivated *PPM1D* by CRISPR/Cas9 were described and validated previously [15,21]. U2OS-TR-WIP1 cells with tetracycline inducible expression of FLAG-tagged WIP1-WT or phosphatase dead WIP1-D314A were described previously [19]. All cell lines were regularly tested for mycoplasma infection and were confirmed as negative.

Antibodies and chemicals

Following antibodies were used: mouse monoclonal WIP1 antibody (clone F-10, sc-376257), rabbit polyclonal WIP1 antibody (sc-20712), mouse monoclonal p53 (clone D01, sc-126), rabbit polyclonal anti-p53 (sc-6243), Chk1 (sc-8408), importin (sc-137016) and TFIIH (sc-293) from Santa Cruz Biotechnology (Dallas, TX, USA); pT180-Y182-p38 MAPK (#9216), p38 MAPK (#9212), DBC1 (#5857), pT454-DBC1 (#4880), pS15-p53 (#9284), pS392-p53 (#9281), acK382-p53

Fig. 7. WIP1 activity impairs interaction between p53 and p300 acetyltransferase. (A) U2OS cells were treated with mock, etoposide (40 μM), Wip1 inhibitor (1 μM), or combination of both and were fixed after 2 h. PLA assay was performed using a rabbit polyclonal antibody to p53 and mouse monoclonal to p300 and cells were imaged using ScanR station. Representative images are shown, size of each field is 22 × 22 μm. (B) Quantification of the PLA signal from A. Each dot represents a single cell ($n = 900$). Statistical significance was evaluated using Mann–Whitney test (****$P < 0.0001$). Shown is mean number of p300/p53 PLA foci per nucleus ± SD. Presented data are from one of three biological replicates that showed comparable results. (C) U2OS cells were treated with WIP1 inhibitor, etoposide or combination of both. PLA assay was performed using mouse monoclonal to p53 and rabbit polyclonal antibody to p300 and cells were imaged using ScanR station. Representative images from one of the three independent replicates are shown, size of each field is 22 × 22 μm. (D) Quantification of the nuclear PLA signal from C. Each dot represents a single cell ($n = 900$). Plotted is mean number of p300/p53 PLA foci per nucleus ± SD. Statistical significance was evaluated using Mann–Whitney test (****$P < 0.0001$). (E) U2OS-TR-WIP1-WT cells were incubated or not with tetracycline for 12 h and treated with etoposide (40 μM) for additional 2 h. After fixation, PLA assay was performed with indicated combination of antibodies. Shown is mean number of p300/p53 PLA foci per nucleus ± SD. Presented data are from one of two biological replicates that showed comparable results. Statistical significance was evaluated using Mann–Whitney test (****$P < 0.0001$). (F) Proposed model of WIP1 impact on p53 acetylation. ATM activated by genotoxic stress induces interaction between p53, p300, and BRCA1 by phosphorylation of the N-terminal domain of p53 and S1524 of BRCA1. WIP1 dephosphorylates p53 and BRCA1, inhibits the p53-p300 interaction, and decreases acetylation of p53 at K382. Phosphorylation events shown in yellow, acetylation in green.

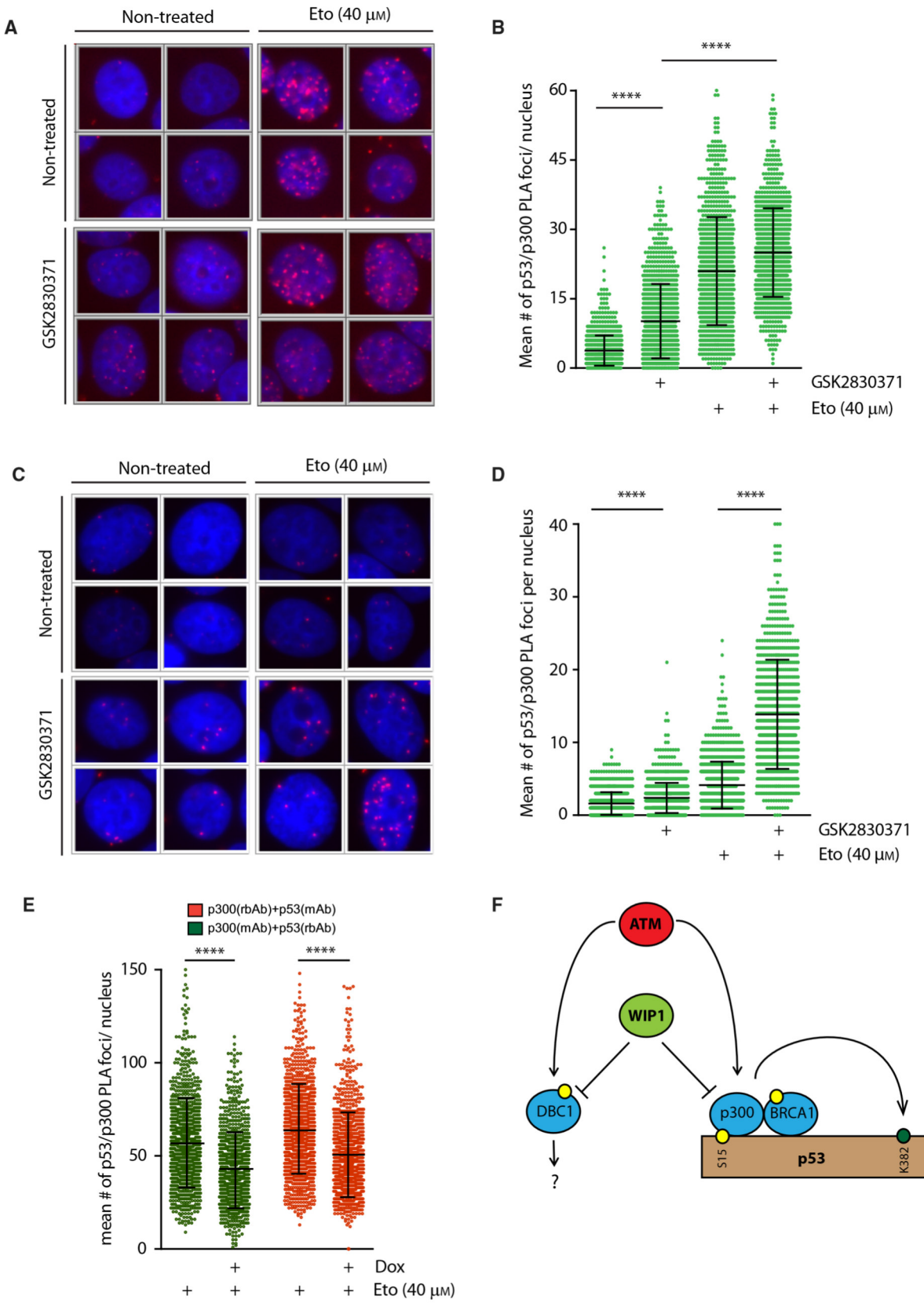

(#2525), pS343-NBS1 (#3001), pS676-MRE11 (#4859), pS296-Chk1 (#2349), pS317-Chk1 (#12302), pS345-Chk1 (#2341S), pT68-Chk2 (#2661), H3 (#14269), SIRT1 (#2493), pT334-MK2 (#3007) from Cell Signalling Technology (Danvers, MA, USA); RPA2 (clone 9H8, ab2175), pS2056-DNA-PKcs (ab124918), pT2609-DNA-PKcs (ab18356), pS1524-BRCA1 (ab2401), and pS1423-BRCA1 (ab-90528) from Abcam (Cambridge, UK); pS33-RPA2 (NB100-544), mouse monoclonal and rabbit polyclonal p300 antibody (NB500-161 and NB100-507), pT2609-DNA-PKcs (NB600-897) from Novus Biologicals (Centennial, CO, USA); pS139-H2AX (05-636), pS4/8-RPA2 (PLA0071), and flag (F 1804) from Merck Millipore (Burlington, MA, USA); pS824-KAP1 (GTX63711), KAP1 (GTX62973) from GeneTex (Irvine, CA, USA); pS473-KAP1 (clone 11G10SC, 654102) from Biolegend (San Diego, CA, USA); His (A00186-100) from GenScript (Piscataway, NJ, USA); secondary Alexa Fluor conjugated antibodies from Thermo Fisher Scientific (Waltham, MA, USA). Antibodies against pS564-DAXX and pS688-Mre11 were described and validated previously [33,60]. WIP1 inhibitor GSK2830371 was obtained from MedchemExpress (Monmouth Junction, NJ, USA), dissolved in DMSO and used at final concentration 1 μM [21,27], doxorubicin and etoposide were from Merck (Darmstadt, Germany).

Protein purification

N terminally His-tagged full-length human Wip1 was expressed from pET21b vector in BL21 *Escherichia coli*. Protein expression was induced by 0.5 mM IPTG at OD = 0.6 for 16 h at 21 °C. After centrifugation, bacteria were resuspended in lysis buffer [50 mM HEPES (pH 7.5), 200 mM NaCl, 10% (v/v) glycerol, 10 mM $MgCl_2$] freshly supplemented with 0.5 mM TCEP, 1 mg·mL^{-1} lysozyme and EDTA-free protease inhibitors (Sigma-Aldrich, St. Louis, MO, USA). Lysate was sonicated on ice and kept on ice for 15 min. Afterward, benzonase 0.1 μL·mL^{-1} (25 U·μL^{-1}) was added and the mixture was incubated for 15 min at RT. Lysate was centrifuged 48 000 ***g*** for 1 h at 4 °C, filter by 0.45-um one-off filter. The clarified eluate was purified using the FPLC purification with His-Trap HP column (Sigma-Aldrich, St. Louis, MO, USA) by gradient elution by 10–500 mM imidazole. The fraction enriched with Wip1 was desalted with HiTrap column (Sigma-Aldrich) into exchange buffer (50 mM HEPES pH 7.5, 10 mM $MgCl_2$, 200 mM NaCl, 5% glycerol) and further purified by ion exchange chromatography on 1 mL SP HiTrap column (Sigma-Aldrich) with gradient elution 200–1000 mM NaCl. Peak fractions were pooled, aliquoted, and stored at −80 °C.

In vitro phosphatase assay

U2OS-WIP1-KO cells treated with etoposide or exposed to UVC were washed with PBS and swollen in hypotonic lysis buffer (10 mM HEPES-KOH pH 7.9, 1 mM MgCl2, 2.5 mM KCl, 0.5 mM DTT, supplemented with EDTA-free protease and phosphatase inhibitors) for 5 min, centrifuged and dounce homogenized in the same buffer using tight pestle on ice. Nuclei were spun down at 500 ***g*** for 5 min at 4 °C and extracted in buffer C (20 mM HEPES pH 7.9, 1.5 mM $MgCl_2$, 0.2 mM EDTA, 25% glycerol, 0.5 mM DTT) supplemented with 600 mM KCl on ice for 15 min before centrifugation at max speed 15 min 4 °C. Supernatants were diluted with buffer C to final concentration 150 mM KCl, clarified by centrifugation at max speed 15 min 4 °C, and stored at −80 °C. For *in vitro* phosphatase assay, 100 μg of NE was incubated with 250 ng of purified His-WIP1 for 15 min at 37 °C. Reactions were stopped by addition of 4× sample buffer. Protein phosphorylations were determined using phospho-specific antibodies by western blotting. Alternatively, purified His-WIP1 (100 ng) was incubated with synthetic phosphopeptides (100 μM) and DMSO or Wip1 inhibitor for 60 min at 37 °C and released phosphate was measured using PiPer Phosphatase Assay Kit (Thermo Fisher Scientific).

Immunoprecipitation

HEK293 cells were transfected with GFP-tagged plasmids using linear polyethylene-imine MAX 40 kDa (Polysciences, Warrington, PA, USA). Cells were treated as indicated, washed with PBS, and harvested in lysis buffer (50 mM Tris pH 8.0, 120 mM NaCl, 1% Tween-20, 0.1% NP-40, 10% glycerol, 2 mM EDTA, 3 mM EGTA, 10 mM $MgCl_2$, complete protease and phosphatase inhibitors). After sonication, EtBr (50 μg·mL^{-1}) and benzonase (100 U·mL^{-1}) were added and cell extract was centrifuged at 20,000 ***g*** for 20 min at 4 °C. Supernatant was incubated with GFP-Trap beads (Chromotek, Planegg, Germany) for 1 h. After washing 4 × with lysis buffer, proteins were eluted with SDS/PAGE loading buffer and analyzed by western blotting. Alternatively, endogenous proteins were immunoprecipitated from U2OS cells using DBC1 or control antibodies immobilized on protein A/G UltraLink resin (Thermo Fisher Scientific).

Mass spectrometry

HEK293 cells stably transfected with EGFP, EGFP-DBC1-WT, and EGFP-DBC1-T524A were treated or not with etoposide (40 μM) for 2 h and immunoprecipitation using GFP Trap was performed as described above. Three independent experiments were performed for every condition. Beads were resuspended in 100 mM TEAB containing 2% SDC. Cysteins were reduced with 5 mM TCEP (60 °C for 60 min) and blocked with 10 mM MMTS (10 min at room temperature). Samples were cleaved on beads with 1 μg of trypsin at 37 °C overnight. After digestion, samples were centrifuged and supernatants were collected and acidified

with 1% TFA and SDC was removed by extraction to ethylacetate [61]. Peptides were desalted using in-house made stage tips packed with Empore C18 SPE disks (CDS Analytical, Oxford, PA, USA). Nano-reversed phase column (EASY-Spray column, 50 cm × 75 μm ID, PepMap C18, 2 μm particles, 100 Å pore size) was used for LC/MS analysis. Eluting peptide cations were converted to gas-phase ions by electrospray ionization and analyzed on a Thermo Orbitrap Fusion (Q-OT-qIT; Thermo Scientific). All data were analyzed and quantified with the MAXQUANT software (version 1.6.2.1) [62].

Proximity ligation assay

Cells were treated with mock, WIP1 inhibitor (1 μM), etoposide (40 μM) or combination of both for 2 h, fixed with PFA, and permeabilized with 0.2% Triton X-100. PLA was performed using indicated antibodies and Duolink red detection reagent (Sigma-Aldrich) according to the manufacturer's protocol. Images were acquired by Olympus ScanR station equipped with 40×/1.3 UPLFN objective (Olympus, Tokyo, Japan). PLA signal was quantified as a number of spots per nucleus. More than 900 cells were quantified per condition, and statistical difference was evaluated using Mann–Whitney test.

Acknowledgements

Authors are thankful to Karel Harant and Pavel Talacko (Faculty of science, Charles University, Prague) for performing MS analysis. This project was supported by Czech Science Foundation (19-15962S). Production of recombinant proteins was supported by Ministry of Education Youth and Sports of the Czech Republic (CZ-OPENSCREEN program LO1220 and LM2015063), microscopy imaging was performed at Light Microscopy Core Facility (IMG ASCR, Prague, Czech Republic) supported by MEYS (Czech-Bio-Imaging, CZ.02.1.01/0.0/0.0/18_046/0016045). Radka Storchova was partly supported by Grant Agency of the Charles University (1394218).

Conflict of interest

Authors declare no conflict of interest.

Author contributions

RS, KB, and MP perfomed investigation; KB, RHM, and LM conceptualized the data; LM wrote original draft; RS, KB, LM, MP, RHM, and LM involved in writing-review and editing; LM contributed funding acquisition.

Peer Review

The peer review history for this article is available at https://publons.com/publon/10.1111/febs.15965.

References

1 Jackson SP & Bartek J (2009) The DNA-damage response in human biology and disease. *Nature* **461**, 1071–1078.
2 Bartek J & Lukas J (2003) Chk1 and Chk2 kinases in checkpoint control and cancer. *Cancer Cell* **3**, 421–429.
3 Blackford AN & Jackson SP (2017) ATM, ATR, and DNA-PK: the trinity at the heart of the DNA damage response. *Mol Cell* **66**, 801–817.
4 Matsuoka S, Ballif BA, Smogorzewska A, McDonald ER III, Hurov KE, Luo J, Bakalarski CE, Zhao Z, Solimini N, Lerenthal Y *et al.* (2007) ATM and ATR substrate analysis reveals extensive protein networks responsive to DNA damage. *Science* **316**, 1160–1166.
5 Bensimon A, Schmidt A, Ziv Y, Elkon R, Wang SY, Chen DJ, Aebersold R & Shiloh Y (2010) ATM-dependent and -independent dynamics of the nuclear phosphoproteome after DNA damage. *Sci Signal* **3**, rs3.
6 Choi BK, Fujiwara K, Dayaram T, Darlington Y, Dickerson J, Goodell MA & Donehower LA (2020) WIP1 dephosphorylation of p27(Kip1) Serine 140 destabilizes p27(Kip1) and reverses anti-proliferative effects of ATM phosphorylation. *Cell Cycle* **19**, 479–491.
7 el-Deiry WS, Tokino T, Velculescu VE, Levy DB, Parsons R, Trent JM, Lin D, Mercer WE, Kinzler KW & Vogelstein B (1993) WAF1, a potential mediator of p53 tumor suppression. *Cell* **75**, 817–825.
8 Reinhardt HC, Aslanian AS, Lees JA & Yaffe MB (2007) p53-deficient cells rely on ATM- and ATR-mediated checkpoint signaling through the p38MAPK/MK2 pathway for survival after DNA damage. *Cancer Cell* **11**, 175–189.
9 Manke IA, Nguyen A, Lim D, Stewart MQ, Elia AE & Yaffe MB (2005) MAPKAP kinase-2 is a cell cycle checkpoint kinase that regulates the G2/M transition and S phase progression in response to UV irradiation. *Mol Cell* **17**, 37–48.
10 Bulavin D, Higashimoto Y, Popoff I, Gaarde W, Basrur V & Potapova O (2001) Initiation of a G2/M checkpoint after ultraviolet radiation requires p38 kinase. *Nature* **411**, 102–107.
11 Shaltiel IA, Aprelia M, Saurin AT, Chowdhury D, Kops GJPL, Voest EE & Medema RH (2014) Distinct phosphatases antagonize the p53 response in different phases of the cell cycle. *Proc Natl Acad Sci USA* **111**, 7313–7318.
12 Fiscella M, Zhang H, Fan S, Sakaguchi K, Shen S, Mercer WE, Vande Woude GF, O'Connor PM &

Appella E (1997) Wip1, a novel human protein phosphatase that is induced in response to ionizing radiation in a p53-dependent manner. *Proc Natl Acad Sci USA* **94**, 6048–6053.
13 Shreeram S, Demidov ON, Hee WK, Yamaguchi H, Onishi N, Kek C, Timofeev ON, Dudgeon C, Fornace AJ, Anderson CW *et al.* (2006) Wip1 phosphatase modulates ATM-dependent signaling pathways. *Mol Cell* **23**, 757–764.
14 Macurek L, Lindqvist A, Voets O, Kool J, Vos H & Medema R (2010) Wip1 phosphatase is associated with chromatin and dephosphorylates gammaH2AX to promote checkpoint inhibition. *Oncogene* **29**, 2281–2291.
15 Burdova K, Storchova R, Palek M & Macurek L (2019) WIP1 promotes homologous recombination and modulates sensitivity to PARP inhibitors. *Cells* **8**, 1258.
16 Jaiswal H, Benada J, Müllers E, Akopyan K, Burdova K, Koolmeister T, Helleday T, Medema RH, Macurek L & Lindqvist A (2017) ATM/Wip1 activities at chromatin control Plk1 re-activation to determine G2 checkpoint duration. *EMBO J* **36**, 2161–2176.
17 Fujimoto H, Onishi N, Kato N, Takekawa M, Xu X & Kosugi A (2006) Regulation of the antioncogenic Chk2 kinase by the oncogenic Wip1 phosphatase. *Cell Death Differ* **13**, 1170–1180.
18 Lu X, Nannenga B & Donehower L (2005) PPM1D dephosphorylates Chk1 and p53 and abrogates cell cycle checkpoints. *Genes Dev* **19**, 1162–1174.
19 Lindqvist A, de Bruijn M, Macurek L, Bras A, Mensinga A & Bruinsma W (2009) Wip1 confers G2 checkpoint recovery competence by counteracting p53-dependent transcriptional repression. *EMBO J* **28**, 3196–3206.
20 Krenning L, Feringa FM, Shaltiel IA, van den Berg J & Medema RH (2014) Transient activation of p53 in G2 phase is sufficient to induce senescence. *Mol Cell* **55**, 59–72.
21 Pechackova S, Burdova K, Benada J, Kleiblova P, Jenikova G & Macurek L (2016) Inhibition of WIP1 phosphatase sensitizes breast cancer cells to genotoxic stress and to MDM2 antagonist nutlin-3. *Oncotarget* **7**, 14458–14475.
22 Emelyanov A & Bulavin DV (2015) Wip1 phosphatase in breast cancer. *Oncogene* **34**, 4429–4438.
23 Bulavin DV, Demidov ON, Saito SI, Kauraniemi P, Phillips C, Amundson SA, Ambrosino C, Sauter G, Nebreda AR, Anderson CW *et al.*(2002) Amplification of PPM1D in human tumors abrogates p53 tumor-suppressor activity. *Nat Genet* **31**, 210–215.
24 Zhang L, Chen LH, Wan H, Yang R, Wang Z, Feng J, Yang S, Jones S, Wang S, Zhou W *et al.* (2014) Exome sequencing identifies somatic gain-of-function PPM1D mutations in brainstem gliomas. *Nat Genet* **46**, 726–730.
25 Kleiblova P, Shaltiel IA, Benada J, Sevčík J, Pecháčková S, Pohlreich P, Voest EE, Dundr P, Bartek J, Kleibl Z *et al.* (2013) Gain-of-function mutations of PPM1D/Wip1 impair the p53-dependent G1 checkpoint. *J Cell Biol* **201**, 511–521.
26 Richter M, Dayaram T, Gilmartin AG, Ganji G, Pemmasani SK, Van Der Key H, Shohet JM, Donehower LA & Kumar R (2015) WIP1 phosphatase as a potential therapeutic target in neuroblastoma. *PLoS One* **10**, e0115635.
27 Gilmartin AG, Faitg TH, Richter M, Groy A, Seefeld MA, Darcy MG, Peng X, Federowicz K, Yang J, Zhang S-Y *et al.* (2014) Allosteric Wip1 phosphatase inhibition through flap-subdomain interaction. *Nat Chem Biol* **10**, 181–187.
28 Yamaguchi H, Minopoli G, Demidov ON, Chatterjee DK, Anderson CW, Durell SR & Appella E (2005) Substrate specificity of the human protein phosphatase 2Cdelta, Wip1. *Biochemistry* **44**, 5285–5294.
29 Yamaguchi H, Durell SR, Chatterjee DK, Anderson CW & Appella E (2007) The Wip1 phosphatase PPM1D dephosphorylates SQ/TQ motifs in checkpoint substrates phosphorylated by PI3K-like kinases. *Biochemistry* **46**, 12594–12603.
30 Kim S, Lim D, Canman C & Kastan M (1999) Substrate specificities and identification of putative substrates of ATM kinase family members. *J Biol Chem* **274**, 37538–37543.
31 Kahn JD, Miller PG, Silver AJ, Sellar RS, Bhatt S, Gibson C, McConkey M, Adams D, Mar B, Mertins P *et al.* (2018) PPM1D truncating mutations confer resistance to chemotherapy and sensitivity to PPM1D inhibition in hematopoietic cells. *Blood* **132**, 1095.
32 Takekawa M, Adachi M, Nakahata A, Nakayama I, Itoh F, Tsukuda H, Taya Y & Imai K (2000) p53-inducible wip1 phosphatase mediates a negative feedback regulation of p38 MAPK-p53 signaling in response to UV radiation. *EMBO J* **19**, 6517–6526.
33 Brazina J, Svadlenka J, Macurek L, Andera L, Hodny Z, Bartek J & Hanzlikova H (2015) DNA damage-induced regulatory interplay between DAXX, p53, ATM kinase and Wip1 phosphatase. *Cell Cycle* **14**, 375–387.
34 Moon S, Lin L, Zhang X, Nguyen T, Darlington Y, Waldman A, Lu X & Donehower LA (2010) Wildtype p53-induced phosphatase 1 dephosphorylates histone variant gamma-H2AX and suppresses DNA double strand break repair. *J Biol Chem* **285**, 12935–12947.
35 Reinhardt HC, Hasskamp P, Schmedding I, Morandell S, van Vugt MA, Wang X, Linding R, Ong SE, Weaver D, Carr SA *et al.* (2010) DNA damage activates a spatially distinct late cytoplasmic cell-cycle checkpoint network controlled by MK2-mediated RNA stabilization. *Mol Cell* **40**, 34–49.
36 Söderberg O, Gullberg M, Jarvius M, Ridderstråle K, Leuchowius KJ, Jarvius J, Wester K, Hydbring P, Bahram F, Larsson LG *et al.* (2006) Direct observation of individual endogenous protein complexes in situ by proximity ligation. *Nat Methods* **3**, 995–1000.

37 Zannini L, Buscemi G, Kim JE, Fontanella E & Delia D (2012) DBC1 phosphorylation by ATM/ATR inhibits SIRT1 deacetylase in response to DNA damage. *J Mol Cell Biol* **4**, 294–303.
38 Zhao W, Kruse JP, Tang Y, Jung SY, Qin J & Gu W (2008) Negative regulation of the deacetylase SIRT1 by DBC1. *Nature* **451**, 587–590.
39 Kim JE, Chen J & Lou Z (2008) DBC1 is a negative regulator of SIRT1. *Nature* **451**, 583–586.
40 Deng K, Liu L, Tan X, Zhang Z, Li J, Ou Y, Wang X, Yang S, Xiang R & Sun P (2020) WIP1 promotes cancer stem cell properties by inhibiting p38 MAPK in NSCLC. *Signal Transduct Target Ther* **5**, 36.
41 Bulavin DV, Phillips C, Nannenga B, Timofeev O, Donehower LA, Anderson CW, Appella E & Fornace AJ (2004) Inactivation of the Wip1 phosphatase inhibits mammary tumorigenesis through p38 MAPK-mediated activation of the p16Ink4a-p19Arf pathway. *Nat Genet* **36**, 343–350.
42 Demidov ON, Kek C, Shreeram S, Timofeev O, Fornace AJ, Appella E & Bulavin DV (2006) The role of the MKK6//p38 MAPK pathway in Wip1-dependent regulation of ErbB2-driven mammary gland tumorigenesis. *Oncogene* **26**, 2502–2506.
43 Shreeram S, Demidov O, Hee W, Yamaguchi H, Onishi N & Kek C (2006) Wip1 phosphatase modulates ATM-dependent signaling pathways. *Mol Cell* **23**, 757–764.
44 Lu X, Ma O, Nguyen T-A, Jones SN, Oren M & Donehower LA (2007) The Wip1 phosphatase acts as a gatekeeper in the p53-Mdm2 autoregulatory loop. *Cancer Cell* **12**, 342–354.
45 Tang Y, Zhao W, Chen Y, Zhao Y & Gu W (2008) Acetylation is indispensable for p53 activation. *Cell* **133**, 612–626.
46 Luo J, Li M, Tang Y, Laszkowska M, Roeder RG & Gu W (2004) Acetylation of p53 augments its site-specific DNA binding both *in vitro* and *in vivo*. *Proc Natl Acad Sci USA* **101**, 2259–2264.
47 Barlev NA, Liu L, Chehab NH, Mansfield K, Harris KG, Halazonetis TD & Berger SL (2001) Acetylation of p53 activates transcription through recruitment of coactivators/histone acetyltransferases. *Mol Cell* **8**, 1243–1254.
48 Gu W & Roeder RG (1997) Activation of p53 sequence-specific DNA binding by acetylation of the p53 C-terminal domain. *Cell* **90**, 595–606.
49 Jenkins LM, Yamaguchi H, Hayashi R, Cherry S, Tropea JE, Miller M, Wlodawer A, Appella E & Mazur SJ (2009) Two distinct motifs within the p53 transactivation domain bind to the Taz2 domain of p300 and are differentially affected by phosphorylation. *Biochemistry* **48**, 1244–1255.
50 Feng H, Jenkins LM, Durell SR, Hayashi R, Mazur SJ, Cherry S, Tropea JE, Miller M, Wlodawer A, Appella E *et al.* (2009) Structural basis for p300 Taz2-p53 TAD1 binding and modulation by phosphorylation. *Structure (London, England: 1993)* **17**, 202–210.
51 Avantaggiati ML, Ogryzko V, Gardner K, Giordano A, Levine AS & Kelly K (1997) Recruitment of p300/CBP in p53-dependent signal pathways. *Cell* **89**, 1175–1184.
52 Sakaguchi K, Herrera JE, Saito S, Miki T, Bustin M, Vassilev A, Anderson CW & Appella E (1998) DNA damage activates p53 through a phosphorylation-acetylation cascade. *Genes Dev* **12**, 2831–2841.
53 Teufel DP, Bycroft M & Fersht AR (2009) Regulation by phosphorylation of the relative affinities of the N-terminal transactivation domains of p53 for p300 domains and Mdm2. *Oncogene* **28**, 2112–2118.
54 Li Q, Hao Q, Cao W, Li J, Wu K, Elshimali Y, Zhu D, Chen Q-H, Chen G, Pollack JR *et al.* (2019) PP2Cδ inhibits p300-mediated p53 acetylation via ATM/BRCA1 pathway to impede DNA damage response in breast cancer. *Sci Adv* **5**, eaaw8417.
55 Li J, Bonkowski MS, Moniot S, Zhang D, Hubbard BP, Ling AJ, Rajman LA, Qin B, Lou Z, Gorbunova V *et al.* (2017) A conserved NAD(+) binding pocket that regulates protein-protein interactions during aging. *Science* **355**, 1312–1317.
56 Uematsu N, Weterings E, Yano K, Morotomi-Yano K, Jakob B, Taucher-Scholz G, Mari PO, van Gent DC, Chen BP & Chen DJ (2007) Autophosphorylation of DNA-PKCS regulates its dynamics at DNA double-strand breaks. *J Cell Biol* **177**, 219–229.
57 Crowe JL, Wang XS, Shao Z, Lee BJ, Estes VM & Zha S (2020) DNA-PKcs phosphorylation at the T2609 cluster alters the repair pathway choice during immunoglobulin class switch recombination. *Proc Natl Acad Sci USA* **117**, 22953–22961.
58 Shao Z, Flynn RA, Crowe JL, Zhu Y, Liang J, Jiang W, Aryan F, Aoude P, Bertozzi CR, Estes VM *et al.* (2020) DNA-PKcs has KU-dependent function in rRNA processing and haematopoiesis. *Nature* **579**, 291–296.
59 Jiang W, Estes VM, Wang XS, Shao Z, Lee BJ, Lin X, Crowe JL & Zha S (2019) Phosphorylation at S2053 in Murine (S2056 in Human). DNA-PKcs is dispensable for lymphocyte development and class switch recombination. *J Immunol* **203**, 178–187.
60 von Morgen P, Burdova K, Flower TG, O'Reilly NJ, Boulton SJ, Smerdon SJ, Macurek L & Horejsi Z (2017) MRE11 stability is regulated by CK2-dependent interaction with R2TP complex. *Oncogene* **36**, 4943–4950.
61 Masuda T, Tomita M & Ishihama Y (2008) Phase transfer surfactant-aided trypsin digestion for membrane proteome analysis. *J Proteome Res* **7**, 731–740.
62 Cox J, Hein MY, Luber CA, Paron I, Nagaraj N & Mann M (2014) Accurate proteome-wide label-free quantification by delayed normalization and maximal peptide ratio extraction, termed MaxLFQ. *Mol Cell Proteomics* **13**, 2513–2526.

cells

MDPI

Article

WIP1 Promotes Homologous Recombination and Modulates Sensitivity to PARP Inhibitors

Kamila Burdova, Radka Storchova, Matous Palek and Libor Macurek *

Cancer Cell Biology, Institute of Molecular Genetics of the Czech Academy of Sciences, CZ14220 Prague, Czech Republic; kamila.burdova@img.cas.cz (K.B.); radka.storchova@img.cas.cz (R.S.); matous.palek@img.cas.cz (M.P.)

* Correspondence: libor.macurek@img.cas.cz; Tel.: +420-241063210

Received: 6 September 2019; Accepted: 10 October 2019; Published: 15 October 2019

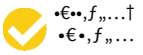

Abstract: Genotoxic stress triggers a combined action of DNA repair and cell cycle checkpoint pathways. Protein phosphatase 2C delta (referred to as WIP1) is involved in timely inactivation of DNA damage response by suppressing function of p53 and other targets at chromatin. Here we show that WIP1 promotes DNA repair through homologous recombination. Loss or inhibition of WIP1 delayed disappearance of the ionizing radiation-induced 53BP1 foci in S/G2 cells and promoted cell death. We identify breast cancer associated protein 1 (BRCA1) as interactor and substrate of WIP1 and demonstrate that WIP1 activity is needed for correct dynamics of BRCA1 recruitment to chromatin flanking the DNA lesion. In addition, WIP1 dephosphorylates 53BP1 at Threonine 543 that was previously implicated in mediating interaction with RIF1. Finally, we report that inhibition of WIP1 allowed accumulation of DNA damage in S/G2 cells and increased sensitivity of cancer cells to a poly-(ADP-ribose) polymerase inhibitor olaparib. We propose that inhibition of WIP1 may increase sensitivity of BRCA1-proficient cancer cells to olaparib.

Keywords: DNA repair; phosphatase; genotoxic stress; chemotherapy; PARP inhibitor; olaparib

1. Introduction

Cells are constantly challenged with DNA damage that comes both from endogenous and exogenous sources. The most deleterious type of DNA damage is double strand breaks (DSBs) that aect both strands of DNA and if not repaired correctly could lead to chromosomal rearrangements. DSBs are repaired by two major pathways—homologous recombination (HR) and non-homologous end joining (NHEJ). NHEJ operates throughout the cell cycle and results in ligation of two ends of DNA that are not extensively processed [1]. HR is restricted to S and G2 phases of the cell cycle as the homologous sequence required as template for repair usually comes from the sister chromatid and the whole process depends on activity of cyclin-dependent kinases [1,2]. Formation of DSBs triggers a highly organized network of protein phosphorylation mediated by PI3-like kinases ATM, ATR and DNA-PK; and ubiquitination mediated by ubiquitin ligases RNF8 and RNF168 [3,4]. DSBs are recognized by either DNA-PK to allow NHEJ or MRE11-RAD50-NBS1 (MRN) complex that starts the process of DNA end resection to allow HR. After initial incision, exonuclease activity of MRE11 removes the DNA towards DSB ends that is followed by long-range resection mediated by Exo1 and DNA2 [2,5]. Resection generates long stretches of single-stranded DNA (ssDNA) that are immediately bound by replication protein A (RPA) that protects it from nucleolytic cleavage [6]. ssDNA-RPA facilitates activation of ATR kinase that further supports repair by HR [7]. In the next step, RPA is exchanged for RAD51 in process mediated by PALB2-BRCA2 that is recruited to sites of damage by BRCA1 or in case of BRCA1 haploinsuciency by RNF168 [8,9]. RAD51 nucleofilament is stabilized by BRCA1-BARD1 complex and invades the sister chromatid to search for homology that is facilitated

by RAD54 [10]. Once homologous sequence is found, DNA is extended using sister chromatid as template. The second end of DNA is eventually captured forming a double holiday junction that is resolved or dissolved yielding either non-crossovers or crossovers.

Two major factors involved in repair pathway choice are TP53-binding protein 1 (53BP1) and Breast cancer type 1 susceptibility protein (BRCA1) [11,12]. BRCA1 association with DSBs is mediated by its interactors RAP80 and BARD1 that mediate binding of the complex to the ubiquitinated histone H2A and histone H4 non-methylated at lysine 20 (H4K20me0), respectively [13,14]. 53BP1 is recruited to DSBs by its BRCT domains that bind phosphorylated histone H2AX (H2AX), by UDR domain that recognizes histone H2A ubiquitinated at lysine 13/15 by RNF168, and by Tudor domains that recognize dimethylated lysine 20 at histone H4 [14–17]. After ATM-mediated phosphorylation of 53BP1 on multiple SQ/TQ sites (including Threonine 543), Rap1-interacting factor 1 homolog (RIF1) binds 53BP1 through its Heat repeats and restricts DNA end resection [18–20]. Binding of BRCA1 and 53BP1 is not exclusive as in S and G2 phases of the cell cycle BRCA1 can be present at the same DSB as 53BP1. 53BP1 is repositioned from the end of DSB by T543 dephosphorylation mediated by PP4C that is brought to the site by BRCA1 and disrupts interaction between 53BP1 and RIF1 [21]. In addition, BRCA1-BARD1 complex promotes 53BP1 repositioning by ubiquitination of the C-terminal lysines of histone H2A and recruitment of a chromatin remodeler SMARCAD1 [22].

Mutations in BRCA1 and other DNA repair genes are common cause of cancer but deficient HR can be also exploited as target for cancer therapy [23]. Inhibition of poly-(ADP-ribose) polymerase (PARP), a key enzyme in base excision repair, eciently kills cancer cells with defective HR and PARP inhibitors (including olaparib) are now used for treatment of BRCA1/2-deficient breast and ovary cancer [24]. Combinations of PARPi with other drugs are now being intensively investigated to prevent development of resistance to PARPi and to extend their use beyond the BRCA1/2 negative tumors [24–29].

WIP1 is a monomeric magnesium-dependent, chromatin-bound phosphatase encoded by PPM1D gene and its expression is increasing towards the G2 phase of the cell cycle [30–32]. WIP1 terminates the DNA damage response by dephosphorylation of H2AX, ATM pS1981 and KAP1 pS824 and promotes release from the cell cycle checkpoint by dephosphorylation of p53 pS15 [30,33–37]. PPM1D locus is amplified in about 10% of breast cancers, in medulloblastoma and ovary cancer [38–40]. Importantly, PPM1D amplifications occur mostly in tumors harboring wild-type p53 [38,41]. Activity of WIP1 can be specifically inhibited by a small-molecule compound GSK2830371 and WIP1 was proposed as perspective pharmacological target particularly in p53-proficient cancers [42–46].

Here we report a novel role of WIP1 in DSB repair through HR. We find that WIP1 stably interacts with BRCA1-BARD1 complex and inhibition of WIP1 delays recruitment of BRCA1 to DSBs. Consistent with WIP1 function in HR, inhibition of WIP1 leads to accumulation of DNA damage in S/G2 cells and sensitizes cancer cells to olaparib. Thus, inhibition of WIP1 may promote eciency of PARP inhibitors in tumors with normal BRCA1 function.

2. Results

2.1. WIP1 Promotes DSB Repair by Homologous Recombination

WIP1 phosphatase was shown to counteract ATM kinase activity at chromatin to terminate DNA damage response and to facilitate recovery form the G2 checkpoint [30,34,35]. In addition, overexpression of WIP1 aects DSB repair eciency through dephosphorylation of H2AX leading to disruption of DDR signaling [30,47]. To evaluate the role of WIP1 in more physiological condition we used dierent established cell based reporter assays together with a recently described specific WIP1 inhibitor GSK2830371 [42,44]. To this end we generated stable Trac light reporter cell lines in U2OS and RPE that allowed us to analyze the overall repair eciency as well as the ratio of repair eciency by homologous recombination (GFP+) and non-homologous end joining (RFP+) (Figure S1A) [48]. As expected, inhibition of DNA-PK increased the HR/NHEJ ratio reflecting its essential role in NHEJ

(Figure S1B). Conversely, inhibition of ATM decreased the HR/NHEJ ratio which is consistent with involvement of ATM in mediating DNA resection (Figure S1B) [49]. Interestingly, inhibition of WIP1 lowered DSB repair eciency by homologous recombination while NHEJ was not aected and thus decreased the HR/NHEJ ratio in two independent clones of both U2OS and RPE cells (Figure 1A–D). To further confirm this phenotype, we used established U2OS DR-GFP and E5J reporter cell lines and consistently we observed decreased HR eciency after inhibition of WIP1 (Figure S1C) [50].

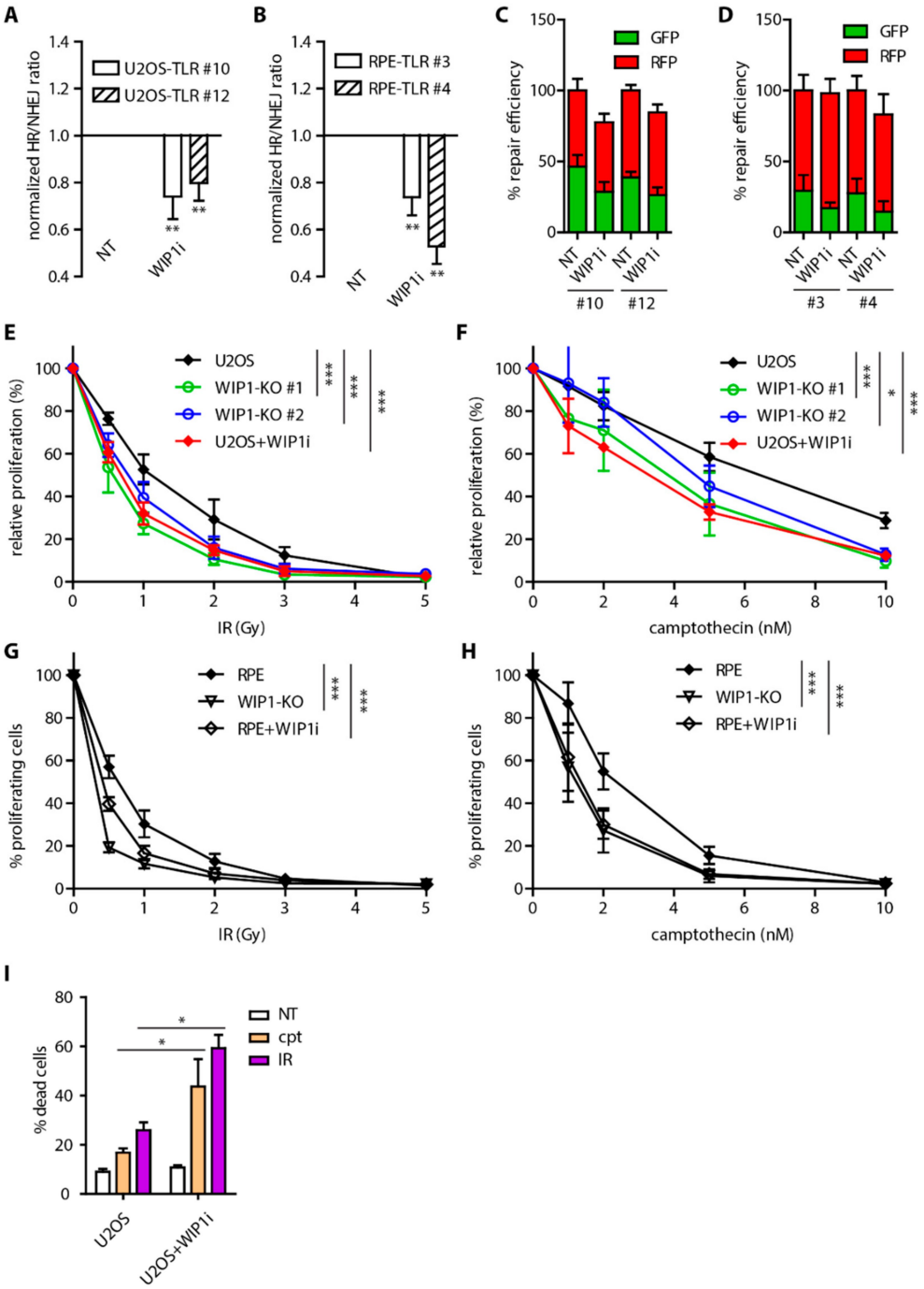

Figure 1. Inhibition of WIP1 impairs homologous recombination (HR). (**A**) Trac light reporter assay in U2OS cells. Two independent stable cell lines (clones #10 and #12) were transfected with ISceI together with BFP-donor vector with or without pretreatment with 1 M WIP1i. Eciency of repair was analyzed 3 days after transfection by FACS. Plotted is mean of normalized ratio of GFP^+/RFP^+ cells.

Bars indicate SD, n 3. Statistical significance evaluated by two-tailed t-test. (**B**) Trac light reporter assay in two independent clones of RPE cells (#3 and #4). Same as A. (**C**) Eciency of repair by H R (GFP^+) and NHEJ (RFP^+) in TLR assay in U2OS cells from A. (**D**) Eciency of repair by HR (GFP^+) and NHEJ (RFP^+) in TLR assay in RPE cells from B. (**E**) Cell survival after irradiation of parental U2OS and two independent U2OS-WIP1-KO cell lines treated or not with WIP1 inhibitor was evaluated after 7 days using resazurin viability assay. Plotted is mean and SD, n 3. Statistical significance evaluated by two-way ANOVA (* P < 0.05; *** P < 0.001). (**F**) Cell survival of parental U2OS and two independent U2OS-WIP1-KO cell lines treated with indicated doses of camptothecin with or without combined treatment with WIP1 inhibitor was evaluated after 7 days using resazurin viability assay. Plotted is mean and SD, n 3. Statistical significance evaluated by two-way ANOVA (* P < 0.05; *** P < 0.001). (**G**) Cell survival after irradiation of parental RPE and RPE-WIP1-KO cell lines assayed as in E. (**H**) Cell survival of parental RPE and RPE-WIP1-KO cell lines with treated with camptothecin and analyzed as in F. (**I**) Percentage of dead cells was evaluated by Hoechst 33258 staining and FACS analysis 7 days after treatment with camptothecin or after irradiation in U2OS cell line with or without combined treatment with WIP1i. Plotted is mean +/ SD. Statistical significance evaluated by two-tailed t-test.

Next, we employed CRISPR/Cas9 technology and generated WIP1 knockout U2OS and RPE cell lines (Figure S1D,E) and tested their sensitivity to gamma irradiation (IR). As reported previously, U2OS-WIP1 knockout cells were more sensitive to IR and their sensitivity was comparable to WIP1 inhibition (Figure 1E,G) [44]. Importantly, increased sensitivity was partially rescued by complementation of knockout cells with wild-type WIP1 but not catalytically inactive mutant D314A (Figure S1F,G). Treatment of cells by topoisomerase I inhibitor camptothecin was shown to induce DNA damage that is repaired by HR [51]. Both RPE and U2OS WIP1 knockout cell lines were found to be more sensitive to camptothecin treatment to similar extent as after WIP1 inhibition (Figure 1F,H). Decreased cell proliferation after inhibition of WIP1 was accompanied by increased cell death after IR or camptothecin treatment (Figure 1I). Consistent with potential role of WIP1 in HR, U2OS-WIP1-KO cells were more sensitive to DNA crosslinking agent mitomycin C (Figure S1H).

Next, we followed DSB repair kinetics in parental U2OS or U2OS-WIP1-KO cells by quantifying 53BP1 foci formation and disassembly after exposure to IR. Interestingly, knockout or inhibition of WIP1 lead to persistence of 53BP1 foci mainly in cells that were in S-phase (EdU+, Figure 2A, and Figure S2A) at time of irradiation and to lesser extent in cells irradiated in G1 or G2 phases of the cell cycle (EdU-, Figure 2B and Figure S2A). Persistence of 53BP1 foci was fully rescued in WIP1 knockout cells complemented with the wild-type WIP1 but not with D314A mutant (Figure 2C,D and Figure S2B). Moreover, persistence of 53BP1 foci in cells irradiated in S-phase was recapitulated in MCF7 cells treated with WIP1 inhibitor (Figure S3A–C).

DNA repair pathway choice is controlled by a balance between 53BP1 and BRCA1 at DNA double strand breaks that have opposing eects on DNA end resection [11,19]. To evaluate possible impact of WIP1 on these proteins, we employed the Trac light reporter assay and depleted 53BP1/RIF1 and/or BRCA1/BARD1 using siRNA in combination with WIP1 inhibition. As expected, depletion of BRCA1 or BARD1 decreased HR frequency, whereas depletion of 53BP1 or RIF1 increased the HR/NHEJ ratio [19,48,52,53]. Importantly, HR was not further decreased upon WIP1 inhibition in BRCA1 and BARD1-depleted cells (Figure 2E–G and Figure S1I). In contrast, increased HR observed in 53BP1 and RIF1-depleted cells was reduced back to normal after inhibition of WIP1 (Figure 2E–G). Combined these data suggest that WIP1 may promote HR through regulation of BRCA1/BARD1 complex.

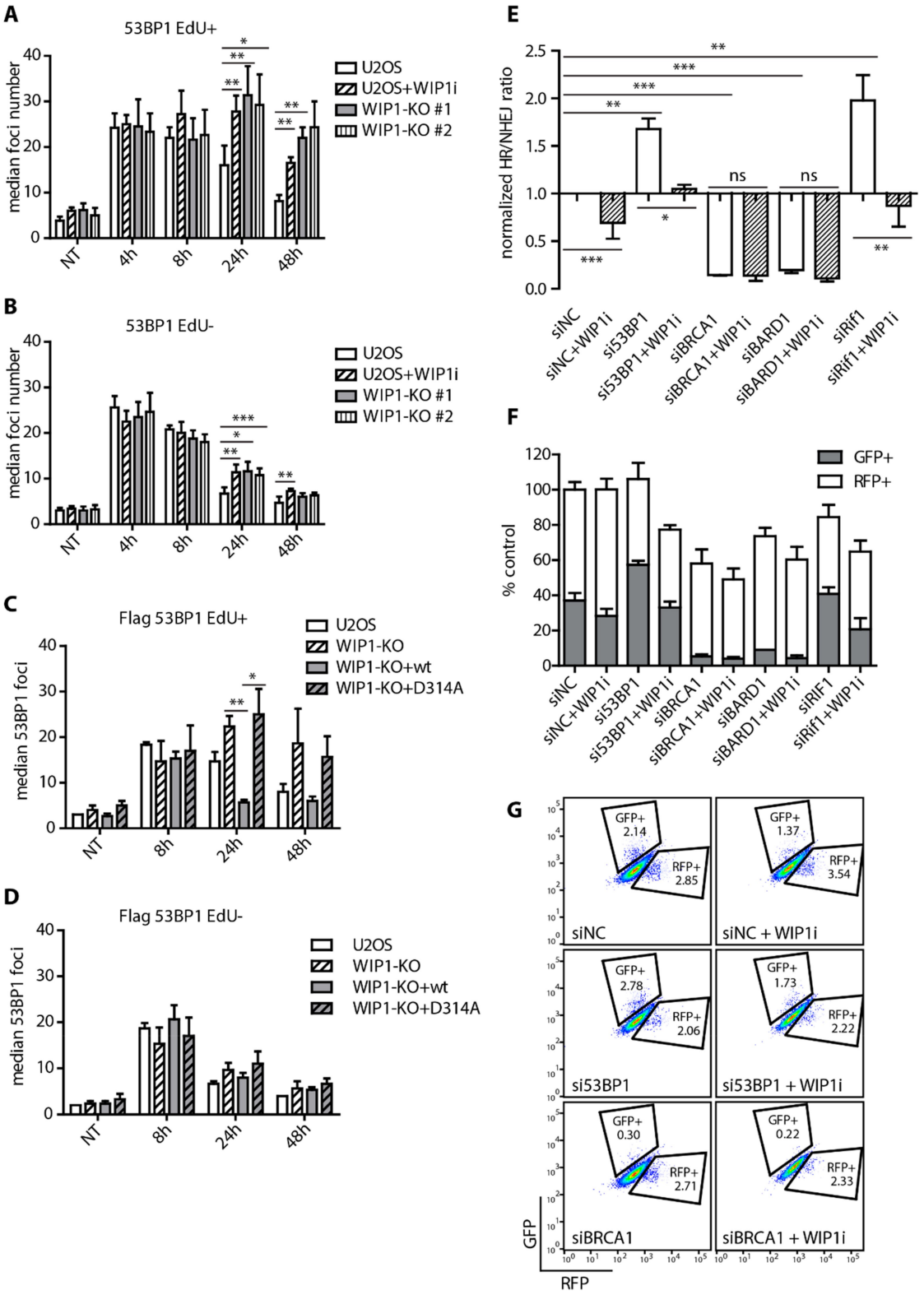

Figure 2. WIP1 plays role in DNA double-strand break repair in S-phase cells. (**A**) Quantification of 53BP1 foci in replicating (EdU+) cells after irradiation. U2OS parental cell lines with or without combined treatment with WIP1i and two independent WIP1 knockout cell lines were pulse-labeled with EdU for 30 min before irradiation. Cells were fixed after pre-extraction at indicated time-points and stained with 53BP1 antibody. Click chemistry was used to visualize EdU. Mean of median foci number +/- SD is plotted (n 3).

Statistical significance evaluated by two tailed t-test. (**B**) Quantification of 53BP1 foci in non-replicating (EdU-) cells after irradiation. As in A. (**C**) Quantification of 53BP1 foci in replicating (EdU+) cells after irradiation. U2OS parental, WIP1 knockout and cell lines complemented with wild-type or phosphatase-dead (D314A) mutant of WIP1 were irradiated and analyzed as in A. (**D**) Quantification of 53BP1 foci in non-replicating (EdU-) cells after irradiation. U2OS parental, WIP1 knockout and cell lines complemented with wild-type or phosphatase-dead (D314A) mutant of WIP1 were irradiated and analyzed as in A. (**E**) Trac light reporter assay in U2OS cells after transfection with indicated siRNA. Cells were transfected with ISceI together with BFP-donor vector with or without pretreatment with 1 M WIP1i 2 days after siRNA transfection. Eciency of repair was analyzed by FACS 3 days after ISceI and BFP-donor transfection. Plotted is mean +/ SD. Statistical significance evaluated by two-tailed t-test. (**F**) Eciency of repair by HR and NHEJ in Trac light reporter assay as in E. (**G**) Representative plots from Trac light reporter assay in E.

2.2. WIP1 Interacts with BRCA1 and Promotes its Recruitment to DSBs

To investigate the impact of WIP1 on BRCA1, we first performed a set of immunoprecipitation assays. We observed that WIP1 co-immunoprecipitated with BRCA1 and BARD1 in non-treated HEK293 and U2OS cells suggesting that WIP1 forms a stable interaction with BRCA1-BARD1 complex (Figure 3A–C). BRCA1 and BARD1 were previously reported to be extensively phosphorylated by ATM/ATR after DNA damage [54–58]. To determine BRCA1 phosphorylation after DNA damage we validated the phosphospecific BRCA1-pS1524 antibody for both immunofluorescence and Western blotting (Figure S4A–D). As expected, total intensity of BRCA1-pS1524 at chromatin was increased in response to IR in both S and G2 cells whereas RNAi-mediated depletion of BRCA1 reduced the signal to the basal level (Figure S4A,B). Next, we performed in vitro phosphatase assay and established that recombinant His-WIP1 was able to dephosphorylate BRCA1 S1524 with a comparable eciency to other substrates including ATM S1981, KAP1 S824 and p53 S15 (Figure S4E). In addition, purified WIP1 dephosphorylated BRCA1 S1524 in the presence of ATM inhibitor and also in fixed cells indicating that removal of the signal was not caused by modulation of ATM activity (Figure S4J,K). Interestingly, basal BRCA1 phosphorylation at S1524 was increased in WIP1 knockout cells and there was no further increase in BRCA1-pS1524 signal after IR compared to untreated condition (Figure 3D,E and Figure S5A). Similar eect was observed in MCF7 cells treated with WIP1 inhibitor confirming that WIP1 dephosphorylates BRCA1 not only after IR but also in unchallenged conditions (Figure 3F). Next, we assayed the recruitment of BRCA1 to the foci formed in S phase cells after exposure to IR. We observed delayed formation of BRCA1 foci in early time-points in WIP1 knockout cell line that could be rescued by complementation with the wild-type WIP1 but not with inactive D314A mutant (Figure 3G and Figure S5B). Combined these data indicate that WIP1 forms a stable complex with BRCA1-BARD1 and its activity is needed for timely recruitment of BRCA1 to DSBs.

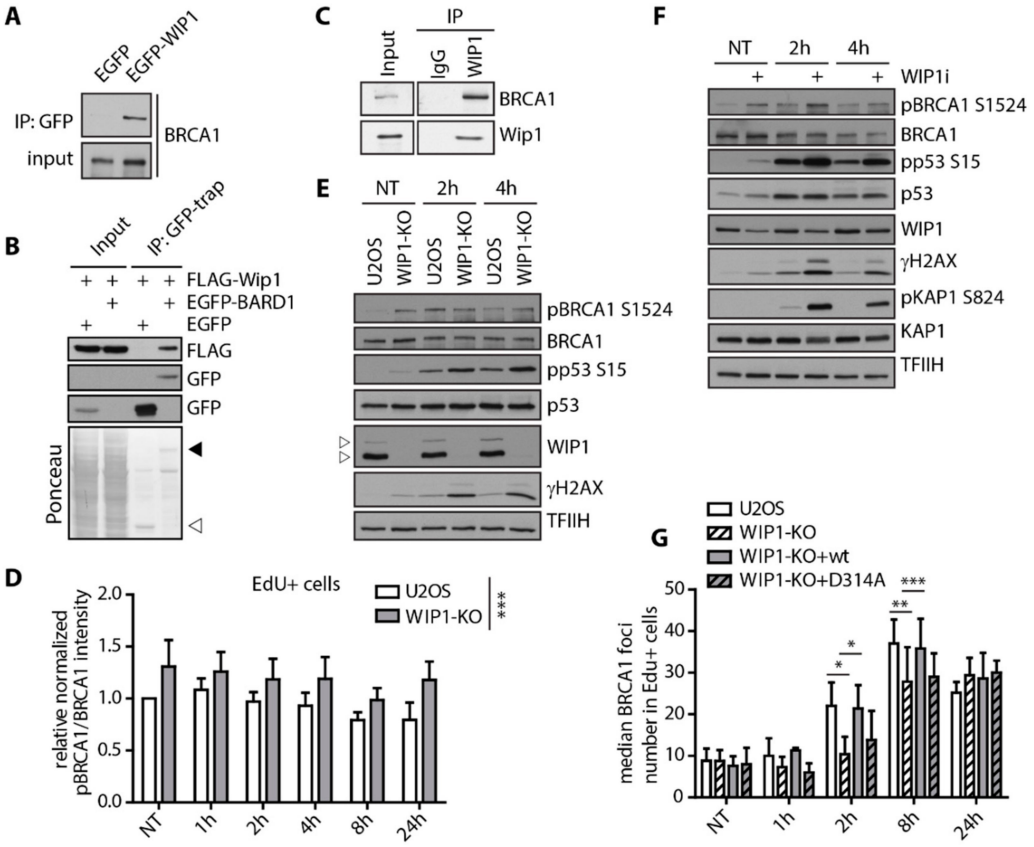

Figure 3. WIP1 interacts with BRCA1 and dephosphorylates S1524. (**A**) Co-immunoprecipitation of WIP1 and BRCA1. HEK293 cells were transfected with either empty GFP or GFP-WIP1, subjected to immunoprecipitation using GFP-Trap and analyzed by Western blotting with BRCA1 antibody. (**B**) Co-immunoprecipitation of WIP1 and BARD1. HEK293 cells were co-transfected with either empty GFP or GFP-BARD1 and Flag-WIP1, subjected to immunoprecipitation using GFP-Trap and analyzed by Western blotting with indicated antibodies. Ponceau staining with indicated positions of GFP (empty arrowhead) and GFP-BARD1 (full arrowhead) are shown. (**C**) Co-immunoprecipitation of endogenous WIP1 and BRCA1. U2OS cell lysates were incubated with 2 g of a control antibody (IgG) or anity-purified antibody against WIP1 for 2 h. Protein complexes were isolated by protein A/G resin and analyzed by immunoblotting. (**D**) Quantification of BRCA1 pS1524 signal intensity in replicating (EdU+) cells after irradiation. U2OS parental and WIP1 knockout cell lines were pulse-labeled with EdU for 30 min before irradiation. At indicated time-points, cells were pre-extracted, fixed and stained with pBRCA1 S1524 and BRCA1 antibodies. Click chemistry was used to visualize EdU. Median total intensity of BRCA1 pS1524 was normalized to total BRCA1 and is plotted +/ SD. Statistical significance evaluated by two-way ANOVA. (**E**) Western blot analysis of U2OS parental and U2OS-WIP1-KO cell lines after irradiation. Cells were irradiated and whole cell lysates were analyzed using Western blotting with indicated antibodies. Arrowheads indicate two isoforms of WIP1 present in U2OS. (**F**) Western blot analysis of MCF7 cells after irradiation with or without combined treatment with WIP1i. Cells were pretreated with WIP1 inhibitor for 30 min before irradiation and whole cell lysates were analyzed by Western blotting with indicated antibodies. (**G**) Quantification of BRCA1 foci in replicating (EdU+) cells after irradiation. Parental U2OS and U2OS-WIP1-KO cells and cell lines complemented with wild-type or phosphatase-dead (D314A) mutant of WIP1 were pulse-labeled with EdU for 30 min before irradiation. Cells were fixed after pre-extraction at indicated time-points and stained with BRCA1 antibody. Click chemistry was used to visualize EdU. Mean of median total intensity +/ SD is plotted. Statistical significance evaluated by two-tailed t-test.

2.3. WIP1 Dephosphorylates 53BP1 at T543 Residue Needed for Interaction with RIF1

Next, we aimed to test possible impact of WIP1 on 53BP1. Using immunoprecipitation, we found that WIP1 interacted with 53BP1 (Figure 4A). However, in contrast to the stable interaction with BRCA1, we observed increased interaction between WIP1 and 53BP1 after exposure to ionizing radiation (Figure 4B). BRCA1 was recently implicated in 53BP1 repositioning after IR by mediating 53BP1 dephosphorylation at threonine 543 and releasing its interaction with RIF1 [21]. Using siRNA of 53BP1 we validated the specificity of the pT543 53BP1 antibody for immunofluorescence and Western Blotting (Figure S4F–H). In addition, we found that WIP1 eciently dephosphorylated 53BP1 at T543 in vitro (Figure S4I–K). Whereas PP4C was originally reported to mediate pT543 dephosphorylation [21], we noted a significant increase of 53BP1 phosphorylation at T543 in WIP1 knockout cell line in response to IR by immunofluorescence and in cells treated with WIP1 inhibitor by immunoblotting (Figure 4C,D and Figure S6). Partial overlap in substrate specificity between PP4C and WIP1 has previously been reported for other substrates including H2AX and KAP1 [30,35,59,60] and similarly both phosphatases may collaborate to control the phosphorylation status of 53BP1. Indeed, at later time-points after IR we observed a more pronounced 53BP1 T543 phosphorylation after combining depletion of PP4C and knockout of WIP1 (Figure 4E).

As WIP1 interacts with and dephosphorylates BRCA1 and 53BP1, we aimed to evaluate its role in DNA resection that is controlled by the balance between BRCA1 and 53BP1 at DSBs. Surprisingly, we did not observe any dierence in formation of RPA2 foci in S-phase cells after inhibition of WIP1 (Figure 4F). Similarly, formation of RAD51 filament was largely unaected in early time-points after irradiation (Figure 4G) suggesting that WIP1 does not influence DNA end resection.

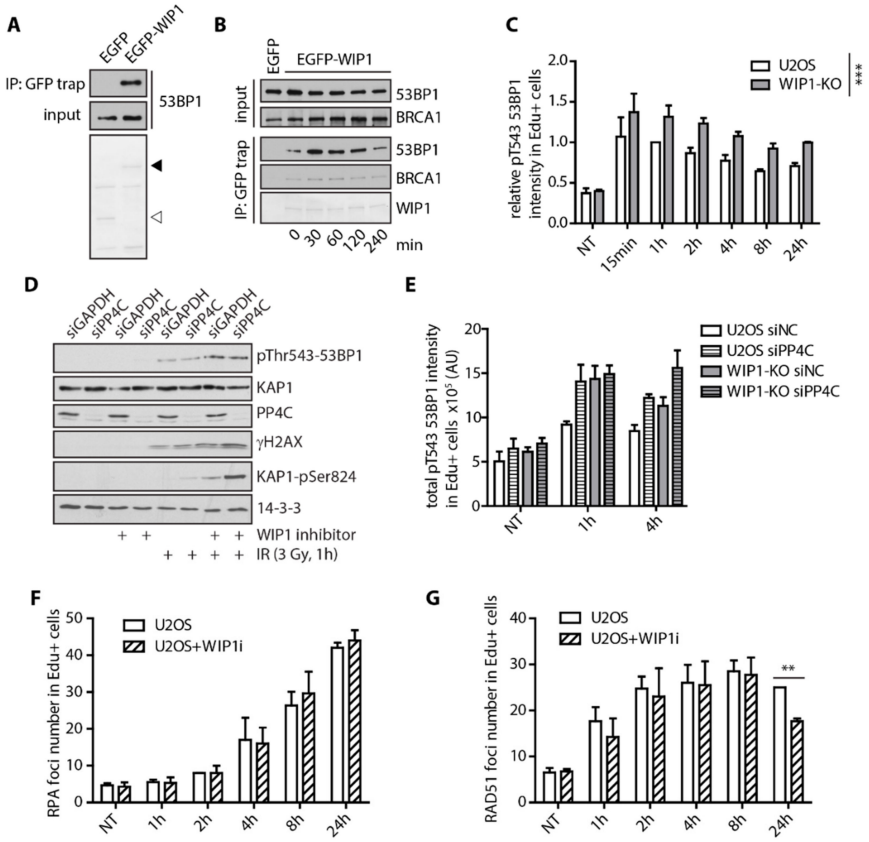

Figure 4. WIP1 delays recruitment of BRCA1 and dephosphorylation of 53BP1 at T543. (**A**) Co-immunoprecipitation of WIP1 and 53BP1. HEK293 cells were transfected with either empty GFP or GFP-WIP1, subjected to immunoprecipitation using GFP-Trap 24 h after transfection and by Western blotting with 53BP1 antibody. Ponceau staining with indicated positions of GFP (empty arrowhead) and GFP-WIP1 (full arrowhead) are shown.

(**B**) HEK293 cells transfected with EGFP or EGFP-WIP1 were exposed to 3 Gy of IR, collected at indicated times and proteins were immunoprecipitated by GFP Trap. (**C**) Quantification of 53BP1 pT543 signal intensity in replicating (EdU+) cells after irradiation. U2OS parental and WIP1 knockout cell lines were pulse-labeled with EdU for 30 min before irradiation. Cells were fixed after pre-extraction at indicated time-points after IR and stained with p53BP1 T543 antibody. Click chemistry was used to visualize EdU. Mean of median total intensity +/ SD is plotted. (**D**) Western blot analysis of whole cell lysates of U2OS cells transfected with GAPDH or PP4C siRNA in response to irradiation and/or WIP1 inhibitor. (**E**) Quantification of 53BP1 pT543 signal intensity in replicating (EdU+) cells after irradiation. U2OS parental and WIP1 knockout cell lines were transfected with control or PP4C siRNA 2 days before irradiation. Cells were processed and analyzed as in C. (**F**) Quantification of RPA2 foci in replicating (EdU+) cells after irradiation. U2OS parental cell lines with or without combined treatment with WIP1i were pulse-labeled with EdU for 30 minutes before irradiation. Cells were fixed after pre-extraction at indicated time-points and stained with RPA2 and RAD51 antibodies. Click chemistry was used to visualize EdU. Mean of median foci number +/ SD is plotted. (**G**) Quantification of RAD51 foci in replicating (EdU+) cells after irradiation as in F.

2.4. WIP1 Deficient Cells are Sensitive to PARP Inhibition in BRCA1 Dependent Manner

Mutations in BRCA1/2 that impair HR are commonly found in breast and ovarian cancers and increase sensitivity to PARP inhibitors. Since inhibition of WIP1 impaired HR, we tested if WIP1 deficiency would lead to sensitization of cells to PARP inhibitors. Indeed, we found that U2OS WIP1 knockout cell lines were more sensitive to olaparib (Figure 5A). Importantly, WIP1 inhibition decreased cell proliferation to the similar extent as the knockout cell lines (Figure 5A) and loss of WIP1 could be rescued by complementation with the wild-type WIP1 but not catalytically inactive D314A mutant (Figure 5B). Decreased cell proliferation after combined treatment with WIP1 inhibitor and olaparib was associated with increased cell death in U2OS cells (Figure 5C). Moreover, similar increase in sensitivity to olaparib and another PARPi A-966492 [61] was observed after inhibition of WIP1 in MCF7 and RPE cell lines (Figure 5D, Figure S7A). Combined depletion of PP4C and inhibition of WIP1 further increased sensitivity of cells to olaparib, suggesting that both phosphatases may target similar substrates involved in regulation of HR (Figure 5E).

WIP1 inhibition increased the number of 53BP1 foci in U2OS and MCF7 cells in response to PARP inhibition (Figure 5F, Figure S7B,C) and was accompanied by increased H2AX intensity suggesting that DNA lesions accumulate after the combined treatment (Figure S7D,E). The increase of 53BP1 foci number was observed mainly in S/G2 phases of the cell cycle which is consistent with accumulation of DNA damage due to failed HR (Figure S7F,G). Importantly, accumulation of 53BP1 foci in S/G2 cells was rescued by complementation with the wild-type WIP1 but not catalytically inactive D314A mutant (Figure 5G).

Next, we analyzed the response of U2OS and WIP1 knockout cells to olaparib treatment. As expected, treatment of U2OS cells with olaparib induced CHK1 and RPA2 phosphorylation after 24 h and was followed by a slight increase of H2AX and p21 levels after 2–3 days (Figure 5H). In contrast, treatment of U2OS WIP1 knockout cells with olaparib lead to additional increase of H2AX and RPA2 phosphorylation accompanied by a strong induction of p21 protein levels which is consistent with an increased load of DNA damage leading to a profound activation of the cell cycle checkpoint (Figure 5H). Indeed, we found that cells treated with a combination of olaparib and WIP1 inhibitor accumulated in the G2 (Figure S7F). Cells that entered mitosis in the presence of olaparib and WIP1 inhibitor showed increased frequency of abnormal anaphases likely reflecting a presence of unrepaired DNA (data not shown). To test if the sensitivity of U2OS WIP1 knockout cells to PARP inhibitors is due to the increased activation of the cell cycle checkpoint mediated by p21, we generated p21 knockout cell line (Figure S7H). Interestingly, the eect of WIP1 inhibition was found to be p21 independent in cell survival assays (Figure S7I). Moreover, inhibition of WIP1 further increased the number of 53BP1 foci induced by olaparib in p21 deficient U2OS cells (Figure S7J). We conclude that the increased

sensitivity of cells observed after combined treatment with WIP1 and PARP inhibitors is not caused by a stronger activation of the cell cycle checkpoint caused by inhibition of WIP1. To test whether the increased load of DNA damage after combined inhibition of PARP and WIP1 was BRCA1 dependent, we depleted MCF7 cells of BRCA1 using siRNA and analyzed number of 53BP1 foci in S/G2 phases of cell cycle. Indeed, we found that depletion of BRCA1 is epistatic with inhibition of WIP1 after olaparib treatment (Figure 5I).

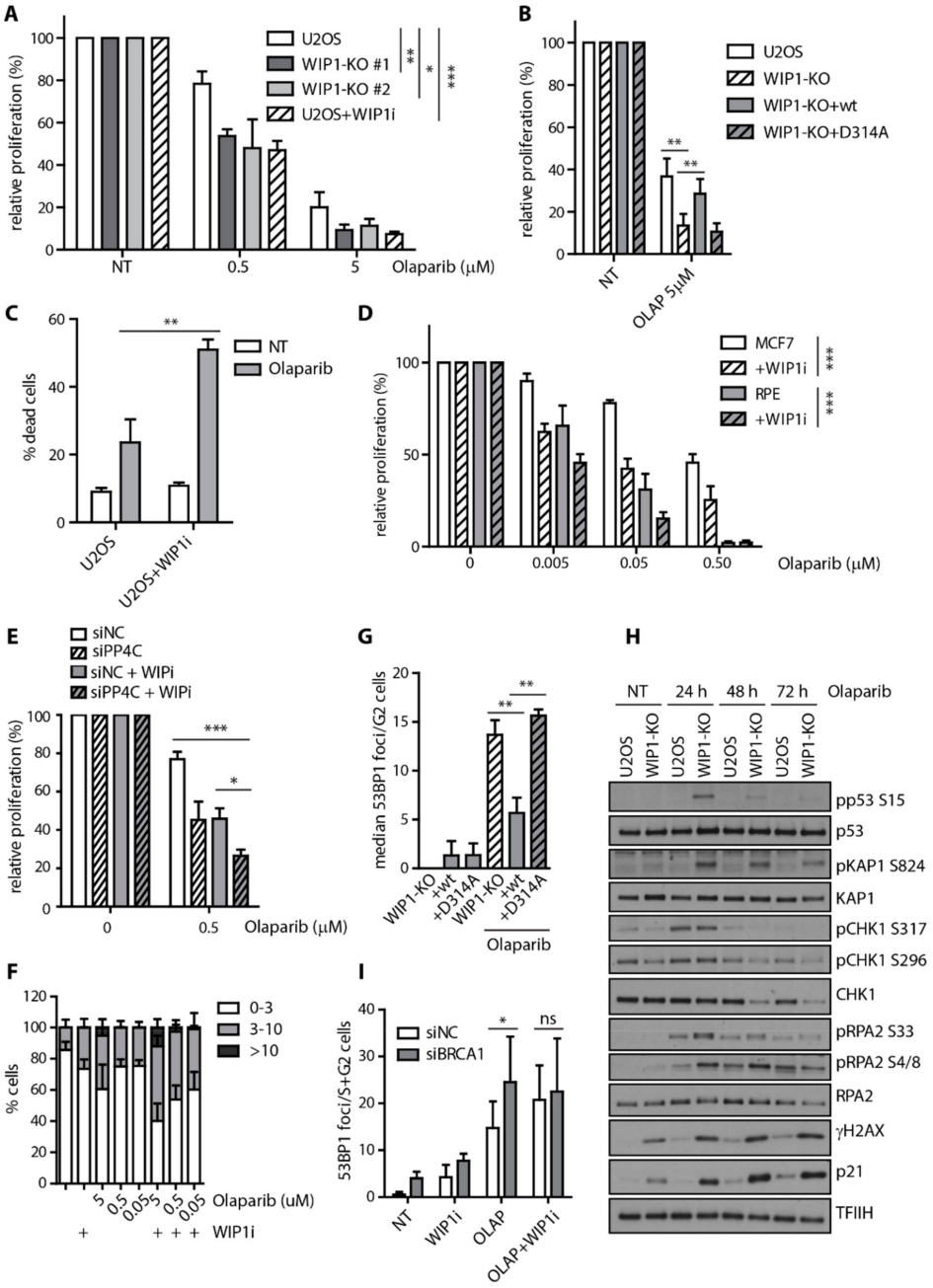

Figure 5. WIP1 deficient cells are more sensitive to PARP inhibition. (**A**) Cell survival of parental U2OS, two independent U2OS-WIP1-KO cell lines with or without combined treatment with WIP1i was evaluated 7 days after treatment with indicated doses of olaparib using resazurin viability assay. Plotted is mean +/ SD, n 3. Statistical significance evaluated by two-way ANOVA. (**B**) Cell survival of parental U2OS, U2OS-WIP1-KO cells and cell lines complemented with wild-type or phosphatase-dead (D314A) mutant of WIP1 in response to 5 M olaparib as in A. Statistical significance evaluated by two-tailed t-test (n 3).

(**C**) Percentage of dead cells was evaluated by Hoechst 33258 staining and FACS analysis 7 days after treatment with 5 M olaparib in U2OS cell line with or without combined treatment with WIP1i. Plotted is mean +/ SD. (**D**) Cell survival of RPE and MCF7 cell lines with or without combined treatment with WIP1i was evaluated 7 days after treatment with indicated doses of olaparib using resazurin viability assay. Plotted is mean +/ SD. N 3. Statistical significance evaluated by two-way ANOVA. (**E**) Cells were transfected with control siRNA (siNC) or siRNA to PP4C (siPP4C). Cell survival was evaluated after 7 days of treatment with olaparib and DMSO or WIP inhibitor. Statistical significance evaluated by two-tailed t-test (n = 3). (**F**) Quantification of 53BP1 foci number 3 days after treatment with olaparib. U2OS cells were treated with indicated doses of olaparib together with or without WIP1i for 3 days, fixed, stained with 53BP1 antibody and percentage of cells having 0–3, 3–10 and >10 foci were quantified. Mean +/ SD is plotted, n 3. (**G**) Quantification of 53BP1 foci after treatment with olaparib. U2OS-WIP1-KO cells and cell lines complemented with wild-type or phosphatase-dead (D314A) mutant of WIP1 were treated with WIP1i and olaparib for 3 days, fixed after pre-extraction and stained with 53BP1 antibody. Number of 53BP1 foci in S/G2 cells was evaluated using DAPI content of >2 n to gate S-G2 cells. Mean of median foci number +/ SD is plotted, n 3. Statistical significance evaluated by two-tailed t-test. (**H**) Response of U2OS and U2OS-WIP1-KO cell lines to treatment with 5 M olaparib for 24–72h was analyzed by Western blotting using indicated antibodies. **I**) Quantification of 53BP1 foci 3 days after treatment with olaparib. MCF7 cells were transfected with indicated siRNAs and treated after 2 days with WIP1i and olaparib alone or combined for further 3 days. Cells were fixed after pre-extraction and stained with 53BP1 antibody. Number of 53BP1 foci in S/G2 cells was evaluated using DAPI content of >2 n to gate S-G2 cells. Mean of median foci number +/ SD is plotted. Statistical significance evaluated by two-tailed t-test.

3. Discussion

WIP1 phosphatase prevents induction of senescence in cells exposed to genotoxic stress and promotes recovery from the G2 checkpoint through targeting the p53 pathway and a nuclear co-repressor KAP1 [35,36,62]. In addition to this established role in checkpoint silencing, WIP1 was also reported to impact on the nucleotide and base excision repair pathways by targeting XPA and UNG2 at chromatin [63,64]. Here we identified a novel role of WIP1 in promoting repair of DSBs through HR in S/G2 cells. Using two distinct reporter assays we showed that HR (but not NHEJ) eciency was decreased upon inhibition of WIP1. This was accompanied by a delayed clearance of the 53BP1 foci indicating the persistent DNA damage in S/G2 cells lacking WIP1. We found that WIP1 interacted with and dephosphorylated BRCA1 whereas loss of WIP1 delayed recruitment of BRCA1 to the DSBs. Loss of WIP1 delayed dephosphorylation of 53BP1 at a residue previously reported to mediate interaction with RIF1 and promote chromatin remodeling. Although we observed a higher impact on T543 53BP1 phosphorylation by inhibiting WIP1 than by depletion of PP4C that was previously reported to target 53BP1, we failed to detect any significant dierence in the DNA resection upon inhibition of WIP1. It is plausible that WIP1 aects 53BP1 repositioning only in a small but physiologically meaningful fraction of DNA lesions depending on the context of the chromatin. Alternatively, WIP1 may fine-tune HR through additional substrates involved in the late steps of HR. One of the candidates is the BRCA1-BARD1 complex that is phosphorylated at multiple sites by ATM/ATR, stably interacts with WIP1 and was recently shown to be important for invasion step of HR [10]. Accumulation of 53BP1 foci in G2 cells caused by a combined treatment with olaparib and WIP1 inhibitor was independent on the ability of cells to activate the cell cycle checkpoint. However, we cannot exclude that WIP1 modulates HR also through inhibition of p53 that was previously shown to directly interact with RAD51 and RAD54 and to suppress RAD51 expression [65–67]. The precise molecular mechanism of WIP1 function in HR will need to be addressed by future research.

PARP inhibitors are currently approved for treatment of BRCA1/2-deficient tumors and new drug combinations are under investigation. Consistent with the WIP1 role in HR, we observed that loss of WIP1 promoted sensitivity of cancer cells to PARP inhibitors. Combined treatment with olaparib and WIP1 inhibitor increased the DNA damage load in G2 cells and significantly increased

cell death. In contrast to other phosphatases, WIP1 activity can be specifically suppressed by a specific inhibitor GSK2830371 and WIP1 inhibition is well tolerated in normal cells. Based on the newly identified role of WIP1 in HR, we propose WIP1 phosphatase as potential pharmacological target in BRCA1-proficient tumors (Figure 6). Inhibition of WIP1 was previously reported to be ecient mainly in p53-proficient cancer types including neuroblastoma, breast adenocarcinoma and melanoma [44,68–70]. We hypothesize that inhibition of HR and stimulation of the p53 response could synergize to eradicate the cancer cells treated with WIP1 inhibitors.

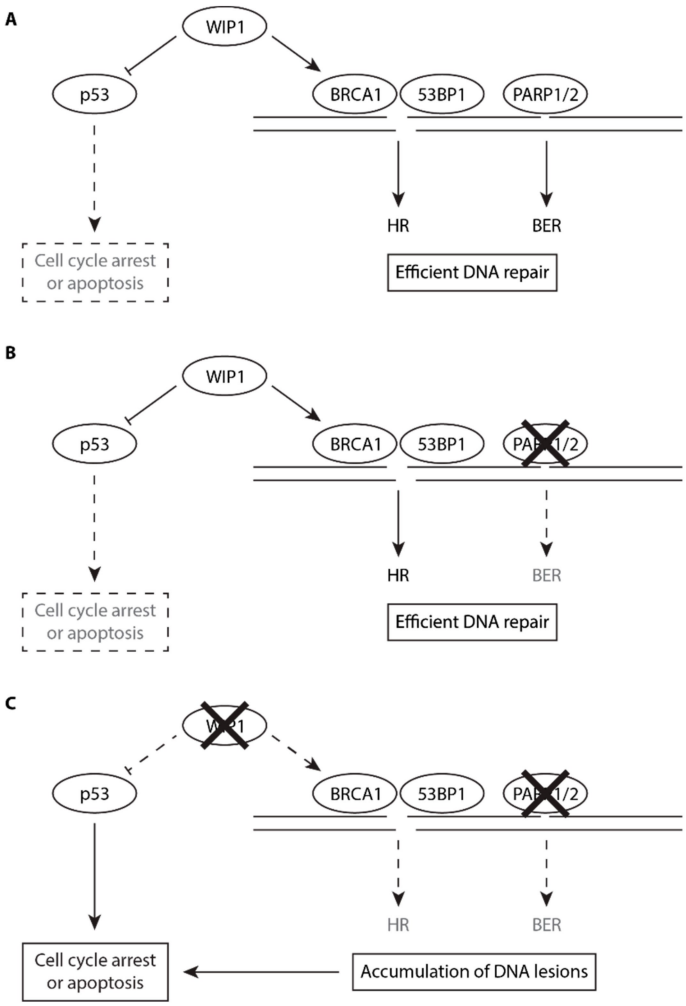

Figure 6. Putative model for the role of WIP1 in HR and in PARP inhibitor sensitivity. (**A**) Under normal conditions, endogenous DNA lesions are eciently repaired by HR and BER. WIP1 promotes eciency of HR and limits the extent of p53 pathway activation allowing cells to proliferate. (**B**) After inhibition of PARP1, BER pathway is impaired (dashed lines) but DNA lesions are eciently repaired by HR. (**C**) Combined inhibition of PARP1 and WIP1 impairs both BER and HR (dashed lines) and enhances p53 response leading to accumulation of DNA lesions in G2 cells. Increased DNA damage load triggers the DNA damage response and allows full activation of p53 pathway leading to cell death.

4. Material and Methods

4.1. Cell Lines

All cell lines used were maintained in DMEM containing 6% FBS, Penicillin (100 U/mL) and Streptomycin (0.1 mg/mL). All cell lines were regularly checked for mycoplasma contamination and were confirmed as negative. U2OS-WIP1-KO cells were described previously [44] and here were stably complemented by transfection of EGFP-WIP1-wt or EGFP-WIP1-D314A followed by three

weeks selection by zeocin and expansion of individual GFP+ clones. WIP1 knockout in RPE cells was generated by transfection of pCMV-CAS9-2A-GFP (Sigma-Aldrich, St. Louis, MO, USA) carrying gRNA sequence tgagcgtcttctccgaccaggg, followed by sorting of single GFP+ cells 48 h after transfection to 96-well plate. Loss of WIP1 was validated by Western blotting in single clones. Knockout of CDKN1A/p21 in U2OS cells was generated using CRISPR-Cas9 and HDR reporter vector (Santa Cruz Biotechnology, Dallas, TX, USA) as described [44]. Cells were sorted as GFP+/RFP+ 48 h after plasmid transfection as single cells to 96-well plate and knockout was validated by Western blotting in single clones. Trac light reporter cell lines were generated by transfection of linearized pCVL Trac Light Reporter 1.1 Ef1a Puro plasmid (Addgene, Watertown, MA, USA, Plasmid #31482) [48] to U2OS or RPE cells using polyethylenimine. Single clones were picked after selection with puromycin for three weeks. Integration of the reporter was confirmed using ISceI with BFP-donor plasmid transfection by FACS. Silencer Select siRNA was transfected at 5 nM final concentration using RNAiMAX using manufacturer's guidelines (Thermo Fisher Scientific, Waltham, MA, USA). Where indicated, cells grown on culture plates were exposed to the indicated dose of ionizing radiation generated by X-RAD 225XL instrument with Cu filter 0.5 mm (Precision X-Ray, North Branford, CT, USA).

4.2. Antibodies and Chemicals

Following antibodies were used: WIP1 antibody (clone F-10, sc-376257), p21 (sc-397), p53 (clone D01, sc-126), BRCA1 (sc-6954), rabbit-53BP1 (sc-22760), RAD51 (sc-6862) and TFIIH (sc-293, used as loading control) from Santa Cruz Biotechnology (Dallas, TX, USA); phoshpo-Thr543-53BP1 (#3428), phospho-S15-p53 (#9284) from Cell Signaling Technology (Danvers, MA, USA); RPA2 (clone 9H8, ab2175), and phospho-Ser1524-BRCA1 (ab2401) from Abcam (Cambridge, UK), H2AX (05-636), and mouse monoclonal 53BP1 (MAB3802) from Merck Millipore (Burlington, MA, USA); phospho-S824-KAP1 (GTX63711), KAP1 (GTX62973) and PP4C (GTX114659) from Genetex (Irvine, CA, USA); secondary Alexa Fluor conjugated antibodies from Thermo Fisher Scientific (Waltham, MA, USA). WIP1 inhibitor GSK2830371 (here referred to as WIP1i and used at 0.5 M unless stated otherwise), olaparib and camptothecin (all Medchemexpress, New York, NJ, USA) and mitomycin C (Santa Cruz Biotechnology, Dallas, TX, USA) were dissolved in DMSO and used at indicated concentrations.

4.3. Immunoprecipitation

HEK293 or U2OS-WIP1-KO cells were transfected with GFP-WIP1 plasmid using polyethylenimine. Cells treated as indicated were extracted in lysis buer [50 mM Tris pH 8.0, 120 mM NaCl, 1% Tween-20, 0.1% NP-40, 1.0% glycerol, 2 mM EDTA, 3 mM EGTA, 10 mM $MgCl_2$, complete protease and phosphatase inhibitors (Sigma-Aldrich, St. Louis, MO, USA)] supplemented with benzonase (100 U/mL), briefly sonicated and EtBr (50 g/mL) was added before centrifugation 30 min 4 C at 20,000 g. GFP-Trap beads (Chromotek, Planegg, Germany) were added to lysate for 1 h before washing 4 with lysis buer. Alternatively, endogenous WIP1 was immunoprecipitated from U2OS cells by a rabbit anity-purified antibody generated against human WIP1 and immobilized on protein A/G UltraLink resin (Thermo Fisher Scientific, Waltham, MA, USA). Bound proteins were eluted with 2 loading buer and analyzed by Western Blotting.

4.4. Immunofluorescence

Cells were seeded on coverslips one day before treatment. Where indicated, cells were pre-extracted 5 min on ice before fixation. Cells were fixed with 4% PFA 15 min RT. Cells were permeabilized using 0.5% Triton-X100 in PBS 5 min and blocked in 1% BSA for 30 min. Where indicated, cells were pulse labeled with EdU 30 min before irradiation and click reaction was performed before primary antibody incubation in 0.1 M Tris pH 8.5, 0.1 M sodium ascorbate, 2 mM $CuSO_4$ and 10 M AlexaFluor 647 azide (Thermo Fisher Scientific, Waltham, MA, USA) for 30 min at RT. Coverslips were incubated with primary antibodies for 2 h in RT, washed 3 in PBS, incubated with secondary antibody for 1 h in RT, washed 3 in PBS, stained with DAPI in PBS for 2 min, washed in dH_2O and dried before mounting

with Vectashield. Images were acquired using Olympus ScanR system equipped with 40/1.3 UPLFN or 40/0.9 objective (Olympus, Tokyo, Japan). Nuclei were segmented based on DAPI intensity and foci were identified using Spot detection module. Total and mean intensities of staining per nucleus were determined. FlowJo v10.6.1 software (TreeStar, Ashland, OR, USA) was used to determine of intensity or foci number in particular cell population.

4.5. Flow Cytometry

For cell cycle analysis, cells were incubated with EdU 30 min before harvesting by trypsinization and fixation in 70% EtOH. Cells were permeabilized with 0.5% Triton-X100 in PBS 15 min RT, washed in BSA, click reaction was performed before incubation with primary and secondary antibodies. DAPI was added in final concentration of 5 g/mL in PBS. Percentage of dead cells was determined 3 days after treatment using Hoechst33258 [71]. To analyze repair eciency by DR-GFP and EJ assays, cells were pretreated 15 min with WIP1i before ISceI transfection using PEI. Percentage of GFP+ cells was determined 3 days after transfection. For trac light reporter, cells stably expressing Trac light reporter 1.1 were seeded at 20,000/well one day before transfection with 5 nM siRNA for 2 days. WIP1i was added 15 min before transfection ISceI and pRRL-SFFV-d20GFP.T2A.mTagBFP Donor plasmid (Addgene, Watertown, MA, USA, ID 31485) [48]. Percentage of GFP and mCherry positive cells in BFP positive singlet cells were analyzed three days after ISceI transfection as described [48]. Data were acquired using BD LSRII flow cytometer (Becton Dickinson, Franklin Lakes, NJ, USA) and analyzed using FlowJo (TreeStar, Ashland, OR, USA).

4.6. Cell Survival Assays

Cells were seeded 1 day before treatment to 96 well plates at 50–500 cells per well, incubated seven days with treatment before resazurin was added in fresh media at final concentration 30 g/mL [44]. Fluorescence at excitation wavelength 560 nm and emission 590 nm was measured using Envision plate reader (PerkinElmer, Waltham, MA, USA) after 2 h incubation.

4.7. Western Blot

Cells were lysed in 2 lysis buer, sonicated and protein concentration was determined using BCA protein assay. A total of 20–50 g lysate was resolved on SDS-PAGE, transferred to nitrocellulose membrane, blocked in 5% milk, incubated with primary and secondary antibodies and developed with ECL.

4.8. In Vitro Phosphatase Assay

U2OS-WIP1-KO cells were treated as indicated and nuclear extracts were prepared using hypotonic lysis as previously described [72]. Briefly, cells were washed with PBS, incubated in buer A (10 mM HEPES-KOH (pH 7.9), 1 mM $MgCl_2$, 2.5 mM KCl, 0.5 mM DTT) for 5 min, centrifuged, resuspended in buer A containing EDTA-free protease and phosphatase inhibitors (Sigma-Aldrich, St. Louis, MO, USA) and dounce homogenized using tight pestle on ice. Nuclei were spun down at 500 g 5 min 4 C and extracted in buer C (20 mM HEPES pH 7.9, 1.5 mM $MgCl_2$, 0.2 mM EDTA, 25% glycerol, 0.5 mM DTT) supplemented with 600 mM KCl on ice for 15 min before centrifugation at max speed 15 min 4 C. Supernatants were diluted with buer C to final concentration 150 mM KCl, clarified by centrifugation max speed 15 min 4 C and stored at 80 C. For in vitro phosphatase assay 100 g of nuclear extract was incubated with 250 ng of purified full-length His-WIP1 phosphatase 15 min at 37 C [30]. Where indicated ATM (KU-55933, 100 M) or DNA-PK (NU-7441, 50 M) inhibitor were added into the phosphatase reaction. Reaction was stopped by addition of 4 sample buer. Protein phosphorylation was determined using phospho-specific antibodies by Western blotting. Alternatively, U2OS cells grown on coverslips were exposed or not to 5 Gy of IR, fixed with 4% paraformaldehyde, permeabilized with 0.5% Triton X-100 and in situ phosphatase assay using purified WIP1-His was performed as described previously [35]. Reaction was stopped by addition of 20 mM

NaF and 20 mM -glycerolphosphate in PBS, samples were stained with H2AX, BRCA1 S1524 or 53BP1 T543 antibodies and total nuclear intensity was determined using Olympus ScanR.

Supplementary Materials: The following are available online at http://www.mdpi.com/2073-4409/8/10/1258/s1, Figure S1: WIP1 inhibition impairs HR and increases sensitivity to DNA damage, Figure S2: Loss of WIP1 delays removal of 53BP1 foci in U2OS cells, Figure S3: WIP1 inhibition delays removal of 53BP1 foci in MCF7 cells, Figure S4: WIP1 dephosphorylates BRCA1 and 53BP1 in vitro and in situ, Figure S5: Loss of WIP1 increases BRCA1 phosphorylation at S1524, Figure S6: Loss of WIP1 increases IR-induced phosphorylation of 53BP1 at T543.

Author Contributions: Conceptualization, K.B. and L.M.; data acquisition K.B., R.S., M.P. and L.M., data interpretation K.B. and L.M.; supervision, L.M.; funding acquisition, L.M.; writing manuscript K.B. and L.M.

Funding: This research was funded by Czech Science Foundation (16-19437S) and Czech Academy of Sciences (RVO 68378050). Light Microscopy Core Facility was supported by MEYS (LM2015062) and OPPK (CZ.2.16/3.1.00/21547). R.S. received a stipend from Charles University.

Acknowledgments: Plasmids for trac light reporter were a gift from Andrew Scharenberg (Seattle Children's Hospital). U2OS DR-GFP and U2OS E5J reporter cell lines were from Jeremy Stark (City of Hope, Duarte). Purified His-Wip1 was provided by Sona Pechackova (IMG, Prague).

Conflicts of Interest: Authors declare no conflict of interests.

References

1. Hustedt, N.; Durocher, D. The control of DNA repair by the cell cycle. Nat. Cell Biol. **2016**, 19, 1. [CrossRef] [PubMed]
2. Ferretti, L.; Lafranchi, L.; Sartori, A. Controlling DNA-end resection: A new task for CDKs. Front. Genet. **2013**, 4, 99. [CrossRef] [PubMed]
3. Jackson, S.P.; Bartek, J. The DNA-damage response in human biology and disease. Nature **2009**, 461, 1071–1078. [CrossRef] [PubMed]
4. Jackson Stephen, P.; Durocher, D. Regulation of DNA Damage Responses by Ubiquitin and SUMO. Mol. Cell **2013**, 49, 795–807. [CrossRef] [PubMed]
5. Himmels, S.-F.; Sartori, A.A. Controlling DNA-End Resection: An. Emerging Task for Ubiquitin and SUMO. Front. Genet. **2016**, 7, 152. [CrossRef] [PubMed]
6. Chen, H.; Lisby, M.; Symington, L.S. RPA coordinates DNA end resection and prevents formation of DNA hairpins. Mol. Cell **2013**, 50, 589–600. [CrossRef] [PubMed]
7. Zou, L.; Elledge, S.J. Sensing DNA Damage Through ATRIP Recognition of RPA-ssDNA Complexes. Science **2003**, 300, 1542–1548. [CrossRef]
8. Zong, D.; Adam, S.; Wang, Y.; Sasanuma, H.; Callén, E.; Murga, M.; Chaudhuri, A.R. BRCA1 Haploinsuciency Is Masked by RNF168-Mediated Chromatin Ubiquitylation. Mol. Cell **2019**, 73, 1267–1281.e7. [CrossRef]
9. Sy, S.M.H.; Huen, M.S.Y.; Chen, J. PALB2 is an integral component of the BRCA complex required for homologous recombination repair. Proc. Natl. Acad. Sci. USA **2009**, 106, 7155–7160. [CrossRef]
10. Zhao, W.; Steinfeld, J.B.; Liang, F.; Chen, X.; Maranon, D.G.; Ma, C.J.; Song, X. BRCA1–BARD1 promotes RAD51-mediated homologous DNA pairing. Nature **2017**, 550, 360. [CrossRef]
11. Chapman, J.R.; Martin, R.G.; Taylor, J.; Simon, J.; Boulton, J. Playing the End Game: DNA Double-Strand Break Repair Pathway Choice. Mol. Cell **2012**, 47, 497–510. [CrossRef] [PubMed]
12. Panier, S.; Boulton, S.J. Double-strand break repair: 53BP1 comes into focus. Nat. Rev. Mol. Cell Biol. **2013**, 15, 7. [CrossRef] [PubMed]
13. Sobhian, B.; Shao, G.; Lilli, D.R.; Culhane, A.C.; Moreau, L.A.; Xia, B.; Greenberg, R.A. RAP80 Targets BRCA1 to Specific Ubiquitin Structures at DNA Damage Sites. Science **2007**, 316, 1198–1202. [CrossRef] [PubMed]
14. Nakamura, K.; Saredi, G.; Becker, J.R.; Foster, B.M.; Nguyen, N.V.; Beyer, T.E.; Chapman, J.R. H4K20me0 recognition by BRCA1–BARD1 directs homologous recombination to sister chromatids. Nat. Cell Biol. **2019**, 21, 311–318. [CrossRef] [PubMed]
15. Fradet-Turcotte, A.; Canny, M.D.; Escribano-Díaz, C.; Orthwein, A.; Leung, C.C.; Huang, H.; Durocher, D. 53BP1 is a reader of the DNA-damage-induced H2A Lys 15 ubiquitin mark. Nature **2013**, 499, 50–54. [CrossRef]

16. Pei, H.; Zhang, L.; Luo, K.; Qin, Y.; Chesi, M.; Fei, F.; Lou, Z. MMSET regulates histone H4K20 methylation and 53BP1 accumulation at DNA damage sites. Nature **2011**, 470, 124–128. [CrossRef]
17. Kleiner, R.E.; Verma, P.; Molloy, K.R.; Chait, B.T.; Kapoor, T.M. Chemical proteomics reveals a H2AX-53BP1 interaction in the DNA damage response. Nat. Chem. Biol. **2015**, 11, 807. [CrossRef]
18. Callen, E.; di Virgilio, M.; Kruhlak, M.J.; Nieto-Soler, M.; Wong, N.; Chen, H.T.; Wesemann, D.R. 53BP1 Mediates Productive and Mutagenic DNA Repair through Distinct Phosphoprotein Interactions. Cell **2013**, 153, 1266–1280. [CrossRef]
19. Chapman, J.R.; Barral, P.; Vannier, J.B.; Borel, V.; Steger, M.; Tomas-Loba, A.; Boulton, S.J. RIF1 Is Essential for 53BP1-Dependent Nonhomologous End Joining and Suppression of DNA Double-Strand Break Resection. Mol. Cell **2013**, 49, 858–871. [CrossRef]
20. Escribano-Díaz, C.; Orthwein, A.; Fradet-Turcotte, A.; Xing, M.; Young, J.T.; Tkáč, J.; Xu, D. A Cell Cycle-Dependent Regulatory Circuit Composed of 53BP1-RIF1 and BRCA1-CtIP Controls DNA Repair Pathway Choice. Mol. Cell **2013**, 49, 872–883. [CrossRef]
21. Isono, M.; Niimi, A.; Oike, T.; Hagiwara, Y.; Sato, H.; Sekine, R.; Petricci, E. BRCA1 Directs the Repair Pathway to Homologous Recombination by Promoting 53BP1 Dephosphorylation. Cell Rep. **2017**, 18, 520–532. [CrossRef] [PubMed]
22. Densham, R.M.; Garvin, A.J.; Stone, H.R.; Strachan, J.; Baldock, R.A.; Daza-Martin, M.; Pearl, L.H. Human BRCA1–BARD1 ubiquitin ligase activity counteracts chromatin barriers to DNA resection. Nat. Struct. Mol. Biol. **2016**, 23, 647. [CrossRef] [PubMed]
23. Lord, C.J.; Ashworth, A. The DNA damage response and cancer therapy. Nature **2012**, 481, 287–294. [CrossRef] [PubMed]
24. Lord, C.J.; Ashworth, A. PARP inhibitors: Synthetic lethality in the clinic. Science **2017**, 355, 1152–1158. [CrossRef]
25. Ibrahim, Y.H.; García-García, C.; Serra, V.; He, L.; Torres-Lockhart, K.; Prat, A.; Rodríguez, O. PI3K Inhibition Impairs BRCA1/2 Expression and Sensitizes BRCA-Proficient Triple-Negative Breast Cancer to PARP Inhibition. Cancer Discov. **2012**, 2, 1036–1047. [CrossRef]
26. Gogola, E.; Rottenberg, S.; Jonkers, J. Resistance to PARP Inhibitors: Lessons from Preclinical Models of BRCA-Associated Cancer. Annu. Rev. Cancer Biol. **2019**, 3, 235–254. [CrossRef]
27. Karakashev, S.; Zhu, H.; Yokoyama, Y.; Zhao, B.; Fatkhutdinov, N.; Kossenkov, A.V.; Bitler, B.G. BET Bromodomain Inhibition Synergizes with PARP Inhibitor in Epithelial Ovarian Cancer. Cell Rep. **2017**, 21, 3398–3405. [CrossRef]
28. Zhong, Q.; Hu, Z.; Li, Q.; Yi, T.; Li, J.; Yang, H. Cyclin D1 silencing impairs DNA double strand break repair, sensitizes BRCA1 wildtype ovarian cancer cells to olaparib. Gynecol. Oncol. **2019**, 152, 157–165. [CrossRef]
29. Kurnit, K.C.; Coleman, R.L.; Westin, S.N. Using PARP Inhibitors in the Treatment of Patients with Ovarian Cancer. Curr. Treat. Opt. Oncol. **2018**, 19, 1. [CrossRef]
30. Macůrek, L.; Lindqvist, A.; Voets, O.; Kool, J.; Vos, H.R.; Medema, R.H. Wip1 phosphatase is associated with chromatin and dephosphorylates gammaH2AX to promote checkpoint inhibition. Oncogene **2010**, 15, 2281–2291.
31. Macurek, L.; Benada, J.; Müllers, E.; Halim, V.A.; Krejčíková, K.; Burdová, K.; Bartek, J. Downregulation of Wip1 phosphatase modulates the cellular threshold of DNA damage signaling in mitosis. Cell Cycle **2013**, 12, 251–262. [CrossRef] [PubMed]
32. Fiscella, M.; Zhang, H.; Fan, S.; Sakaguchi, K.; Shen, S.; Mercer, W.E.; Appella, E. Wip1, a novel human protein phosphatase that is induced in response to ionizing radiation in a p53-dependent manner. Proc. Natl. Acad. Sci. USA **1997**, 94, 6048–6053. [CrossRef] [PubMed]
33. Lu, X.; Ma, O.; Nguyen, T.A.; Jones, S.N.; Oren, M.; Donehower, L.A. The Wip1 Phosphatase Acts as a Gatekeeper in the p53-Mdm2 Autoregulatory Loop. Cancer Cell **2007**, 12, 342–354. [CrossRef] [PubMed]
34. Shreeram, S.; Demidov, O.N.; Hee, W.K.; Yamaguchi, H.; Onishi, N.; Kek, C.; Minami, Y. Wip1 Phosphatase Modulates ATM-Dependent Signaling Pathways. Mol. Cell **2006**, 23, 757–764. [CrossRef]
35. Shreeram, S.; Demidov, O.N.; Hee, W.K.; Yamaguchi, H.; Onishi, N.; Kek, C.; Minami, Y. ATM/Wip1 activities at chromatin control Plk1 re-activation to determine G2 checkpoint duration. EMBO J. **2017**, 36, 2161–2176.
36. Shaltiel, I.A.; Aprelia, M.; Saurin, A.T.; Chowdhury, D.; Kops, G.J.; Voest, E.E.; Medema, R.H. Distinct phosphatases antagonize the p53 response in dierent phases of the cell cycle. Proc. Natl. Acad. Sci. USA **2014**, 111, 7313–7318. [CrossRef]

37. Cha, H.; Lowe, J.M.; Li, H.; Lee, J.S.; Belova, G.I.; Bulavin, D.V.; Fornace, A. JWip1 Directly Dephosphorylates -H2AX and Attenuates the DNA Damage Response. Cancer Res. **2010**, 70, 4112–4122. [CrossRef]
38. Bulavin, D.V.; Demidov, O.N.; Saito, S.I.; Kauraniemi, P.; Phillips, C.; Amundson, S.A.; Kallioniemi, A. Amplification of PPM1D in human tumors abrogates p53 tumor-suppressor activity. Nat. Genet. **2002**, 31, 210. [CrossRef]
39. Tan, D.S.; Lambros, M.B.; Rayter, S.; Natrajan, R.; Vatcheva, R.; Gao, Q.; Fenwick, K. PPM1D Is a Potential Therapeutic Target in Ovarian Clear Cell Carcinomas. Clin. Cancer Res. **2009**, 15, 2269–2280. [CrossRef]
40. Castellino, R.C.; de Bortoli, M.; Lu, X.; Moon, S.H.; Nguyen, T.A.; Shepard, M.A.; Kim, J.Y. Medulloblastomas overexpress the p53-inactivating oncogene WIP1/PPM1D. J. Neurooncol. **2008**, 86, 245–256. [CrossRef]
41. Le Guezennec, X.; Bulavin, D.V. WIP1 phosphatase at the crossroads of cancer and aging. Trends Biochem. Sci. **2010**, 35, 109–114. [CrossRef] [PubMed]
42. Gilmartin, A.G.; Faitg, T.H.; Richter, M.; Groy, A.; Seefeld, M.A.; Darcy, M.G.; Minthorn, E. Allosteric Wip1 phosphatase inhibition through flap-subdomain interaction. Nat. Chem. Biol. **2014**, 10, 181–187. [CrossRef] [PubMed]
43. Richter, M.; Dayaram, T.; Gilmartin, A.G.; Ganji, G.; Pemmasani, S.K.; van der Key, H.; Kumar, R. WIP1 Phosphatase as a Potential Therapeutic Target in Neuroblastoma. PLoS ONE **2015**, 10, e0115635.
44. Pechackova, S.; Burdova, K.; Benada, J.; Kleiblova, P.; Jenikova, G.; Macurek, L. Inhibition of WIP1 phosphatase sensitizes breast cancer cells to genotoxic stress and to MDM2 antagonist nutlin-3. Oncotarget **2016**, 7, 14458–14475. [CrossRef] [PubMed]
45. Pecháčková, S.; Burdová, K.; Macurek, L. WIP1 phosphatase as pharmacological target in cancer therapy. J. Mol. Med. **2017**, 95, 589–599. [CrossRef] [PubMed]
46. Stolte, B.; Iniguez, A.B.; Dharia, N.; Robichaud, A.; Conway, A.; Morgan, A.; Alexe, G. Genome-scale CRISPR-Cas9 screen identifies druggable dependencies in TP53 wild-type Ewing sarcoma. J. Exp. Med. **2018**, 215, 2137–2155. [CrossRef]
47. Moon, S.H.; Lin, L.; Zhang, X.; Nguyen, T.A.; Darlington, Y.; Waldman, A.S.; Donehower, L.A. Wildtype p53-induced phosphatase 1 dephosphorylates histone variant gamma-H2AX and suppresses DNA double strand break repair. J. Biol. Chem. **2010**, 285, 12935–12947. [CrossRef]
48. Certo, M.T.; Ryu, B.Y.; Annis, J.E.; Garibov, M.; Jarjour, J.; Rawlings, D.J.; Scharenberg, A.M. Tracking genome engineering outcome at individual DNA breakpoints. Nat. Methods **2011**, 8, 671. [CrossRef]
49. Jazayeri, A.; Falck, J.; Lukas, C.; Bartek, J.; Smith, G.C.; Lukas, J.; Jackson, S.P. ATM-and cell cycle-dependent regulation of ATR in response to DNA double-strand breaks. Nat. Cell Biol. **2006**, 8, 37–45. [CrossRef]
50. Gunn, A.; Stark, J.M. I-SceI-Based Assays to Examine Distinct Repair Outcomes of Mammalian Chromosomal Double Strand Breaks. In DNA Repair Protocols; Bjergbæk, L., Ed.; Humana Press: Totowa, NJ, USA, 2012; pp. 379–391.
51. Saleh-Gohari, N.; Bryant, H.E.; Schultz, N.; Parker, K.M.; Cassel, T.N.; Helleday, T. Spontaneous Homologous Recombination Is Induced by Collapsed Replication Forks That Are Caused by Endogenous DNA Single-Strand Breaks. Mol. Cell. Biol. **2005**, 25, 7158–7169. [CrossRef]
52. Noordermeer, S.M.; Adam, S.; Setiaputra, D.; Barazas, M.; Pettitt, S.J.; Ling, A.K.; Annunziato, S. The shieldin complex mediates 53BP1-dependent DNA repair. Nature **2018**, 560, 117–121. [CrossRef] [PubMed]
53. Schmidt, C.K.; Galanty, Y.; Sczaniecka-Clift, M.; Coates, J.; Jhujh, S.; Demir, M.; Jackson, S.P. Systematic E2 screening reveals a UBE2D–RNF138–CtIP axis promoting DNA repair. Nat. Cell Biol. **2015**, 17, 1458. [CrossRef] [PubMed]
54. Tibbetts, R.S.; Cortez, D.; Brumbaugh, K.M.; Scully, R.; Livingston, D.; Elledge, S.J.; Abraham, R.T. Functional interactions between BRCA1 and the checkpoint kinase ATR during genotoxic stress. Genes Dev. **2000**, 14, 2989–3002. [CrossRef] [PubMed]
55. Xu, B.; O'Donnell, A.H.; Kim, S.T.; Kastan, M.B. Phosphorylation of Serine 1387 in Brca1 Is Specifically Required for the Atm-mediated S-Phase Checkpoint after Ionizing Irradiation. Cancer Res. **2002**, 62, 4588–4591.
56. Scully, R.; Chen, J.; Ochs, R.L.; Keegan, K.; Hoekstra, M.; Feunteun, J.; Livingston, D.M. Dynamic Changes of BRCA1 Subnuclear Location and Phosphorylation State Are Initiated by DNA Damage. Cell **1997**, 90, 425–435. [CrossRef]
57. Kim, H.S.; Li, H.; Cevher, M.; Parmelee, A.; Fonseca, D.; Kleiman, F.E.; Lee, S.B. DNA Damage–Induced BARD1 Phosphorylation Is Critical for the Inhibition of Messenger RNA Processing by BRCA1/BARD1 Complex. Cancer Res. **2006**, 66, 4561–4565. [CrossRef]

58. Filipponi, D.; Muller, J.; Emelyanov, A.; Bulavin, D.V. Wip1 Controls Global Heterochromatin Silencing via ATM/BRCA1-Dependent DNA Methylation. Cancer Cell **2013**, 24, 528–541. [CrossRef]
59. Chowdhury, D.; Xu, X.; Zhong, X.; Ahmed, F.; Zhong, J.; Liao, J.; Lieberman, J. A PP4-phosphatase complex dephosphorylates gamma-H2AX generated during DNA replication. Mol. Cell **2008**, 31, 33–46. [CrossRef]
60. Lee, D.H.; Goodarzi, A.A.; Adelmant, G.O.; Pan, Y.; Jeggo, P.A.; Marto, J.A.; Chowdhury, D. Phosphoproteomic analysis reveals that PP4 dephosphorylates KAP-1 impacting the DNA damage response. EMBO J. **2012**, 31, 2403–2415. [CrossRef]
61. Penning, T.D.; Zhu, G.D.; Gong, J.; Thomas, S.; Gandhi, V.B.; Liu, X.; Fry, E.H. Optimization of Phenyl-Substituted Benzimidazole Carboxamide Poly(ADP-Ribose) Polymerase Inhibitors: Identification of (S)-2-(2-Fluoro-4-(pyrrolidin-2-yl)phenyl)-1H-benzimidazole-4-carboxamide (A-966492), a Highly Potent and Ecacious Inhibitor. J. Med. Chem. **2010**, 53, 3142–3153. [CrossRef]
62. Lindqvist, A.; de Bruijn, M.; Macurek, L.; Brás, A.; Mensinga, A.; Bruinsma, W.; Medema, R. HWip1 confers G2 checkpoint recovery competence by counteracting p53-dependent transcriptional repression. EMBO J. **2009**, 28, 3196–3206. [CrossRef] [PubMed]
63. Lu, X.; Bocangel, D.; Nannenga, B.; Yamaguchi, H.; Appella, E.; Donehower, L.A. The p53-Induced Oncogenic Phosphatase PPM1D Interacts with Uracil DNA Glycosylase and Suppresses Base Excision Repair. Mol. Cell **2004**, 15, 621–634. [CrossRef] [PubMed]
64. Nguyen, T.A.; Slattery, S.D.; Moon, S.H.; Darlington, Y.F.; Lu, X.; Donehower, L.A. The oncogenic phosphatase WIP1 negatively regulates nucleotide excision repair. DNA Repair **2010**, 9, 813–823. [CrossRef] [PubMed]
65. Linke, S.P.; Sengupta, S.; Khabie, N.; Jeries, B.A.; Buchhop, S.; Miska, S.; Yang, Q. p53 Interacts with hRAD51 and hRAD54, and Directly Modulates Homologous Recombination. Cancer Res. **2003**, 63, 2596–2605. [PubMed]
66. Arias-Lopez, C.; Lazaro-Trueba, I.; Kerr, P.; Lord, C.J.; Dexter, T.; Iravani, M.; Silva, A. p53 modulates homologous recombination by transcriptional regulation of the RAD51 gene. EMBO Rep. **2006**, 7, 219–224. [CrossRef]
67. Gatz, S.A.; Wiesmüller, L. p53 in recombination and repair. Cell Death Dier. **2006**, 13, 1003–1016. [CrossRef]
68. Sriraman, A.; Radovanovic, M.; Wienken, M.; Najafova, Z.; Li, Y.; Dobbelstein, M. Cooperation of Nutlin-3a and a Wip1 inhibitor to induce p53 activity. Oncotarget **2016**, 7, 31623–31638. [CrossRef]
69. Chen, Z.; Wang, L.; Yao, D.; Yang, T.; Cao, W.M.; Dou, J.; Zhao, Y. Wip1 inhibitor GSK2830371 inhibits neuroblastoma growth by inducing Chk2/p53-mediated apoptosis. Sci. Rep. **2016**, 6, 38011. [CrossRef]
70. Wu, C.E.; Esfandiari, A.; Ho, Y.H.; Wang, N.; Mahdi, A.K.; Aptullahoglu, E.; Lunec, J. Targeting negative regulation of p53 by MDM2 and WIP1 as a therapeutic strategy in cutaneous melanoma. Br. J. Cancer **2017**, 118, 495.
71. Kasibhatla, S.; Amarante-Mendes, G.P.; Finucane, D.; Brunner, T.; Bossy-Wetzel, E.; Green, D.R. Staining of Suspension Cells with Hoechst 33258 to Detect. Apoptosis. Cold Spring Harb. Protoc. **2006**, 2006, pdb.prot4492. [CrossRef]
72. Shiotani, B.; Zou, L. Single-Stranded DNA Orchestrates an ATM-to-ATR Switch at DNA Breaks. Mol. Cell **2009**, 33, 547–558. [CrossRef] [PubMed]